



Studies of star formation in small molecular clouds and Bok globules

Author:

Bourke, Tyler Leonard

Publication Date:

1994

DOI:

<https://doi.org/10.26190/unsworks/6675>

License:

<https://creativecommons.org/licenses/by-nc-nd/3.0/au/>

Link to license to see what you are allowed to do with this resource.

Downloaded from <http://hdl.handle.net/1959.4/60601> in <https://unsworks.unsw.edu.au> on 2024-04-27

PLEASE TYPE

UNIVERSITY OF NEW SOUTH WALES
Thesis/Project Report Sheet

Surname or Family name: BOURKE
First name: Tyler Other name/s: Leonard
Abbreviation for degree as given in the University calendar: MSc
School: Department of Physics Faculty: University College
Title: Studies of Star Formation in Small Molecular Clouds and Bok Globules
.....
.....

Abstract 350 words maximum: (PLEASE TYPE)

A comprehensive study of a set of small, southern molecular clouds (globules) has been undertaken, primarily through radio observations of ammonia, in order to determine their physical characteristics, their role in the formation of low mass stars, and what physical mechanism triggers the star formation process, or stabilizes the globules against collapse.

The globule list was chosen on the basis of size ($< 10'$) and density (only the densest globules were chosen). The *IRAS* database was used to search the sample for associated point sources. A total of 83 sources were found lying toward 76 of the globules. The *IRAS* sample is dominated by cool sources, with *IRAS* colours of those of embedded sources.

To determine the densities, temperatures and masses of the globules, a major survey was undertaken in the (1,1) and (2,2) inversion transitions of ammonia. Half of the globules were detected in ammonia, but only 5% of the detections were "strong" ($T_a^* \geq 0.35$ K)). Comparing the globule properties with those of Benson and Myers (1989) for cores within complexes, we find that the globules are less opaque and less dense, and are less active sites of star formation. Other properties are comparable. The Vela cometary globules were detected more readily in ammonia, and are more active star formation sites, than the more isolated globules. These results suggest that the dense core's environment plays a significant role in initiating the star formation process.

Dynamical analysis suggests that the globules are not in virial equilibrium. It may be that the star formation process is providing support for the globules against further collapse (outflows? turbulence?) which is revealed in the larger line widths for globules with *IRAS* sources. However, the Jeans masses suggest the globules are in a state of critical equilibrium, and so the mechanism causing the large velocity dispersions may not be sufficient to provide support. Of ten mapped globules, only one shows signs of rotation, and this rotation cannot be significant in the globule dynamics and support, in agreement with earlier globule studies.

Declaration relating to disposition of project report/thesis

I am fully aware of the policy of the University relating to the retention and use of higher degree project reports and theses, namely that the University retains the copies submitted for examination and is free to allow them to be consulted or borrowed. Subject to the provisions of the Copyright Act 1968, the University may issue a project report or thesis in whole or in part, in photostate or microfilm or other copying medium.

The University recognises that there may be exceptional circumstances requiring restrictions on copying or conditions on use. Requests for restriction for a period of up to 2 years must be made in writing to the Registrar. Requests for a longer period of restriction may be considered in exceptional circumstances if accompanied by a letter of support from the Supervisor or Head of School. Such requests must be submitted with the thesis/project report.

FOR OFFICE USE ONLY

Date of completion of requirements for Award:

Registrar and Deputy Principal

Library
of the
Australian Defence Force Academy



University College
The University of New South Wales

Donor: Tyler L. Bourke

**Studies of Star Formation
in
Small Molecular Clouds
and
Bok Globules**

by
Tyler Leonard Bourke
BSc. (Hons), Australian National University

Thesis submitted in accordance with the regulations for the
Degree of Master of Science

Department of Physics
University College
The University of New South Wales
February 1994



301255

I hereby declare that this submission is my own work and that, to the best of my knowledge and belief, it contains no material previously published or written by another person nor material which to a substantial extent has been accepted for the award of any other degree or diploma of a university or other institution of higher learning, except where due acknowledgement is made in the text of the thesis.

Tyler Bourke

*To my parents,
for their unquestioned support over the years,
and to Lyman.*

Acknowledgements

Firstly, I would like to thank my supervisors, Professor Harry Hyland and Dr Garry Robinson, for their advice and guidance over the course of this work, and for their approachability in all matters.

Many people assisted with the observations at the Parkes radio telescope, which is much appreciated. To Steve James, Chris Wright, Simon Duchesne, Robert Smith, Peter McGregor, Andrew Walsh, Craig Smith, Liam Waldron, and Chris Lidman, thank you.

I am extremely grateful to those who assisted me with the data reduction and analysis, and who helped me to understand the reduction procedures involved, when it seemed I was going to be lost in a sea of bits and bytes. In particular I would like to acknowledge the assistance given by Rick Forster, John Whiteoak and Jim Caswell with the Parkes data reduction, and David Allen, Michael Burton, and Peter McGregor for their assistance with the use of IRIS and the near-infrared data reduction. For help with all things computing, many, many thanks go to Henrietta May, Jason Spyromilio, Steve James and Stephen Metheringham.

I was allowed access to facilities at Mt Stromlo Observatory, CSIRO Radio-physics, and the Anglo-Australian Observatory. I would like to thank each of these institutions for granting me this access, and to the staff at each facility who assisted me in any way. This thesis would not have been possible without it.

Financially I would like to thank the Department of Physics for support through demonstrating and research assisting, and the Australian Research Council for part support of the project through a grant. The generous allocation of time on the Parkes radio telescope, the Anglo-Australia Telescope, and the 40

inch telescope at Siding Spring Observatory is gratefully acknowledged.

To the many friends I have made through the International Space University (too many to list), thanks for much needed doses of sanity and inspiration. Chris, thanks for the good times in the e-room, but get off my computer! Many friends at home have helped make life great, in particular Jeppo, Sam, Philthy, Brutal, and various other party-animals (you know who you are), and Nicki and Judy, for more refined pursuits. To Jodie, who somehow always believes I can, and makes me believe it too, words are never enough. Michelle, thanks for your support and caring, and many long distracting phone calls.

Finally, the biggest thanks of all go to my parents, who have supported me financially and morally over many years of my education. I know I am very lucky to have such special people for parents.

*When I heard the learn'd astronomer,
When the proofs, the figures, were ranged in columns before me,
When I was shown the charts and diagrams, to add, divide, and measure them,
When I sitting heard the astronomer where he lectured with much applause in
the lecture-room,
How soon unaccountable I became tired and sick,
Till rising and gliding out I wander'd off by myself,
In the mystical moist night-air, and from time to time,
Look'd up in perfect silence at the stars.*

Walt Whitman

“Mein Gott, da ist ein Loch im Himmel!”

Wilhelm Herschel

Abstract

A comprehensive study of a set of small, southern molecular clouds (globules) has been undertaken, primarily through radio observations of ammonia, in order to determine their physical characteristics, their role in the formation of low mass stars, and what physical mechanism triggers the star formation process, or stabilizes the globules against collapse.

The globule list was chosen on the basis of size ($< 10'$) and density (only the densest globules were chosen). The *IRAS* database was used to search the sample for associated point sources. A total of 83 sources were found lying toward 76 of the globules. The *IRAS* sample is dominated by cool sources, with *IRAS* colours of those of embedded sources.

To determine the densities, temperatures and masses of the globules, a major survey was undertaken in the (1,1) and (2,2) inversion transitions of ammonia. Half of the globules were detected in ammonia, but only 5% of the detections were “strong” ($T_a^* \geq 0.35$ K). Comparing the globule properties with those of Benson and Myers (1989) for cores within complexes, we find that the globules are less opaque and less dense, and are less active sites of star formation. Other properties are comparable. The Vela cometary globules were detected more readily in ammonia, and are more active star formation sites, than the more isolated globules. These results suggest that the dense core’s environment plays a significant role in initiating the star formation process.

Dynamical analysis suggests that the globules are not in virial equilibrium. It may be that the star formation process is providing support for the globules against further collapse (outflows? turbulence?) which is revealed in the larger line widths for globules with *IRAS* sources. However, the Jeans masses suggest the globules are in a state of critical equilibrium, and so the mechanism causing

the large velocity dispersions may not be sufficient to provide support. Of ten mapped globules, only one shows signs of rotation, and this rotation cannot be significant in the globule dynamics and support, in agreement with earlier globule studies.

Contents

1	Molecular Clouds and Star Formation – A Review	1
1.1	Introduction	1
1.2	Classification of Molecular Clouds	3
1.2.1	Diffuse Interstellar Clouds	4
1.2.2	Cold Dark Cloud Complexes	4
1.2.3	Globules and Isolated Dark Clouds	5
1.2.4	Giant Molecular Clouds	5
1.3	Star Formation	8
1.4	Previous Studies of Dark Clouds	15
1.4.1	Optical Surveys	15
1.4.2	Molecular Line Surveys	18
1.4.3	Infrared Surveys	26
1.5	Isolated Dark Clouds and Bok Globules	33
1.5.1	Properties of the Dust and Gas Components	37

1.5.2	Star Formation in Bok Globules	42
1.6	The Work of this Thesis	43
1.6.1	Unanswered Questions	43
1.6.2	Thesis Aims	44
1.6.3	Thesis Outline	46
2	The Dark Cloud Sample	48
2.1	Introduction	48
2.2	The Southern Bok Globule Catalogue	49
2.3	Optical Properties	58
2.4	IRAS properties	70
2.4.1	Comparison with CB associations	71
2.4.2	Comparison with Beichman <i>et al.</i> associations	78
2.5	Conclusions	88
3	The Ammonia Survey	91
3.1	Introduction	91
3.2	Observations and Data Reduction	92
3.3	Data Analysis	95
3.3.1	Ammonia Analysis	95
3.3.2	Distances	104

3.4	Results	107
3.4.1	Survey	107
3.4.2	Derived Properties	113
3.5	Discussion	117
3.5.1	Comparison with Cores in Complexes	117
3.5.2	Globule Sizes	125
3.5.3	Cometary Globules	127
3.5.4	IRAS sources in Globules and Complexes	134
3.6	Conclusions	137
4	Ammonia Mapping and Dynamical Analysis	140
4.1	Introduction	140
4.2	Observations and Data Reduction	141
4.3	Results	141
4.3.1	Source Mapping	141
4.3.2	Mapped Sources	145
4.3.3	Dynamical Analysis	176
4.4	Conclusions	203
5	Conclusions and Future Work	206
5.1	Results of this Thesis	206

5.2 Future Work	210
References	213
Appendix A Molecular Excitation and Radiative Transfer	228
A.1 Molecular Excitation	228
A.2 Radiative Transfer	230
Appendix B The Ammonia Molecule	234
B.1 Physics of the Ammonia Molecule	234
B.2 Ammonia as a Diagnostic Probe	235

Chapter 1

Molecular Clouds and Star Formation – A Review

1.1 Introduction

Interstellar space is not empty. Clouds of gas and dust reveal themselves within our Galaxy as bright nebulae, and dark molecular clouds seen silhouetted against the background stars. It is deep within some dark molecular clouds that stars form, as a result of the collapse of the cloud under the strain of its own gravitational forces. The early stages of a star's formation are rendered optically invisible to us due to the shroud of gas and dust in which they are born. Our knowledge of the star formation process has developed slowly as a result. It is only in the past twenty years, with the advent of radio and infrared astronomical instrumentation, that we have been able to probe the dense stellar nurseries.

That the dark clouds are molecular was first suggested by Bok (1955), who compared the ratio of dust extinction to neutral atomic hydrogen (HI) column

density toward a sample of local dark clouds, and found that it is lower than it is in the more diffuse clouds (as defined by their optical appearance). He proposed that the missing atomic hydrogen exists in the form of molecular hydrogen (H_2). Direct observations of molecules in dark clouds began in the late 1960s, with the detection of OH (Heiles, 1968), ammonia (NH_3) (Cheung *et al.*, 1968), and formaldehyde (H_2CO) (Palmer *et al.*, 1969) at centimetre wavelengths. Densities greater than 10^3 cm^{-3} are required to excite NH_3 to detectable levels at the temperatures typical of dark clouds (see e.g., Ho and Townes, 1983). Only H_2 could be so dense as to cause this excitation but remain undetected. Molecular hydrogen is undetectable at the low temperatures found in most molecular clouds ($T < 100 \text{ K}$) due to its small moment of inertia and the fact that it has no permanent electric dipole (Scoville and Sanders, 1987).

However, it was the detection of carbon monoxide (CO) at millimetre wavelengths toward HII regions (Wilson *et al.*, 1970) and dark clouds (Penzias *et al.*, 1972) that has led to the great advances in our knowledge of the star formation process over the past twenty years. CO is the best general tool for the observational study of molecular clouds for a number of reasons. Due to its low dipole moment, the lowest rotational states require only a modest density (i.e., $n(\text{H}_2) \sim 300 \text{ cm}^{-3}$) to populate them to significant levels via collisional excitation at the kinetic temperatures inferred for the more diffuse dark clouds ($T > 20 \text{ K}$). It is orders of magnitude more abundant than all other molecular species in interstellar space, with the obvious exception of H_2 , and its most common isotopes (^{12}CO , ^{13}CO and C^{18}O), are observable almost at will toward dark clouds. The ratio CO/H_2 is fairly constant over a wide range of physical conditions, allowing cloud densities to be inferred from direct observations of CO . Its ubiquity has made CO the most popular observational tool for the tracing of molecular gas throughout the Galaxy.

Observations of molecules allow us to probe a wide range of physical conditions, in particular density and temperature. Many molecular transitions are detectable throughout the radio and submillimetre wavebands, as a result of their ground state rotational levels being characterised by low energies, allowing their excitation by collisions and radiation under a wide range of interstellar conditions. We have mentioned above that CO is able to provide density and temperature information at relatively low densities. At higher densities other probes of density and temperature are required. Diatomic species with simple single-ladder energy schemes and many allowed transitions serve as good densitometers (Turner, 1988), the most widely used being carbon monosulphide (CS) which is able to trace densities to 10^7 cm^{-3} . Isotopes of CO, such as C^{18}O , are also popular as densitometers. Symmetric tops with many transitions separated by small energies act as sensitive thermometers, the most common example being NH_3 , which, being able to act as a densitometer as well, has been used in many studies of molecular cloud conditions (see e.g., Walmsley and Ungerechts, 1983; Benson and Myers, 1989).

1.2 Classification of Molecular Clouds

Various authors have proposed classification schemes for molecular clouds based on the different morphologies that are evident. The brief description given below is based on that of Turner (1988), and only includes regions of relevance to the current study.

1.2.1 Diffuse Interstellar Clouds

These clouds have been mentioned briefly in section 1.1 when discussing Bok's suggestion that the dark clouds are molecular. They are defined as having column densities $2 \times 10^{19} \leq N \leq 2 \times 10^{21} \text{ cm}^{-2}$, where $N = N(\text{H}) + 2N(\text{H}_2)$. The column density in this range is inversely correlated with temperature. At the low end range of N these clouds have little molecular content, but appreciable molecular content at the high- N end (see e.g., Blitz *et al.*, 1984). Their connection, if any, to the dense molecular clouds is unclear. There is observational evidence to support the suggestion that they are "halos" surrounding the denser clouds (Kazes and Crovisier, 1981; Federman and Willson, 1982), and some evidence against this hypothesis (Phillips and Huggins, 1981).

1.2.2 Cold Dark Cloud Complexes

Cold dark cloud complexes appear as optically well defined extended regions of extinction with $A_V \geq 2$ mags ($N > 2 \times 10^{21} \text{ cm}^{-2}$) and sizes 6 – 20 pc (Goldsmith, 1987). They are generally not associated with nebulosity and are mostly molecular in content. Temperatures of 10 K and densities in the range 10^2 to 10^4 cm^{-3} are typical for these clouds. Dense cores are found within the dark clouds (Myers and Benson, 1983), with densities 10 – 100 times greater than the surrounding cloud. Typical masses are of the order of $10^4 M_\odot$. Examples of this type of cloud include the complexes in Taurus ($10^4 M_\odot$), Ophiuchus ($3 \times 10^3 M_\odot$), Lupus ($3 \times 10^4 M_\odot$), the Coalsack ($3 \times 10^3 M_\odot$), Corona Australis ($7 \times 10^4 M_\odot$) and Chamaeleon ($8 \times 10^3 M_\odot$).

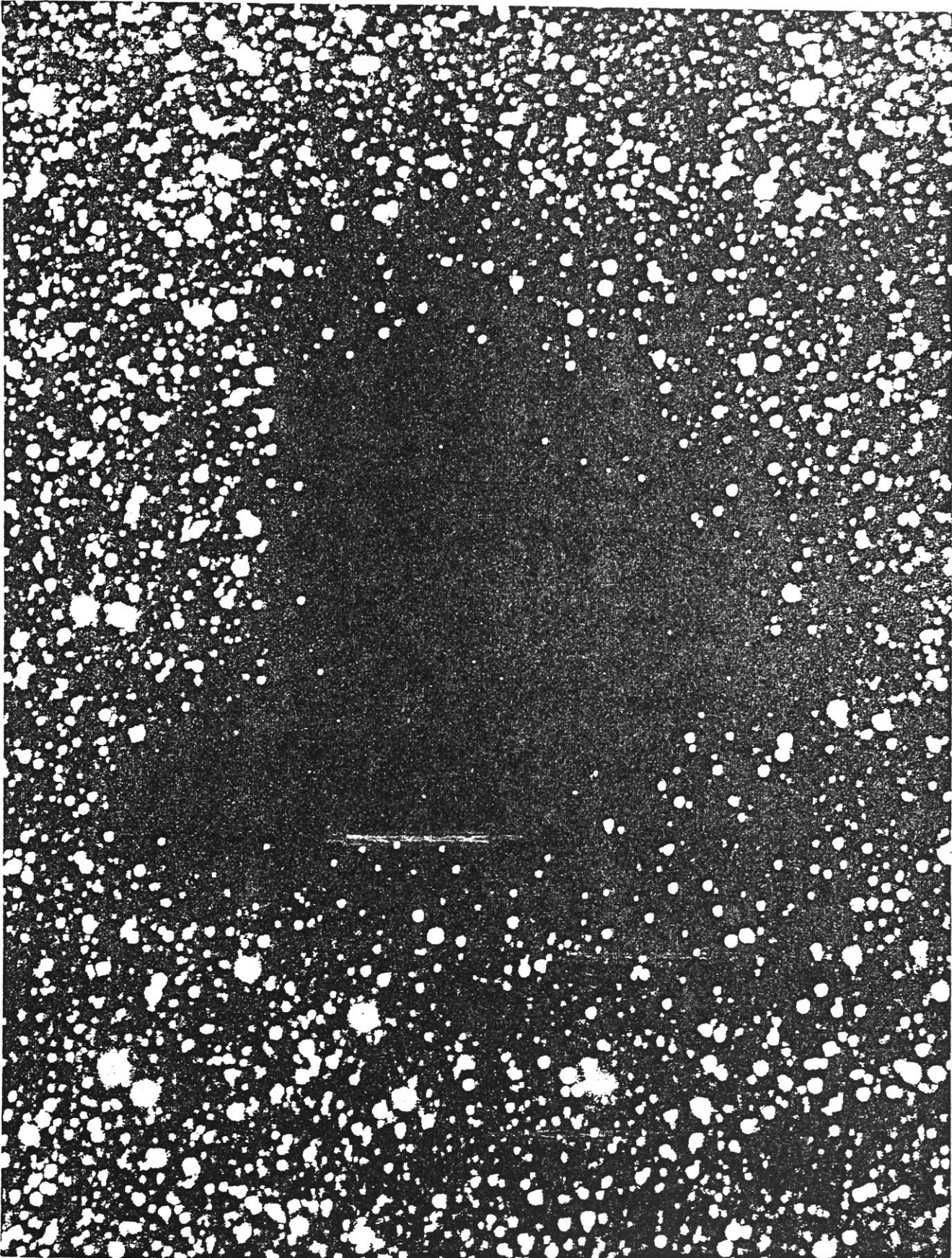
1.2.3 Globules and Isolated Dark Clouds

Globules, as defined by Bok *et al.* (1971) and Bok (1977), are similar in their physical state to the dense cores found in the dark cloud complexes (see e.g., Benson and Myers, 1989). Bok and Reilly (1947) first suggested that this class of object may be the precursors to the formation of low mass stars. They form a remarkably heterogeneous group of objects, being well defined, generally roundish, with angular diameters ranging from a few arcminutes to $\sim 20'$, corresponding to linear sizes up to about 3 pc. They are in general well isolated from other dark clouds and regions of bright nebulosity, one classic example being Barnard 68 (see figure 1.1). All the larger globules we see must lie within 2 kpc of the Sun, otherwise they would not be distinguishable as dark clouds due to the presence of foreground stars. The majority are found within 20° of the galactic plane, where the background star density is greatest. Derived parameters are kinetic temperatures ~ 10 K, column densities $> 10^{22}$ cm $^{-2}$, densities of the order of 10^4 cm $^{-3}$, sizes in the range 0.1 – 3.0 pc, and masses of a few $\times 10 M_\odot$ (Leung, 1985). Globules will be discussed in more detail in section 1.5.

1.2.4 Giant Molecular Clouds

Giant Molecular Clouds (GMCs) were first discovered during CO emission surveys within the past 20 years (see e.g., Blitz, 1991, and references therein). These objects are almost always associated with clusters of OB stars. Densities range from 100 cm $^{-3}$ (Dame *et al.*, 1986) to 10^3 cm $^{-3}$ (Blitz and Shu, 1980), sizes up to 200 pc are quoted (Goldsmith, 1987) and masses $> 10^3 M_\odot$ are inferred. The GMCs contain hot molecular cores which are the sites of ongoing star formation, as indicated by the presence of OB stars (Blitz, 1991). Temperatures as high as 2000 K have been reported for some cores (Elias, 1980), with densities up to 10^8

Figure 1.1: Image of B68, taken by Bart Bok with the CTIO 4 metre reflector at prime focus with an exposure time of 200 minutes at $\sim 0.8 \mu\text{m}$ (*I* band). Taken from Bok (1977), figure 4.



cm^{-3} . The most famous member of this class is the Orion GMC, in which both low and high mass star formation is occurring.

1.3 Star Formation

Three pieces of evidence support the argument that star formation is an ongoing process within the Galaxy (Bowers and Deeming, 1984). There exist in the current epoch massive, luminous stars (e.g., OB stars) with short main-sequence lifetimes of a few million years. So stars have certainly formed within the past few million years, and there is no reason to suppose that they are not continuing to do so. Further support comes from the existence of unbound stellar clusters such as the Orion association. The members of these clusters experience differing amounts of differential rotation about the centre of the Galaxy, and it can be shown that such a cluster lying at a distance from the Galactic Centre greater than about 3 kpc will have dispersed within 10^{10} years (Bowers and Deeming, 1984). These associations must therefore consist of young stars. Further indirect support for ongoing star formation is offered by the location of hot, young stars near to the interstellar molecular clouds, presumably from which they formed. It is obvious that at some stage the interstellar medium has evolved through very dense phases (i.e., stars), and the densest regions are found within the molecular clouds.

Arguments have been put forward by Herbig (1962) and Mezger and Smith (1977) that the regions of high ($M \gg M_{\odot}$) and low ($M \sim M_{\odot}$) mass star formation are spatially distinct and involve different mechanisms. Herbig noted that in the Taurus dark cloud complex there are no stars more massive than $\sim 2 M_{\odot}$, whereas in Orion there exists young stellar objects (YSOs) of both high and low mass. He surmised that low mass stars form before high mass stars and star

formation occurs within a molecular cloud over a few tens of millions of years. Mezger and Smith noted high mass stars, such as the OB stars, form in the larger molecular complexes within the spiral arms of the Galaxy. The formation of low mass stars of the T Tauri type occurs in both small and large molecular clouds distributed throughout the Galactic disk. It is therefore envisaged that high mass star formation is occurring in the more active clouds, possibly as a result of cloud collisions within the tightly packed spiral arms, while low mass star formation is a more quiescent process occurring throughout the Galactic disk.

The dense molecular clouds from which stars form may be separated into two general categories, which transgress the molecular cloud regions defined in section 1.2 above. The earliest schemes (e.g., Turner, 1978) divided the clouds based on their mass, the dividing line being $\sim 10^3 M_{\odot}$. This may seem rather arbitrary, but this mass does appear to delimit regions of low and high mass star forming regions, with high mass star formation requiring a cloud mass greater than this value to proceed. More recently the clouds have been grouped according to gas kinetic temperature (Evans, 1978; Solomon *et al.*, 1985). Evans classified those clouds which have temperatures less than 20 K throughout as Group A, and those where the temperature rises above 20 K somewhere within the cloud as Group B. The Group A clouds have an almost one to one correspondence with the small molecular clouds defined by Turner (1978). The Group B clouds contain the hot cores from which high mass stars are thought to form, and there is a similar correspondence between the Group B clouds and the GMCs. Solomon *et al.* placed their dividing line at 10 K, although more recent results would suggest a temperature of 15 K as a more definitive separator (e.g., Benson and Myers, 1989). The warm clouds are in general more massive, spatially larger, and exhibit signposts characteristic of massive star formation,

such as visible nebulae (HII regions) and radio continuum emission, compact HII regions and associated maser activity (Evans, 1981; Churchwell, 1991; Kylafis, 1991) and strong infrared emission (Evans, 1981).

The signposts of low mass star formation are more subtle than those of high mass star formation. We know that high mass stars are born within molecular clouds, as shown by the association of the hot, luminous O and B stars with nearby dark clouds and the more distant molecular clouds seen in CO emission. It was thus natural that the first search for young, low mass stars should be directed toward the nearby dark cloud complexes. T Tauri stars were first recognized as a distinct class of objects through the pioneering work of Joy in the 1940s (Joy, 1945, 1949), who searched for stars exhibiting strong H α emission in the direction of the Taurus–Auriga dark cloud complex. T Tauri stars are named after the brightest member of their class identified by Joy. These T Tauri stars were quickly recognized as being low mass young stars (Herbig, 1962), born within the dark clouds with which they are associated spatially and kinematically (Herbig, 1977). T Tauri stars exhibit a number of unusual features which suggest they are young and of low mass (see e.g., Rydgren *et al.*, 1976; Bertout, 1989):

- i) Variability. All T Tauri stars are irregularly variable at optical wavelengths (Herbig, 1962), and some are reported variable in the near-infrared (Mendoza, 1966, 1968). This is probably due to different temperatures present on their photospheres (i.e., star-spots).
- ii) Emission lines. T Tauri stars display prominent emission lines, notably those of the Balmer series, Fe II and Ca II, superimposed on a relatively cool (~ 4000 K) photosphere, similar to the chromospheric spectrum of the Sun.

- iii) Veiling. Joy (1949) noted that the ultraviolet and B spectral regions of many T Tauri stars are “veiled” by an apparent overlying continuous emission arising from non-photospheric regions in T Tauri atmospheres.
- iv) Broad absorption lines. T Tauri stars exhibit exceptionally broad and shallow photospheric absorption lines (Herbig, 1957). This phenomena was originally interpreted as indicating rapid stellar rotation which we now know is not the case.
- v) P Cygni Profiles. Many T Tauri stars display P Cygni profiles in their strongest emission lines which are taken as evidence of outflow of matter. Mass loss rates of the order of 10^{-7} to $10^{-9} M_{\odot} \text{ yr}^{-1}$ have been inferred (Kuhi, 1964). Inverse P Cygni profiles are seen in a few T Tauri stars (Walker, 1972), indicating possible mass infall.
- vi) Infrared excess. The spectral energy distributions (SEDs) of many T Tauri stars display excess near-infrared radiation (Mendoza, 1966, 1968). Mendoza suggested that this excess arises from circumstellar dust grains.

The high lithium abundances observed in T Tauri stars (Bonsack and Greenstein, 1960) is cited as further evidence for their young nature, since lithium is quickly destroyed by stellar nuclear reactions when a star reaches the main sequence (Herbig, 1962).

Cohen and Kuhi (1979) surveyed ~ 500 $H\alpha$ emission stars, mainly in Taurus–Auriga, to determine their bolometric luminosities and effective temperatures, enabling them to be placed on the Hertzsprung-Russell (HR) diagram. Their results show that T Tauri stars lie on convective tracks in the HR diagram, as predicted by the classical pre-main-sequence theory of Hayashi *et al.* (1962; see also Hayashi, 1966 for a review), and their distribution does not correspond to any dynamical evolutionary tracks (see e.g., Larson, 1969). Radii and masses

inferred from the HR diagram lie between 1 and 5 R_{\odot} and 0.2 and 3.0 M_{\odot} respectively. The inferred age of T Tauri stars range from 10^4 to 10^7 years, based on their position in the HR diagram.

Shu *et al.* (1987) have suggested that the observed activity of the T Tauri stars may simply be a result of their continual adjustment to the transfer of material around them into their stellar environments. Cohen and Kuhi (1979) noted that the correlation of emission line strength with bolometric luminosity is suggestive of a decrease in stellar activity with increasing age. Other properties, such as their unpredictable variability and infrared excess, also show a decrease with age, adding support to the above suggestions.

T Tauri stars thus represent a late stage of low mass pre-main-sequence stellar evolution. The evolutionary state of the most deeply embedded YSOs are much harder to determine, since they are not visible at optical wavelengths and their luminosities and temperatures cannot be measured directly. Lada (1987) defined a spectral index α such that:

$$\alpha = -\frac{d \log(\nu F_{\nu})}{d \log \nu}$$

for wavelengths longer than 2.2 μm , where ν is the frequency and F_{ν} the flux at that frequency. When the SEDs of YSOs are classified by this spectral index then most fall into three distinct morphological classes (see also Adams *et al.*, 1987). This classification scheme is illustrated in figure 1.2 (from Lada, 1991).

The three classes may be summarized as follows:

1. Class I : SEDs are broader than a single blackbody with positive α . These sources are often identified with protostars, i.e., they are deriving the bulk of their energy from the accretion of circumstellar matter.
2. Class II : SEDs which are also broader than a single blackbody, but have

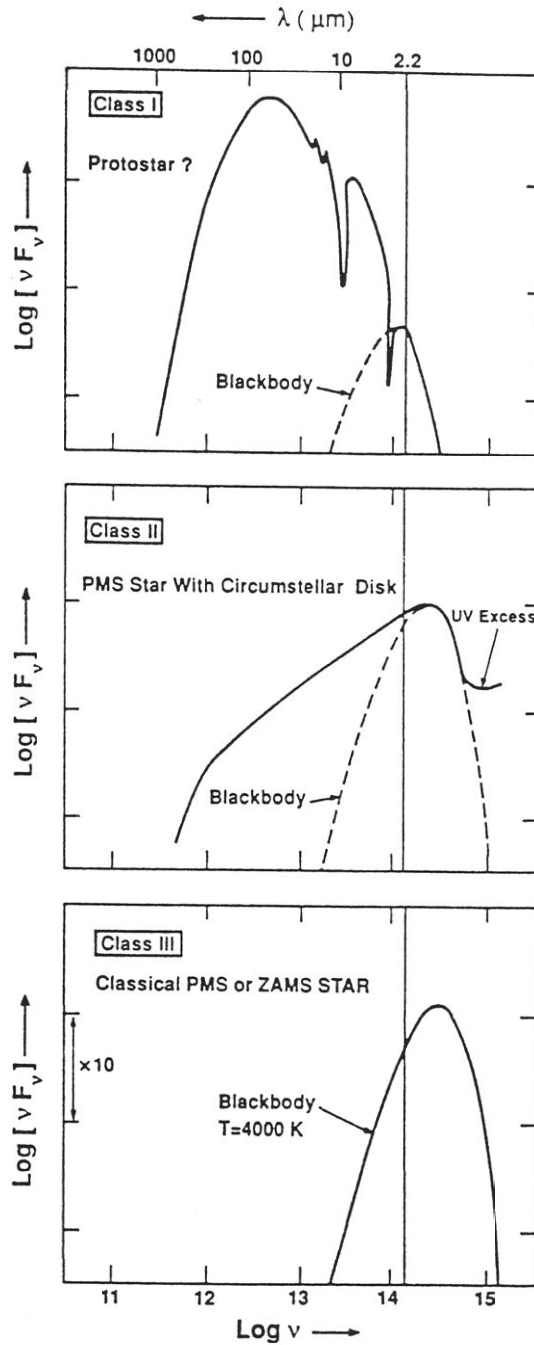


Figure 1.2: Classification scheme for spectral energy distributions of young stellar objects. This figure is from Lada, 1991, figure 4.

values of α which are negative.

3. Class III : SEDs characterized by negative values of α , but widths which are comparable to single blackbody functions.

The class I sources are usually deeply embedded within the molecular clouds, their steep spectral indices resulting from the presence of large amounts of circumstellar dust (see review by Lada, 1991). The class II sources are almost always visible optically as well as in the infrared. Almost all class II sources can be identified with known T Tauri stars (see e.g., Rucinski, 1985). Class II sources are surrounded by far less circumstellar matter than the class I objects. Class III objects are usually optically visible with little or no emission in the near- and mid-infrared. This class includes both young main sequence stars and pre-main-sequence stars, such as the “naked” T Tauri stars (Walter, 1987). Some YSOs cannot be distinctly placed in any of these three classes, not being defined by a single value of α . They may usually be identified as a sub-class of one of the three main classes (Lada, 1991). In fact, a continuous variation in SED shape is observed through the class I to class III sources, which is suggestive of an evolutionary sequence for YSOs based on their SEDs (Lada, 1987).

Myers *et al.* (1987) attempted to model a number of class I sources using circumstellar dust shells, with only limited success. Their best model fits indicated that a class I stellar source is surrounded by a cavity 10 – 100 AU in extent. They were unable to reproduce the mid-infrared (5 – 20 μm) spectral range with their models, an excess of radiation being observed. Radiation in the mid-infrared implies dust temperatures in the range 150 – 300 K, which in turn implies that dust must exist within the cavity region, though in a non-spherically symmetric distribution. Adams *et al.* (1987), have successfully modelled class I SEDs by the addition of a rotating accretion disk within the cavity. Shu *et al.*

(1987) have presented one self-consistent model for the collapse of a molecular cloud core to form a star which is able to successfully reproduce the SEDs of the class I – III objects (see also Adams *et al.*, 1987). In their scenario, the first stage of star formation is the formation of a slowly rotating cloud core, which forms through slow ambipolar diffusion. In the second stage the cloud core becomes gravitationally unstable and undergoes dynamical “inside-out” collapse, resulting in a central protostar with disk embedded within an infalling envelope of dust and gas. The model SEDs for this stage fit very well the observed SEDs of class I sources. Stage three begins with the onset of deuterium burning and convection, resulting in a stellar wind which emerges through the channels of least resistance, i.e., the rotational poles, leading to the observed collimated jets and bipolar outflows. In stage four the stellar wind opening angle gradually increases to sweep away the circumstellar shell and reveal the low-mass YSO (i.e., a T Tauri star) with a disk. Lynden-Bell and Pringle (1974) predicted successfully the observed SEDs of T Tauri stars by surrounding them with a luminous accretion disk, while passive disks (Adams and Shu, 1986) have also been successful in reproducing the SEDs of T Tauri stars.

1.4 Previous Studies of Dark Clouds

1.4.1 Optical Surveys

The first optical surveys for dark clouds were made by Barnard (1919, 1927), based on his own photographic survey of the Milky Way. The major optical surveys which have formed the basis for studies of dark clouds over the past twenty years are those of Lynds (1962), Sandqvist (1977) and more recently Hartley *et al.* (1986), although many objects are still referred to by their Barnard

designation through the early work of Bok and co-workers (Bok and Reilly, 1947; Bok and Cordwell, 1971; Bok and McCarthy, 1974). Lynds made a complete survey of dark clouds north of -33° using the Palomar Observatory Sky Survey (POSS). Her survey lists the coordinates, surface area and visual estimates of the opacity (on a scale of 1 to 6, 6 being the most opaque) for 1802 clouds, most being areas of enhanced visual extinction within larger cloud complexes. A large number of quoted positions in the Lynds catalogue have been found over the years to be inaccurate (see e.g., Parker, 1989). Parker (1989) has remeasured the positions of all class 6 clouds from the Lynds list.

The Lynds catalogue has been the workhorse of studies of dark clouds in the north. The first substantial list of dark clouds south of declination -33° was published by Sandqvist and Lindroos (1976) and Sandqvist (1977), who used the Whiteoak extension of the Palomar survey and the European Southern Observatory (ESO) Schmidt survey plates for their list. These lists included some 136 clouds of Lynds opacity 4 – 6, although in each case plates for only one waveband were used for the estimate, unlike Lynds who used both red and blue plates. Feitzinger and Stüwe (1984) published a list of southern dark clouds between the galactic longitudes 240° and 360° based on the ESO survey and the United Kingdom Schmidt Telescope Survey (hereinafter the SERC survey). They also estimated the visual opacities of all the 489 dark clouds and 331 globules in their list. The major catalogue of southern dark clouds was compiled by Hartley and co-workers (Hartley *et al.*, 1986), and represents a complete survey of the sky at declinations south of -33° . Their catalogue of 1101 clouds was compiled from visual inspections of the ESO/SERC Southern J survey plates (blue plates) as a direct complement to the Lynds catalogue. They listed both galactic and equatorial positions for all clouds, with estimates of the cloud's size (major axis \times minor axis) and opacity. A three level opacity scheme (class

A being the most dense) was used as it was not felt a division into six classes was appropriate based on observations with plates of only one waveband. Apart from its more extensive coverage, the Hartley catalogue is preferred to that of Feitzinger and Stüwe as its positions appear to be more accurate (Hartley *et al.*, 1986), and attempts to identify globules within complexes and not just identify the complex.

Hyland *et al.* (1993) have pointed out some shortcomings in the use of these catalogues as the basis of surveys of isolated dark clouds at other wavelengths, particularly the smaller clouds. These include:

- i) the bias of dark clouds from these surveys towards small distances, because the surveys are photographic (at optical wavelengths), and only nearby dark clouds can easily be picked out. At larger distances the smaller angular sizes of the clouds are such that the globule structure may be masked by foreground stars;
- ii) the suspect nature of the opacity data in many cases. The dimensions and opacity data often refer to the extensions to a well formed globule (rather than the globule itself), and therefore give the wrong impression of its structure;
- iii) imprecise catalogued positions, and catalogued positions which do not necessarily refer to the most opaque portion of the cloud;
- iv) the omission of many smaller dark clouds.

Visual inspection of the original survey plates is therefore required when compiling new lists with selection criteria which are more strict than was used in compiling the original more general catalogues described above. Many researchers have found this to be the case, not being able to rely solely on the published

catalogue data to determine their list of objects for study (see e.g., Clemens and Barvainis, 1988; Parker, 1989; Benson and Myers, 1989).

1.4.2 Molecular Line Surveys

The importance of molecular spectroscopy to our understanding of the physical conditions within dark clouds cannot be understated. The bulk of our knowledge of the physical conditions within dark clouds has come from radio and submillimetre observations of rotational transitions of a wide variety of molecules. As indicated earlier, H_2 is not directly observable at the temperatures found in molecular clouds, and so we have had to rely on a number of tracer molecules to derive our information on the physical conditions within molecular clouds. The most popular of these have been CO, NH_3 , H_2CO , and CS. Below are described some of the larger surveys of dark clouds that have been performed.

Carbon Monoxide Surveys

Observations of the submillimetre rotational transitions of CO and its isotopes, in particular the $J = 1 \rightarrow 0$ and $J = 2 \rightarrow 1$ transitions at 115 GHz and 230 GHz respectively, have been most important in expanding our knowledge of the physical conditions within molecular clouds. The ^{12}CO $J = 1 \rightarrow 0$ transition is almost universally optically thick and therefore fully thermalised, so measurement of the ^{12}CO intensity leads directly to an estimation of the gas kinetic temperature toward the cloud. Dickman (1975, 1978) used this knowledge to determine the kinetic temperature toward a sample of 68 dark clouds, finding $T_K = 8 - 15$ K. He also determined a relationship between the observed CO column density and H_2 density toward dark clouds, by comparing his CO column densities with H_2 densities determined by other means. In the years since, this relationship

has been confirmed, extended and used extensively to infer H_2 densities of dark clouds (see e.g., Scoville and Sanders, 1987).

The major CO surveys of dark clouds have concentrated on the northern sky, due to the lack of suitable receivers in the Southern Hemisphere. Myers *et al.* (1983) surveyed 90 opaque regions selected from the Lynds catalogue through visual inspection of the POSS plates, to determine the positions of maximum visual opacity. This resulted in some cases in the surveyed positions differing from the Lynds positions. They observed the $J = 1 \rightarrow 0$ transitions of C^{18}O and ^{13}CO , with a sensitivity sufficient to detect essentially every cloud observed, and a resolution fine enough to observe line shape asymmetries. The prime objective of their survey was to determine the CO column density toward a large sample of dark clouds, with many of their clouds lying within the Taurus and Ophiuchus dark cloud complexes. Typically they infer from the C^{18}O emission cloud sizes of ~ 0.3 pc, $A_V \sim 11$ mag., $M \sim 30 M_\odot$, $\Delta v \sim 0.6$ km s $^{-1}$, $T_{\text{ex}} \sim 10$ K and $N(\text{CO}) \sim 2 \times 10^{15}$ cm $^{-2}$. These numbers imply column densities of $N(\text{H}_2) \sim 10^{22}$ cm $^{-2}$. The dynamical nature of the clouds is not clear from these results. If the total line width results from turbulent motion then the data is consistent with stable equilibrium, while if turbulent motions make up only part of the width then the data is consistent with gravitational contraction.

One other major survey of CO emission from dark clouds has been performed by Clemens and Barvainis (1988) and Clemens *et al.* (1991). From the POSS survey they compiled a catalogue of 248 small dark clouds with declinations between $+90^\circ$ and -36° (angular size $< 10'$, mean size $4'$) which are reasonably well isolated and centrally opaque. Concern about the lack of smaller clouds in the Lynds catalogue lead them to conduct their own survey of the POSS prints for clouds fulfilling their selection criteria. Of the resulting list of 248 clouds, $\sim 30\%$ had not previously been catalogued. Their search list was observed in the

$^{12}\text{CO } J = 1 \rightarrow 0$ line. From these observations they found, for the majority of the clouds, $T_K \sim 8.5$ K and $M \sim 11 M_\odot$. When plotting CO temperature against linewidth, they identified three subgroups within the sample. One subgroup exhibits warm and narrow lines, another cool and wide lines. The majority (74%) fall into the third category which have $T_{line} \sim 4.5$ K and $\Delta v \sim 1 - 1.5 \text{ km s}^{-1}$, indicating that the majority of the clouds are cool and quiescent. Supplementing their work with data from the Infrared Astronomical Satellite (*IRAS*) Point Source Catalogue, they found no correlation between the dust and gas properties of the clouds, suggesting that they are poorly coupled, if at all.

Yun and Clemens (1992) performed follow-up observations of 41 of the globules from Clemens and Barvainis (1988), of which 36 contain *IRAS* point sources. Molecular outflows were found toward 14 of the 36 *IRAS* associated globules. They found that the outflows seem to be associated with the youngest *IRAS* sources, as indicated by their spectral index between 12 and 25 μm . Five of the globules show evidence for rotation.

There has been only a limited amount of work performed on dark clouds south of -33° , due to a lack of suitable instrumentation, as mentioned above. de Vries *et al.* (1984) observed ~ 80 dark clouds in the $J = 2 \rightarrow 1$ line of ^{12}CO , with a detection rate of 50%. They were not using instruments designed specifically for submillimetre work – in fact they used a suite of ESO optical telescopes, modified to allow limited submillimetre observations. The resulting beam sizes were often larger than the clouds they were observing, resulting in many their observations suffering badly from beam dilution. They did however map seven sources with $1.9'$ resolution, finding five of them to have signs of mass outflows. They also found that clouds associated with nebulosity have greater line widths, which they conclude probably indicates the existence of internal heating sources.

Nyman *et al.* (1989) performed a CO survey of the Coalsack with $8.8'$ resolu-

tion. Although we are concerned here with the smaller isolated dark clouds, the situation in the Coalsack appears unique among the larger dark cloud complexes. Unlike other large complexes, i.e. the ρ Ophiuchus dark cloud, the Coalsack appears on smaller scales to consist of a series of fragmented clouds and globules rather than as one relatively large, connected cloud. At present there are no indications that star formation is taking place within the Coalsack, in contrast to most other dark cloud complexes. Their survey covered 26.5 square degrees, showing the Coalsack to be complex in structure, with numerous clumps and velocity components. An interesting result to emerge is that the densest globules within the Coalsack cannot be distinguished in CO emission, either because the CO is optically thick in the surrounding gas, or because the beam size is greater than the globule size ($< 6'$), and so only the surrounding gas is being probed.

Other studies of small dark clouds in CO have concentrated on only a small number of clouds and so are not described here, except to note that the general properties found in these smaller studies are the same as for the large surveys (see e.g., Martin and Barrett, 1978; Snell, 1981).

With the advent of the Swedish-ESO Submillimetre Telescope (SEST), CO observations of southern dark clouds at sub-arcminute resolution is now possible. Various researchers at ESO (e.g., see Henkel, 1989) have begun observing the cometary globules associated with the Gum nebula (e.g., Harju *et al.*, 1990), and have detected a CO outflow associated with the Herbig-Haro objects HH 46/47 in the globule DC 267.4-7.5 (Olberg *et al.*, 1992). However, to date most CO observations of southern sources with SEST have concentrated on large cloud complexes, i.e., R Coronae Australis (Harju *et al.*, 1993).

Formaldehyde Surveys

Formaldehyde (H_2CO) was the first molecule to be used as a tracer of high density gas [$n(\text{H}_2) > 10^4 \text{ cm}^{-3}$] in interstellar space. Densities this high cannot easily be probed by the CO molecule. Unlike most other molecules, H_2CO is almost always seen in absorption in its lowest rotational levels. Palmer *et al.* (1969) first observed the $1_{10} \rightarrow 1_{11}$ rotational transition at 4830 MHz ($\sim 6 \text{ cm}$) against the cosmic background radiation. For this phenomena to occur, the excitation temperature of the 6 cm line must be less than the cosmic background temperature of 2.7 K. Since this excitation temperature is far less than the inferred kinetic temperature for dark clouds, it appears that some non-equilibrium process is causing the excitation of this transition.

The first major survey of dark clouds in the 6 cm transition of H_2CO was reported by Dieter (1973), who searched for H_2CO absorption toward 381 clouds selected from the Lynds catalogue. All clouds of opacity class 5 and 6 with angular sizes greater than the antenna beamwidth of $10'$ were searched, as well as some clouds with smaller sizes and a selection of clouds from other opacity classes. Of the 322 large clouds observed, 109 showed detectable H_2CO absorption, with the maximum depth of the H_2CO line being strongly correlated with the position of greatest visual opacity within the clouds. The narrow line widths seen with high density gas tracers toward dark clouds were first revealed by this survey.

Two other large H_2CO surveys of dark clouds at 6 cm have been performed, both concentrating on clouds in the south. Sandqvist and Lindroos (1976) compiled a list of 42 southern dark clouds of high visual opacity from the Whiteoak extension to the POSS survey. Formaldehyde absorption was observed toward 33 of these clouds, and analysis of the hyperfine structure was performed on 27

of these. Compared to the survey of Dieter, Sandqvist and Lindroos found for their sample greater optical depths and even narrower lines. This is most likely to be a result of restricting their observations to the highest opacity clouds.

Goss *et al.* (1980) surveyed 226 positions of high opacity selected from the preliminary version of the Hartley catalogue, using the Parkes 64 metre radio telescope with a beamwidth of $4.4'$, the smallest used to date in H_2CO work at 6 cm. Absorption was detected toward 169 of the clouds ($\sim 75\%$), and extended observations made of 12 of the sources for analysis of the hyperfine structure. As with the earlier surveys a strong correlation between the observed line depth and the visual opacity of the clouds was found.

Rickard *et al.* (1977) observed 7 isolated globules in H_2CO absorption, and found their derived parameters to be similar to those of larger dark clouds. The absorption was found to be localized to the globules. The analysis indicated that the densities of the globules are $\lesssim 10^5 \text{ cm}^{-3}$, with line widths consistent with equilibrium conditions.

The analysis of H_2CO absorption observations have in general been limited to the derivation of excitation temperatures and optical depths. However, more important quantities such as the kinetic temperature and density are not reported. This is a result of the wide spacing of H_2CO rotational transitions within the radio waveband, making it difficult to use the assumption of a common excitation mechanism in the comparison of the different lines observed. The two easily accessible transitions of H_2CO occur at 6 cm and 2 cm, both appearing in absorption. This is not the case with NH_3 and CS, which have either transitions close together in frequency from the one isotope (NH_3) or different isotopes with closely spaced transitions (CS). For density studies CS has become the favoured probe over the past decade, since its simple linear structure allows easier calculation of rate constants than does H_2CO , and available beam sizes

in the submillimetre waveband (where the most commonly observed CS transitions occur) are an order of magnitude smaller than those in the centimetre region. However, recent investigations of the possible use of H₂CO as a probe of temperature and density in the millimetre and submillimetre wavebands, where H₂CO is seen in emission, have been made by Magnum and Wootten (1993, and references therein). They investigated a number of transitions between 211 and 365 GHz, which may be used together with large velocity gradient models to determine kinetic temperatures and densities over a wide range of physical conditions. They claim that H₂CO is the most unbiased and potentially accurate probe of temperature and density in the interstellar medium.

Ammonia Surveys

Densities greater than 10^3 cm^{-3} are required to excite the $(J,K) = (1,1)$ rotation inversion transition of ammonia to observable strength in dark clouds at a temperature of 10 K (Ho and Townes, 1983). These inversion doublets are further split by hyperfine interactions, allowing the optical depth for the transition to be deduced directly from the observed ratios of the hyperfine components. Thus the usual problem of determining optical depths, that of determining isotopic ratios, is circumvented. Analysis of the formaldehyde spectrum at 6 cm suffers from the closeness of its hyperfine components in frequency, requiring good signal to noise data for accurate determination of its optical depth. This is not a problem with ammonia. Although ammonia is used widely as a tracer of high density gas, its most important property is its sensitivity as a thermometer (Walmsley and Ungerechts, 1983; Danby *et al.*, 1988). Ammonia possesses many transitions situated close together in frequency, but requiring different excitation mechanisms. The relative populations of the different metastable ($J = K$) levels are thought to be determined primarily by collisional processes. By comparing

the population distribution within these levels as a function of excitation with that predicted by the Boltzmann law, an estimate of the kinetic temperature may be determined. The properties of the ammonia molecule are discussed in more detail in the appendix.

The first major survey of dark clouds for ammonia emission was undertaken by Myers and Benson during the 1980s (Myers and Benson, 1983; Benson and Myers, 1989). They searched 144 dark cloud positions, chosen mainly from the Lynds catalogue, for $(J,K) = (1,1)$ emission. Their search list evolved over time from the lists of Lynds (1962), Bernes (1977) and Schneider and Elmegreen (1979). This resulted in a non-systematic list, with the main selection criteria being that the clouds should be of Lynds opacity classes 5 and 6 and have a galactic latitude $|b| \leq 10^\circ$. In all $\sim 50\%$ of clouds were detected, with the detections well correlated with positions of high visual opacity. Myers and Benson (1983) refer to the positions of NH_3 detection as “dense cores”. This terminology is now in common use and will be used throughout this thesis. Forty-one of the strongest sources detected were mapped, and observations of the $(2,2)$ transition attempted, to allow the determination of density and temperature. These dense cores have $T_K \sim 10 - 15$ K, $n(\text{H}_2) \sim 2 \times 10^3 - 2 \times 10^5 \text{ cm}^{-3}$ and $\Delta v \sim 0.2 - 0.9 \text{ km s}^{-1}$, with masses of the order of a few $\times M_\odot$. Most of the cores mapped are not spherical in shape, suggesting that there are significant forces other than random forces and self-gravity are present. Benson and Myers (1989) found that $\sim 70\%$ of the strong ammonia detections are associated with *IRAS* sources. This suggests to them that cores without infrared sources are in the process of forming stars, while those with infrared sources have already done so. Cores with *IRAS* sources were found to be larger and have broader lines than those cores without sources. No statistical differences in shape, temperature or density in cores with and without *IRAS* sources were found. No significant differences were

found between globules and condensations within cores, in agreement with the work of Rickard (1977), but only a few globules were studied.

A small survey of 29 dark clouds was performed by Ho, Martin and Barrett (1978), with NH_3 being detected from 12 sources. Temperatures around 10 K, densities $> 5 \times 10^3 \text{ cm}^{-3}$ and line widths $\sim 0.35 \text{ km s}^{-1}$ were derived from the observed spectra, consistent with the later large survey of Benson and Myers (1989).

No large surveys of Bok globules for NH_3 emission have previously been performed, though individual globules have been observed in NH_3 (see e.g., Martin and Barrett, 1978; Menten *et al.*, 1984; Benson and Myers, 1989).

1.4.3 Infrared Surveys

Infrared surveys have proved important in our study of dark clouds within the past 15 years. Near-infrared ground based surveys, generally restricted to the 1 – 5 μm region, have been extremely valuable in identifying low luminosity young stellar objects such as T Tauri stars and embedded protostellar objects, which are hidden within the dense molecular clouds, rendering them invisible at optical wavelengths. The majority of surveys have been aimed at identifying objects located within the dark clouds, discriminating them from background field stars on the basis of their near-infrared colours, since YSOs are known to possess an infrared excess. The probability of an object with a near-infrared excess lying in the direction of a dark cloud but not being associated with it is very small. These surveys have concentrated on the large dark cloud complexes, where the likelihood of finding a number of embedded sources is enhanced, enabling different evolutionary stages within the one cloud to be probed, and as a result surveys of the smaller isolated clouds in the near-infrared are rare. The best

studied of these complexes are those in Ophiuchus (see e.g., Wilking, 1991) and Chamaeleon (see e.g., Schwartz, 1991), where numerous YSOs have been identified on the basis of their infrared emission alone.

Far-infrared observations ($\lambda > 35 \mu\text{m}$) are able to probe directly the dust within dark clouds. Dust grains are heated by absorption of starlight in the ultraviolet and visible, where their absorption cross-sections are high, and cooled by the emission of thermal radiation in the infrared. Interstellar radiation in the far-infrared peaks at $\sim 100 \mu\text{m}$, and is dominated by thermal radiation from interstellar dust grains in the temperature range 15 – 30 K. Far-infrared observations of dark clouds have, however, been limited due to a lack of suitable instrumentation. Until recently only the NASA Kuiper Airborne Observatory (KAO) has been able to successfully probe this spectral region on a regular basis.

In 1983 the Infrared Astronomical Satellite (*IRAS*) was launched to survey the whole sky at wavelengths 12 μm , 25 μm , 60 μm , and 100 μm , with a sensitivity sufficient to detect young, cool, star forming cores within dark clouds. However, *IRAS* did not target dark clouds specifically, but as mentioned above performed an all sky survey. The resulting Point Source Catalogue (PSC) contains over 250,000 entries, including many candidate YSOs. Sources with fluxes increasing toward the longer wavelengths are identified as the most likely YSO candidates, but as many authors have pointed out *IRAS* data alone is insufficient to discriminate YSOs from other objects. We shall see below that the *IRAS* database has been used extensively to search for possible young embedded sources in dark clouds.

Only one unbiased survey of dense cores in dark clouds has been performed in the near-infrared, although various isolated dark clouds have been studied individually by different authors to search for YSOs. Benson *et al.* (1984) surveyed 25 dense cores identified by Myers and Benson (1983) for associated embedded

stars at K ($2.2 \mu\text{m}$). They found 5 stars to the limit of the survey ($K = 10.5$), with three of the stars associated with cores and optically invisible. In most cases they found the infrared source position and dense core peak position to coincide, with the infrared source being visible in two cases as indicated above. Follow-up photometry at J ($1.25 \mu\text{m}$), H ($1.65 \mu\text{m}$), K ($2.2 \mu\text{m}$), L ($3.45 \mu\text{m}$) and M ($4.75 \mu\text{m}$) and circular variable filter (CVF) spectroscopy between 2.0 and $2.5 \mu\text{m}$ was performed on these sources. All three sources were detected by *IRAS*, with spectra available for two of them. The complete $2 - 100 \mu\text{m}$ spectrum for two sources were compared with those of well studied pre-main-sequence (PMS) objects of low luminosity and low mass. The spectral shape and luminosity were found to be very similar to that of HL Tau, which is one of the youngest T Tauri stars known. Many of the cores in the Myers and Benson (1983) sample are found in the Taurus and Ophiuchus dark cloud regions, but Benson *et al.* do not list the clouds they searched, so it is not clear whether they included both isolated clouds and cores within complexes in their infrared search.

In the far-infrared only one small survey has been conducted to study isolated dark clouds (not including studies undertaken with the *IRAS* database). Keene (1981) studied nine globules with the KAO, finding a remarkable uniformity in their emission, which argues against any dominant internal heating sources, instead pointing towards the interstellar radiation field (ISRF) as the dominant heating source. Her observed spectra peak at $\sim 225 \mu\text{m}$, and the spectra are well fitted by blackbodies with temperatures in the range $13 - 16 \text{ K}$, implying dust temperatures slightly higher than the observed gas temperatures ($8 - 10 \text{ K}$). It was later found that one globule observed by Keene, B335, does have an internal heating source in the form of a compact far-infrared object (Keene *et al.*, 1983). The surface brightness of B335 quoted in her 1981 paper is twice that quoted for the other globules, providing an important pointer to the effect such a compact

source has on the far-infrared emission from a globule.

Emerson (1987) attempted to select a candidate group of protostellar objects lying within the boundaries of southern dark clouds from the *IRAS* PSC, based on a comparison of the *IRAS* colours of known objects with *IRAS* sources found toward dark clouds. He constructed *IRAS* colour-colour plots for objects of known type and used the densest clustering of each object type in colour-colour space to define the colour regions occupied by the different objects. Of particular interest to the current work are the regions occupied by T Tauri stars and embedded cores. The cores region is based on a sample of *IRAS* objects found associated with dense cores by Beichman *et al.* (1986; see below), and the T Tauri region on a sample of 338 T Tauri stars (Emerson, 1987). There exists an overlap between these two regions. Emerson searched the Hartley catalogue for *IRAS* sources lying within a radius equal to the cloud's minor axis, restricting his search to the 1055 clouds not defined as complexes by Hartley. This search yielded 1099 possible sources associated with 436 of the clouds. Of these, a total of 247 *IRAS* sources have colours of embedded sources. If the majority of these embedded sources are in fact field stars, then we would expect an even distribution of them, in projection, over the cloud area. This is not observed; in fact the number decreases with distance from the cloud centre, implying they are most likely physically associated with the clouds. Emerson concludes that there is no evidence in this data to suggest that low mass star formation in dark clouds is externally triggered.

Beichman *et al.* (1986) searched the *IRAS* PSC for sources lying toward 95 dense cores, mostly selected from the lists of Benson and Myers (1983) and Benson (1983). For inclusion in their study, the *IRAS* sources had to be within 6' of the molecular line peak (CO or NH₃) and be detected at either 25 μm or at both 60 μm and 100 μm . Almost half the clouds have *IRAS* sources associated

with them based on this selection criteria. Over half of these sources have no visible counterparts, while most of the visible sources can be identified with known T Tauri stars, or have infrared properties similar to those stars. On the basis of statistical arguments they claim that as many as one-third of these invisible sources may be protostars. The cores (i.e., the invisible sources) were found to occupy a well defined region on colour-colour plots, with a broad range of temperatures inferred from the *IRAS* colours. This large range of temperature is consistent with dominant heating from an internal source and not from the ISRF (Leung, 1985; Beichman *et al.*, 1986).

Myers *et al.* (1987) followed up the work of Beichman *et al.* (1986) by undertaking photometry from 0.4 to 20 μm for 34 sources from Beichman *et al.*, of which approximately half of the sources are optically invisible (and so photometry for wavelengths longer than J only are reported). Their results show that nearly all of the *IRAS* sources examined are reddened stars with flux increasing with wavelength. The sources with the steepest slopes are generally optically invisible and located within the dense cores, with visual extinctions $A_V > 30$ magnitudes implied. Modelling of the spectral energy distributions of typical sources show that a circumstellar disk of size 10 – 100 AU is required to produce the observed mid-infrared (5 – 30 μm) excess seen over the spherically symmetric dust shell models.

Parker (1989) searched all the Lynds opacity class 6 clouds for associated *IRAS* sources, with the criteria that the sources must lie within the optical cloud boundary and satisfy the flux criteria $S_{100} > S_{25}$, in an attempt to discriminate against stars. Out of a total of 147 clouds, 136 *IRAS* sources were detected toward 73 clouds. However, only 24 of these sources had detections of sufficient quality in three adjacent *IRAS* wavebands to be studied in detail. The inadequacies of using *IRAS* data alone in selecting embedded protostel-

lar objects is highlighted by Parker’s observation that of 12 sources with *IRAS* colours characteristic of embedded cores, 4 have visible counterparts. Clearly candidate YSOs selected on the basis of *IRAS* data require further investigation to determine their true nature.

Clemens and Barvainis (1988; hereinafter CB) searched the *IRAS* PSC for sources associated with their catalogue of 248 small dark clouds. They found 346 possible associations with 149 clouds. Their search included a wide area around each cloud by defining three search regions, “core”, “envelope” and “reference”, with the core region defined to be equal to the cloud optical area, and the reference region used to estimate the likelihood that the core and envelope sources are chance associations. Of the 145 sources found in the core region, 51 are expected to be there by chance alignments. Associations in the core regions are dominated by sources with strong 60 and 100 μm detections. Applying the selection criteria of Beichman *et al.* to their sample, and comparing the 60 and 100 μm properties of the two samples, CB find that their sample is cooler and not as bright at 100 μm implying a physical difference between sources in the small isolated clouds of CB and the molecular cores of Beichman *et al.* CB show that if the *IRAS* sensitivity could be improved by a factor of three, then almost every cloud in their sample would be detected at 100 μm , whether it contains a point source or not. This is shown to be the case by Clemens *et al.* (1991) with the use of coadded *IRAS* data, which allowed the detection threshold to be lowered by a factor of three and did result in the detection of almost every cloud in their sample. Clemens *et al.* do not discriminate against the point sources, and so emission from the whole cloud, including any point sources that may be present, are included in their cloud photometry. The average far-infrared luminosity of the CB clouds derived from the coadded data is equal to that expected if the ISRF is fully thermalised by the globules, i.e., it is their predominant heating

source. Globules which differ significantly from this average must not be in thermal equilibrium, most likely due to the presence of an internal heating source. Clemens *et al.* observe a wide range of dust temperatures for the globules, which may be interpreted as a signpost of internal heating or of different sized dust grains within the globule.

Persi *et al.* (1990) used the PSC to search 482 southern dark clouds for evidence of YSOs. From the Hartley catalogue they chose clouds with small angular dimensions ($< 64 \text{ arcmin}^2$) or with associated nebulosities. *IRAS* sources were detected in 190 dark clouds, with 19% of these sources being detected in three to four adjacent wavebands (91 sources). From this a subsample of 53 sources with $S_{100} > S_{60} > S_{25}$, where S_i is the flux at wavelength i , were selected for further study. Forty of this subsample have *IRAS* colours typical of YSOs (i.e., T Tauri stars and embedded cores). Follow-up near-infrared photometry on the subsample found 13 to have a near-infrared excess, suggesting that these sources are low-luminosity YSOs at different evolutionary stages. They also found that 4 of the sources without a near-infrared excess can be classified as pre-main-sequence stars. These 4 objects may be T Tauri stars in a late evolutionary stage.

It is clear from the above review that the majority of infrared surveys of dark clouds or molecular cores are based on the *IRAS* Point Source Catalogue. Until recently surveys in the near-infrared were restricted by the lack of detector sensitivity and spatial resolution, since most detectors consisted of only one element, which had to be scanned across the area of interest for use in “survey mode”. With the availability of new near- and mid-infrared detector array cameras in the late 1980s we can expect an increase in the number of large surveys for embedded sources within molecular clouds, as well as the determination of cloud dust distributions by observations of the reddening of background stars seen behind the cloud (see e.g., *Astrophysics with Infrared Arrays*, 1991, Astro-

nomical Society of the Pacific Conference Series Volume 14, ed. R. Elston). The first such survey of small molecular clouds (Bok globules) has been undertaken by Yun (1992), who imaged 34 globules with known *IRAS* point source associations at *J*, *H* and *K*, and found that 11 of the near-infrared counterparts of the *IRAS* sources are associated with near-infrared nebulosities. Yun found that the brightest *K* band nebulosities are associated with the youngest YSOs (as defined by their spectral index between 12 and 25 μm). Combining these results with earlier work on CO outflows (Yun and Clemens, 1992), Yun found that *K* band nebulosities are good morphological tracers of CO molecular outflows.

1.5 Isolated Dark Clouds and Bok Globules

Bok and Reilly (1947) first called attention to the class of dark cloud which have become to be known as Bok globules. They identified two types of globule; the small globules seen against a background of nebulosity or HII region, and the larger globules seen projected against the general background of stars. Bok and Reilly suggested that the large globules represent the evolutionary stage just preceding star formation. More recently, Leung (1985) identified four classes of globules based on their optical morphology; (a) elephant-trunk and speck globules, (b) cometary globules, (c) globular filaments and (d) isolated dark globules. These classes are described below.

Elephant-trunk and Speck Globules

These two types of globule are seen in projection against HII regions with which they are physically associated. Herbig (1974) suggested that the speck globules are simply fragments of the elephant-trunk globules, suggesting a possible evo-

lutionary connection between them. Recent studies by Sugitani *et al.* (1991) of ~ 50 bright rimmed globules seen against HII regions and associated with *IRAS* sources indicate that intermediate mass stars ($2 - 6 M_{\odot}$) are forming within these globules. This class of globule will not be discussed further in this thesis.

Cometary Globules

Cometary Globules (CGs) were first noted by Hawarden and Brand (1976) on Schmidt survey prints as isolated dark clouds having a compact, dusty, opaque head with a bright rim on one side and a long, faint, luminous tail on the other. Optical measurements indicate that their tail length varies from 0.2 to 7.0 pc, with head sizes in the range 0.1 – 1.0 pc and masses $< 1 M_{\odot}$ to several M_{\odot} . Most of the known CGs are located within the Vela–Gum region (Reipurth, 1983; Zealey *et al.*, 1983), having their tails directed away from a common origin located near the Vela pulsar, the energetic O star ζ Puppis and the binary star γ^2 Velorum. The favoured scenario for their formation (Reipurth, 1983) suggests that CGs formed when UV radiation from ζ Pup and γ^2 Vel caused evaporation of small clumpy molecular clouds, leaving behind the dense cores in the form of the CGs with their bright rims representing an ionisation front and the faint tails the eroded, windswept material that once surrounded the core. In this picture the CGs will eventually form isolated dark globules. Star formation is occurring in some globules (see review by Pettersson, 1991), possibly as a result of external compression. Calculations by Sandford *et al.* (1982, 1984) support this CG formation scenario.

Globular Filaments

Globular filaments are elongated dark clouds with a filamentary appearance. Many show signs of internal fragmentation or condensation along their length. Schneider and Elmegreen (1979) catalogued 23 of these filaments. They suggested the globular filaments may form when an initially uniform filament fragments and aligns with the interstellar magnetic field, followed by gravitationally induced condensation into individual globules along their length. It has been suggested that these condensations may be the precursors of the isolated globules. Figure 1.3 indicates such a possible connection between the filament Barnard 72 (B72 – the snake) and the isolated globule B68. Another example of a globular filament is the Lupus 2 dark cloud complex. The star forming properties of these filaments are uncertain (McGregor, 1992), but certainly for the Lupus 2 cloud low mass star formation is taking place (see review by Krautter, 1991).

Isolated Dark Clouds

These are the large globules first identified by Bok and Reilly from the lists of dark clouds by Barnard (1919, 1927). Early optical studies of these globules were performed almost exclusively by Bok and co-workers (Bok and Cordwell, 1971; Bok and McCarthy, 1974; Bok *et al.*, 1977; Bok, 1977, 1978). As a result this class of globule have become known as Bok globules, or sometimes large Bok globules (Bok, 1977). These dense clouds display a strikingly simple structure (usually round) with well defined sharp boundaries and sizes in the range 3' – 20' (Bok, 1977). This simple structure means the range of physical processes which may occur in these objects is likely to be small, so that even a limited study of a small number of globules may result in substantial increase in our knowledge of their properties. Their simple geometry and environment also allows the globules

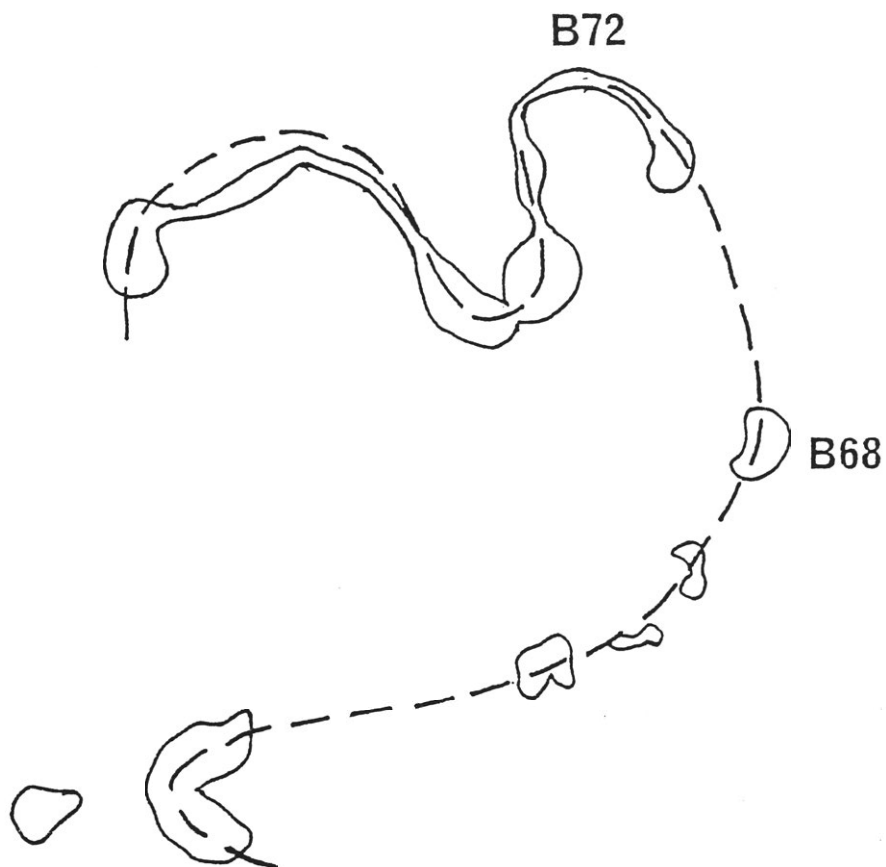


Figure 1.3: Sketch of the region around B72 and B68, showing a possible connection between the larger, filamentary dark cloud B72 and the isolated Bok globule B68. Both may have once been part of a larger filament which has fragmented due to magnetic field effects.

to be modelled in detail (see e.g., Leung, 1975, 1978; Spencer and Leung, 1978; Villere and Black, 1980; Dickman and Clemens, 1983; Krügel *et al.*, 1983; Lee and Rogers, 1987; Leung *et al.*, 1989; De Luca *et al.*, 1993). In recent years studies in the optical, infrared and radio have provided evidence that low mass star formation may occur in some globules (Bok, 1978; Clemens and Barvainis, 1988; Yun and Clemens, 1992; Bourke *et al.*, 1993). The physical properties of the smallest ($< 10'$) isolated dark globules appear similar to those of the dense cores in the dark cloud complexes (Leung, 1985; Benson and Myers, 1989), i.e., $M \sim 1 - 10 M_{\odot}$, $R \sim 0.05 - 0.2$ pc, $\log(n) \sim 4 - 5$, $T_K \sim 10$ K, and $\Delta v \sim 0.2 - 0.9$ km s $^{-1}$. The physical properties of isolated globules have been well summarized by Leung (1985). Figure 1.4 shows a schematic overview of the physical processes occurring in an isolated globule without a significant internal heat source (from Leung, 1985).

1.5.1 Properties of the Dust and Gas Components

The Dust Component

There are three methods which enable the dust component of isolated Bok globules to be probed. They are; (a) measurements in the visible of surface brightness profiles, (b) observations in the visible and near-infrared of the reddening of background stars, and (c) observations of the far-infrared dust emission (Leung, 1985).

It is observed that many globules have a visible surface brightness which increases with distance from the globule centre, exhibiting bright rims with dark cores (Lynds, 1968; FitzGerald *et al.*, 1976; Dickman and Clemens, 1983). This phenomena is thought to be due to strong anisotropic scattering of starlight by

the dust (Leung, 1985).

Various star counting techniques in the visible have been used to determine the dust opacity and distribution within Bok globules (see e.g., Bok and Cordwell, 1971). Studies by various workers (e.g., Schmidt, 1975; Dickman, 1978; Tomita *et al.*, 1979) point to a dust density distribution that is centrally condensed. However, the use of star counts in the visible suffers badly when the central region is so dense that no stars are visible through it. This technique is therefore restricted to the less opaque globules (Hyland, 1981).

The extinction is much lower at wavelengths longer than $1 \mu\text{m}$ and so near-infrared surveys of background stars are a far more useful probe of globules (see review by Hyland, 1981). This technique has been used successfully to probe the inner structure of the dense globule 2 in the Coalsack by Jones *et al.* (1980, 1984). They found no signs of a central density enhancement down to the $15''$ level, and concluded that the globule is not collapsing. Aligned grains were observed towards globule 2, which Jones *et al.* interpreted as mild evidence for a weakly compressive magnetic field. However, three more globules studied in this manner failed to show any such field (Klebe and Jones, 1990). It may be that significant ambipolar diffusion has taken place within these globules and so has lessened the role of magnetic support (Klebe and Jones, 1990), which has not yet happened for globule 2. Despite the obvious advantages of using the near-infrared reddening of background stars to determine the dust density distribution within globules, this technique has not been widely used. It is expected that with the new generation of infrared array cameras this situation will change.

Studies of far-infrared emission allows one to directly observe the dust in globules and to determine whether the grains are heated predominately by an internal source or the ISRF (Leung, 1985). The work of Keene and co-workers (Keene *et al.*, 1980; Keene, 1981; Keene *et al.*, 1983) has shown that the dust

temperature of isolated globules is ~ 15 K, slightly greater than the observed gas temperature of 10 K, and the dust mass lies in the range $0.07 - 0.17 M_{\odot}$, which implies a gas-to-dust ratio of 100. The work of Clemens *et al.* (1991) shows that most of the far-infrared emission we observe from globules results from grain heating by the ISRF.

The Gas Component

Observations of a wide variety of molecular lines allows one to sample different density regions of globules. The density distribution may be well determined by observations of the high density tracers such as CS, H₂CO, C¹⁸O and NH₃ (see e.g., Snell *et al.*, 1982; Menten *et al.*, 1984). Such observations indicate that the gas density distribution is centrally condensed with densities $> 10^4 \text{ cm}^{-3}$ (see e.g., Snell *et al.*, 1982). These distributions are usually well fitted by inverse square laws (Fulkerson and Clarke, 1984; Snell, 1981) and indicate that globules consist of a core-envelope structure (Leung, 1985). Observations of the CO J = 1→0 transition, which is assumed to be optically thick and fully thermalised, point to gas temperatures in the range 8 - 15 K (Dickman, 1975). Recent observations of the CO 2→1 transition for a large number of globules confirms this result (Clemens and Barvainis, 1988). Ammonia observations of dense cores and globules also indicate kinetic gas temperatures of ~ 10 K (Ungerechts *et al.*, 1982; Benson and Myers, 1989). Theoretical studies show that the observed gas temperatures can be explained by cosmic ray heating of the cloud cores (see e.g., Goldsmith and Langer, 1978).

Observations of molecular transitions also allow details of the cloud internal velocity structure to be determined. These show that a power law relation exists between the cloud size and velocity dispersion of the form $\Delta v \propto R^{0.5}$ and that virial equilibrium is well satisfied by these clouds, i.e. $\Delta v \propto n^{0.5} R$ (Myers,

1983). Indeed, Leung *et al.* (1982) showed that most globules appear to be in virial equilibrium, and a few may have even undergone significant gravitational contraction. The observed velocity dispersion in the inner core regions is smaller than that observed within the outer parts of globules, which has been interpreted as evidence for gravitational collapse (Martin and Barrett, 1978; Myers *et al.*, 1978). Rotation has been observed in only a few globules, e.g. B361 (Milman, 1977). Observations of B335 by Menten *et al.* (1984) indicate that rotation plays a negligible role in the internal dynamics within that cloud. The lack of significant rotation on large scales (i.e., 10^{17} cm) suggests that rotation cannot play an important role in the support of globules in virial equilibrium (Goldsmith and Arquilla, 1985).

Theoretical Studies

The theoretical study of globules may be divided into two categories (Leung, 1985):

- i) those which study the chemical and thermal structure and radiation transport in some detail, but ignore the hydrodynamical processes (see e.g., Leung, 1975, 1978; Spencer and Leung, 1978; Clavel *et al.*, 1978; de Jong *et al.*, 1980; Dickman and Clemens, 1983; Lee and Rogers, 1987)
- ii) those that study the dynamical evolution, emphasizing the role of gravitation, rotation and magnetic fields, but generally ignore the effects of chemistry, thermal structure and radiation transport. Observational comparison with these models are difficult (see e.g., Villere and Black, 1980; Tarafdar *et al.*, 1984; Myers and Goodman, 1988; Mouschovias, 1991).

The details of the theoretical modelling is outside the scope of this thesis. Relevant comparisons between observation and theory will be made when appropri-

ate.

1.5.2 Star Formation in Bok Globules

Bok and Reilly (1947) first suggested that isolated globules represent an early phase of star formation. However, it was not accepted until very recently that stars may form in Bok globules and are in fact doing so (see e.g., Yun and Clemens, 1990). In particular, two well studied globules, B335 and DC 267.4–7.5 (ESO 210–6a) show all the characteristic signs of low mass star formation, such as the presence of far-infrared point sources (Keene *et al.*, 1983; Cohen *et al.*, 1984), bipolar molecular outflows (Goldsmith *et al.*, 1984; Olberg *et al.*, 1992), Herbig-Haro objects (Reipurth *et al.*, 1991; Schwartz, 1977), dense ammonia cores (Menten *et al.*, 1984; Kuiper *et al.*, 1987), and in the case of DC 267.4–7.5 a corresponding near-infrared point source (Graham and Heyer, 1989).

Star formation is occurring or has occurred in a number of cometary globules (see review by Pettersson, 1991). The best studied of this class of globule is CG30, with its associated infrared source and Herbig-Haro object (Pettersson, 1984). The number density of H α emission stars in the vicinity of globules is at least as twice as high as that seen in the ordinary galactic field, presumably indicating that some of these young stars have recently emerged from their parent globule (Ogura and Hasegarva, 1983). Indeed, *IRAS* has detected many point sources towards dark cloud cores (Beichman *et al.*, 1986) and globules (Clemens and Barvainis, 1988; Yun and Clemens, 1990). These studies point to many globules containing internal heat sources of low mass. Bipolar outflows are seen in a number of globules (Parker, 1989; Yun and Clemens, 1992) and many of the *IRAS* point sources found by Clemens and Barvainis (1988) have SEDs characteristic of YSOs seen in molecular cloud complexes (Yun, 1992). It should

no longer be doubted that star formation is an ongoing process in Bok globules.

1.6 The Work of this Thesis

1.6.1 Unanswered Questions

Bok globules are active sites of star formation. However, there is still much we do not understand about them, and many problems that require answers if we are to understand the role of globules in the overall picture of galactic star formation. One of the main problems in the study of Bok globules is the lack of a wide range of observations of the properties of a large number of globules. The number of individual test cases available for theoretical study is very limited, with possibly only B335 and DC 267.4–7.5 having a sufficient number of different observations for indepth modelling to be performed. The work of Clemens and co-workers (Clemens and Barvainis, 1988; Yun and Clemens, 1990; Clemens *et al.*, 1991; Yun and Clemens, 1992) has gone a long way to addressing this situation, with a comprehensive study of 248 globules using the *IRAS* database and CO observations with follow-up observations to search for molecular outflows and near-infrared observations of a sample of the *IRAS* point sources. This lack of a suitable database had been identified previously by Hyland (1981). Aside from expanding the relevant database, a number of direct questions require further investigation. These are outlined below.

- i) What are the relationships between the different types of globules? Are the cometary globules precursors to the isolated dense globules? Do globules begin as dense cores within dark clouds, then pass through a cometary phase on their way to becoming isolated globules? Do the condensations

in globular filaments develop into isolated globules?

- ii) What are the gas and dust density distributions within the globules, and what are their shapes?
- iii) Why do most globules appear to be in virial equilibrium?
- iv) What physical mechanisms appear to trigger star formation or stabilize globules against collapse, i.e., magnetic fields, rotation, turbulence?
- v) What fraction of globules appear to be the sites of current star formation, or have densities sufficient to indicate they may have undergone significant ambipolar diffusion, and thus be on the way to irreversible gravitational contraction?
- vi) Are there any significant differences between the isolated globules and the dense cores found in the larger dark cloud complexes?
- vii) What are the physical characteristics and evolutionary status of the embedded sources found within the globules?

1.6.2 Thesis Aims

In this thesis an attempt has been made to shed some light on a number of questions presented above.

We have seen earlier in this chapter that the major study of dense cores in dark cloud complexes has been undertaken by Myers and co-workers (Myers *et al.*, 1983, Myers and Benson, 1983; Benson and Myers, 1989), who primarily used NH_3 to determine the temperature, density, mass, and dynamical state of a number of dense cores. For Bok globules the major study is that performed by Clemens and co-workers (Clemens and Barvainis, 1988; Yun and Clemens, 1990;

Clemens *et al.*, 1991; Yun and Clemens, 1992), who primarily used CO spectroscopy and the *IRAS* database to determine the gas and dust temperatures of a comprehensive sample of small Bok globules in the northern sky. They also determined unequivocally that some Bok globules are active sites of star formation, through analysis of the SEDs of a number of YSO candidates identified in their globules, and the detection of CO molecular outflows towards a number of these.

Despite the findings of these two major studies, the physical nature of the Bok globules remains unclear. It has been noted by a number of authors (see e.g., Fuller and Myers, 1987) that the different high density gas tracers appear to sample different spatial regimes within molecular clouds. This then makes the comparison between different types of molecular clouds observed with different density tracers difficult. Ideally one would desire to use a single diagnostic tool to observe the various types of molecular clouds to enable direct comparisons to be made, and differences to be identified.

In order to examine the physical properties of the Bok globules, it is desirable to study a large number of globules to determine their physical parameters and dynamical states. This is the major thrust of this thesis. Clemens and co-workers have limited their study by not mapping their globules to determine their sizes and the density distributions within them, and by not determining the densities of the globules in their sample. Though they have shown that Bok globules are active sites of low mass star formation, their physical and dynamical nature remain unclear, and their relationship to other regions of low mass star formation also remains unclear.

This thesis aims to determine for a complete sample of southern small molecular clouds, mostly isolated Bok globules, their temperatures, densities, masses, dynamical state and star forming state. It also aims to compare the dense cores

found within globules with those found in the larger dark cloud complexes, as identified by Benson and Myers (1989). By examining the smallest isolated globules we hope to identify differences between them and the cores found in complexes which are of direct importance to the study of low mass star formation, since the linear sizes and masses of these globules are likely to be of the most relevance in the study of isolated low mass star formation. Do we see the “laws” relating line width, core size and core density that were first identified by Larson (1981) over a large range of cloud size, and further supported by other studies (Myers, 1983; Sanders *et al.*, 1985; Dame *et al.*, 1986), or do the laws break down on the smallest scales of most importance to low mass star formation? Are the smallest isolated globules in virial equilibrium, as the larger globules appear to be (Leung *et al.*, 1982)? These questions may be addressed by surveying a large sample of Bok globules in the high density tracer ammonia (NH_3), which allows the determination of temperature and density, by comparing the results with the work of Benson and Myers (1989), and by combining this survey with a search of the *IRAS* database for possible associated embedded sources. This is exactly the study described in this thesis.

1.6.3 Thesis Outline

Chapter 1 presents a brief review of molecular clouds in general, and examines the formation of stars in molecular clouds. Previous studies of molecular clouds in the optical, radio and infrared are also discussed, in particular large surveys of the smaller molecular clouds, which are not as common as studies of the large cloud complexes. Finally, the Bok globules as a separate group are discussed and their known properties outlined. A number of unanswered questions about the Bok globules are listed, and the work of this thesis discussed briefly.

In Chapter 2 the catalogue of small southern molecular clouds is presented, and their optical properties discussed and compared with the properties of the northern catalogue of Bok globules presented by Clemens and Barvainis (1988). The results of a search of the *IRAS* Point Source Catalogue for possible associated YSOs is also presented, and the properties of the resultant list of sources compared to those found by Clemens and Barvainis (1988) toward their sample of Bok globules, and those found by Beichman *et al.* (1986) toward a sample of dense cores located in dark cloud complexes.

Chapter 3 presents the results of the survey for ammonia emission toward the southern Bok globules, and a comparison of the properties of the dense cores found within the globules with those found in the dark cloud complexes is made. The properties of the cometary globules as a distinct group are examined, as well as a comparison made between the *IRAS* sources found in the globule cores and those found in the dense cores within complexes.

A dynamical analysis of a subsample of Bok globules from this study and that of Benson and Myers (1989) is presented in Chapter 4, along with a discussion of the properties of the few strong ammonia emitting globules we have successfully mapped in this study.

Finally, in Chapter 5 the main conclusions of the thesis are presented, along with suggestions for future research based on these results and the questions which have remained unanswered despite this study.

Chapter 2

The Dark Cloud Sample

2.1 Introduction

Bok globules are the ideal laboratory for the study of isolated low mass star formation. Their simple structure allows them to be modelled in detail, since the number of physical processes occurring within them is likely to be limited. Due to their optical appearance the Bok globules are thought to be relatively nearby (< 500 pc) and so linear scales of a few tenths of a parsec may be readily resolved with current instruments. Their isolation also means that they are relatively unaffected by the problems associated with the study of the larger more complex molecular clouds, i.e., large scale motions which may mask the smaller scale motions of direct interest, energetic HII regions, and multiple star formation within the one cloud which may destroy much of the evidence sought on the single star forming events.

Earlier studies of Bok globules (e.g., Leung *et al.*, 1982) concentrated on the larger globules ($> 10'$), which are relatively massive and may contain multiple

sites of star formation (see e.g., Beichman *et al.*, 1984). Therefore in order to examine single low mass star forming events in an isolated environment one must turn to the smaller ($< 10'$) isolated Bok globules. The choice of the smallest clouds for study means that a relatively large survey may be undertaken in a reasonable number of observing sessions, using current single dish millimetre and radio telescopes, and optical CCDs and infrared array cameras (Clemens and Barvainis, 1988; hereafter CB). It also means that the largest globules in the sample ($10'$) will have a linear size of only 0.7 pc at a distance of 500 pc, not much larger than the typical core size found in the dark cloud complexes (~ 0.4 pc).

CB compiled a catalogue of 248 small molecular clouds located in the northern sky. In this chapter we present a similar catalogue of small molecular clouds for the southern sky, with the clouds selected from the Hartley *et al.* (1986) catalogue. The *IRAS* PSC has been searched for point sources lying within the optical boundaries of the selected clouds. The optical and *IRAS* properties of the clouds are compared with those in the CB catalogue, and the *IRAS* properties of this catalogue and the CB catalogue are compared with those of the dense cores in dark cloud complexes studied by Beichman *et al.* (1986).

2.2 The Southern Bok Globule Catalogue

The Catalogue of Southern Dark Clouds by Hartley *et al.* (1986) has been searched to choose a candidate set of small dark clouds and Bok globules for study. This catalogue, which we shall refer to as the Hartley catalogue, lists the positions of 1101 dark clouds south of -33° declination. The merits of the Hartley catalogue over other southern dark cloud catalogues (e.g., Feitzinger and Stüve, 1984; Sandqvist and Lindroos, 1976) have been outlined in section 1.4.1.

The clouds were selected on the basis of i) density and ii) size as described below. Only the densest (class A) clouds from Hartley were considered initially, and from this group only small clouds, or particularly dense and obvious condensations within larger clouds were selected, the upper limit to the cloud diameter being 10 arcminutes. This upper limit also enables a complete molecular line survey of the clouds to be undertaken in a reasonable time, using beam sizes $\sim 1' - 2'$. The search was aimed particularly at identifying isolated clouds satisfying the above criteria, although, as indicated, for completeness the sample does include some dense clouds which appear to be connected to surrounding regions of less dense interstellar matter, and some globular condensations within dark cloud filaments, to enable comparisons of these different types of globules. The shape of the cloud was not important in the cloud selection, for the same reasons that shape was not a selection criteria in the Bok globule catalogue of Clemens and Barvainis (1988), i.e., because the shape may depend on the cloud's dynamical evolution and magnetic structure, properties which we wish to probe.

All class A clouds (432) from Hartley were inspected visually on the SERC Schmidt survey J plates for their suitability in this program. Though Hartley lists the cloud sizes, it was found after the initial inspection of the plates that quoted sizes sometimes referred to extensions to what otherwise appeared as well defined globules (Hyland *et al.*, 1993), which therefore resulted in their exclusion in the initial search. All class A clouds were therefore inspected so as to avoid missing these occasional exceptions. Some clouds classified by Hartley as class B were also included in the final list after inspection of the Schmidt plates, as they satisfied our criteria for opaqueness and size. This search rendered a survey list of 169 dark clouds satisfying the selection criteria outlined above.

Parker (1989) noted that a large number of the quoted positions of the Lynds opacity class 6 clouds are in error, or do not relate to the most opaque position

within the cloud. A similar problem has been found with the Hartley catalogue during this search, though to a far lesser extent. In order to check the positional accuracy of the clouds in our sample a method similar to that employed by Parker was used. Overlays using stars from the SAO, AGK3 and Perth70 catalogues were generated for a $1.5^\circ \times 1.5^\circ$ field about each cloud position quoted by Hartley. If the Hartley position did not correspond to either the cloud or the densest location within the cloud, then the cloud position was remeasured with respect to the Hartley position directly from the Schmidt plate. The scale of the Schmidt plates is ~ 67 arcsecond mm^{-1} and so the estimated accuracy of the revised positions is ~ 30 arcsecond (i.e., ~ 0.5 mm). This is smaller than the size of the Parkes radio telescope beam ($1.4'$) at the frequency of the (1,1) inversion transition of ammonia (~ 23.7 GHz), which we shall see in the next chapter is our main diagnostic probe of the physical conditions within the clouds. All the class A clouds listed by Hartley were able to be identified on the Schmidt plates, whereas Parker was unable to identify 3 of the 150 Lynds class 6 clouds. Approximately 30% of the clouds catalogued by CB had not previously been identified by earlier catalogues, while in the present work only two clouds not catalogued by Hartley were identified. They are, using the nomenclature of Hartley, DC 322.7+4.0 and DC 322.7+3.9. However, we were not searching for previously undetected clouds, as were CB, but choosing a subsample of clouds from the Hartley catalogue satisfying certain criteria, and so not all the southern Schmidt plates have been searched in this study, nor a thorough search made of the plates we have inspected. It is thus possible that we have not identified all clouds with sizes $< 2'$, which are difficult to detected at the scale of the plates ($2' \sim 2$ mm) and make up the majority of the new clouds in the CB catalogue. Table 2.1 lists the clouds which satisfy our selection criteria and which therefore represent our list of southern isolated dark clouds (for convenience they shall often be referred to simply as Bok globules). Column 1 identifies the DC cloud

name as given by Hartley, which is based on the cloud's galactic coordinates. Clouds identified with an asterisk have positions which differ from those given by Hartley, i.e., the position has been remeasured. Columns 2 and 3 give the cloud's right ascension and declination in 1950.0 coordinates. Columns 4 and 5 list the major and minor axes of the clouds, which in general are the same as those listed by Hartley. Column 6 attempts to identify the cloud type, where I means the cloud is well isolated, CG indicates a cometary globule, F a globule within a filament, C a globule within a less opaque complex and N an associated reflection nebula. Combinations of these types are possible, as indicated in the table. Column 7 lists other catalogued names for the clouds where they exist and are known to us, where CG refers to Zealey *et al.* (1983) and Reipurth (1983), Sa to Sandqvist and Lindroos (1976) and Sandqvist (1977), B to Barnard (1927), L to Lynds (1962) and CB to Clemens and Barvainis (1988). Other popular names and Herbig-Haro identifications are also given.

The majority of positions listed in table 2.1 which are different from those of Hartley arise from the subjective determination of the cloud centre or the most opaque position within the cloud. Most of the positions from Hartley do in fact lie within the cloud optical boundaries (for the clouds on our list at least). As a result, very few remeasurements were a result of inaccurate positional quotations in the Hartley catalogue, but simply represent a personal bias. This serves only to reinforce our arguments that the Hartley catalogue is the prime catalogue for studies of southern dark clouds due to its completeness and accuracy.

Of the 169 clouds in table 2.1, 40 are cometary globule like in appearance. Of these 40 CGs, 32 have been identified by Zealey *et al.* (1983) and Reipurth (1983) as possibly being associated with the Gum Nebula.

Globules which appear as condensations within filaments account for 6 of the clouds, while larger clouds which appear as condensations within still larger

Table 2.1: Catalogue of southern Bok globules, taken from the Southern Dark Cloud Catalogue of Hartley *et al.* (1986).

DC Name	RA (1950.0) <i>h m s</i>	Dec (1950.0) <i>° ' "</i>	<i>a</i>	<i>b</i>	Type	Other Names
249.7-2.1	07 56 09	-33 10 06	6	6	I	
251.7+0.2	08 10 29	-33 36 36	2	1	CG	CG27
251.8+0.0*	08 10 28	-33 46 48	1	1	CG	CG28
251.9+0.0	08 10 27	-33 52 00	1	1	CG	CG29
252.2+0.7	08 14 03	-33 41 30	2	1	CG	CG26
252.3+0.5*	08 13 29	-33 55 30	0.8	0.6	CG	CG33
252.5+0.1*	08 12 23	-34 21 08	3	1.5	CG	CG32
253.1-1.7A	08 07 10	-35 52 24	4	2	CG	CG31A
253.1-1.7B	08 06 55	-35 54 14	2	2	CG	CG31B
253.1-1.7C	08 06 40	-35 50 44	3	2	CG	CG31C
253.1-1.7D	08 06 24	-35 52 58	1	1	CG	CG31D
253.3-1.6	08 07 39	-35 55 54	3	2	CG	CG30/HH120
253.6+2.9	08 26 48	-33 35 48	5	3	CG	CG22
253.8-10.9	07 27 53	-41 04 12	3	1	CG	CG34
255.3-14.4	07 14 28	-43 52 18	2	2	CG	CG2
255.4-3.9	08 03 39	-39 00 18	6	2	I	
256.2-14.1*	07 17 49	-44 29 36	2	2	CG	CG1
256.9+2.6	08 35 23	-36 27 24	1	1	CG	CG36
257.2-10.3	07 39 16	-43 42 06	1	0.5	CG	CG5
259.0-13.2	07 29 05	-46 37 18	3	1	CG	CG6
259.4-12.7	07 32 41	-46 47 42	4	1	CG	CG4
259.5-16.4	07 12 50	-48 23 54	5	3	CG	CG13
259.9-0.0	08 33 43	-40 28 06	5	3	I/N	NGC2626
260.0-3.8	08 17 33	-42 45 18	1	1	CG	CG24
260.7-12.4	07 37 42	-47 46 12	3	1.5	CG	CG3
262.5-13.4	07 37 18	-49 43 48	3	1	CG	CG14
262.9-14.7	07 31 03	-50 39 06	3	1	CG	CG15
262.9-15.5	07 26 20	-50 58 18	2	1	CG	CG16
264.5+5.6	09 11 29	-40 17 06	5	1	I	
265.3-0.0	08 51 57	-44 36 36	4	2	I	Sa3
265.7-7.7	08 17 11	-49 34 24	3	3	I	
266.0+4.3	09 12 14	-42 17 36	2	1.5	CG	CG7
266.0-4.3*	08 35 24	-47 54 07	3	3	I/N	
267.2-7.2	08 25 06	-50 30 00	2	2	I	
267.4-0.9	08 55 45	-46 46 42	5	3	I	
267.4-7.5	08 24 17	-50 52 12	4	3	I	Sa111/HH46-47/ESO210-6a
267.5-7.4	08 25 12	-50 51 42	2	2	I	Sa112
267.6-6.0a*	08 32 38	-50 08 00	5	2	I/F	Sa113
267.6-6.0b*	08 32 49	-50 14 09	5	2	I/F	Sa113
267.6-6.4	08 30 31	-50 22 36	2	2	I	

Table 2.1 *continued*

DC Name	RA (1950.0) <i>h m s</i>	Dec (1950.0) <i>° ' "</i>	<i>a</i>	<i>b</i>	Type	Other Names
267.7-7.4	08 26 04	-51 00 42	5	4	I	
267.9-7.8	08 24 46	-51 29 24	3	1.5	I	
269.4+3.0	09 20 29	-45 36 00	3	3	I/C	Sa115
269.5+4.0	09 24 27	-44 58 00	8	4	I	Sa116
269.7-3.9	08 51 04	-50 28 42	0.5	0.5	CG	CG18
270.6-4.7	08 51 04	-51 40 30	1	1	CG	CG17
272.5+2.0	09 29 15	-48 25 06	4	2	I	
273.2+2.4	09 34 15	-48 40 06	6	4	I	
273.3+2.5	09 34 55	-48 38 24	4	3	I	
273.8+3.2	09 39 50	-48 27 00	7	1	I	
274.1+3.9	09 44 00	-48 04 18	1.5	1	CG	
274.1+2.7	09 39 22	-48 59 12	8	3	I	
274.2-0.4	09 27 05	-51 23 30	5	3	I	Sa120
274.3+3.4	09 43 10	-48 37 30	4	2	I	
275.9+1.9*	09 45 03	-50 52 29	4	3	I/C	Sa121
276.2-10.6	08 43 07	-59 43 06	4	3	I/N	
285.3-1.6	10 23 39	-59 09 54	3	2	I	
289.3-2.8	10 47 05	-62 07 12	3	3	I	
291.1-1.7	11 05 03	-61 49 36	6	3	I	Sa125
291.4-0.2	11 12 19	-60 36 42	4	2	I	Sa127
293.1+0.6	11 27 16	-60 25 54	1.5	1.5	I	
293.2+0.4	11 27 39	-60 41 42	3	1	I	
293.3+0.1	11 27 53	-60 56 48	2	1	I	
293.3-0.9	11 25 36	-61 53 24	3	2.5	C	Sa129
294.3+2.7	11 41 06	-58 45 54	3	2	I	
294.3-0.1	11 35 12	-61 28 00	2	1	I	
294.9+0.1	11 40 27	-61 27 42	2	1	I	
295.0+3.4	11 47 31	-58 16 24	6	4	I	Sa1
295.4+0.5	11 45 34	-61 09 24	3	2	I	
295.5+0.4	11 45 43	-61 13 54	2	2	I	
297.7-2.8	11 59 10	-64 52 24	8	3	I	Sa136
298.3-2.8	12 04 31	-65 02 00	4	1.5	I	
299.6+5.6	12 23 54	-56 49 12	6	3	I	
300.0-3.7	12 19 21	-66 10 30	3	2	I	
300.2-3.5	12 21 24	-65 54 06	8	4	I	Sa139
300.6-3.1	12 25 27	-65 37 24	9	4	I	Sa140
300.7-1.0*	12 28 38	-63 28 15	6	6	C	Tapia 2
301.2-0.4	12 33 25	-62 56 06	5	2	I/C	Sa144
301.7-6.7	12 33 55	-69 14 12	7	6	I/N	Sa147
301.7-7.2	12 34 07	-69 43 24	7	2	CG	CG21/Sa149

Table 2.1 *continued*

DC Name	RA (1950.0) <i>h m s</i>	Dec (1950.0) <i>° ' "</i>	<i>a</i>	<i>b</i>	Type	Other Names
301.7-2.6	12 36 42	-65 10 00	5	2	I/C	Sa148
302.0-7.0*	12 37 57	-69 35 14	4	1.5	CG	CG20/Sa151
302.1+7.4	12 42 48	-55 09 00	2	1	CG	CG19
302.6-15.9	12 40 59	-78 31 48	6	3	I/N	TPN
303.3+1.3	12 51 19	-61 16 48	9	4	I	Sa155
303.8-14.2	13 03 02	-76 44 54	10	6	I/N	Sa160
307.3+2.9	13 22 34	-59 27 18	3	3	I	
314.8-5.1*	14 44 30	-65 03 24	9	5	I/N	Sa165
315.8-27.5a	19 02 16	-78 40 48	2	2	I/N	
315.8-27.5b	19 03 05	-78 40 54	3	1	I/N	
316.3+4.9	14 23 27	-55 14 06	4	3	I	
316.5+21.2*	13 54 34	-39 40 49	4	3	CG/N	CG12/NGC5367
316.5-4.0	14 54 09	-63 15 42	8	3	I/F	
316.9-4.9	15 01 00	-63 56 18	4	2	I	
316.9-2.1	14 49 24	-61 23 48	5	1.5	I	
317.0-4.6	15 00 30	-63 36 24	6	3	I	
319.9-4.8	15 22 59	-62 12 48	3	2	I	
320.1-4.3	15 22 16	-61 45 30	3	1	I	
320.5-3.5	15 20 56	-60 51 06	2	1	I	
320.5-3.6	15 21 38	-60 56 36	3	2	I	
320.7-1.7	15 14 51	-59 10 48	5	3	I/C	
320.7-2.0	15 16 16	-59 27 12	6	4	I/C	
320.9-2.1	15 17 35	-59 25 06	3	1	I	
322.7+4.0*	15 06 04	-53 19 26	1	1	I	
322.7+3.9*	15 06 19	-53 21 41	2	1	I	
323.0+4.0	15 07 34	-53 07 06	3	2	I	
325.2+5.8	15 13 38	-50 25 42	3	3	I	
325.9+5.9	15 17 27	-50 01 30	3	2	I	
326.8+5.6	15 22 42	-49 49 00	3	2	I	
326.9+5.5	15 23 27	-49 50 12	3	2	I	
327.2+1.8*	15 38 34	-52 38 21	10	4	I	
330.7-1.3*	16 09 58	-52 45 52	7	7	I	Sa178
331.0-0.7	16 09 00	-52 09 01	7	1	I	
331.1-2.3	16 16 10	-53 11 12	3	2	I	
332.7+6.8*	15 46 49	-45 21 24	6	2	I	
334.2+0.0	16 19 53	-49 26 00	3	1	I	Sa179
334.6+4.6	16 02 44	-45 47 12	8	5	I	
334.6-1.4*	16 28 10	-50 01 38	8	7	C	
335.9+7.0*	15 59 38	-43 09 30	7	3	I	Sa181
336.7+7.8	15 59 49	-41 58 12	4	3	I	

Table 2.1 *continued*

DC Name	RA (1950.0) <i>h m s</i>	Dec (1950.0) <i>° ' "</i>	<i>a</i>	<i>b</i>	Type	Other Names
337.1-4.9	16 54 50	-50 31 12	8	2	I	Sa185
337.7-4.0	16 52 49	-49 30 54	4	4	I	Sa186
337.8-1.6	16 42 09	-47 54 06	6	4	I/C	
337.9-1.4*	16 41 13	-47 39 42	1.5	1	F	
338.2+0.8	16 33 02	-45 55 12	2	2	I	
338.6+9.5	16 01 07	-39 29 36	5	3	I	
338.6+11.9*	15 53 50	-37 38 30	9	5	F	Sa11/Lupus2
339.1+11.7a*	15 55 22	-37 31 12	4	3	F	Lupus2
339.1+11.7b*	15 55 47	-37 27 51	5	4	F	Lupus2
339.1-0.8	16 43 05	-46 22 00	2	2	I	Sa190
339.3-0.3	16 42 22	-45 53 24	7	5	F	Sa191
340.4+5.5	16 22 38	-41 08 36	3	2	I	
340.5+0.5	16 43 09	-44 25 24	7	2	I	Sa15
340.9+9.2	16 10 36	-38 09 06	7	5	I	
343.4+3.5	16 41 23	-40 17 36	7	2	I	Sa18
344.5+2.0	16 51 04	-40 26 03	1	1	CG	
344.6-4.3	17 18 10	-44 05 54	5	3	I/N	
345.0-3.5	17 16 00	-43 24 00	2	2	I	
345.2-3.6*	17 17 15	-43 17 30	6	5	I	
345.4-4.0	17 19 19	-43 19 48	10	6	I	
345.8+7.6	16 33 33	-35 50 30	3	2	I	
346.2-11.7	17 59 18	-46 39 54	3	1.5	I	Sa193
346.4-5.0	17 27 02	-43 06 12	2	2	I	
346.4+7.9	16 34 10	-35 07 54	4	2	I	
347.5-8.0	17 44 23	-43 42 12	6	3	I	Sa195
347.9-4.4	17 28 50	-41 32 18	7	5	I	
348.0+3.7	16 55 04	-36 37 42	4	3	I	
349.0+3.0	17 01 05	-36 14 42	2.5	2.5	I	
349.2+3.1a	17 01 06	-36 04 18	3	1	I	
349.2+3.1b	17 01 25	-36 06 12	1	1	I	
349.3+3.1	17 01 28	-35 59 05	2	1	I	
351.0+3.9	17 03 22	-34 09 54	4	3	I	
351.2+5.1	16 59 28	-33 12 12	7	4	I	B49/Sa31/CB69
351.2+5.2	16 59 04	-33 12 18	2	2	I	CB69
351.7+0.5*	17 18 44	-35 32 29	9	5	I	Sa33
351.8+2.8	17 10 11	-34 11 54	2	1	I	
352.9+4.8	17 05 31	-32 03 00	6	3	I	B56/L1685/CB73
352.9+5.0	17 04 48	-31 59 00	2.5	2	I	
353.1+2.3	17 15 56	-33 23 48	4	2	I	
353.3+2.4	17 15 39	-33 12 54	2.5	2.5	I/N	

Table 2.1 *continued*

DC Name	RA (1950.0) <i>h m s</i>	Dec (1950.0) <i>° ' "</i>	<i>a</i>	<i>b</i>	Type	Other Names
353.5+3.5	17 12 15	-32 21 36	3	1.5	F	
354.1+2.9a*	17 15 57	-32 12 48	1.5	1.5	CG	
354.1+2.9b*	17 15 44	-32 15 36	3	1	CG	
354.1+2.9c*	17 15 44	-32 12 48	3	1.5	CG	
354.1+2.9d*	17 16 26	-32 11 41	3	3	CG	
354.1+2.9e*	17 15 52	-32 08 20	4	2	CG	
354.2+3.2	17 15 13	-32 01 30	6	4	I/C	
356.5-4.5*	17 51 50	-34 13 31	4	1	I	
4.9-24.6	19 37 23	-34 54 36	2.5	1.5	CG	CG11

Notes:**Cloud Type:**

- I = isolated
- CG = cometary globule
- N = nebula associated
- F = filamentary
- C = complex

Other Name:

- B = Barnard (1919, 1927)
- CB = Clemens and Barvainis (1988)
- CG = Zealey *et al.* (1983); Reipurth (1983)
- L = Lynds (1962)
- Sa = Sandqvist and Lindroos (1976); Sandqvist (1977)
- Tapia 2 = Tapia Coalsack Globule 2 (Tapia, 1973)
- TPN = Thumbprint Nebula (FitzGerald *et al.*, 1976)

regions of obscuration account to only 3 of the clouds. The most well known example of this type of globule is Tapia's globule 2 in the Coalsack (Tapia, 1973; Jones *et al.* 1980, 1984). The remaining 120 clouds appear well isolated on the whole, though some may be part of larger complexes (8) or appear as well formed globules with less opaque extensions (Hyland *et al.*, 1993), and others appear to form part of a filamentary chain (3), but the connections to other parts of the filament are not distinct. Nebulosities are associated with 10 of the isolated globules.

The majority of clouds in our list thus satisfy our selection criteria of being small isolated globules. Only a small number of the clouds (9 of 169) appear to be doubtful inclusions, but they still appear as well formed small globules. For example the Coalsack globule 2 mentioned above is a distinct globule, but cannot be classified as truly isolated. Similarly the filamentary globules associated with the stringy Lupus dark clouds cannot be said to be truly isolated. In the next section we will see that the 169 clouds selected here form a remarkably uniform dark cloud sample.

2.3 Optical Properties

Our selection criteria closely resembles that of Clemens and Barvainis (1988), as we have both attempted to identify the smaller ($< 10'$) isolated Bok globules seen in the sky. In this section a comparison will be made between the optical and infrared properties of the CB catalogue, which contains 248 clouds, and the 169 clouds listed in table 2.1.

Figure 2.1 shows a histogram of the apparent mean optical sizes of the clouds in the two samples. The mean optical size is defined to be \sqrt{ab} where a and

b represent the cloud major and minor axes respectively, as listed in table 2.1. The two samples have a similar distribution in cloud size. The CB sample has a peak between 2' and 4', whilst this sample has a narrower peak between 2' and 3'. This is reflected in the mean sizes of the two samples, the mean size being 4' for the CB sample and 3' for this work.

Figure 2.2 shows a histogram of the ellipticities of the two samples. Again the distributions are very similar, with the CB mean ellipticity being 2.0 and the mean of this work 1.9. Both samples have a greatest ellipticity of about 7. Approximately 14% of our sample have ellipticities greater than 3 while for the CB sample the same percentage is about 9, so the difference is not significant. It is apparent that the majority of the globules are not spherical, and so spherical cloud models may not be suitable for their modelling.

Thus, figures 2.1 and 2.2 show that the optical properties of the two samples are very similar and so they represent complementary catalogues of northern and southern Bok globules.

Figure 2.3 shows the combined galactic distribution of the two samples. The CB sample is represented by open circles and the present work by filled circles. The majority of clouds are seen to lie within $|b| < 10^\circ$. Also plotted is the approximate position of Gould's Belt, which is the plane locating the major concentration of local O and B stars (see e.g., Clube, 1967; Westin, 1985; Comeron *et al.*, 1992). Hartley has noted that there is no connection between the southern dark clouds and Gould's Belt. Figure 2.3 certainly shows no evidence for a connection between Gould's Belt and the galactic distribution of isolated Bok globules. Figure 2.4, which plots mean galactic latitude against galactic longitude (binned into intervals of 10°) for the combined sample, reinforces this lack of correlation. This should come as no surprise, since the dark clouds are thought to be regions of preferentially low mass star formation, while the O and

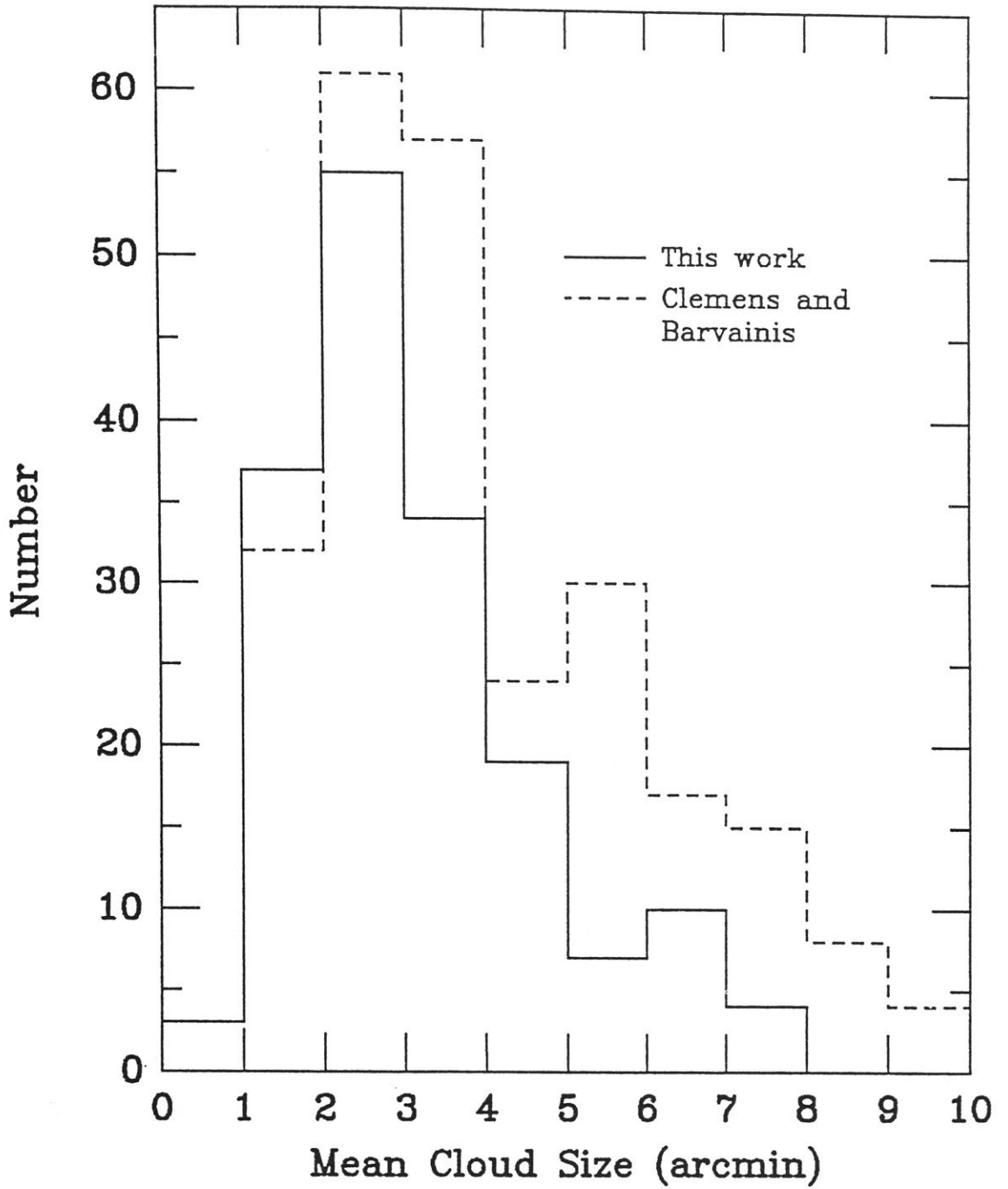


Figure 2.1: The distribution of the mean cloud size for the catalogued clouds. Also shown is the distribution of the CB clouds.

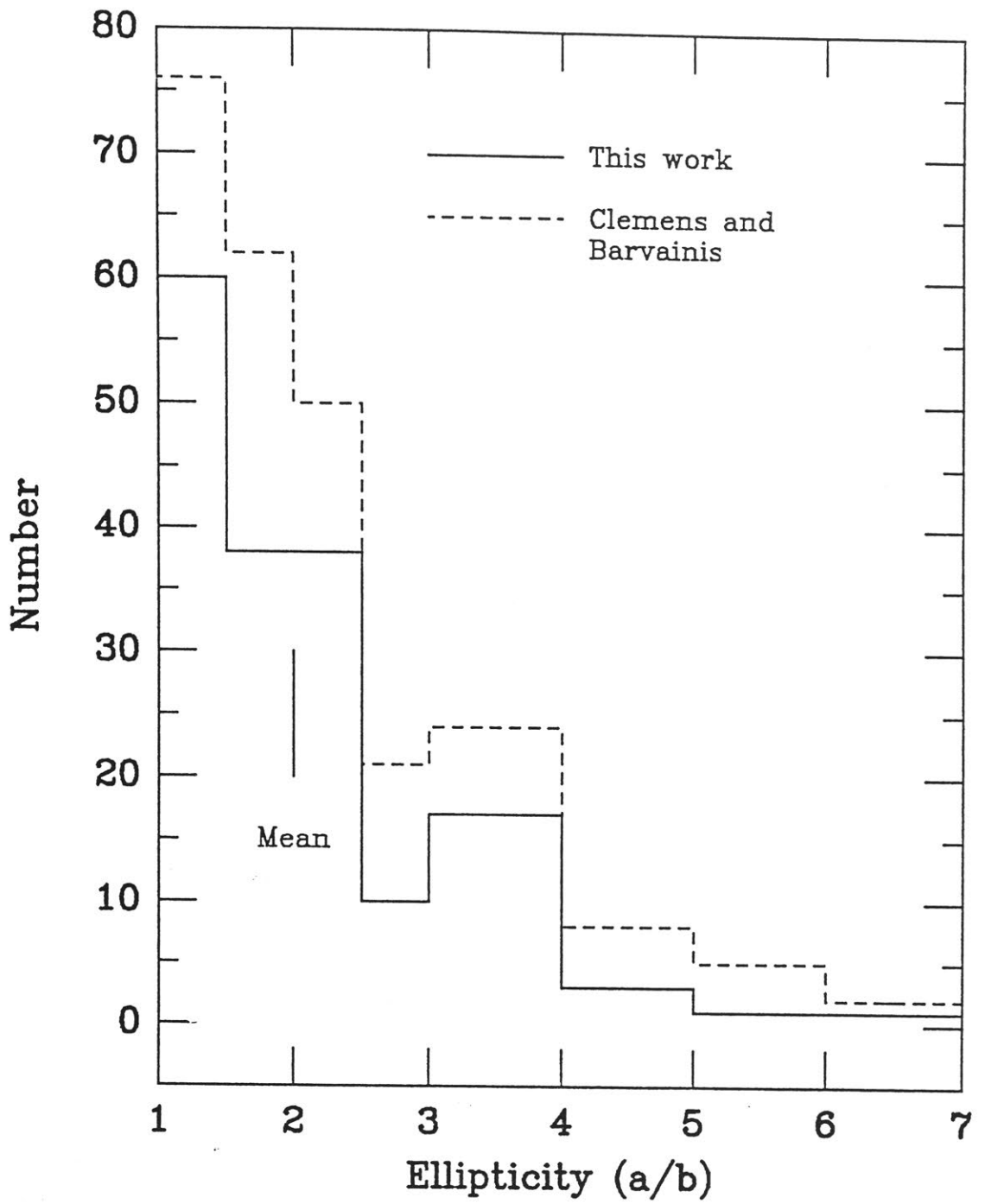


Figure 2.2: The distribution of the ellipticities (a/b) for the catalogued clouds and the CB sample.

B stars are the children of the high mass star formation process. We have seen in section 1.3 that the regions of high and low mass star formation are spatially distinct, a view which is supported by these figures.

The galactic distribution of the clouds in this work is shown in figure 2.5. Also shown in this figure are the locations of three major southern dark cloud complexes, those of Chamaeleon (I, II and III), Lupus (clouds 1 – 4) and the Coalsack, as well as the annulus bounding the Vela–Gum cometary globules. The two globules located in Chamaeleon are bright rimmed globules. One, the Thumbprint nebula, has previously been studied by FitzGerald *et al.* (1976), and both are currently under thorough investigation by Lehtinen and co-workers (K. Lehtinen, private communications 1993). The Lupus dark clouds are a series of globular filaments and the globules in this work from the Lupus complex are thus representative of condensations within globular filaments. The Coalsack is familiar and identifiable as a large collection of globules and small clouds contained within a larger though less opaque molecular complex. The Vela cometary globule annulus, with an inner radius of $\sim 6^\circ$ and outer radius of $\sim 11^\circ$, centered on RA(1950) $\sim 08^h18^m$, Dec(1950) $\sim -44^\circ$, $[(l,b) \sim (261.1,-4.5)]$, is taken from Zealey *et al.* (1983). This catalogue of southern Bok globules contains 6 clouds from within the Lupus complex, 2 from Chamaeleon, 7 from the Coalsack and 32 cometary globules thought to be associated with the Vela–Gum complex. The vast majority of globules in table 2.1 lie outside the major southern dark cloud complexes. No bias, however, was used to include or exclude globules from these complexes in the selection criteria. The CB sample is also bias free with respect to globules within the major northern dark cloud complexes (i.e, Taurus, Orion).

In figure 2.6 the galactic latitude of the sample has been binned in the same way as figure 4 of CB. Plotted are the histograms of the raw counts for both

Figure 2.3: The galactic distribution of Bok globules from this work (filled circles) and CB (open circles). The dashed line indicates the approximate plane of Gould's Belt.

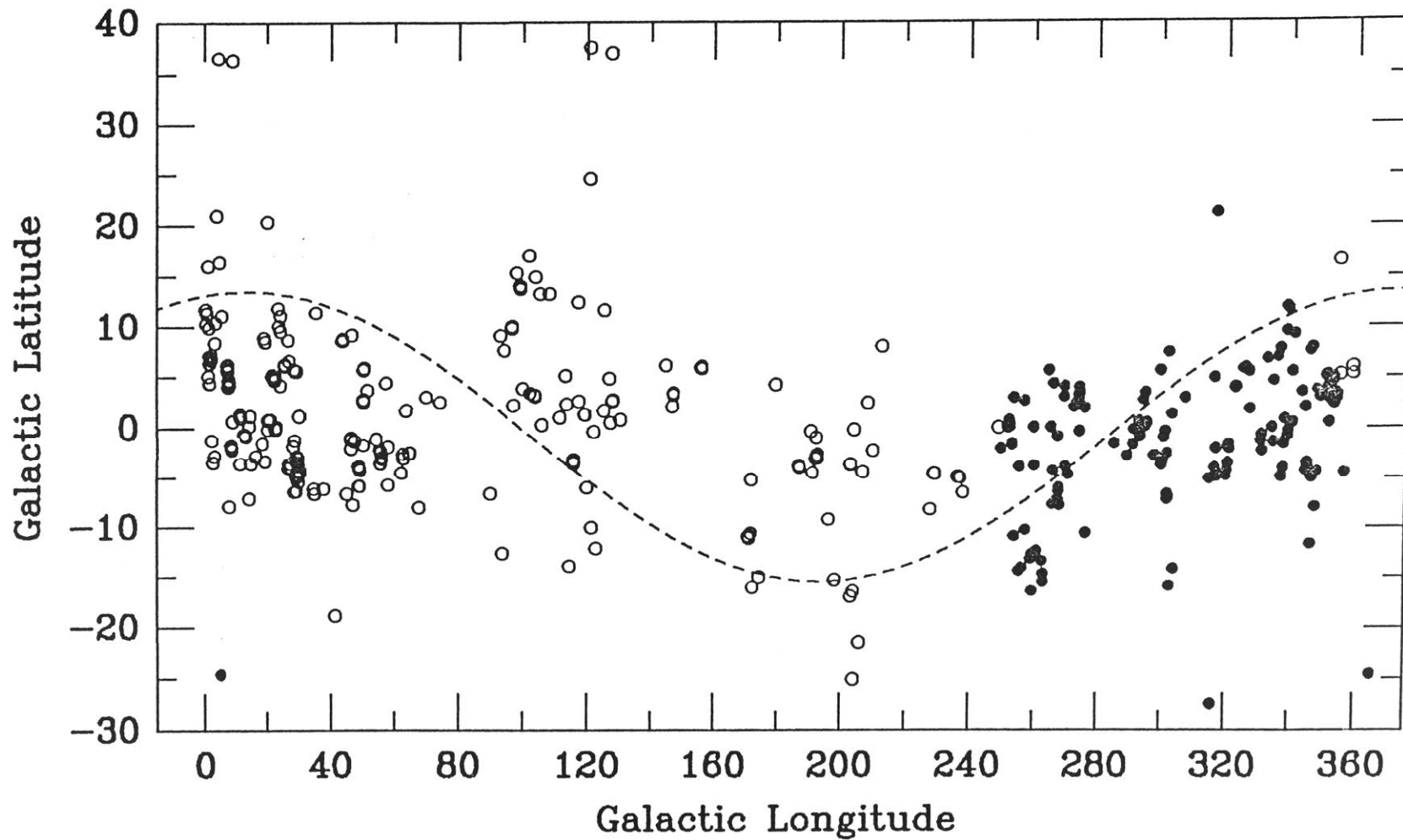


Figure 2.4: The galactic distribution of the clouds in this work and those in CB, binned into intervals of 10° in longitude. The plane locating Gould's Belt is shown as a solid line. No correlation is seen between the globule distribution and Gould's Belt.

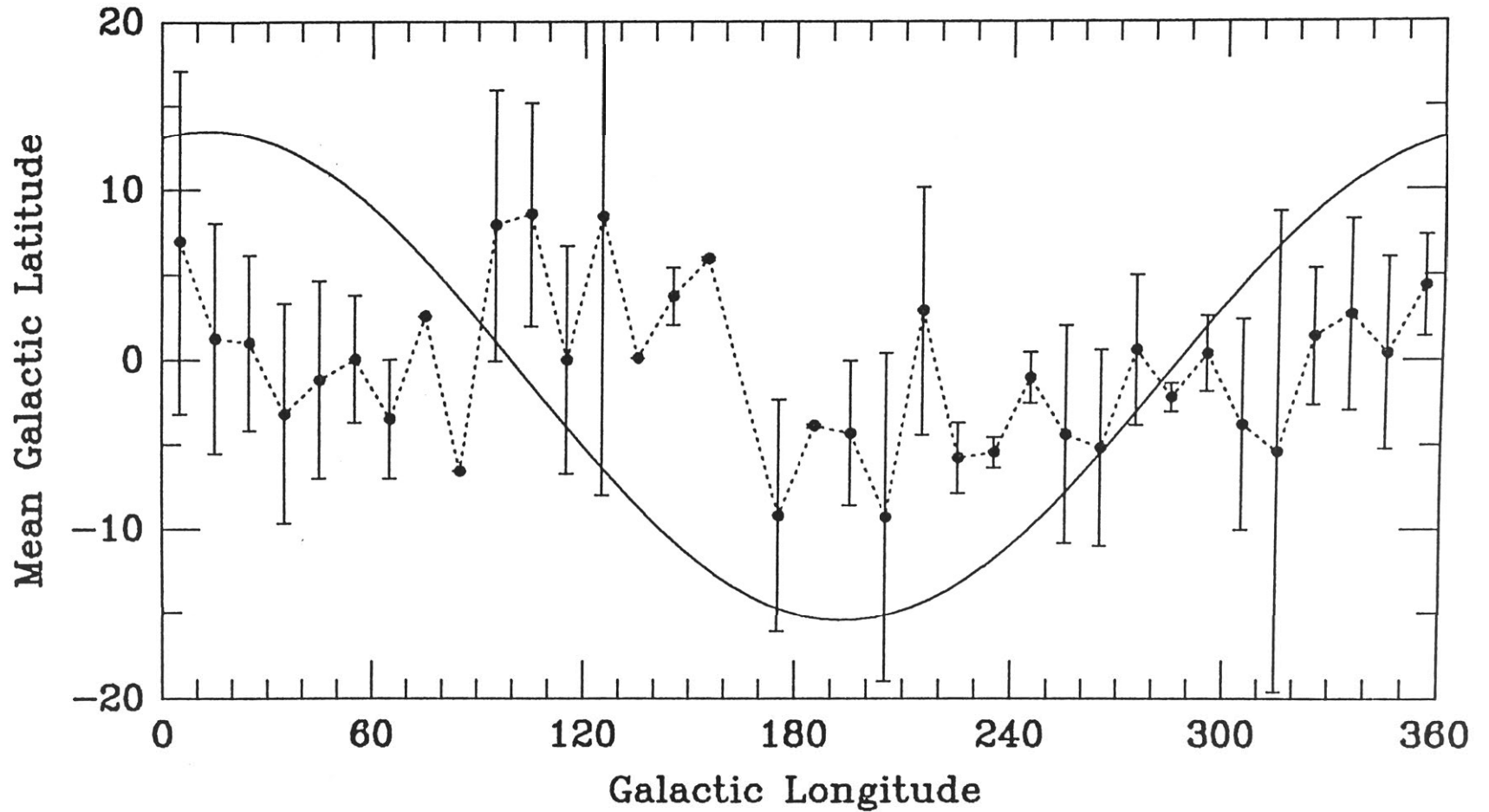
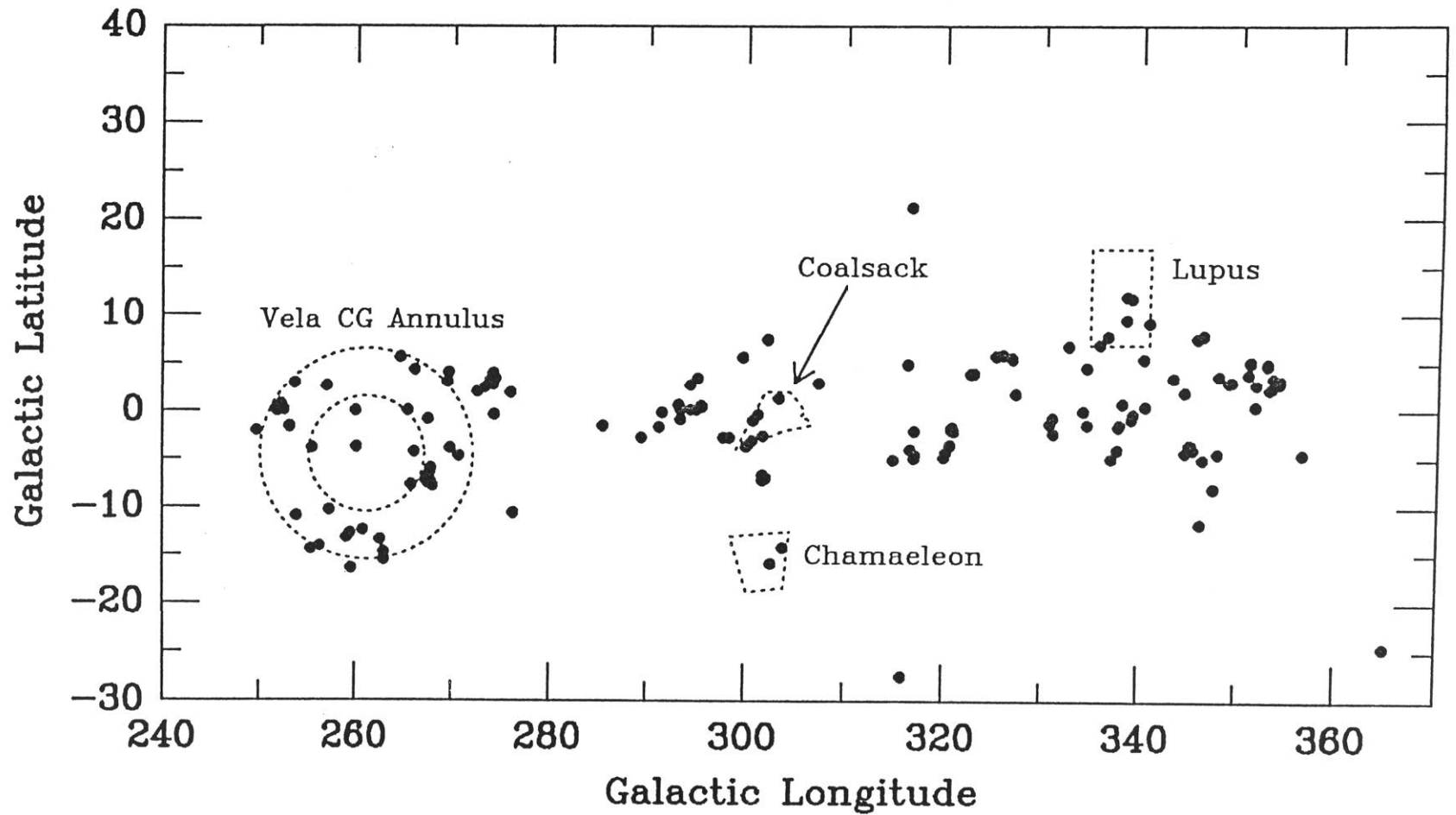


Figure 2.5: The galactic distribution of only the clouds in this work. The three major southern dark cloud complexes of Chamaeleon, Lupus and the Coalsack are indicated, as is the annulus locating the majority of cometary globules (CGs) in the Vela-Gum complex. Note that not all the clouds in this annulus are CGs.



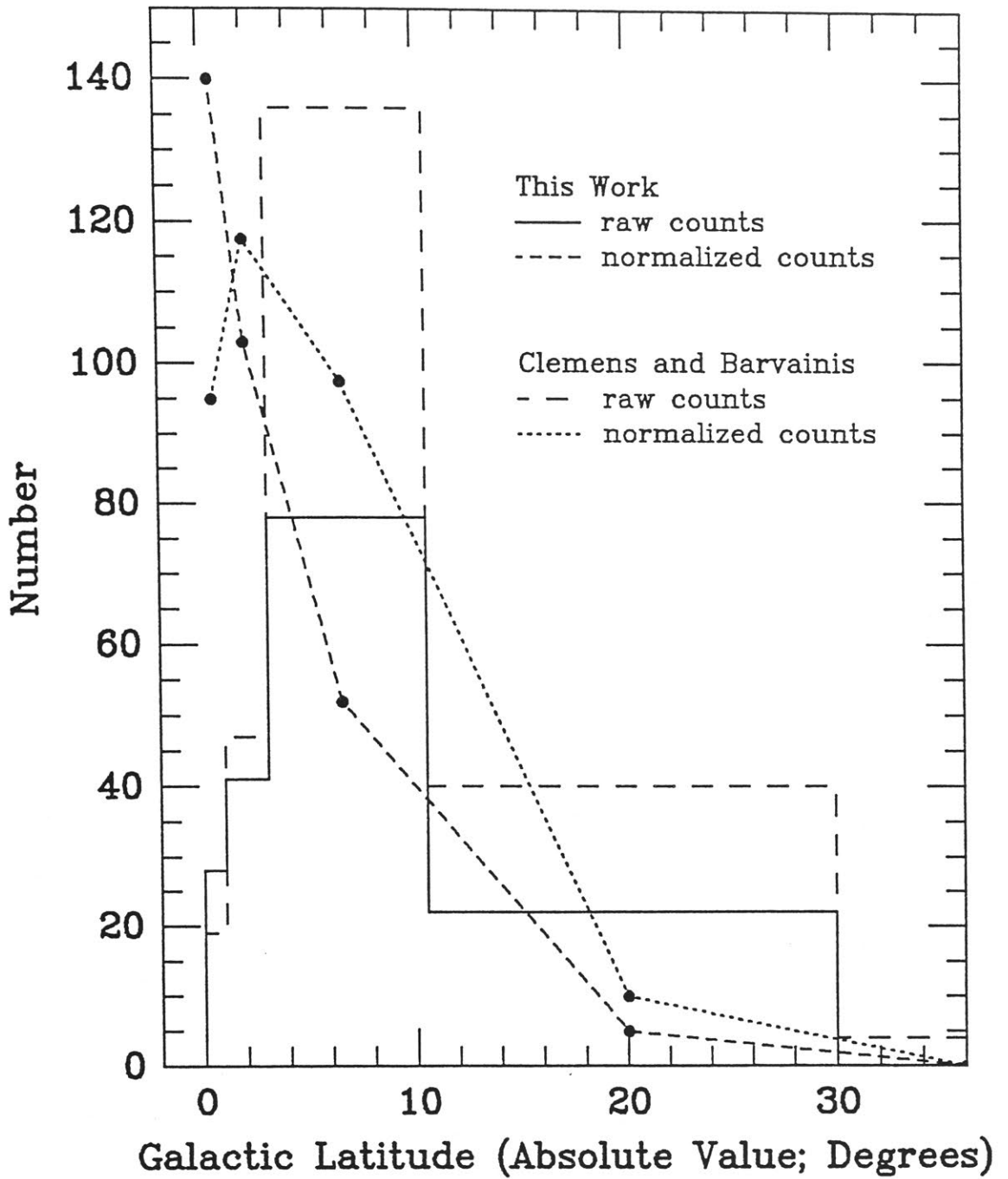


Figure 2.6: The galactic latitude distribution of the clouds in this work and CB. The latitude axis has been folded about $b = 0^\circ$. To produce the normalized counts, the raw counts have been divided by the solid angle subtended by each bin.

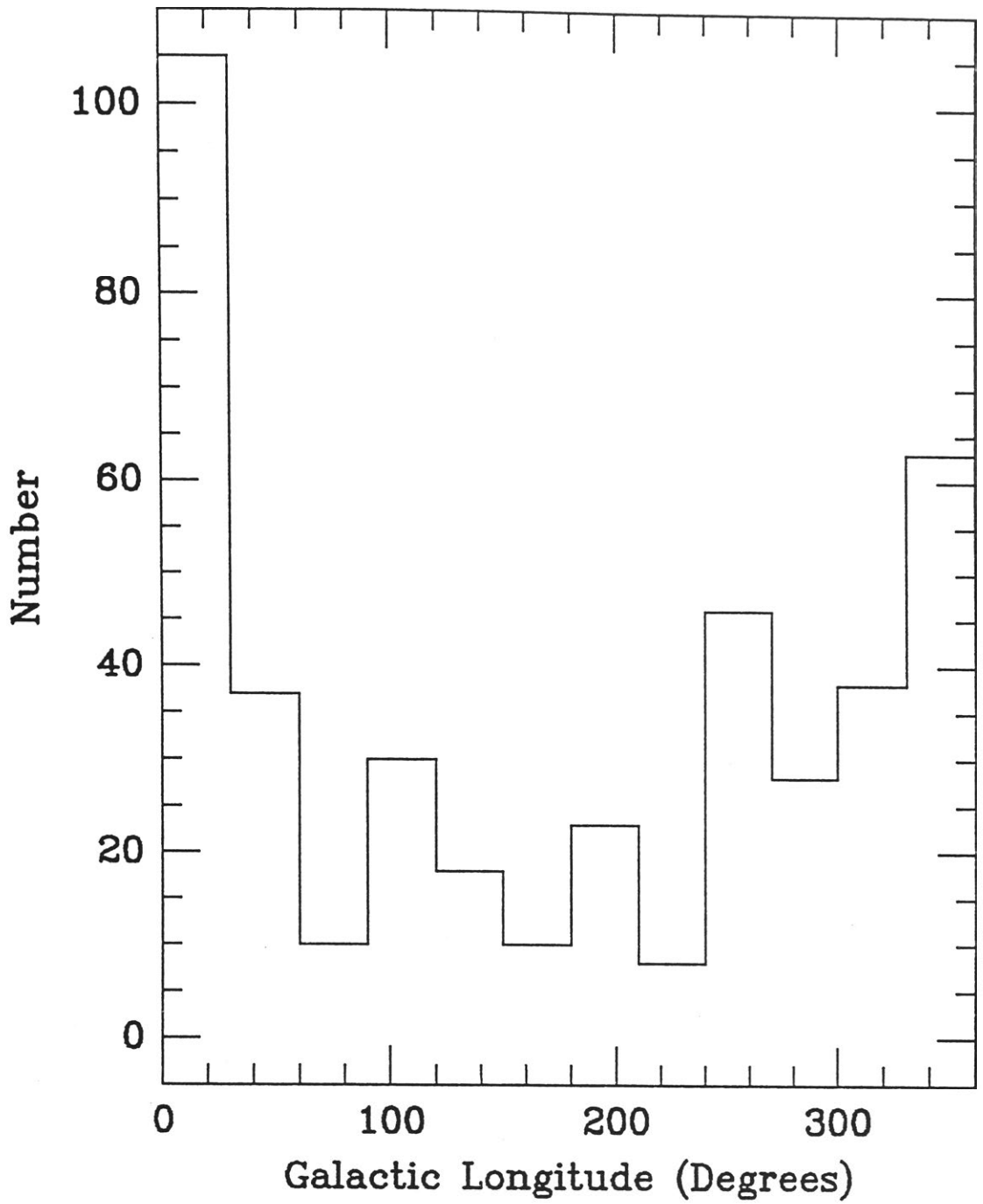


Figure 2.7: The combined galactic longitude distribution of the clouds in this work and CB.

samples, and the normalized counts, where the raw counts have been normalized by the solid angle subtended by each bin. In this plot the latitude distribution has been folded about $b = 0^\circ$. The width of the normalized distribution in b is a measure of the proximity of the sample, assuming the scale height is the same as that of the larger molecular cloud complexes seen in CO emission (Clemens, Solomon and Sanders 1988; CB). We expect the majority of the sample to be nearby (i.e., < 1 kpc) because of the lack of foreground stars seen towards the clouds. Assuming this, the width of the CB normalized distribution, $10^\circ - 12^\circ$, implies a mean distance of ~ 600 pc (CB). The normalised CB sample lacks a central peak due to bias against selecting clouds near the galactic equator. For this work, no bias exists against selecting clouds near the galactic equator, which is reflected in the central peak of the normalized distribution. The peak of this distribution, at $\sim 5^\circ$, is much narrower than the CB peak, implying a mean distance of more than 1 kpc with the assumption of similar scale heights. This does not seem to be a realistic figure for such a sample of small optically selected dark clouds, particularly as noted above the lack of foreground stars seen toward them.

The assumption of similar scale heights for the large and small molecular clouds must be treated with caution, since the large clouds are identified by their CO emission and are in general more distant. The spatial distribution of the large and small clouds may also differ significantly, as pointed out in chapter 1. While not doubting that the CB sample may have a mean distance of 600 pc, the method used to infer this figure appears doubtful, since it does not seem applicable for our sample. By selecting against clouds near the Galactic plane, CB have introduced a bias into their sample which shows up in their assumption of similar scale heights, i.e., their assumption produces reasonable distance estimates when there is no reason to suggest that it should. If CB had

not selected against the low galactic latitude clouds then we may expect their distribution to be peaked about $b = 0^\circ$, as ours is, since the high density of background stars in this region would result in the identification of a significant number of new clouds. Alternatively, in our study we are mostly likely biased against clouds with $|b| > 10^\circ$, since they are difficult to distinguish as dense clouds due to the lack of a sufficient number of background stars to highlight them, particularly on the blue J plates. Inclusion of more of these clouds in our sample would widen our normalized distribution and lower our distance estimates based on equal scale heights.

Figure 2.7 show the combined galactic longitude distribution of both samples. CB note that the strong peak at $0^\circ - 30^\circ$ is most likely caused by the large number of background stars in this region. The peak is also seen in the $330^\circ - 360^\circ$ range for the same reason, although it is not as strong. This may be due to CB using both blue and red Schmidt plates to identify their clouds, since the density of background stars is likely to be greater in the red, and so identification of the smallest clouds would be made easier. It may also be due to the Scorpius–Ophiuchus dark cloud lying in the $330^\circ - 360^\circ$ Galactic longitude range, resulting in less globules being distinguishable, combined with the Scutum–Sagittarius star cloud lying within the $0^\circ - 30^\circ$ longitude range, enhancing the identification of globules in this range. CB found no correlation between the cloud position angle and the direction of the galactic plane, concluding that the Bok globules “retain no memory of the galactic plane orientation in their optical shapes”. A similar comparison has not been made in this study, since it would seem unlikely that we should find the opposite is true for our sample.

2.4 IRAS properties

The Infrared Astronomical Satellite (*IRAS*) was launched in January 1983 as a joint venture between the United States, the Netherlands and the United Kingdom to survey the sky at four wavebands centred on 12, 25, 60 and 100 μm . *IRAS* ceased operations in November 1983 when its liquid helium supply was exhausted. During its 10 month operation *IRAS* successfully surveyed 96% of the sky down to a limiting flux level of ~ 0.5 Jy at the three shortest wavelengths and ~ 1.5 Jy at 100 μm . The resulting Point Source Catalogue (PSC) contains some 250,000 sources, including many candidate YSOs. A complete description of the *IRAS* mission and the resulting catalogues may be found in Beichman *et al.* (1985). In this section *IRAS* point sources associated with the clouds in table 2.1 are identified, and comparisons made with other studies of *IRAS* point sources associated with dark clouds.

In order to study the *IRAS* properties of their sample of dark clouds, CB defined “core”, “envelope” and “reference” regions for each of their clouds. The core region was taken to be the cloud optical area, the envelope region to have twice the semi-major and semi-minor axes of the core region but not including it, and the reference region to have axes twice that of the envelope region but not including the other two regions. They then located every *IRAS* source lying within these regions from the PSC.

In this work, we have searched for *IRAS* point sources lying within the cloud’s optical boundaries, and have not been concerned with envelope and reference regions. Thus we are only interested in detecting “core” sources. The procedure used to identify the *IRAS* sources associated with the dark clouds is similar to that used by Parker (1989). For each cloud in table 2.1, a search radius of 2 arcminutes greater than the cloud’s semi-major axis was used to locate all

possible *IRAS* associations for each cloud. Such a search radius ensures that all sources lying within the optical cloud area will be detected, plus some outside of this region. No flux criteria were imposed at this stage, to enable comparison with other works which have varying criteria for the selection of *IRAS* sources (i.e., CB; Beichman *et al.*, 1986; Benson and Myers, 1989).

The position of the *IRAS* source with respect to the cloud was then checked by generating positional overlays for each possible association, as described in section 2.2, and locating the point source on the Schmidt plates. This search found 83 *IRAS* sources located within the optical boundaries of 76 clouds. Table 2.2 lists the dark clouds which have one or more *IRAS* associations. Column 1 lists the dark cloud name, column 2 the *IRAS* name, which is derived from the source's 1950.0 co-ordinates specified in hours, minutes and tenths of minutes of right ascension, and degrees and minutes of declination. Columns 3 and 4 list respectively the seconds of time in right ascension and seconds of arc in declination for the source. Combining columns 2, 3 and 4 then gives the position of the *IRAS* source. Columns 5 – 8 give the flux in each *IRAS* waveband, with the flux detection quality in parentheses (see below).

2.4.1 Comparison with CB associations

In this section, the properties of the *IRAS* associations are compared with those of CB subjecting our sample to their selection criteria.

The PSC contains a correlation flag which indicates the point like nature of the sources (labelled 'CORR1' in the PSC 2.0). Correlation coefficients below 95 indicate that the source is not well represented by a point source and contains some spatial structure. The PSC also tabulates a detection quality flag (FQUAL) for each *IRAS* waveband, shown in parentheses in columns 5 – 8 of table 2.2. A

Table 2.2: *IRAS* sources associated with southern Bok globules listed in table 2.1.

DC Name	<i>IRAS</i> Name	α (sec)	δ (")	<i>IRAS</i> flux density (Jy)			
				12 μm	25 μm	60 μm	100 μm
259.5-16.4	07127-4828	46	32	0.27 (1)	0.25 (1)	0.85 (3)	5.16 (1)
259.5-16.4	07128-4820	51	55	0.30 (1)	0.25 (1)	0.76 (3)	6.27 (1)
255.3-14.4	07144-4352	28	41	0.25 (1)	0.37 (1)	0.44 (2)	8.88 (3)
256.2-14.1	07178-4429	54	24	6.68 (3)	7.60 (3)	13.12 (3)	33.59 (3)
262.9-14.7	07309-5039	58	38	0.29 (1)	0.25 (1)	0.62 (1)	6.55 (3)
262.5-13.4	07372-4945	13	20	0.25 (1)	0.25 (1)	0.61 (2)	8.92 (3)
260.7-12.4	07378-4745	50	17	0.25 (1)	0.25 (1)	1.79 (3)	13.15 (3)
257.2-10.3	07391-4342	06	07	0.25 (1)	0.25 (1)	0.94 (3)	4.80 (3)
253.3-1.6	08076-3556	40	07	0.63 (3)	3.73 (3)	18.25 (3)	47.54 (2)
251.8+0.0	08103-3346	22	06	0.25 (1)	0.25 (1)	0.64 (1)	5.43 (3)
251.7+0.2	08105-3335	32	52	0.25 (1)	0.25 (1)	0.40 (1)	4.08 (3)
252.5+0.1	08124-3422	29	02	0.25 (1)	0.30 (3)	11.85 (3)	40.55 (3)
252.2+0.7	08140-3340	04	43	0.25 (1)	0.25 (1)	0.40 (1)	3.31 (3)
265.7-7.7	08171-4933	11	47	0.25 (1)	0.25 (1)	0.72 (1)	13.06 (3)
267.4-7.5	08242-5050	16	44	0.82 (3)	6.31 (3)	26.13 (3)	58.27 (2)
267.2-7.2	08250-5030	03	34	0.25 (1)	0.25 (1)	1.20 (3)	17.08 (3)
267.7-7.4	08261-5100	11	39	0.91 (3)	2.50 (3)	4.29 (3)	10.91 (3)
253.6+2.9	08267-3336	44	31	0.39 (3)	1.09 (3)	3.20 (3)	14.28 (3)
259.9-0.0	08337-4028	42	02	0.25 (1)	39.95 (3)	347.60 (1)	1266.00 (2)
259.9-0.0	08337-4024	43	40	0.47 (3)	0.90 (3)	2.31 (1)	35.21 (1)
256.9+2.6	08354-3626	24	09	0.25 (1)	0.25 (1)	0.70 (3)	5.44 (3)
276.2-10.6	08433-5945	22	06	0.32 (1)	0.18 (3)	1.83 (3)	9.74 (2)
272.5+2.0	09293-4824	21	57	0.25 (1)	0.28 (1)	0.46 (1)	3.03 (3)
274.3+3.4	09430-4838	02	59	0.25 (1)	0.25 (1)	0.40 (1)	3.30 (3)
275.9+1.9	09449-5052	57	06	0.25 (1)	0.27 (1)	8.16 (3)	22.30 (3)
289.3-2.8	10471-6206	07	22	0.25 (1)	0.27 (2)	5.36 (3)	37.11 (3)
294.9+0.1	11403-6126	23	47	0.60 (1)	0.52 (3)	3.57 (3)	43.91 (2)
297.7-2.8	11590-6452	03	11	0.25 (1)	6.53 (3)	77.38 (3)	192.90 (3)
299.6+5.6	12239-5649	54	46	0.25 (1)	0.25 (1)	0.76 (1)	6.16 (3)
301.7-6.7	12345-6910	32	33	1.07 (3)	2.41 (3)	4.44 (3)	14.63 (1)
301.7-2.6	12369-6509	56	10	0.37 (3)	0.25 (1)	0.92 (1)	11.99 (1)
302.1+7.4	12427-5508	43	38	0.25 (1)	0.25 (1)	2.23 (3)	12.17 (3)
303.8-14.2	13036-7644	41	03	0.25 (1)	1.05 (3)	6.38 (3)	22.57 (3)
307.3+2.9	13224-5928	26	07	1.20 (3)	2.35 (3)	8.19 (3)	37.21 (3)
316.5+21.2	13546-3941	41	45	0.47 (2)	1.13 (3)	0.40 (1)	201.90 (1)
316.5+21.2	13547-3944	42	07	7.81 (3)	8.94 (3)	67.49 (3)	201.90 (3)
314.8-5.1	14437-6503	43	30	0.40 (3)	0.25 (1)	0.67 (1)	44.64 (1)
314.8-5.1	14451-6502	07	55	1.26 (3)	1.46 (3)	4.66 (3)	22.71 (2)
323.0+4.0	15075-5307	33	34	0.25 (1)	0.25 (1)	0.67 (1)	11.34 (3)
323.0+4.0	15075-5308	33	56	0.43 (3)	0.26 (3)	1.58 (3)	7.82 (1)

Table 2.2 *continued*

DC Name	IRAS Name	α (sec)	δ (")	IRAS flux density (Jy)			
				12 μm	25 μm	60 μm	100 μm
325.2+5.8	15133-5025	23	42	0.25 (1)	0.65 (1)	0.42 (1)	8.46 (3)
320.7-1.7	15148-5911	52	23	1.33 (1)	1.15 (3)	10.69 (3)	123.50 (1)
320.5-3.5	15210-6051	00	51	0.25 (1)	0.25 (1)	1.43 (2)	12.31 (3)
320.5-3.6	15215-6056	32	19	0.25 (1)	0.49 (3)	3.39 (3)	16.55 (3)
320.1-4.3	15223-6146	21	04	0.25 (1)	0.25 (1)	2.01 (3)	11.59 (2)
326.8+5.6	15227-4948	42	55	0.25 (1)	0.25 (1)	0.46 (1)	7.09 (3)
319.9-4.8	15230-6211	00	52	0.25 (1)	0.20 (2)	2.01 (3)	15.38 (3)
326.9+5.5	15233-4949	22	46	0.25 (1)	0.25 (1)	0.40 (1)	6.78 (3)
332.7+6.8	15468-4521	53	45	0.25 (1)	0.27 (1)	0.47 (1)	7.89 (3)
338.6+9.5	16009-3927	55	56	1.27 (3)	0.44 (2)	0.58 (1)	6.56 (2)
334.6+4.6	16029-4548	57	08	1.56 (3)	1.10 (3)	1.04 (1)	49.54 (1)
330.7-1.3	16097-5247	45	03	0.83 (3)	1.06 (1)	5.92 (1)	49.95 (2)
334.6-1.4	16277-5001	46	41	1.35 (3)	3.68 (1)	3.82 (2)	99.48 (1)
334.6-1.4	16282-5002	15	27	6.80 (1)	4.30 (1)	2.45 (3)	304.00 (1)
338.2+0.8	16328-4553	53	59	4.04 (1)	5.05 (1)	35.59 (1)	323.00 (3)
339.3-0.3	16415-4550	33	07	2.15 (3)	1.82 (3)	11.07 (3)	222.30 (1)
344.5+2.0	16510-4026	05	47	0.96 (3)	1.68 (2)	15.87 (2)	56.80 (1)
337.1-4.9	16549-5030	59	58	0.41 (3)	0.28 (1)	0.63 (1)	12.21 (2)
337.1-4.9	16554-5031	27	00	0.36 (1)	0.84 (3)	1.98 (3)	48.65 (1)
351.2+5.2	16590-3313	01	14	0.80 (2)	1.30 (3)	1.75 (1)	8.82 (1)
351.2+5.1	16594-3315	25	08	2.71 (3)	2.92 (3)	0.88 (1)	10.02 (1)
351.2+5.1	16595-3311	31	15	1.61 (3)	1.49 (3)	1.45 (1)	26.75 (3)
349.0+3.0	17011-3613	09	59	0.37 (2)	0.54 (3)	4.50 (3)	35.59 (3)
349.2+3.1a	17012-3603	12	10	0.30 (1)	0.89 (3)	5.31 (3)	30.70 (3)
349.2+3.1b	17014-3606	30	17	0.45 (1)	0.39 (1)	5.79 (3)	25.77 (1)
349.3+3.1	17015-3559	35	01	3.25 (3)	1.64 (3)	3.69 (3)	23.92 (1)
352.9+5.0	17048-3158	49	52	0.41 (1)	0.30 (1)	2.84 (1)	17.32 (3)
352.9+4.8	17056-3204	39	26	0.42 (3)	0.44 (1)	2.81 (1)	16.70 (3)
351.8+2.8	17102-3411	12	55	1.04 (1)	1.83 (1)	2.93 (3)	42.10 (1)
353.5+3.5	17122-3222	17	06	1.55 (1)	0.36 (1)	3.25 (3)	22.46 (1)
354.2+3.2	17151-3202	08	24	1.65 (1)	1.05 (2)	10.81 (3)	43.68 (2)
353.3+2.4	17156-3312	36	45	1.55 (1)	1.75 (1)	15.31 (3)	71.84 (3)
354.1+2.9c	17157-3212	42	58	1.12 (3)	3.11 (3)	16.61 (3)	44.17 (1)
345.0-3.5	17159-4324	54	04	0.50 (1)	0.30 (1)	2.72 (3)	48.22 (1)
353.1+2.3	17159-3324	55	16	0.64 (2)	3.82 (3)	16.13 (3)	278.50 (1)
345.2-3.6	17169-4314	56	39	0.25 (1)	0.72 (1)	3.18 (1)	23.99 (3)
345.2-3.6	17172-4316	15	54	0.39 (3)	0.78 (3)	4.18 (2)	29.01 (3)
344.6-4.3	17181-4405	09	48	2.65 (3)	3.63 (3)	59.88 (3)	170.00 (2)
351.7+0.5	17187-3531	45	57	1.83 (3)	3.48 (1)	99.61 (1)	446.60 (1)
345.4-4.0	17193-4319	18	24	0.25 (1)	0.68 (3)	4.74 (3)	22.98 (3)
345.4-4.0	17195-4320	30	07	0.54 (3)	0.96 (1)	4.74 (1)	25.43 (1)
356.5-4.5	17518-3414	54	03	0.44 (1)	0.37 (1)	1.40 (2)	15.85 (3)
315.8-27.5a	19025-7840	30	39	0.25 (1)	0.25 (1)	0.40 (1)	4.36 (3)

quality flag equal to 3 (a good detection) or 2 (a moderate detection) indicates that the source was detected by *IRAS* in that waveband on more than one survey pass. A flux quality of 1 indicates that the detection is an upper limit.

Detection quality at 100 μm and 60 μm

The mean point source correlation coefficient for the 56 sources in table 2.2 detected at 100 μm is 98.5 with a 1σ of 1.7. CB found for their 74 sources with 100 μm detections a mean of 98.2 ($1\sigma = 1.7$). Our sample has 1 source with a coefficient below 95 (at 92), while CB found two sources below 95. The mean coefficient for sources detected at 60 μm (52 sources) is 98.6 ($1\sigma = 1.6$), with 1 source having a coefficient below 95 (at 94). CB found 56 sources with detections at 60 μm having a mean coefficient of 98.2 ($1\sigma = 2.2$), with 6 sources below 95. The majority of sources detected at 60 μm and 100 μm thus satisfy the *IRAS* criteria of being point sources and would appear to suffer little from confusion with nearby cirrus.

Contamination at 100 μm

CB argue that their 100 μm detections are not strongly affected by the presence of nearby cirrus, for reasons outlined below. The *IRAS* cirrus flag indicates the number of 100 μm only detections in a $1/2^\circ \times 1/2^\circ$ box about each point source, with values of greater than three indicating cirrus contamination. CB point out that for a sample of optically selected small molecular clouds with a mean size of $4'$, the cirrus quality flag would have to be greater than about 36 to indicate cirrus contamination. Their arguments apply equally well to our sample of clouds with a mean size of $3'$. The mean value of the cirrus flag for the CB sample is 6.6 ± 2.4 . They estimate from this figure that the mean

contamination from cirrus will be about 9%. The mean value for the cirrus flag of this sample is also 6.6 ± 2.4 ; therefore the clouds of this work are also relatively unaffected by cirrus contamination, for the same reason. CB reinforce their argument that the $100 \mu\text{m}$ detections are cirrus free by a comparison with the sources found in their reference regions. They find that $100 \mu\text{m}$ only sources are more strongly associated with the core regions than the reference regions. The $100 \mu\text{m}$ detections of Bok globules by *IRAS* thus represent true globule detections uncontaminated by cirrus.

Core Sources

A comparison is shown in figure 2.8 of the types of sources found in the core regions of the two samples. In this plot, each *IRAS* source is characterised by the band showing the largest detected flux. Both samples are dominated by $100 \mu\text{m}$ detections and are therefore relatively cool sources. However, note that $\sim 28\%$ of the CB sources are characterised by $12 \mu\text{m}$ detections, while this figure is only $\sim 6\%$ for the current sample. Our distribution is almost totally 60 and $100 \mu\text{m}$ dominated ($\sim 89\%$) without correcting each band for the number of chance associations, while the same figure for the CB sample is $\sim 66\%$. This figure for the CB sample increases to $\sim 90\%$ after correction for chance associations (by comparison with the CB reference regions). A possible explanation for the difference seen in the two samples is given below, but it does not seem satisfactory.

Sources which have $S_{12} \geq S_{25}$ (where S_i is the flux in Janskys at the wavelength i in microns) when detected in both wavebands, or have $12 \mu\text{m}$ only detections are most likely to be stars. CB found that 41 of their 145 core sources have these flux characteristics ($\sim 28\%$), while the present work contains only 10 such sources ($\sim 12\%$). CB conclude from the galactic distribution of their

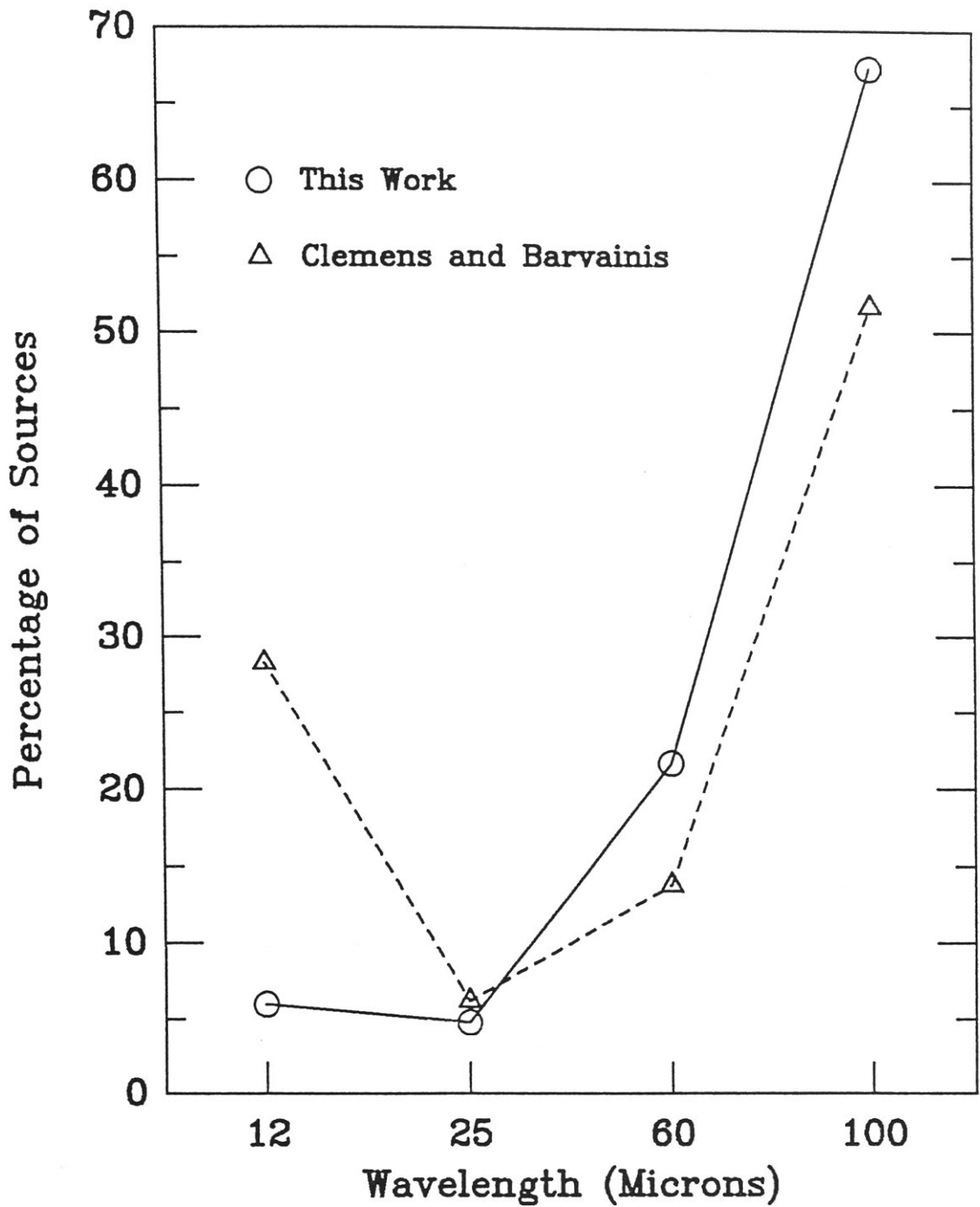


Figure 2.8: Normalized distribution of *IRAS* PSC detections located within the optical boundaries of the clouds of this work and CB, verses the band containing the dominant detection. Both samples are dominated by 100 μm sources.

IRAS sources (peaked strongly between 0° and 30° in longitude) that the majority of these sources are obscured background giant stars in the Galactic bulge. Our smaller sample is peaked between 320° and 350° which would also indicate that these stellar like sources are most likely background giant stars. Of the 10 sources, 4 have possible optical counterparts and so may be foreground stars. We have seen for the CB dark cloud sample that the Galactic longitude distribution is peaked between 0° and 30° , as is the *IRAS* sample characterised by detections in the two lowest wavebands. The large density of background stars in this longitude range, due mainly to the presence of the Scutum–Sagittarius star cloud, is the most likely reason for these peaks, as well as the relatively large number of core sources with star-like detections (28% for the CB sample). These features are not seen in the sources of the present work. A clue to the difference may exist in the relative number of clouds found about galactic longitude 0° for the two samples. As mentioned above, CB found a large number of their clouds in the range $0^\circ - 30^\circ$ ($\sim 42\%$), most likely due to a combination of the large number of background stars in this region and the use of survey plates of two wavelengths. In the range $330^\circ - 360^\circ$, we find $\sim 34\%$ of our clouds. However, the CB sample covers a much larger range in Galactic longitude ($0^\circ - 240^\circ$, $330^\circ - 360^\circ$) than the present sample ($240^\circ - 360^\circ$), and so the difference in these percentages may be significant. As mentioned previously, the Scutum–Sagittarius star cloud lies in the range $0^\circ - 30^\circ$, and so may be responsible for both the large number of identified globules and $12\ \mu\text{m}$ background sources in this region. There does not appear to be any bias in the *IRAS* catalogue for either direction in longitude about the Galactic Centre (i.e., due to *IRAS* not having surveyed that part of the sky). In fact the plot of $12\ \mu\text{m}$ only sources in the *IRAS* Explanatory Supplement appears relatively symmetric about $b = 0^\circ$. We have not been able to come up with a satisfactory reason as to why this difference should be seen in the two samples.

CB define warm *IRAS* cores to be those with $S_{25} > S_{12}$ or 25 μm only detections, of which they found 8 (6%), while in the present work there are 4 such sources (5%). In neither sample is there a source which shows detected $S_{60} \gtrsim S_{100}$, though CB found 21 sources (14%) with detections at 60 μm which had larger 100 μm upper limits, compared with 15 (21%) for this work. In both samples the majority of sources are cool, i.e. $S_{100} \gtrsim S_{60}$ (52% for CB, 65% for this work).

Following CB, the globules may be divided into two categories, bright and dark, where bright globules are those with bright rims (such as the cometary globules) or contain embedded reflection nebulosity. For the clouds in this work, 33 *IRAS* point sources were detected toward 55 bright globules (60%) and 50 toward 114 dark globules (44%). For CB, the corresponding figures are 22 of 31 (71%) for bright globules and 87 of 217 (40%) for the dark globules. For the bright globules in our work which are not labelled ‘CG’ in table 2.1 we find 13 point sources toward 15 clouds (87%). It would appear that the bright rims of the CGs do not appear bright in the infrared, or that they are not a good indication of sights of infrared point sources (20 detections from 40 cometary globules), while the reflection nebulosities and the like, or their embedded exciting sources, are readily detected and are therefore a good indicators of the sites of star formation.

2.4.2 Comparison with Beichman *et al.* associations

In this section a comparison is made of the *IRAS* sources in this work with those of CB and Beichman *et al.* (1986, hereinafter BM86) with all sources subject to the selection criteria of BM86.

BM86 searched for *IRAS* sources associated with a sample of dark cloud cores embedded in larger cloud complexes, where the cores are defined by their

emission in CO or NH₃ as well as by their optical appearance. These cores come from the lists of Myers, Linke and Benson (1983) and Myers and Benson (1983). BM86 required that their *IRAS* associations have detections in the 25 μm band, or in both the 60 and 100 μm bands, in an attempt to exclude 12 μm only sources (stars) and 100 μm only sources (which may be contaminated by cirrus). In order to compare all three samples the selection criteria of BM86 have been applied to the sources in table 2.2.

Figure 2.9 shows two $\log(S_{12}/S_{25})$ versus $\log(S_{25}/S_{60})$ colour-colour space plots. The upper is taken from CB and shows the *IRAS* sources from both CB and BM86 which have been detected at 12, 25 and 60 μm where the CB sample has been subjected to the selection criteria of BM86. The lower figure shows the same plot for associations in table 2.2 satisfying the BM86 criteria. There appears to be no significant differences between the three samples in these plots. However, it does appear as though the sources associated with dark clouds in our sample and detected in the 12–25–60 μm wavebands are warmer than the bright clouds, based on their position along the $\log(S_{12}/S_{25})$ axis. One might reasonably expect the opposite to have been the case, i.e. sources associated with visible nebulosity are warmer and more energetic, therefore brighter at the shorter wavelengths. However, there are so few sources that this result may not be significant. Figure 2.10 shows a $\log(S_{25}/S_{60})$ versus $\log(S_{60}/S_{100})$ plot of sources detected in these three bands for the three samples. The BM86 sources populate a preferentially warmer region than the CB sample or the sources in this work. It would appear that the *IRAS* sources found in globules tend to be cooler than the sources found in the molecular cloud cores of the dark cloud complexes. The bright cloud sources in this sample appear to occupy a warmer region in $\log(S_{60}/S_{100})$ space than the dark sources, which is opposite to that seen in the 12–25–60 colour-colour plot. There are however only 10 sources common

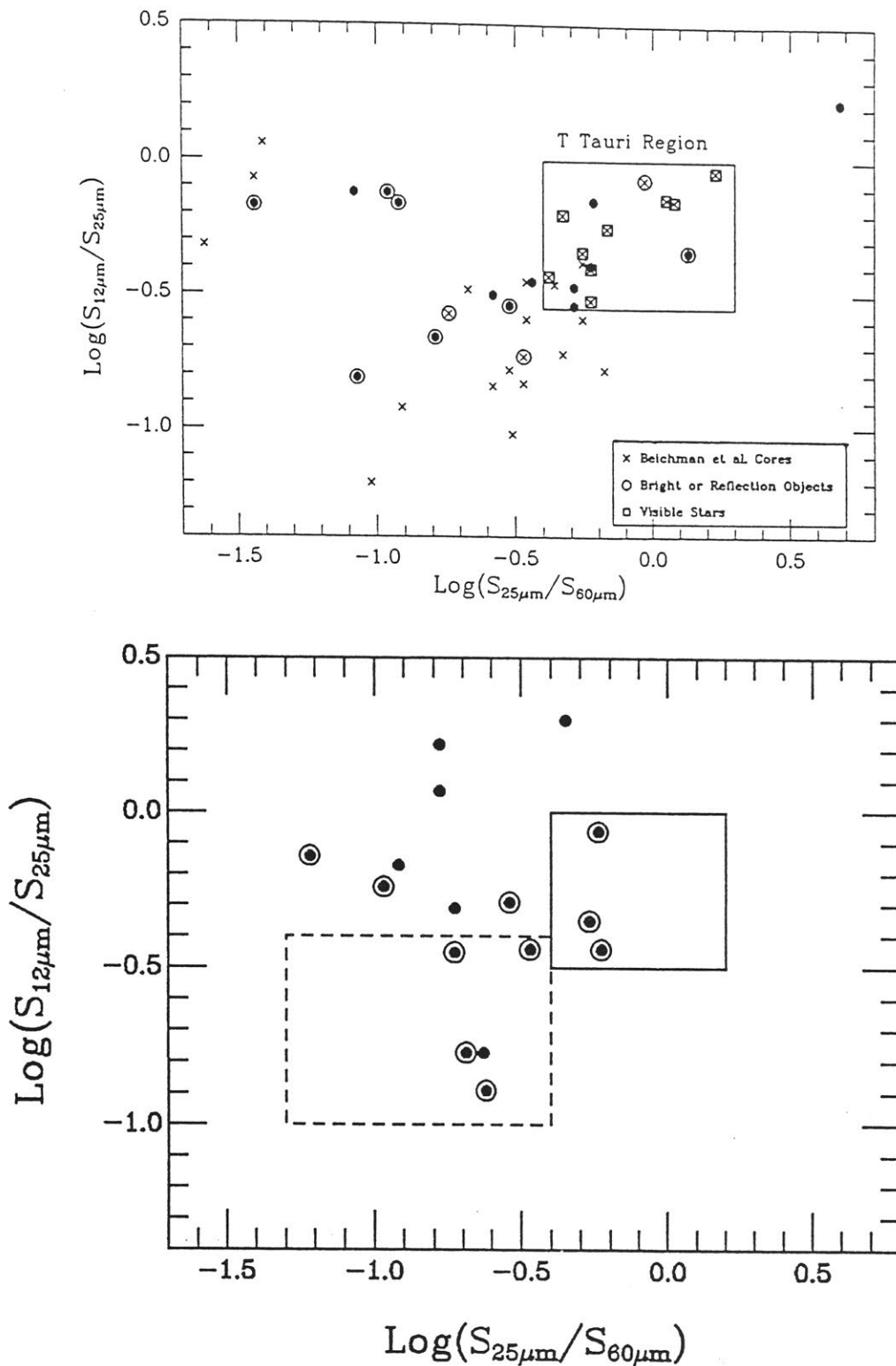


Figure 2.9: The distribution in 12–25–60 μm colour-colour space for the sources in BM86 and CB (upper plot) and this work (lower plot). Also indicated in the lower plot are the regions occupied by T Tauri stars (solid line) and embedded invisible sources (dashed line) (Emerson 1987).

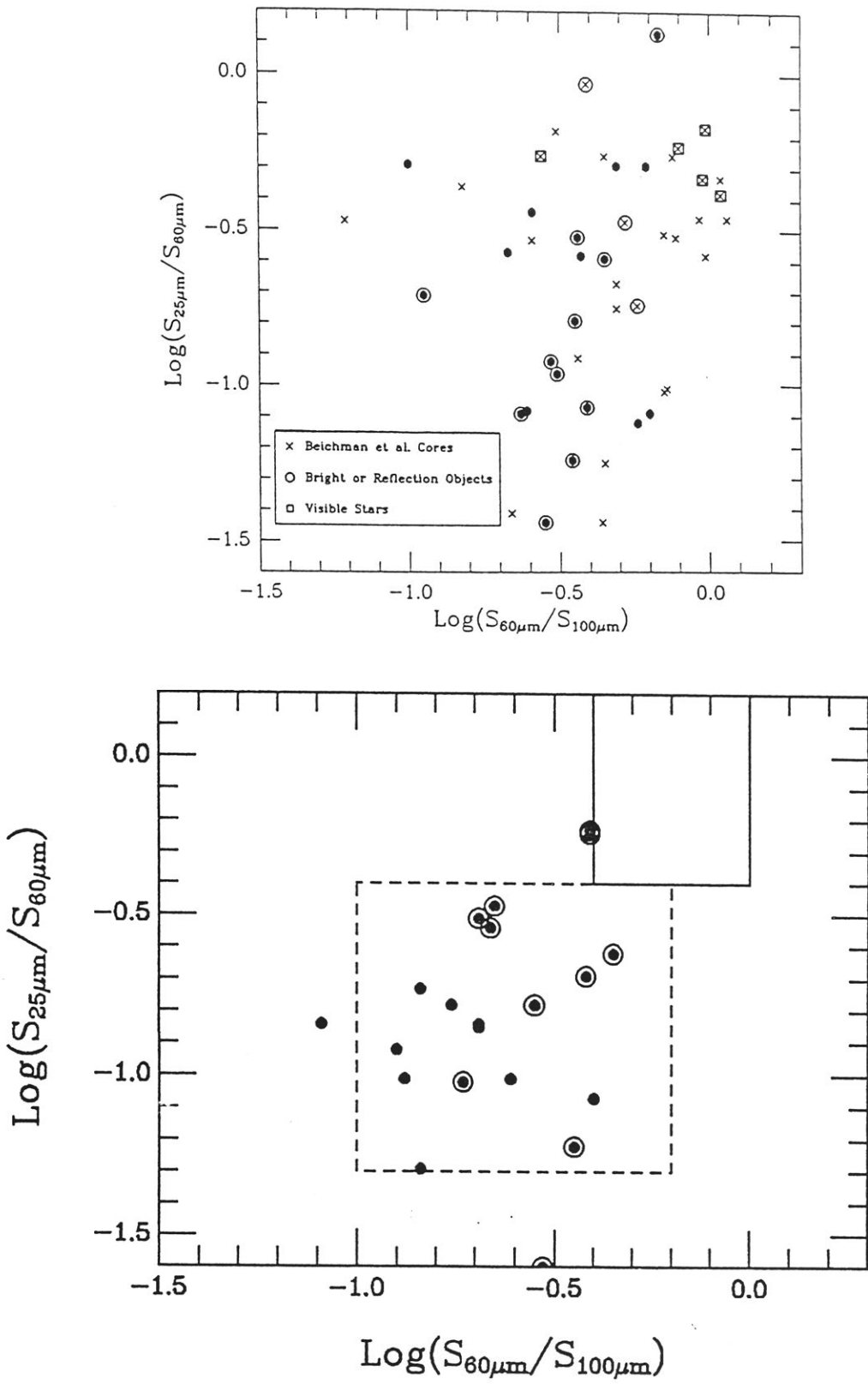


Figure 2.10: As for figure 2.9 but showing the 25–60–100 μm colour-colour space distribution.

to both plots, and so not much significance is placed on this difference.

Emerson (1987) empirically defined regions in *IRAS* colour-colour space occupied by different types of objects. He found that T Tauri stars occupy a range in colour-colour space as defined below:

$$-0.5 \lesssim \log(S_{12}/S_{25}) \lesssim 0.0,$$

$$-0.4 \lesssim \log(S_{25}/S_{60}) \lesssim 0.2,$$

$$-0.4 \lesssim \log(S_{60}/S_{100}) \lesssim 0.0.$$

Emerson also defined an embedded core region, based on those associations in BM86 which do not possess an optical counterpart. As has been seen, the $\log(S_{60}/S_{100})$ colours of the BM86 sample indicate that their sources are warmer than the CB sample and the associations in the present work. It would seem that the BM86 sample does not probe the coldest *IRAS* sources associated with dark clouds, and so the region in colour-colour space occupied by the BM86 associations does not reflect the true distribution of embedded core sources. The BM86 cores lie in the range $-0.7 \lesssim \log(S_{60}/S_{100}) \lesssim 0.0$ while figure 2.10 shows that the CB cores occupy a region bounded by $-1.0 \lesssim \log(S_{60}/S_{100}) \lesssim -0.2$. As a result the definition of the embedded cores region in this work are thus defined to be:

$$-1.0 \lesssim \log(S_{12}/S_{25}) \lesssim -0.4,$$

$$-1.3 \lesssim \log(S_{25}/S_{60}) \lesssim -0.4,$$

$$-1.0 \lesssim \log(S_{60}/S_{100}) \lesssim -0.2.$$

The T Tauri and embedded core regions are plotted in figures 2.9 and 2.10 for our sample. Note that in both plots very few of our sources fall into the T Tauri region, while in the second plot the majority of sources detected are located in the embedded cores region. It is thought that those sources occupying the embedded core region are the best “protostellar” candidates to be found in the PSC (BM86; Myers *et al.*, 1987; Parker, 1989). It is encouraging then that a

large number of our sources are found in this region since we are attempting to identify possible protostellar sources.

Figure 2.11 show the $\log(S_{60}/S_{100})$ verses $\log(S_{100})$ plot for the three samples. The distribution of CB sources in this plot is similar to the present work. All three samples indicate that the brighter globules (as defined by their $\log(S_{100})$) are warmer (as defined by their $\log(S_{60}/S_{100})$ ratio). Note that one of our sources has $\log(S_{100}) > 3$, indicating a very bright 100 μm source.

For sources having blackbody spectra modified by an extinction law, and which have dust temperatures such that $e^{hc/\lambda k T_d} \gg 1$ (which is generally true at the *IRAS* wavelengths), the temperature of the emitting dust is given by (Parker 1989):

$$T_d \simeq \frac{\frac{hc}{k} \left(\frac{1}{\lambda_2} - \frac{1}{\lambda_1} \right)}{(3 + \beta) \ln \left(\frac{\lambda_1}{\lambda_2} \right) + \ln \left(\frac{S_{\lambda_1}}{S_{\lambda_2}} \right)} \quad (2.1)$$

where the emissivity is assumed to follow a power law $\lambda^{-\beta}$, and $\lambda_2 > \lambda_1$. The dust temperatures for the three samples in the longest wavebands are shown in table 2.3, assuming various values of β . The value of $\beta = 0$ corresponds to the dust grains acting purely as blackbodies, while $\beta = 2$ corresponds to crystalline grains. Table 2.3 shows that the BM86 sample is warmer and that the dust temperatures of the CB sample and this work are very similar.

A comparison of the mean 100 μm fluxes of the three samples shows that the BM86 sample is brighter in the far-infrared. The mean 100 μm flux of the BM86 sample is 80 ± 30 Jy, the CB sample 25 ± 5 and this work 34 ± 40 Jy (excluding the source with $S_{100} > 1000$ Jy). That the Beichman *et al.* sources are both warmer and brighter than the sources found in the Bok globules may be a result of those sources heating a larger region of material surrounding the dense cores than is possible by the sources in globules. It may also suggest that

the cloud cores within the complexes are denser than those in globules, and so more radiation from the embedded source is reprocessed into the far-infrared.

Finally, figure 2.12 plots the distribution of 100 μm fluxes for the detected sources in our sample. The dashed line shows the best fit to the upper four flux bins. The slope of this line is essentially the same as that found by CB for a similar plot of their sample (CB figure 11, slope = -0.69 , compared with a slope of -0.63 in figure 2.12). The PSC is incomplete below 3 Jy ($\log(S_{100}) = 0.5$), which is reflected in the size of the first flux bin, i.e. no sources were detected below this value. If the PSC were complete down to 1 Jy ($\log(S_{100}) = 0$) and the same fit were to apply, then the total number of clouds detected at 100 μm would be ~ 120 , i.e. $\sim 70\%$ of the clouds would have been detected by *IRAS*. CB estimated that more than 80% of their clouds would have been detected by *IRAS* using the above analysis. A comparison with figure 11 of CB may indicate that bin 1 ($\log(S_{100}) = 0.5\text{--}1.0$) in figure 2.12 is also incomplete for our sample. This may be seen in table 2.2, where in cases where the 100 μm detections are quoted as upper limits, the flux is generally greater than the *IRAS* sensitivity of 3 Jy at 100 μm . Parker (1989) has noted that the low quality 100 μm detections for sources close to the Galactic plane arises from confusion with background sources and nearby cirrus. As a result, the flux limits for detection at 100 μm are not constant but depend on the surroundings. If we include point sources with upper limits only at 100 μm then the corresponding fit would imply that ~ 170 clouds would have been detected, i.e. a detection rate of 100%. Clemens, Yun and Heyer (1991) have shown with the use of co-added *IRAS* survey data that the cloud detection rate is almost 100% down to the 1 Jy level for the CB clouds. As noted by CB, the clouds with detections below 3 Jy may represent the most quiescent clouds in the sample, i.e. those that are not forming stars. The identification and study of these clouds is important in the overall study of

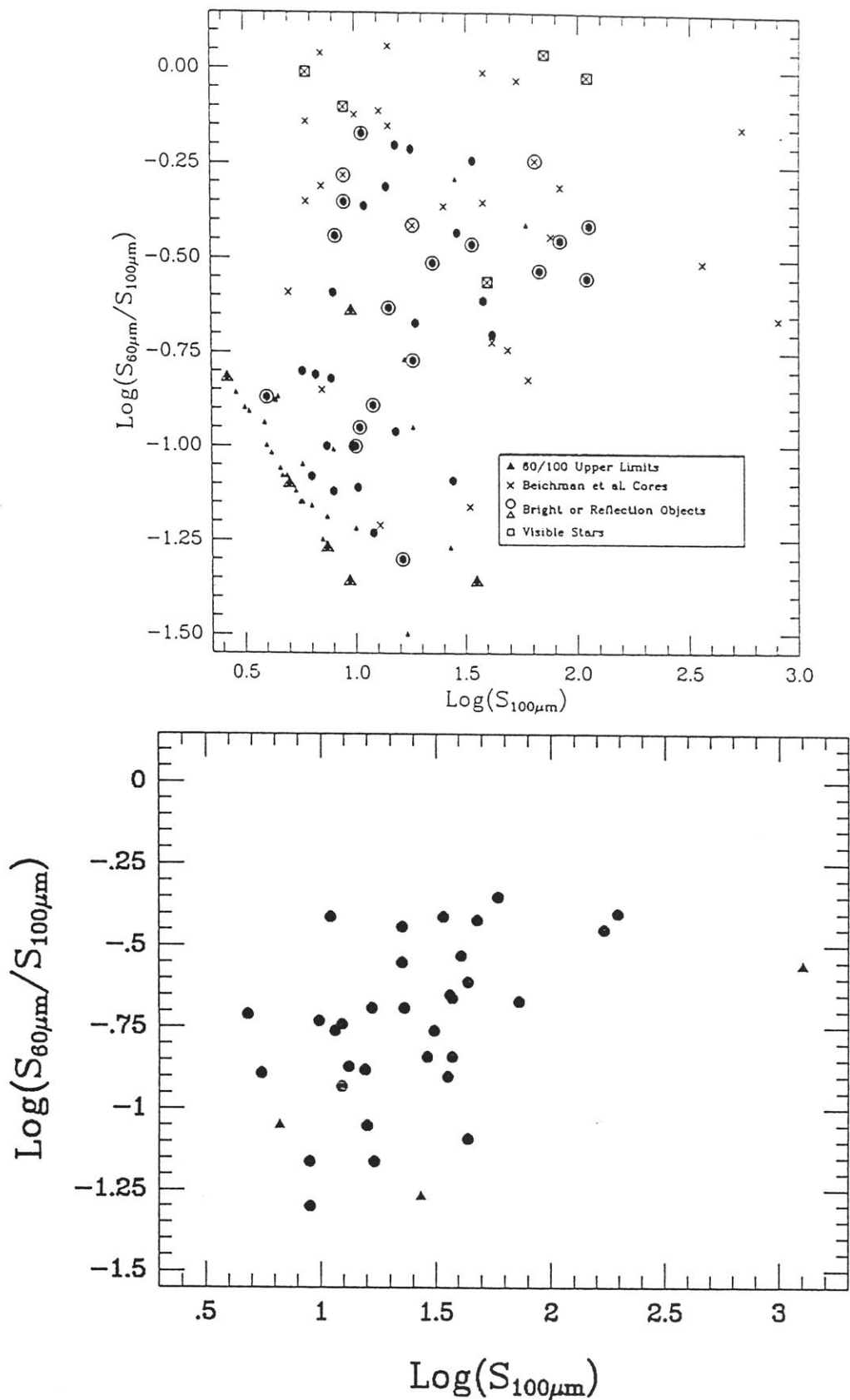


Figure 2.11: The 60–100 μm colour-magnitude distribution for sources in BM86 and CB (upper plot) and this work (lower plot). These plots indicate that the brighter sources are warmer, and that the BM86 sources are warmer than the CB sources or the sources in this work.

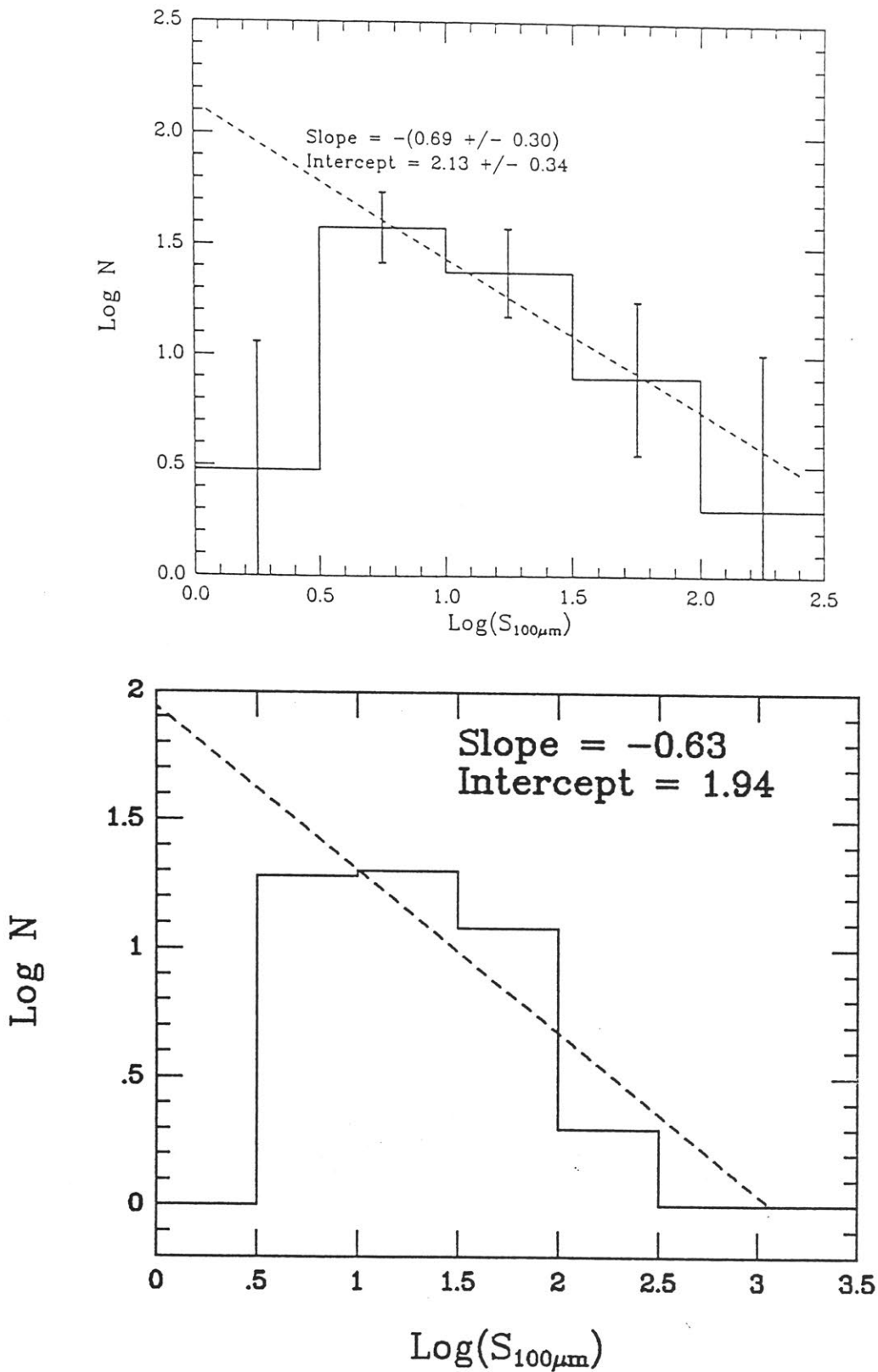


Figure 2.12: The *IRAS* 100 μm detected flux distribution for CB (upper plot) and this work (lower plot). In both figures, the dashed line represents the best fit to the upper four flux bins ($\text{log}(S_{100}) = 0.5\text{--}2.5$).

Table 2.3: Dust temperatures of *IRAS* sources based on *IRAS* 60–100 μm colours.

Sample	β	T(100–60) (K)
Beichman <i>et al.</i>	0	41
	1	34
	2	29
CB	0	31
	1	27
	2	24
This work	0	32
	1	27
	2	24

the star formation process in Bok globules.

2.5 Conclusions

The Catalogue of Southern Dark Clouds by Hartley *et al.* (1986) has been searched for a candidate set of Bok globules satisfying the criteria that they be small ($< 10'$), optically dense and generally isolated from bright nebulosities and other dark clouds. The final list of 169 clouds includes only two clouds not identified by Hartley, and ~ 40 cometary globules, the majority of which are associated with the Vela-Gum complex. These cometary globules may represent an early stage in the formation of isolated Bok globules (Reipurth, 1983; Leung, 1985). The positions quoted by Hartley were found to be very reliable in locating the densest positions within the clouds, with minor revisions necessary in only a small number of cases. This can be compared with the Lynds catalogue of northern dark clouds (Lynds, 1962) where numerous inaccuracies have been found in the quoted positions of the smallest clouds in this list (see e.g., Parker, 1989). The majority of Bok globules in our catalogue have not previously been studied in any form.

The optical properties of the Bok globules in this work are very similar to the globules catalogued by Clemens and Barvainis (1988). The two samples have very similar mean sizes ($3'$ compared to $4'$) and ellipticities (1.9 compared to 2.0, with a greatest ellipticity of 7 in both samples). Both samples include globules of a wide range of shape which may indicate differences in the rotational and magnetic properties of the clouds. The major dark cloud complexes in the southern sky, those of Chamaeleon, Lupus and the Coalsack, are represented in the catalogue, although the vast majority of the sample are well isolated from these complexes. By combining the two catalogues it has been shown that there

is no correlation between the Bok globules (sights of low mass star formation) and Gould's Belt (location of nearby high mass star formation), which represents the plane locating the major concentration of local O and B stars. This lack of correlation supports the view that the regions of low and high mass star formation are spatially distinct.

From the galactic distribution of their sample CB infer a mean distance of 600 pc, assuming a scale height similar to that seen for the larger molecular cloud complexes. Applying the same argument to our sample of Bok globules implies a mean distance > 1 kpc, which is unreasonable considering the lack of foreground stars seen toward the clouds and distance estimates based on other methods, such as star counts. It would thus appear unreasonable to assume that the scale heights of large molecular clouds identified by their CO emission and the optically selected Bok globules are similar. However, source selection biases need to be fully accounted for before this assumption can be completely rejected.

A total of 83 *IRAS* associations were found toward 76 of the clouds ($\sim 45\%$). A comparison with the *IRAS* sources associated with the CB catalogue shows that the properties of the two samples are very similar. Detections in the two longest wavebands are in general uncontaminated by the ubiquitous infrared cirrus, as shown by CB. Both samples are dominated by sources with 60 and 100 μm detections and therefore consist primarily of cool sources.

A comparison of these two samples with the work of Beichman *et al.* (1986) shows that the isolated Bok globules are cooler and not as bright in the far-infrared as the dense cores located within larger cloud complexes. This may be due to the cores within complexes being denser than the cores found within the isolated globules. The fact that the sources within the cores in complexes lie in regions of greater extinction may account for their appearing warmer, since there are more dust grains to reprocess the radiation from the source into the

far-infrared. The majority of *IRAS* associations in this work detected at 60 and 100 μm are located in the embedded cores region of 25–60–100 μm colour-colour space. This group of associations represent a candidate set of “protostellar” objects and thus deserve closer study.

The PSC is incomplete below 3 Jy at 100 μm . If this detection limit could be lowered to 1 Jy then almost every Bok globule would have been detected by *IRAS* in its longest waveband (CB). Clemens *et al.* (1991) have shown with the use of coadded *IRAS* data that this is the case for the CB sample. The globules with detections below 3 Jy represent a quiescent class of globule which are not likely to be forming stars at the present time (CB) and therefore deserve closer attention.

Chapter 3

The Ammonia Survey

3.1 Introduction

A survey of the list of the small molecular clouds presented in chapter 2 was undertaken for emission of the $(J,K) = (1,1)$ rotation inversion transition of ammonia. Ammonia is an excellent tracer of high density gas, requiring densities greater than 10^3 cm^{-3} to excite the $(1,1)$ transition to observable strength at the low temperatures inferred for dark molecular clouds (Ho and Townes, 1983).

The large CO survey of small molecular clouds by Clemens and co-workers (Clemens and Barvainis, 1988; Clemens *et al.*, 1991) was able to provide information on the temperatures and velocity dispersions of this type of cloud, but was unable to provide much information on properties such as the cloud densities and core sizes, nor did it provide information on the gas distribution or the internal velocity structure of the clouds. Moreover, while ^{12}CO is a good diagnostic tool for temperature determinations and outflow identifications, it does not trace high density gas, and so is unable to identify the dense cores which are

the sites of low mass star formation (Benson and Myers, 1989).

The many hyperfine components of the (1,1) transition of ammonia enable the intrinsic line width, optical depth and excitation temperature of the transition to be determined. Combining observations of the (1,1) line with the (2,2) line then enables the determination of the kinetic temperature and density of the cloud. Mapping of the cloud allows the core size and, when the density is known, the core mass to be determined. Ammonia is therefore an extremely versatile diagnostic probe of the conditions in dense molecular clouds.

There are two main thrusts to this survey. The first is to survey the dark cloud sample presented in the previous chapter for dense cores, and to determine the physical properties of these dense cores. The second is to compare the properties of the cores found within the small, isolated molecular clouds with those found in the larger dark cloud complexes, specifically those studied by Benson and Myers (1989) in their ammonia survey.

3.2 Observations and Data Reduction

The ammonia observations were undertaken at the Parkes radio telescope in August–September 1990, January 1991, November 1991, June 1992 and March 1993 with a K-band maser receiver. The author was involved in the latter three observing sessions. A number of different bandwidths and resolutions were employed during the various sessions. For the 1990 and January 1991 sessions, the Parkes 1024 channel digital correlator was split into 4 sections of 256 channels with a bandwidth of 5 MHz (velocity resolution $\Delta v = 0.25 \text{ km s}^{-1}$). In November 1991 the correlator was split into two sections of 512 channels, allowing for a higher resolution ($\Delta v = 0.12 \text{ km s}^{-1}$). Some observations were also made in

January 1991 with $\Delta v = 0.12 \text{ km s}^{-1}$. In June 1992 the new Parkes correlator was used, first with two sections of 1024 channels and a bandwidth of 8 MHz ($\Delta v = 0.10 \text{ km s}^{-1}$), then with a bandwidth of 16 MHz ($\Delta v = 0.20 \text{ km s}^{-1}$), and finally two sections of 2048 channels with a bandwidth of 16 MHz ($\Delta v = 0.10 \text{ km s}^{-1}$), allowing a greater velocity range to be observed. The different setups in 1992 were a result of problems with the correlator. In March 1993 the bandwidth was either 8 MHz over 512 channels (new correlator) or 5 MHz over 512 channels (old correlator), providing velocity resolutions of 0.20 km s^{-1} and 0.12 km s^{-1} respectively. Since we were mainly concerned with mapping during this session a large velocity range was not required. Furthermore, problems with the new correlator meant that we were forced to switch between the two. System temperatures of 70–100 K were recorded in good weather. The beam size at the observed frequencies ($\sim 23.7 \text{ GHz}$) is $1.4'$, and the beam efficiency as determined from observations of Virgo A was 0.32. Pointing checks indicate that the pointing accuracy was better than about $10''$ for all sessions.

The initial search for ammonia emission from the (1,1) transition within the complete list of dark clouds was completed in June 1992. Observations of the (2,2) line were primarily undertaken during November 1991 and March 1993. Difficulties with the prime focus feed at the end of our March 1993 session resulted in a series of (2,2) observations which were not taken with an optimal telescope setup. These results have therefore not been included here. Mapping of the strongest sources was begun in November 1991 and essentially completed in March 1993. Some weaker sources have also been partially mapped.

The observations were performed in total power mode. In most survey positions the total integration time was 60 minutes, consisting of alternate pairs of observations of 5 minutes on source and 5 minutes off source. The off source observations were alternated between 5 minutes west in time (for reference spec-

tra taken before the source spectra) and 5 minutes east in time (for reference spectra taken after source spectra) of the survey position, therefore minimizing the problem of elevation dependent corrections between source and reference spectra. A quotient was formed from each pair, and the quotients averaged to produce the spectra. The spectra were then corrected for atmospheric attenuation and the variation of telescope gain with elevation (see below). Polynomials of up to order three were used to baseline the data. In most cases the spectra have been Hanning smoothed. The rms noise in the off-line channels of the reduced spectra were typically ~ 0.03 K or less. All data reduction was performed with the Australia Telescope National Facility (ATNF) in-house spectral line reduction package SPC.

To correct for the variation of gain with elevation it was necessary to derive a gain curve for the telescope at 23.7 GHz, since one did not exist at the time of our observations. This was done during the June 1992 session by scanning the telescope across Centaurus A at various zenith angles, and comparing the observed flux with that received from Virgo A, which was observed at a nearly constant zenith angle of $\sim 45^\circ$. All observations of Virgo A were scaled to be equal and the Centaurus A observations scaled accordingly. The observations of Centaurus A were performed over a number of clear winter days in June 1992, and thus the effect of atmospheric attenuation on the observations was minimal. Sky dips (plots of system temperature against zenith angle) derived from observations on these days show that this was the case.

A cubic was fitted to the data points using the routine POLFIT in Bevington (1969), which uses the method of least squares and iterates until χ^2 is minimized. The gain curve is shown in figure 3.1. Two scans of Centaurus A in both Right Ascension and Declination were made for each observation and the results averaged, the resulting uncertainty being indicated by the error bars in

the figure.

As can be seen in figure 3.1, the derived gain drops off sharply at zenith angles $> 50^\circ$, but the limited number of data points in this region casts doubt on the reality of this decrease. To minimize any uncertainty we avoided making observations at these zenith angles whenever possible. The best fit to the data is given by:

$$y = 0.81348 + 1.9936 \times 10^{-3}x + 3.6063 \times 10^{-4}x^2 - 7.5879 \times 10^{-6}x^3 \quad (3.1)$$

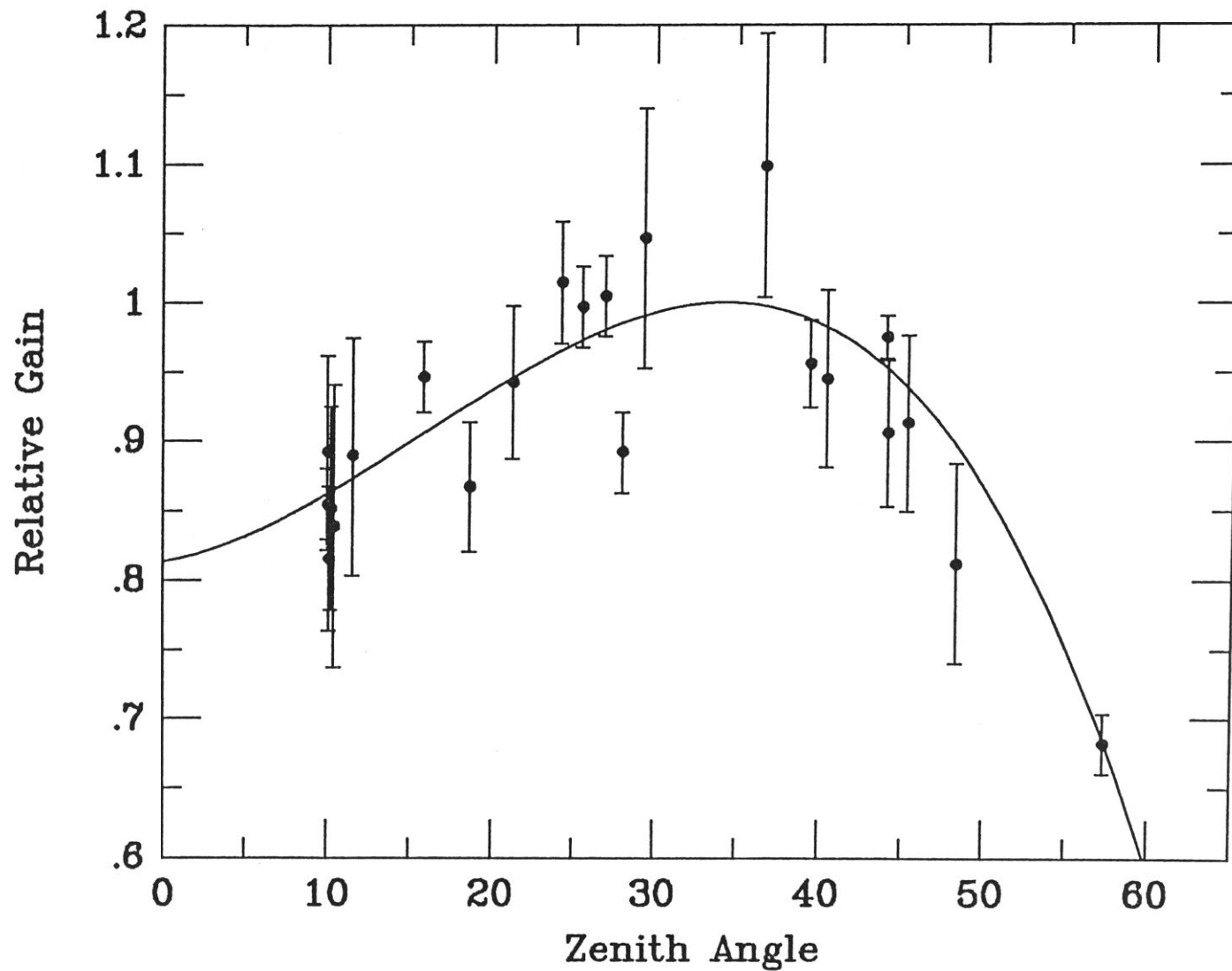
where y is the relative gain and x is the zenith angle. This gain curve has been incorporated into the CAL routine of SPC by the author.

3.3 Data Analysis

3.3.1 Ammonia Analysis

The 18 hyperfine components of the (1,1) transition were fitted to spectra where the satellite features were clearly visible, to allow the determination of the line optical depth, line velocity and intrinsic line width Δv . The fitting program, NH₃fit, in SPC is a least squares fit based on the fitting routine CURFIT of Bevington (1969). Modifications were made to NH₃fit by the author to include all 18 hyperfine components in the analysis. The data for the hyperfine components (offset frequencies and relative intensities) are taken from Ungerechts *et al.* (1980). The fitting routine is similar to that used by other authors (see e.g., Benson and Myers, 1989 (hereafter, BM89); Pauls *et al.*, 1983), and is therefore not discussed here. Model spectra generated with the fitting program and showing the effect of different optical depths on the observed spectra are shown in figure 3.2. An example of a spectrum where the satellites are clearly visible

Figure 3.1: Gain Curve for Parkes Radio Telescope at 23.7 GHz. The data points used to derive the fit are shown with their error bars. The derived gain curve is given in equation 3.1.



and its best fit spectrum are shown in figure 3.3.

The analysis outlined below follows closely that of Harju *et al.* (1993). The general equations from which the following specific equations given here are derived are given in the appendix. A discussion of the ammonia molecule is also given in the appendix.

Excitation Temperature

If the optical depth τ is known then the excitation temperature T_{ex} of the (1,1) transition may be derived from:

$$T_a^* = \eta \phi \frac{h\nu}{k} [F(T_{ex}) - F(T_{bg})] (1 - e^{-\tau(1,1,m)}) \quad (3.2)$$

where T_a^* is the corrected antenna temperature, ϕ is the beam filling factor, T_{bg} the cosmic background temperature, taken to be equal to 2.7 K, η is the beam efficiency, and the letter m refers to the main hyperfine group. The function $F(T)$ is defined to be:

$$F(T) = \frac{1}{e^{h\nu/kT} - 1} \quad (3.3)$$

For the (1,1) transition $h\nu/k$ is equal to 1.14 K. For the mapped sources we were able to derive a core size, $\theta_x' \times \theta_y'$, where θ_x' and θ_y' are the major and minor axes respectively of the map half power contour. This assumes that the source shape may be well approximated by an ellipse, which for almost all the sources presented here is certainly the case. The half power contour thus defines the core. The beam filling factor ϕ may then be found from (Benson, 1983):

$$\phi = \left\{ \left[1 + \left(\frac{\theta_b}{\theta_x} \right)^2 \right] \left[1 + \left(\frac{\theta_b}{\theta_y} \right)^2 \right] \right\}^{-1/2} \quad (3.4)$$

where θ_b is the FWHM of the telescope beam. For sources where we have not been able to deduce a filling factor (because we have not mapped the source), we

Figure 3.2: Spectra generated with the model fitting program of SPC, showing the effects of different optical depths on the observed spectra. The upper spectrum has a main group optical depth of 5, and the lower spectrum an optical depth of 1. The upper spectrum is offset by 1.1 from the lower spectrum. The other parameters used are $T_a^* = 1.0$ K, $\Delta v = 0.35$ km s⁻¹.

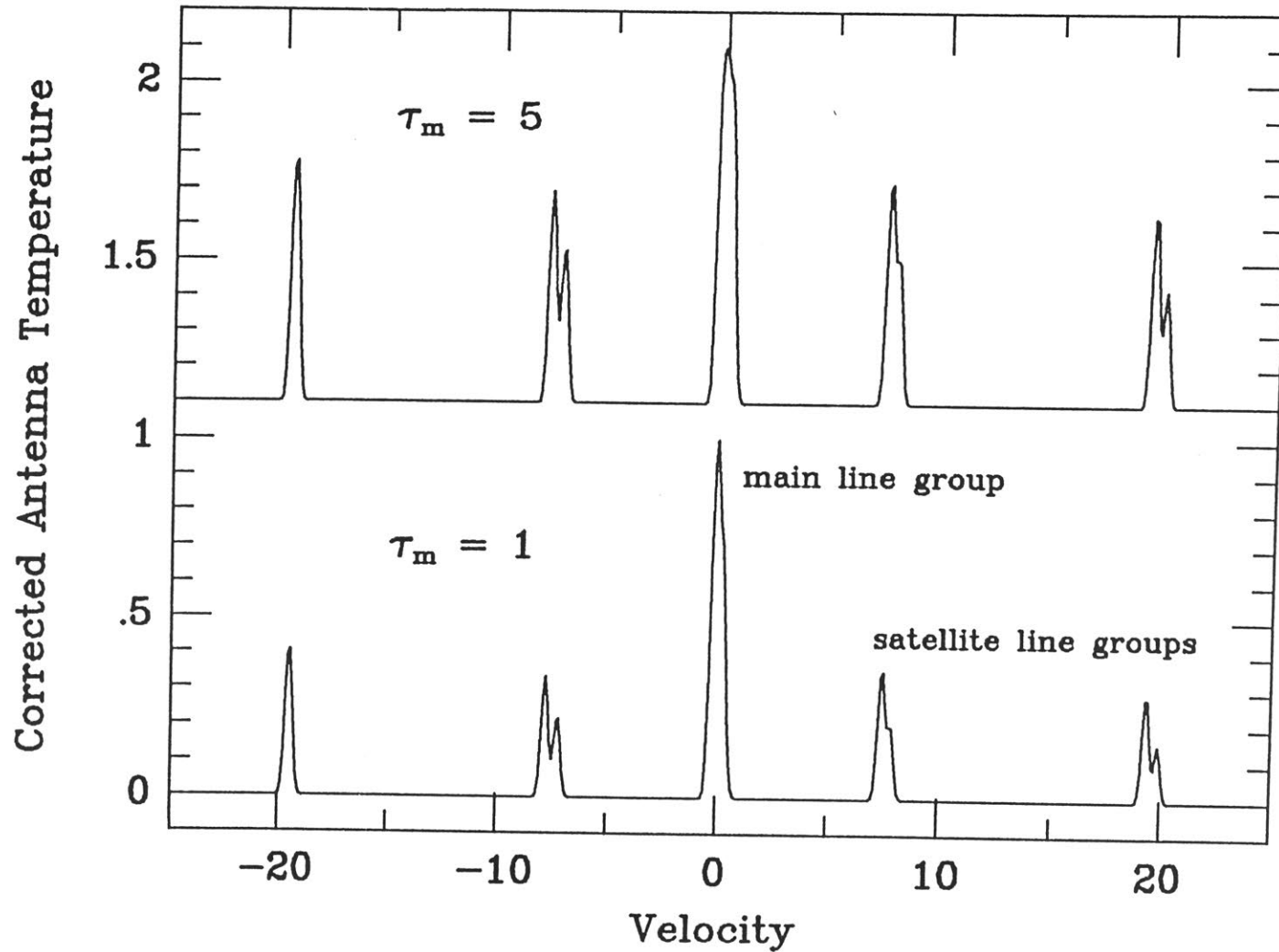
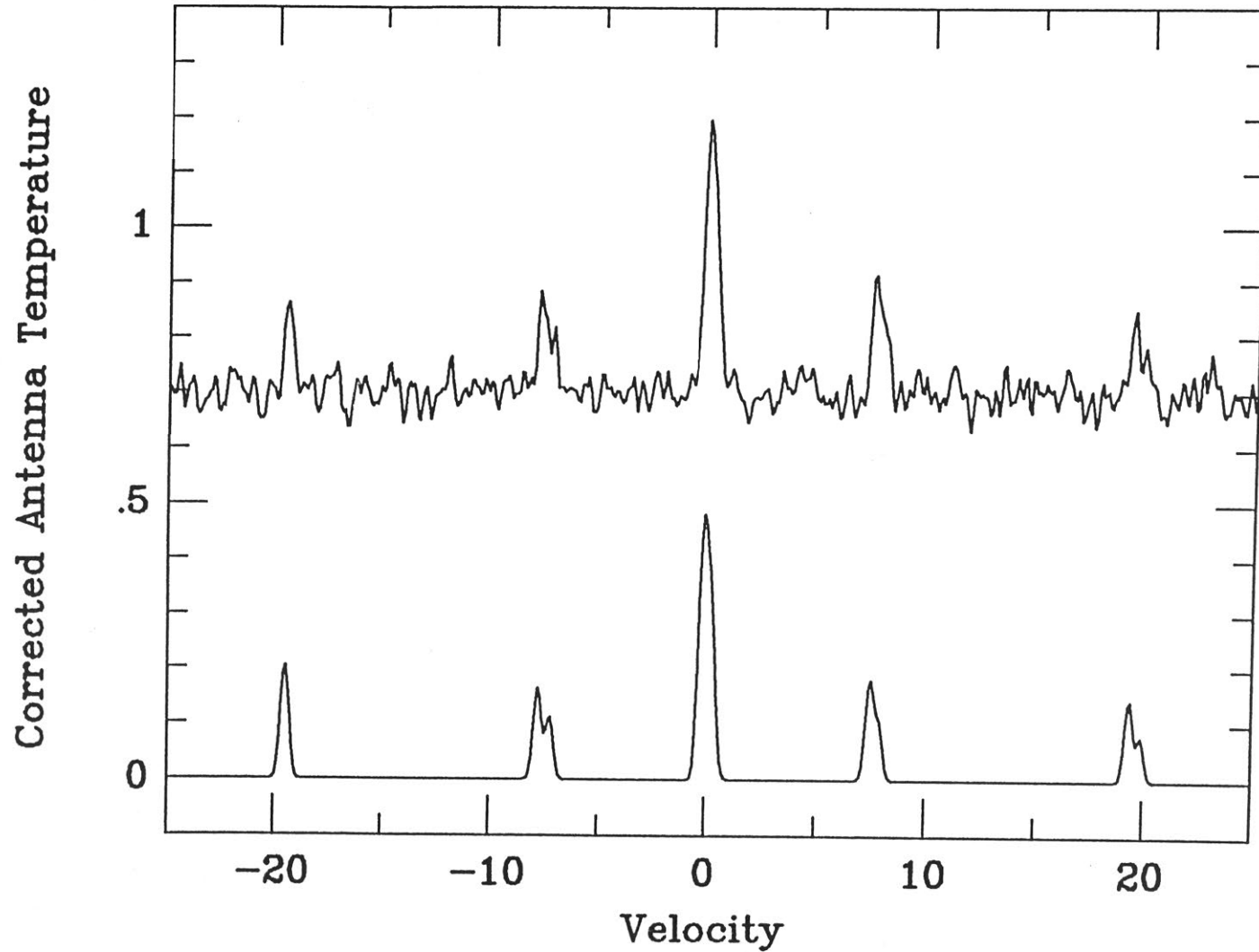


Figure 3.3: The NH_3 (1,1) spectrum of DC 327.2+1.8 (upper) and the model best fit spectrum (lower). The observed spectrum is offset from the model spectrum by 0.7. The splitting of the hyperfine components are clearly visible in this figure.



have assumed that $\phi = 0.75$, based on the average value of the mapped sources in this work. For comparison, BM89 found an average value of 0.7 for the sources they mapped with the Haystack telescope, for which $\theta_b = 1.45'$.

Column Densities

Appendix 1 shows how the various equations outlined below are derived. Here we outline the important results. To obtain the column density of molecules in the upper (1,1) state we assume that all the hyperfine components have the same excitation temperature, and that the excitation conditions along the line of sight are uniform. The column density is then given by:

$$N_u(1,1) = 1.6 \times 10^{13} F(T_{ex}) \Delta v \tau(1,1,m) \quad (3.5)$$

where Δv is in kms^{-1} . For sources with either low signal to noise ratios, or where the optical depth is low (as implied by the model fit), then it is possible to determine N_u by integrating over the (1,1) satellites, or in cases where they are not visible, by integrating over the main group, and assuming optically thin conditions in both cases. In practice one has to calculate the area under the observed line or lines, which is aided greatly by first applying the fitting program to identify the satellite lines. In this case the expression for the column density is:

$$N_u(1,1) = \frac{1}{\phi} 1.3 \times 10^{13} \frac{1}{1 - \frac{F(T_{bg})}{F(T_{ex})}} \int dv T_B(1,1,s) \quad (3.6)$$

where T_B refers to the beam brightness temperature, which is found by dividing the corrected antenna temperature T_a^* by the beam efficiency ($= 0.32$), and the letter s refers to the satellite lines as shown in figure 3.2. The integral is over all four satellite groups. Equation 3.6 still applies when integrating over the main line group instead of the satellites. For the (2,2) line the integral is over the main line only and the numerical factor in equation 3.6 is 6.1×10^{12} .

For spectra where equation 3.5 was applied, the results have been compared with those derived from equation 3.6. The results in almost all cases are similar, since the optical depths are usually low. However, in cases where the excitation temperature cannot be derived a value must be assumed in order to calculate N_u . Harju *et al.* (1993) used an average value of T_{ex} from positions where they were able to determine it. For our sources the average value of T_{ex} is ~ 6 K, while for the BM89 sources the average is ~ 7.5 K. In the analysis presented here, T_{ex} is taken to be 6 K when it has not been determined directly, and so the term $f(T_{ex}) \equiv [1 - F(T_{bg})/F(T_{ex})]^{-1}$ in equation 3.6 is equal to 1.7. For the weaker sources, where an attempt has been made to fit the spectra (with varying degrees of success) the derived excitation temperatures are usually lower than those determined for the stronger sources (the optical depths are usually similar) and so setting $T_{ex} = 6$ K to derive a lower limit on N_u appears to be a valid assumption for these sources. If one puts $T_{ex} = 10$ K then $f(T_{ex}) = 1.3$ (Harju *et al.* 1993) which results in a lower, but not significantly different result to that found with $T_{ex} = 6$ K. The uncertainties in the calibration of the spectra (estimated by many authors to be of the order of 20%, e.g., Bachiller *et al.*, 1987) and in calculating the line areas that follow as a result imply that the choice of T_{ex} is not crucial, as long as it is kept significantly higher than T_{bg} , so that $f(T_{ex})$ is not significantly greater than 1.

The total number of molecules in the (1,1) state is then found by assuming a Boltzmann distribution between the upper and lower states:

$$N(1,1) = N_u + N_l = N_u(1 + e^{h\nu/kT_{ex}}) \quad (3.7)$$

Rotation and Kinetic Temperatures

If the (2,2) transition has been observed then it is possible to determine the rotation temperature between the (1,1) and (2,2) transitions from:

$$\frac{N(2,2)}{N(1,1)} = \frac{5}{3} e^{-\Delta E/kT_R} \quad (3.8)$$

where 5/3 is the ratio of statistical weights and $\Delta E/k = 41.5$ K is the energy difference between the (1,1) and (2,2) states. The rotation temperature may also be calculated directly from the observed antenna temperatures and the optical depth of the (1,1) line, $\tau(1,1,m)$ ($\equiv \tau_m$) when it has been derived (Ho and Townes, 1983):

$$T_R = \frac{-\Delta E/k}{\ln \left[\frac{-0.282}{\tau_m} \ln \left(1 - \frac{T_a^*(2,2,m)}{T_a^*(1,1,m)} (1 - e^{-\tau_m}) \right) \right]} \quad (3.9)$$

In principle the values of T_R calculated should be the same for both methods. In practice we see that they are very similar and overlap within their uncertainties. The values found from equation 3.8 are used in the following discussions.

The rotation temperature slightly underestimates the kinetic temperature in the cold dark clouds, and the deviation between the two becomes greater at higher temperatures. The kinetic temperature may be found from the three level equation of Walmsley and Ungerechts (1983), using the rate constants calculated by Danby *et al.*, (1988) for the rotational excitation of NH_3 by H_2 :

$$T_R = \frac{T_K}{1 + \frac{kT_K}{\Delta E} \ln \left(1 + \frac{C_{23}}{C_{21}} \right)} \quad (3.10)$$

where $\Delta E/k$ is the energy difference between the (1,1) and (2,2) levels, C_{23} represents the rate of collisional transfer of population between the (2,2) and (2,1) level and C_{21} the rate between the (1,1) and (2,2) levels. The (2,1) population is considered to be negligible compared to the (1,1) level.

The total column density of ammonia molecules is found by assuming that the metastable levels are the only ones populated (Ungerechts *et al.*, 1986). The expression for the total column density $N(NH_3)$ is then:

$$N(NH_3) = N(1, 1) \left[\frac{1}{3} e^{23.4/T_R} + 1 + \frac{5}{3} e^{-41.5/T_R} + \frac{14}{3} e^{-101.5/T_R} \right] \quad (3.11)$$

where the terms greater than the (3,3) level have been ignored, as they are insignificant at the temperatures of a typical dark cloud core (~ 10 K).

Densities, Abundances and Masses

With T_{ex} and T_K known the local molecular hydrogen density may then be found, by balancing collisions and stimulated and spontaneous emission, via (Ho and Townes, 1983):

$$n(H_2) = \frac{A F(T_{ex}) - F(T_{bg})}{C F(T_K) - F(T_{ex})} [1 + F(T_K)] \quad (3.12)$$

where A is the Einstein A coefficient ($= 1.7 \times 10^{-7} \text{ s}^{-1}$ for the (1,1) transition) and C is the collisional de-excitation rate of the (1,1) transition, which is equal to $8.5 \times 10^{-11} \text{ cm}^3 \text{ s}^{-1}$ at the temperatures derived here (Danby *et al.* 1988). We are then able to determine the fractional abundance of ammonia, $\chi(NH_3)$, which for a homogeneous cloud is given by:

$$\chi(NH_3) \sim \frac{N(NH_3)}{2d n(H_2)} \quad (3.13)$$

where d is the cloud diameter, taken by Harju *et al.* (1993) to be the half-power diameter at the peak intensity.

There are two ways to determine the core masses. The first makes use of the local molecular hydrogen density and assumes that the cores are homogeneous and spherical clumps with radii estimated from the map half power contour. Some authors choose the half power diameter as the radius (e.g., BM89; Harju *et al.*, 1993). Others use half of this diameter (e.g., Ungerechts *et al.* 1982).

Consistency in the choice is the key here, particularly when comparisons are being made with previous workers. The mass is found from:

$$M(R) = \frac{4\pi}{3} R^3 n(H_2) \langle m \rangle \quad (3.14)$$

where R is the cloud ‘radius’ and $\langle m \rangle$ is the mean mass per hydrogen molecule, including heavier elements ($= 4.3 \times 10^{-24}$ g). The core mass may also be estimated from the hydrogen column density $N(H_2)$, assuming the ammonia column density and abundance are known:

$$M(R) = \frac{4\pi}{3} R^2 N(H_2) \langle m \rangle \quad (3.15)$$

If the core size is not known the above equation can be used to estimate the beam averaged mass (i.e., the mass within the telescope beam) from the beam averaged column density, $\langle N(H_2) \rangle = \phi [N(H_2)]$, and the beam size.

3.3.2 Distances

Determining the distance to a dark cloud is difficult, particularly if there are no stellar or nebulous objects associated with the cloud. For clouds whose distance is unknown, the most commonly used method today is to examine the reddening of stars in the direction of the dark cloud. The central idea is that the dark clouds exist in large groups and are located in discrete layers with respect to distance from the Sun (see e.g., Lynds, 1968; Dickman and Clemens, 1983), and that these layers may be traced over many square degrees on the sky. Plotting the stellar reddening of a sufficiently large number of stars in a given region against their distance corrected for reddening will thus show “steps” of reddening at one or more discrete distances, implying the existence of an intervening cloud or group of clouds at each step. The colours and spectral types of a large number of stars is thus needed for this method to work successfully.

The stellar reddening may be determined if the B and V magnitudes are known, which means that the colour, $(B-V)$ is known, and if the MK spectral type, and hence the star's intrinsic colour, $(B-V)_o$, is known. The reddening, E_{B-V} , is then found from:

$$E_{B-V} = (B-V) - (B-V)_o$$

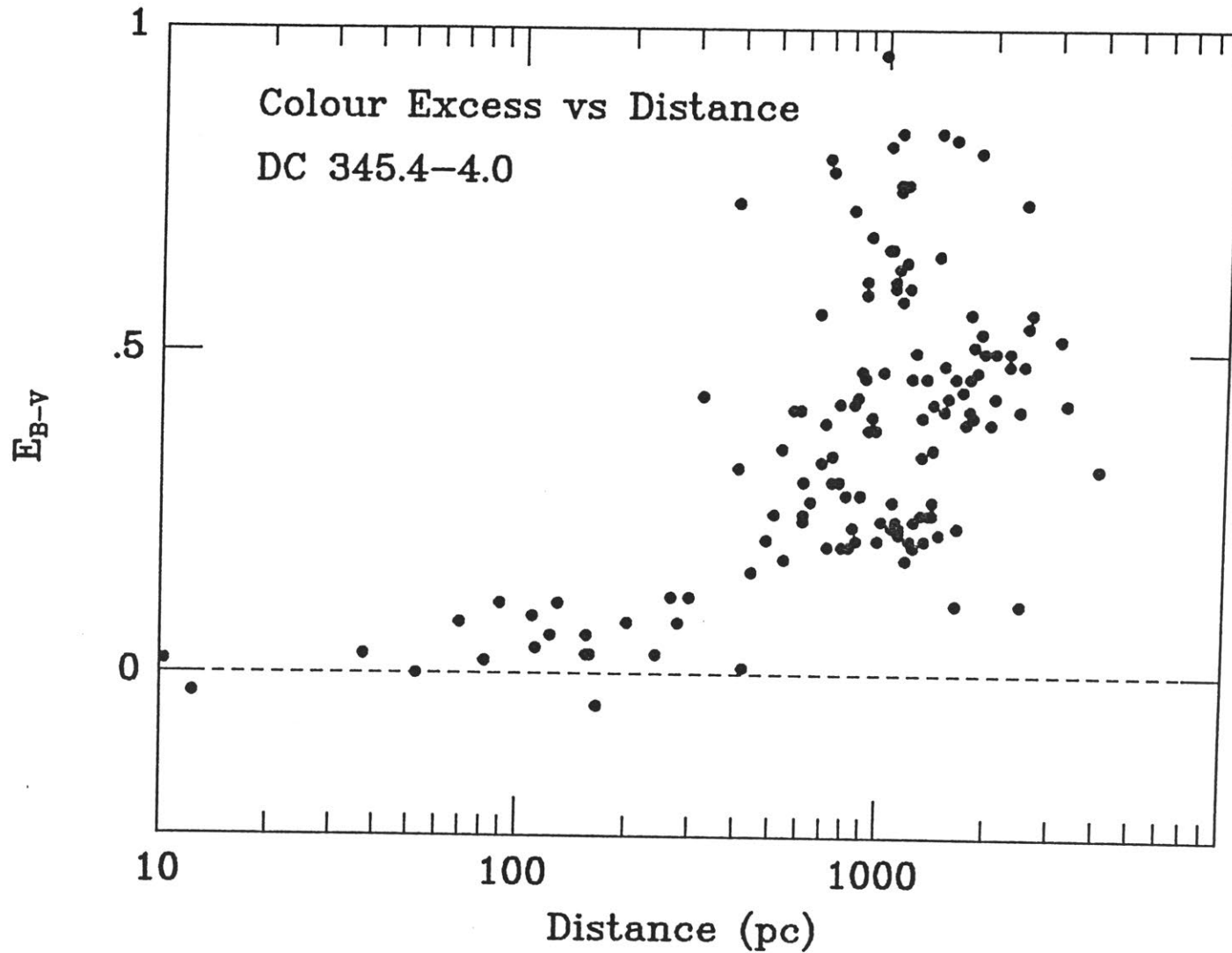
The distance corrected for the reddening may then be found by assuming some value for the ratio of total to selective absorption, $R = A_V/E_{B-V}$, where A_V is the visual extinction. Here R is taken to be equal to 3.1 (Whittet, 1992). The distance is then found from:

$$m_V - M_V = 5 \log r - 5 + A_V \quad (3.16)$$

where m_V is the measured V magnitude, M_V the absolute V magnitude and r the distance in parsecs.

Large areas of sky must be searched to obtain enough stars for plotting due to the limited number of stars for which MK spectral types and colours are available. Snell (1981) used a region of $20^\circ \times 20^\circ$ centered on his cloud positions, and Dickman and Clemens (1983) searched a region $11^\circ \times 16^\circ$ in their study. In this study, the MK Classification Extension Catalogue of Morris-Kennedy (1983) has been searched for stars lying within a given radius centered on the globule. Since this catalogue is available in electronic form the search has been greatly simplified, and allows the possibility to quickly search a smaller area around the globule in the hope of finding a sufficient number of stars. Larger areas may then be searched if an insufficient number of stars have been found. Where possible a search radius of 5° has been used. If not enough stars were found, then the radius was increased to 7.5° , and then to 10° if necessary. A plot of reddening against distance is shown in figure 3.4 in the direction of the dark cloud DC 345.4-4.0.

Figure 3.4: A plot of reddening against distance in the direction of the dark cloud DC 345.4-4.0. A discontinuity in the reddening is evident at a distance of around 400 pc, indicating the probable cloud distance.



One shortcoming of the above method is the uncertainty of deciding which cloud layer the small globules belong to, particularly considering the large search areas used. In some instances more than one jump in reddening may be visible, indicating more than one layer of intervening matter. Without any other knowledge to the contrary, it is assumed that the dense globules are associated with the nearest obscuration, since their opaqueness and general lack of foreground stars imply that they are at least one of the closest clouds in that direction. This method of interstellar reddening has been used in the last instance to determine cloud distances in this study. If other information was available it was used, such as the proximity of the globule to other dark clouds of known distance. For example, clouds which appear to be visually associated with the Southern Coalsack, and which have similar ammonia velocities ($V_{lsr} \sim -5 \text{ km s}^{-1}$), are assumed to lie at a similar distance of 175 pc (Rodgers, 1960). It was also possible for many globules with similar velocities and located near to each other to use a common search area and to assume that they lie at a similar distance.

3.4 Results

3.4.1 Survey

All 169 clouds were surveyed in at least one position for ammonia emission. Gaussians were fitted to the main line of the reduced spectra when visible, and the results of this fit are given in table 3.1. Column 1 lists the cloud name. Column 2 attempts to identify the cloud type, as in the previous chapter. Column 3 lists the rms noise level, which is the 1σ level in the off-line channels of the spectrum. Columns 4–6 list the results of the gaussian fit to the central component, with the uncertainties in the fit quoted in parentheses. When no signal

Table 3.1: Ammonia Survey Results

DC Name	Cloud Type	rms (K)	T_a^* (K)	V_{lsr} (kms $^{-1}$)	ΔV (kms $^{-1}$)	V_{other} (kms $^{-1}$)	Session	IRAS
249.7-2.1	I	0.042	...	0.00	...	ND ¹	N91	
251.7+0.2	CG	0.032	0.24 (0.02)	5.09 (0.03)	0.69 (0.07)		N91	Y
251.8+0.0*	CG	0.030	...	0.00	...		Ju92c	Y
251.9+0.0	CG	0.037	...	0.00	...		Ju92c	
252.2+0.7	CG	0.028	0.23 (0.02)	2.03 (0.02)	0.64 (0.06)		Ju92c	Y
252.3+0.5*	CG	0.022	...	0.00	...		Ju92c	
252.5+0.1*	CG	0.025	0.22 (0.01)	4.85 (0.02)	0.78 (0.04)	ND ¹	Ju92c	Y
253.1-1.7A	CG	0.034	0.35 (0.01)	6.04 (0.02)	0.95 (0.04)	5.9 ¹	N91	
253.1-1.7B	CG	0.026	0.19 (0.02)	5.87 (0.03)	0.71 (0.07)		N91	
253.1-1.7C	CG	0.029	0.24 (0.01)	6.32 (0.03)	1.02 (0.06)		N91	
253.1-1.7D	CG	0.027	...	6.00	...		N91	
253.3-1.6	CG	0.019	0.61 (0.05)	6.18 (0.04)	1.02 (0.09)	5.4 ¹ 6.0 ² 5.2 ³	Ja91a	Y
253.6+2.9	CG	0.034	0.14 (0.02)	6.57 (0.04)	0.64 (0.10)	6.4 ¹ 6.5 ²	N91	Y
253.8-10.9	CG	0.015	0.24 (0.02)	-1.04 (0.03)	0.75 (0.08)	ND ²	Ju92b	
255.3-14.4	CG	0.023	0.11 (0.02)	4.00 (0.03)	0.81 (0.08)	3.5 ¹ 4.1 ²	N91	Y
255.4-3.9	I	0.030	...	0.00	...		Ju92c	
256.2-14.1*	CG	0.015	0.10 (0.01)	3.47 (0.06)	1.00 (0.13)		Ju92b	Y
256.9+2.6	CG	0.020	...	0.00	...		Ju92c	Y
257.2-10.3	CG	0.024	0.09 (0.01)	-3.42 (0.06)	0.68 (0.14)		N91	Y
259.0-13.2	CG	0.045	0.19 (0.03)	0.93 (0.06)	0.89 (0.14)		N91	
259.4-12.7	CG	0.027	0.20 (0.02)	1.45 (0.03)	0.61 (0.06)	1.2 ^{2,3}	N91	
259.5-16.4	CG	0.024	0.12 (0.01)	3.84 (0.06)	0.98 (0.13)	4.0 ¹ 3.5 ^{2,3}	N91	Y
259.9-0.0	I/N	0.016	0.24 (0.02)	7.68 (0.06)	1.75 (0.14)	7.5 ^{2,3}	Ju92b	Y
260.0-3.8	CG	0.020	0.07 (0.01)	-11.88 (0.06)	0.75 (0.13)		Ju92c	
260.7-12.4	CG	0.032	0.17 (0.01)	-0.05 (0.03)	0.71 (0.07)	ND ²	N91	Y
262.5-13.4	CG	0.028	0.11 (0.01)	-0.88 (0.05)	0.83 (0.11)	-1.0 ¹	N91	Y
262.9-14.7	CG	0.032	0.19 (0.03)	-0.83 (0.04)	0.59 (0.09)	ND ¹	N91	Y
262.9-15.5	CG	0.031	0.26 (0.02)	-0.73 (0.02)	0.70 (0.05)		N91	
264.5+5.6	I	0.022	...	0.00	...		Ju92c	
265.3-0.0	I	0.023	...	0.00	...	ND ⁴	Ju92c	
265.7-7.7	I	0.013	0.05 (0.01)	2.87 (0.07)	0.62 (0.16)		Ju92b	Y
266.0+4.3	CG	0.035	...	0.00	...	-1.5 ²	N91	
266.0-4.3*	I/N	0.025	...	0.00	...		Ju92c	
267.2-7.2	I	0.031	0.20 (0.01)	4.95 (0.06)	0.78 (0.20)		M93b	Y
267.4-0.9	I	0.017	0.06 (0.01)	-2.70 (0.13)	0.64 (0.31)	ND ²	A90	
267.4-7.5	I	0.015	0.39 (0.03)	5.28 (0.03)	0.96 (0.07)	5.3 ^{3,6}	A90	Y
267.5-7.4	I	0.021	0.30 (0.02)	5.99 (0.03)	0.86 (0.08)		A90	
267.6-6.0a*	I/F	0.017	0.18 (0.01)	5.85 (0.03)	0.78 (0.07)		Ju92b	
267.6-6.0b*	I/F	0.028	0.10 (0.01)	5.72 (0.03)	0.39 (0.08)		Ju92c	
267.6-6.4	I	0.021	0.07 (0.01)	5.63 (0.11)	0.82 (0.26)	5.3 ²	Ja91a	

Table 3.1 *continued*

DC Name	Cloud Type	rms (K)	T_a^* (K)	V_{lsr} (km s ⁻¹)	ΔV (km s ⁻¹)	V_{other} (km s ⁻¹)	Session	IRAS
267.7-7.4	I	0.030	0.60 (0.02)	5.43 (0.02)	0.76 (0.04)	5.3 ²	N91	Y
267.9-7.8	I	0.032	0.08 (0.01)	6.21 (0.13)	1.57 (0.31)		N91	
269.4+3.0	I/C	0.026	0.08 (0.02)	-1.69 (0.06)	0.69 (0.14)	-2.3 ^{2,3}	N91	
269.5+4.0	I	0.028	0.08 (0.01)	-3.24 (0.11)	0.83 (0.26)		N91	
269.7-3.9	CG	0.023	...	0.00	...		Ju92c	
270.6-4.7	CG	0.053	...	5.00	...	-6.7 ¹	N91	
272.5+2.0	I	0.028	...	0.00	...		Ju92c	Y
273.2+2.4	I	0.026	...	0.00	...		Ju92c	
273.3+2.5	I	0.029	...	0.00	...		Ju92c	
273.8+3.2	I	0.027	...	0.00	...		Ju92c	
274.1+3.9	CG	0.034	...	0.00	...		Ju92c	
274.1+2.7	I	0.015	0.06 (0.01)	-3.71 (0.07)	0.92 (0.16)	-3.5 ²	Ju92b	
274.2-0.4	I	0.047	0.19 (0.03)	5.70 (0.08)	0.78 (0.20)		Ja91a	
274.3+3.4	I	0.031	...	0.00	...		Ju92c	Y
275.9+1.9*	C	0.026	0.41 (0.01)	-5.45 (0.01)	0.84 (0.03)		Ju92c	Y
276.2-10.6	I/N	0.018	...	0.00	...		A90	Y
285.3-1.6	I	0.047	...	2.00	...		N91	
289.3-2.8	I	0.017	0.12 (0.01)	-6.98 (0.08)	1.73 (0.20)		A90	Y
291.1-1.7	I	0.016	0.26 (0.02)	-4.52 (0.03)	0.87 (0.06)	-4.8 ^{2,3}	A90	
291.4-0.2	I	0.032	0.15 (0.02)	-6.52 (0.13)	1.12 (0.29)	-6.5 ²	A90	
293.1+0.6	I	0.046	...	2.00	...		N91	
293.2+0.4	I	0.015	...	0.00	...		Ju92b	
293.3+0.1	I	0.022	...	0.00	...		Ju92a	
293.3-0.9	C	0.019	0.20 (0.02)	-27.47 (0.05)	1.29 (0.12)		A90	
294.3+2.7	I	0.024	...	0.00	...		N91	
294.3-0.1	I	0.021	...	0.00	...		Ju92c	
294.9+0.1	I	0.031	0.10 (0.01)	-10.78 (0.05)	0.56 (0.11)		Ju92c	Y
295.0+3.4	I	0.018	0.37 (0.03)	-7.55 (0.03)	0.85 (0.07)	-7.7 ^{2,3}	Ju92b	
295.4+0.5	I	0.028	...	0.00	...		Ju92c	
295.5+0.4	I	0.027	...	0.00	...		Ju92c	
297.7-2.8	I	0.049	0.97 (0.03)	-4.43 (0.01)	0.94 (0.03)	-4.8 ²	N91	Y
298.3-2.8	I	0.028	0.07 (0.01)	-4.71 (0.08)	0.89 (0.20)		Ju92c	
299.6+5.6	I	0.012	...	0.00	...		Ju92b	Y
300.0-3.7	I	0.017	0.12 (0.02)	-5.78 (0.06)	0.73 (0.14)		A90	
300.2-3.5	I	0.030	...	-4.00	...	-5.8 ²	M93a	
300.6-3.1	I	0.015	0.07 (0.01)	-5.37 (0.06)	0.65 (0.14)	-5.6 ²	Ja91a	
300.7-1.0*	C	0.026	0.15 (0.02)	-5.34 (0.02)	0.44 (0.06)	-6.2 ² -6.1 ³	Ju92c	
301.2-0.4	I/C	0.027	0.15 (0.01)	-4.80 (0.03)	0.69 (0.07)	-5.1 ³	N91	
301.7-6.7	I/N	0.026	...	0.00	...		Ju92c	Y
301.7-7.2	CG	0.029	...	0.00	...	ND ²	Ju92c	

Table 3.1 *continued*

DC Name	Cloud Type	rms (K)	T_a^* (K)	V_{lsr} (km s ⁻¹)	ΔV (km s ⁻¹)	V_{other} (km s ⁻¹)	Session	IRAS
301.7-2.6	I/C	0.018	...	0.00	...		Ju92b	Y
302.0-7.0*	CG	0.028	0.19 (0.02)	4.76 (0.03)	0.65 (0.06)		Ju92c	
302.1+7.4	CG	0.025	0.12 (0.01)	-15.12 (0.03)	0.75 (0.25)		Ju92c	Y
302.6-15.9	I/N	0.045	...	-5.00	...		N91	
303.3+1.3	I	0.028	0.09 (0.02)	-3.71 (0.04)	0.52 (0.09)	-3.9 ²	N91	
303.8-14.2	I/N	0.016	0.08 (0.01)	3.95 (0.07)	1.26 (0.17)	3.7 ²	Ju92b	Y
307.3+2.9	I	0.028	0.10 (0.02)	32.72 (0.05)	0.53 (0.11)		M93a	Y
314.8-5.1*	I/N	0.019 ^a	0.06 (0.02)	-4.16 (0.11)	0.69 (0.25)	-4.5 ²	Ju92b	Y
315.8-27.5a	I/N	0.030	...	-40.00	...		N91	Y
315.8-27.5b	I/N	0.052	0.21 (0.04)	-37.84 (0.04)	0.32 (0.10)		N91	
316.3+4.9	I	0.028	...	0.00	...		N91	
316.5+21.2*	CG/N	0.019	0.11 (0.01)	-5.60 (0.06)	1.52 (0.15)	ND ¹ -6.1 ²	Ju92b	Y
316.5-4.0	I/F	0.030	0.13 (0.02)	-6.49 (0.04)	0.66 (0.10)		N91	
316.9-4.9	I	0.023	...	0.00	...		Ju92c	
316.9-2.1	I	0.047	...	2.00	...		N91	
317.0-4.6	I	0.016	0.07 (0.01)	-6.33 (0.05)	0.54 (0.11)		Ju92b	
319.9-4.8	I	0.020	...	0.00	...		A90	Y
320.1-4.3	I	0.031	...	0.00	...		N91	Y
320.5-3.5	I	0.029	...	2.00	...		M93a	Y
320.5-3.6	I	0.028	0.15 (0.02)	-0.61 (0.03)	0.61 (0.08)		N91	Y
320.7-1.7	I/C	0.029	0.11 (0.03)	-0.33 (0.08)	0.59 (0.19)		N91	Y
320.7-2.0	I/C	0.024	...	0.00	...		Ju92c	
320.9-2.1	I	0.054	...	-5.00	...		N91	
322.7+4.0*	I	0.035	...	0.00	...		M93b	
322.7+3.9*	I	0.026	...	0.00	...		Ju92b	
323.0+4.0	I	0.029	...	-5.00	...		N91	Y
325.2+5.8	I	0.039	0.15 (0.03)	-5.75 (0.05)	0.29 (0.11)		N91	Y
325.9+5.9	I	0.028 ^a	...	0.00	...		Ju92c	
326.8+5.6	I	0.027	...	0.00	...		Ju92c	Y
326.9+5.5	I	0.019	0.10 (0.01)	-10.41 (0.04)	0.52 (0.08)	ND ²	Ju92c	Y
327.2+1.8*	I	0.024	0.49 (0.01)	0.00 (0.01)	0.71 (0.02)		Ju92a	
330.7-1.3*	I	0.023	...	0.00	...	-4.8 ²	Ju92c	Y
331.0-0.7	I	0.021	0.20 (0.01)	-5.07 (0.02)	0.77 (0.05)		Ju92c	
331.1-2.3	I	0.025	...	0.00	...		Ju92c	
332.7+6.8*	I	0.022	...	0.00	...		Ju92a	Y
334.2+0.0	I	0.021	0.10 (0.01)	-20.28 (0.03)	0.81 (0.07)		Ju92c	
334.6+4.6	I	0.034	0.17 (0.02)	3.52 (0.04)	0.61 (0.09)	3.6 ²	N91	Y
334.6-1.4*	C	0.026	...	0.00	...		Ju92c	Y
335.9+7.0*	I	0.030	...	0.00	...	4.0 ²	M93a	
336.7+7.8	I	0.020	...	0.00	...		Ju92c	

Table 3.1 *continued*

DC Name	Cloud Type	rms (K)	T_a^* (K)	V_{lsr} (km s ⁻¹)	ΔV (km s ⁻¹)	V_{other} (km s ⁻¹)	Session	IRAS
337.1-4.9	I	0.029	...	-20.00	...	ND ²	N91	Y
337.7-4.0	I	0.033	0.16 (0.02)	3.59 (0.05)	0.65 (0.11)	3.5 ²	N91	
337.8-1.6	I/C	0.024	...	0.00	...	-10.7 ²	Ju92c	
337.9-1.4*	F	0.023	...	0.00	...		Ju92c	
338.2+0.8	I	0.023	...	0.00	...		Ju92c	Y
338.6+9.5	I	0.032	...	0.00	...		Ju92c	Y
338.6+11.9*	F	0.030	...	0.00	...		M93a	
339.1+11.7a*	F	0.030	...	0.00	...		Ju92c	
339.1+11.7b*	F	0.027	...	0.00	...		Ju92c	
339.1-0.8	I	0.029	0.11 (0.02)	-30.17 (0.04)	0.35 (0.09)		N91	
339.3-0.3	F	0.020	...	0.00	...		Ju92c	Y
340.4+5.5	I	0.025	0.13 (0.02)	4.61 (0.03)	0.39 (0.06)		Ju92c	
340.5+0.5	I	0.050	0.23 (0.04)	5.11 (0.04)	0.47 (0.10)	5.0 ² 4.9 ⁴	N91	
340.9+9.2	I	0.026	...	0.00	...		Ju92c	
343.4+3.5	I	0.027	0.08 (0.02)	4.53 (0.06)	0.64 (0.15)	4.72 ⁴	N91	
344.5+2.0	CG	0.027	...	0.00	...		N91	Y
344.6-4.3	I/N	0.026	0.17 (0.01)	-12.51 (0.04)	1.40 (0.10)	ND ²	Ju92c	Y
345.0-3.5	I	0.012	0.12 (0.01)	7.66 (0.04)	0.92 (0.10)		Ju92b	Y
345.2-3.6*	I	0.037	...	0.00	...		Ju92a	Y
345.4-4.0	I	0.020	0.67 (0.06)	-8.33 (0.06)	1.39 (0.14)	-8.2 ²	Ju92b	Y
345.8+7.6	I	0.028	...	0.00	...		Ju92c	
346.2-11.7	I	0.052	0.19 (0.04)	-22.75 (0.06)	0.65 (0.13)		N91	
346.4-5.0	I	0.028	...	0.00	...		Ju92b	
346.4+7.9	I	0.020	0.07 (0.01)	3.73 (0.05)	0.64 (0.12)		Ju92c	
347.5-8.0	I	0.058	0.31 (0.04)	7.65 (0.03)	0.62 (0.08)	7.3 ²	N91	
347.9-4.4	I	0.040	...	0.00	...		N91	
348.0+3.7	I	0.020	...	0.00	...		A90	
349.0+3.0	I	0.033	...	0.00	...		Ja91b	Y
349.2+3.1a	I	0.032	0.09 (0.02)	10.86 (0.08)	0.98 (0.19)		N91	Y
349.2+3.1b	I	0.030	...	0.00	...		N91	Y
349.3+3.1	I	0.028	...	0.00	...		Ju92c	Y
351.0+3.9	I	0.029	...	0.00	...		Ju92c	
351.2+5.1	I	0.029	...	15.00	...		M93a	Y
351.2+5.2	I	0.032	0.11 (0.02)	17.19 (0.06)	0.56 (0.13)	ND ⁴ 18.52 ⁵	Ju92c	Y
351.7+0.5*	I	0.029	...	0.00	...	5.8 ⁴	Ju92c	Y
351.8+2.8	I	0.055	...	0.00	...		Ju92c	Y
352.9+4.8	I	0.029	...	0.00	...	13.77 ⁵	Ju92c	Y
352.9+5.0	I	0.022	...	0.00	...		Ju92c	Y
353.1+2.3	I	0.018	0.08 (0.02)	7.91 (0.11)	1.26 (0.25)		Ja91a	Y
353.3+2.4	I/N	0.032	...	0.00	...		Ju92c	Y

Table 3.1 *continued*

DC Name	Cloud Type	rms (K)	T_a^* (K)	V_{lsr} (kms $^{-1}$)	ΔV (kms $^{-1}$)	V_{other} (kms $^{-1}$)	Session	IRAS
353.5+3.5	F	0.028	...	0.00	...		M93a	Y
354.1+2.9a*	CG	0.040	...	0.00	...		Ju92c	
354.1+2.9b*	CG	0.031	0.11 (0.01)	12.05 (0.05)	0.73 (0.11)		Ju92a	
354.1+2.9c*	CG	0.023	0.06 (0.01)	11.39 (0.11)	1.31 (0.25)		Ju92a	Y
354.1+2.9d*	CG	0.017	0.05 (0.01)	9.77 (0.14)	1.30 (0.34)		Ju92b	
354.1+2.9e*	CG	0.020	0.05 (0.01)	11.85 (0.09)	1.29 (0.21)		Ju92c	
354.2+3.2	I/C	0.031	...	0.00	...		Ju92c	Y
356.5-4.5*	I	0.028	...	0.00	...		Ju92c	Y
4.9-24.6	CG	0.028	...	-30.00	...		N91	
		0.045	...	30.00	...		N91	

Notes:**Cloud Type:**

- I = isolated
- CG = cometary globule
- N = nebula associated
- F = filamentary
- C = complex

V_{lsr} : When no signal was observed the velocity of the central channel is given.

 V_{other} :

- 1 = Zealey *et al.* (1983)
- 2 = Goss *et al.* (1980)
- 3 = de Vries *et al.* (1984)
- 4 = Sandqvist and Lindroos (1976)
- 5 = Clemens *et al.* (1991)
- 6 = Kuiper *et al.* (1987)

Session:

- A90 = August/September 1990 ($\Delta v = 0.25$ kms $^{-1}$)
- Ja91a = January 1991 ($\Delta v = 0.25$ kms $^{-1}$)
- Ja91b = January 1991 ($\Delta v = 0.12$ kms $^{-1}$)
- N91 = November 1991 ($\Delta v = 0.12$ kms $^{-1}$)
- Ju92a = June 1992 ($\Delta v = 0.10$ kms $^{-1}$, 1024 channels)
- Ju92b = June 1992 ($\Delta v = 0.20$ kms $^{-1}$)
- Ju92c = June 1992 ($\Delta v = 0.10$ kms $^{-1}$, 2048 channels)
- M93a = March 1993 ($\Delta v = 0.20$ kms $^{-1}$)
- M93b = March 1993 ($\Delta v = 0.12$ kms $^{-1}$)

IRAS: Y = IRAS source associated.

was visible the velocity of the central channel is quoted. Column 7 indicates the velocity of the signal observed in previous studies, where 1 = Zealey *et al.*, 1983 (H₂CO), 2 = Goss *et al.*, 1980 (H₂CO), 3 = de Vries *et al.*, 1984 (CO), 4 = Sandqvist and Lindroos, 1976 (H₂CO), 5 = Clemens *et al.*, 1991 (CO) and 6 = Kuiper *et al.*, 1987 (NH₃). Column 8 indicates the observing session when the spectrum was obtained and the velocity resolution. The legend to this column is given at the end of the table. Column 9 indicates whether there is an *IRAS* point source associated with the cloud. The detection statistics are discussed in section 3.5.1 where a comparison with cores in complexes is presented, and throughout the Discussion section.

3.4.2 Derived Properties

We have only been able to successfully fit the ammonia hyperfine pattern to 13 of the sources listed in table 3.1, allowing the opacity to be estimated and hence the excitation temperature to be derived for a limited number of sources. Another 23 sources have hyperfine components visible in their spectra, but the model fit implies either a low optical depth or low signal-to-noise ratio, or the uncertainties in the fit are large (usually a result of hyperfines with varying heights, perhaps implying non-LTE conditions, see e.g., Stutzki *et al.*, 1984; Stutzki and Winnewisser, 1985a). For these sources the integral over the hyperfine components has been used to determine the column densities. As explained earlier, for these sources where we have not been able to determine the excitation temperature directly a value of 6 K has been assumed. For the 10 globules which have been mapped, the mean value for the filling factor is 0.75. As mentioned previously, this value of 0.75 has been assumed for the beam filling factor for the unmapped sources in the analysis. Based on the derived values of T_R and those determined by previous workers, we have assumed that $T_R = 10$ K when we have not been

able to derive it, in order to estimate the total column density of NH_3 . For the cometary globules we have assumed that $T_R = 13$ K for similar reasons. The column densities are not highly sensitive to the value of T_R used. In determining the core masses, half of the half power diameter shown in table 4.1 has been used as the cloud radius.

The determination of the total density requires a knowledge of both the kinetic and excitation temperature. In some cases it has been possible to determine only one of these temperatures, and so in order to estimate the density the other temperature has been assumed. These cases are indicated in table 3.2, which shows the results of the analysis. In this table, column 1 lists the cloud name. Column 2 indicates the value of the optical depth derived from the best fit spectrum, and column 3 the derived excitation temperature. Column 4 lists the column density of the (1,1) transition, and column 5 indicates how this density was derived, where 1.0 indicates the column density is found from the model fit (equation 3.5), and 0.5 indicates it was derived from the integral over the satellite lines (equation 3.6). Column 6 lists the value of T_R used, and column 7 the total column density of NH_3 . Column 8 lists the derived values of T_K . Column 9 lists the derived values of $n(\text{H}_2)$, and column 10 how the density was derived, where 1.0 indicates it was derived from a knowledge of both T_{ex} and T_K , and 0.5 indicates that one of T_{ex} or T_K was assumed. Column 11 lists the beam average column density, and column 12 the assumed cloud distance, which is found from stellar reddening as described earlier, unless otherwise indicated. Column 13 lists the core mass, where the core radius is used (half of the half power contour diameter), which is found either from mapping the source, or in the case of the CGs, assumed to be equal to the optical size, and Column 14 indicates the beam averaged mass. Note that in many of the columns in table 3.2 too many significant figures are quoted, but that these were used in the

Table 3.2: Derived parameters from ammonia spectra.

Notes:

- (a) $m_1 = 1.0$ if $N(1, 1)$ determined from fit of model spectrum.
 $m_1 = 0.5$ if $N(1, 1)$ determined from the integral over the satellite lines.
- (b) If T_R undetermined then $T_R = 10$ K assumed for globules, $T_R = 13$ K assumed for CGs.
- (c) $m_2 = 1.0$ if $n(H_2)$ determined from know values of T_{ex} and T_K .
 $m_2 = 0.5$ if $n(H_2)$ determined assuming a value for one of T_{ex} or T_K .
- (d) Beam averaged column density.
- (e) Distance estimates:
 - 1 = Vela/Gum CG ($D = 400$ pc)
 - 2 = Bok (1977)
 - 3 = Proximity to Coalsack ($D = 175$ pc)
 - Others from reddening.
- (f) Radius found either from mapping, or for CGs assumed to be equal to the cloud head when not mapped.

Table 3.2 continued

Name	τ_m	T_{ex} (K)	$N(1,1)$ $\times 10^{14} \text{ cm}^{-2}$	$m_1^{(a)}$	$T_R^{(b)}$ (K)	$N(NH_3)$ $\times 10^{14} \text{ cm}^{-2}$	T_K (K)	$n(H_2)$ $\times 10^4 \text{ cm}^{-3}$	$m_2^{(c)}$	$\langle N(H_2) \rangle^{(d)}$ $\times 10^{22} \text{ cm}^{-2}$	D ^(e) (pc)	$M^{(f)}$ M_\odot	$\langle M \rangle$ M_\odot
253.3-1.6	1.46	6.37	2.01	1.0	13.2	6.10	13.9	1.23	1.0	1.51	400 ¹	9.0	8.6
267.4-7.5	0.92	4.77	0.97	1.0	16.2	2.47	17.7	0.61	1.0	0.70	400 ¹	13.0	4.0
267.7-7.4	2.42	5.55	1.85	1.0	11.1	7.00	11.4	1.02	1.0	1.75	400 ¹	7.5	10.0
275.9+1.9	1.01	5.19	0.83	1.0	11.0	3.18	11.3	0.84	1.0	0.87	300	4.9	2.8
295.0+3.4	1.22	4.78	1.38	1.0	10.6	5.61	10.9	0.68	1.0	1.51	350	6.1	6.6
297.7-2.8	1.83	7.16	2.39	1.0	11.5	8.59	11.9	2.03	1.0	2.35	150 ³	1.9	1.9
327.2+1.8	1.29	5.65	0.84	1.0	11.0	3.22	11.3	1.07	1.0	0.78	250	2.1	1.8
345.4-4.0	2.79	5.82	4.61	1.0	8.9	25.99	9.0	1.62	1.0	6.50	400	11.8	37.2
B68	1.98	5.34	0.84	1.0	14.7	2.30	15.8	0.72	1.0	0.54	200 ²	0.7	0.8
252.2+0.7			0.43	0.5	13	1.33				0.33	400 ¹		1.9
252.5+0.1	1.78	3.84	1.18	1.0	13	3.64	14	0.28	0.5	0.91	400 ¹	1.3	5.2
253.1-1.7A			0.74	0.5	13.6	2.18	14.4	1.03	0.5	0.57	400 ¹	13.4	3.3
235.1-1.7B			0.30	0.5	13	0.93				0.23	400 ¹		1.3
253.6+2.9			0.40	0.5	13	1.23				0.31	400 ¹		1.8
253.8-10.9	1.89	3.92	0.94	1.0	13	2.90	14	0.30	0.5	0.73	400 ¹	1.1	4.1
256.2-14.1			0.32	0.5	13	0.99				0.25	400 ¹		1.4
259.9-0.0			0.97	0.5	10	4.35				1.09	500		9.7
260.7-12.4			0.52	0.5	13	1.61				0.40	400 ¹		2.3
262.9-15.5	1.87	3.78	1.04	1.0	13	3.21	14	0.26	0.5	0.80	400 ¹	0.5	4.6
267.2-7.2			0.33	0.5	10	1.48				0.37	400 ¹		2.1
267.5-7.4	1.39	4.50	0.99	1.0	10	4.44	10	0.55	0.5	1.11	400 ¹	1.9	6.4
267.6-6.0A			0.37	0.5	10	1.66				0.42	450		3.0
274.2-0.4			0.38	0.5	10	1.71				0.43	500		3.8
289.3-2.8			0.49	0.5	10	2.20				0.55	250		1.2
291.1-1.7			0.35	0.5	10	1.57				0.39	250		0.9
293.3-0.9			0.62	0.5	10	2.78				0.70	900		20.0
300.0-0.7			0.27	0.5	10	1.21				0.30	175 ¹		0.4
302.1+7.4			0.37	0.5	10	1.66				0.42	300		1.3
331.0-0.7			0.42	0.5	13	1.30				0.32	200		0.5
334.6+4.6			0.29	0.5	10	1.30				0.33	250		0.7
344.6-4.3			0.89	0.5	10	3.99				1.00	700		17.5
345.0-3.5			0.29	0.5	10	1.30				0.33	400		1.5
347.5-8.0			0.65	0.5	10	2.92				0.73	450		5.3

calculations to avoid rounding errors.

For clouds where the core sizes are unknown, we have determined the beam averaged mass (i.e., the mass within the telescope beam) from the beam averaged column density and equation 3.15, assuming an ammonia abundance of 3×10^{-8} , which is the average value derived for the clouds in this work, where we have been able to determine it. By comparison with masses derived from the core sizes we can see that the beam averaged masses are not a bad approximation of the core mass. If we calculate the beam averaged masses for sources where we have determined the abundances, and use this abundance instead of the group average, then the agreement improves (i.e., for the sources in table 3.2 for which $m_2 = 1.0$).

3.5 Discussion

3.5.1 Comparison with Cores in Complexes

We wish to investigate whether there are any important differences between cores found in dark cloud complexes and those found in small isolated dark clouds. The major study of dense cores in complexes was undertaken by Myers and co-workers during the 1980s, culminating in the publication of a major survey of dense cores for ammonia emission BM89. The properties of these cores have been outlined in the first chapter. The following is a comparison between the results of BM89 and the survey undertaken here.

BM89 divided their survey results into four categories. They defined strong detections as those having $T_a^* \geq 0.35$ K, moderate detections as those with 0.35 K $> T_a^* > 3\sigma$, questionable detections as those with a possible signal in the

range $2 - 3\sigma$ at the correct velocity, and the fourth group as those with no detectable emission. In this work, 9 sources were found to be strong (5%), 67 to be moderate (40%), 8 had questionable detections (5%) and 85 of the 169 clouds had no observable signal (50%). These results, along with those of BM89, are shown in table 3.3. In this table, column 1 lists the type of detection, as indicated above, column 2 the number of each type of detection in this work, column 3 the same numbers for the BM89 sample, column 4 the same numbers for the BM89 sample with their Taurus sources removed, and column 5 the same numbers for the BM89 sample with both their Taurus and Ophiuchus sources removed.

Several points are worth noting. Firstly, the number of non-detections in both samples is similar at about 50%. This would seem to imply that at least 50% of the sources surveyed have densities sufficient to suggest that they may be in the process of gravitational contraction leading to star formation, or at least are gravitationally bound. Some sources may not have been detected because they are too distant or too small compared to the beam size, resulting in beam dilution, or because we have yet to observe the densest part of the cloud (for the larger clouds).

The number of strong sources is significantly less than that found by BM89 for the cores in complexes, with only 5% of the globules in this survey being strong, while 28% of the BM89 sample are strong detections. BM89 include in their sample many cores from the Taurus and Ophiuchus dark clouds, which are nearby (~ 150 pc) and are known to be undergoing relatively efficient star formation. It may be that the cores in these clouds are significantly affecting the BM89 results, since it is unlikely that many of the globules lie this close to the Sun. To test this, table 3.3 also shows the BM89 results with the Taurus and Ophiuchus sources removed. It can be clearly seen that the removal of these sources has not significantly changed the detection statistics of BM89. It

Table 3.3: Results of survey for ammonia emission in southern dark clouds. Also shown are the results of Benson and Myers (1989).

Detection Type	This Work	BM89	BM89 ^(a) (-Taurus)	BM89 ^(b) (-Taurus and Ophiuchus)
strong ($T_a^* \geq 0.35$ K)	9 (5%)	42 (28%)	29 (25%)	19 (23%)
moderate ($3\sigma \leq T_a^* < 0.35$ K)	67 (40%)	24 (16%)	21 (18%)	11 (13%)
weak ($T_a^* \sim 2-3\sigma$)	8 (5%)	12 (8%)	10 (9%)	10 (12%)
No Detection	85 (50%)	71 (48%)	54 (47%)	44 (52%)
Totals	169	149	114	84

Notes:

(a) Taurus sources removed from sample.

(b) Taurus and Ophiuchus sources removed from sample.

would appear that on the whole the cores in complexes are stronger emitters of ammonia than the cores found in globules. The most obvious reason would seem to be that the cores found within complexes are denser, as a result of their interactions with the dark cloud in which they live.

One way to test this idea is to examine the opacities and excitation temperatures of the two samples. Equation 3.2 shows the relationship between the measured intensity from the cloud (the antenna temperature), the excitation temperature of the transition and the opacity. Equation 3.12 then shows how the density of the cloud affects the excitation temperature. We will assume that the kinetic temperature of the different clouds are about equal, which has been shown to be true for both complexes and globules by many workers (see e.g., BM89; Leung *et al.*, 1982). The globules in the BM89 sample are excluded from their sample in this comparison. For this work we find that the average value of the derived optical depth for 13 sources is 3.5 ± 1.0 (this is the total optical depth τ_o of the transition), while for the BM89 sample of 48 sources it is 6 ± 3 (see figure 3.5). If we include the 6 BM89 globules (L1512, L1544, L63, B335, B361, L1262A), then the average optical depth for globules is 4 ± 2 (for 18 sources, where L1544 has been excluded from the calculation since $\tau_o = 13$). The cores in complexes thus show a greater opacity in the (1,1) line of ammonia. This should come as no surprise, since we know the cores in complexes are surrounded by a medium which is denser than the general interstellar medium surrounding the isolated globules.

The average value of the excitation temperature for the globules in this work is ~ 6 K, which is probably an upper limit for the weaker sources, as has been discussed earlier. For the BM89 sample $T_{ex} \sim 7.5$ K, and so the excitation temperature of the cores in complexes is also on average greater than that found in globules. Equation 3.2 thus shows that we should expect the measured intensity

to be lower on average for the globules. It should then follow that the density derived for the globules is also lower, since for a constant kinetic temperature the variation in excitation temperature depends directly on the density. This is suggested by the ammonia column densities of the two samples, as shown in figure 3.6. For this work the average is $\log N \sim 14.4 \pm 0.2$ (33 sources) while for BM89 $\log N \sim 14.8 \pm 0.3$ (48 sources). More conclusive is the fact that 85% of the globules have $\log N \leq 14.6$ while 85% of the cores in complexes have $\log N \geq 14.6$. For the sources where we have been able to determine the total density, combined with 6 globules from BM89, we find an average value of $\log n \sim 4.1 \pm 0.4$ (20 sources), where $n = 1.2 n(H_2)$ (see figure 3.7). For the cores in complexes we find $\log n \sim 4.5 \pm 0.5$ (48 sources). To compare the densities of the two samples, the densities of the BM89 sources have been recalculated using equation 3.12 and the values of T_{ex} and T_K quoted by BM89. The densities of the cores within complexes are thus on average more than twice that found in the isolated globules, though as can be seen in figure 3.7 the argument is not as strong as it is for the differences in the column densities.

Why are the globules less dense than the cores in complexes? It may be that, since the cores in complexes are subject to an external pressure greater than that found in the interstellar medium, they have a greater density as a counterbalance, since most studies show that the physical state of a typical dense core is close to equilibrium (see e.g., Myers, 1983, 1985). These cores may also be subject to larger magnetic fields than the isolated globules, which would provide a mechanism of support to the cores, allowing them to reach greater densities via ambipolar diffusion before they begin to contract irreversibly. However, the observed correlation $\Delta v \propto R^{0.5}$ over three orders of magnitude implies that the magnetic field does not vary strongly from region to region (Shu *et al.*, 1987). This is examined in section 4.3.3, where we show that this law may break down

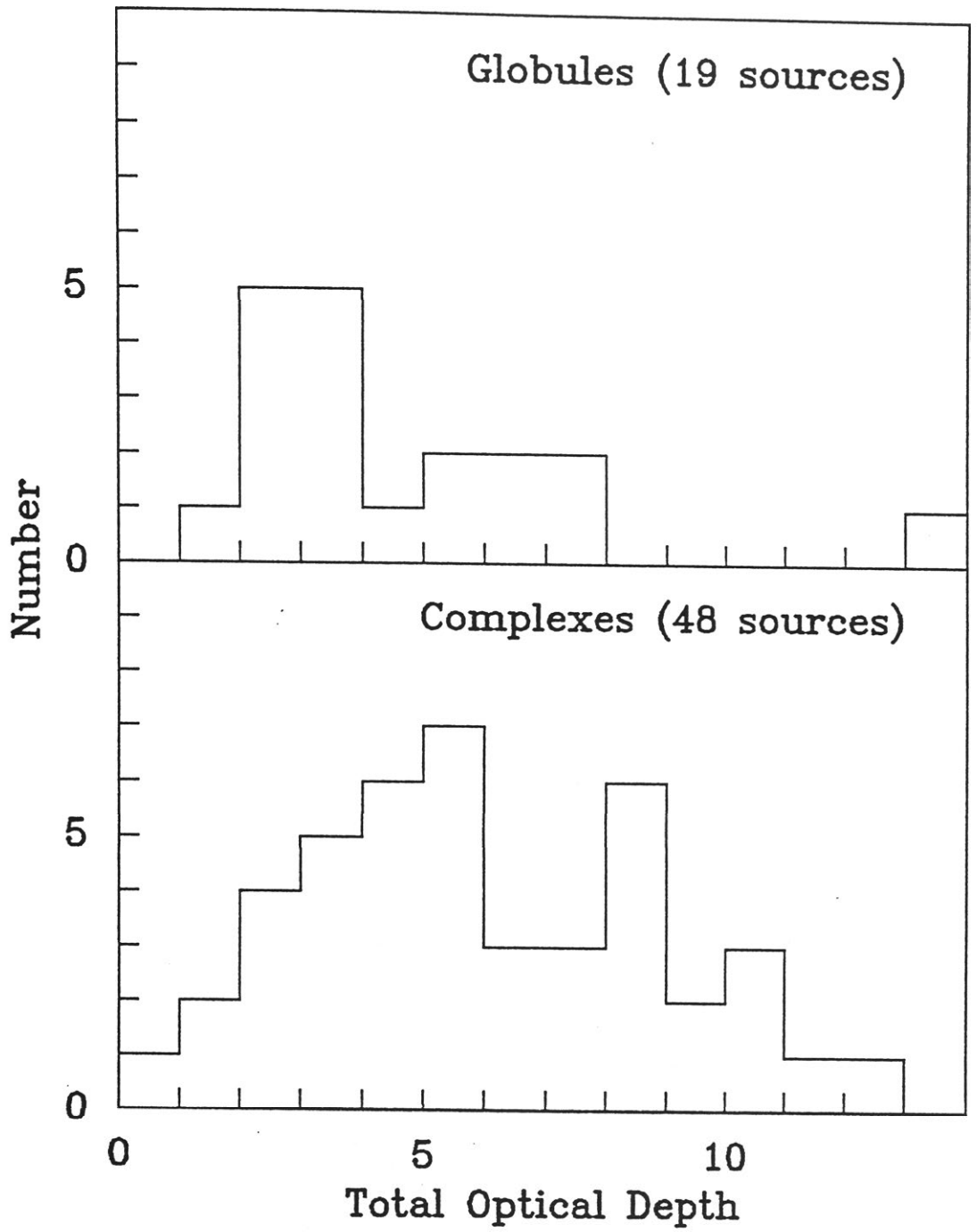


Figure 3.5: Histograms of the total optical depth of the (1,1) inversion transition of NH_3 for globules (top) and cores in complexes (bottom).

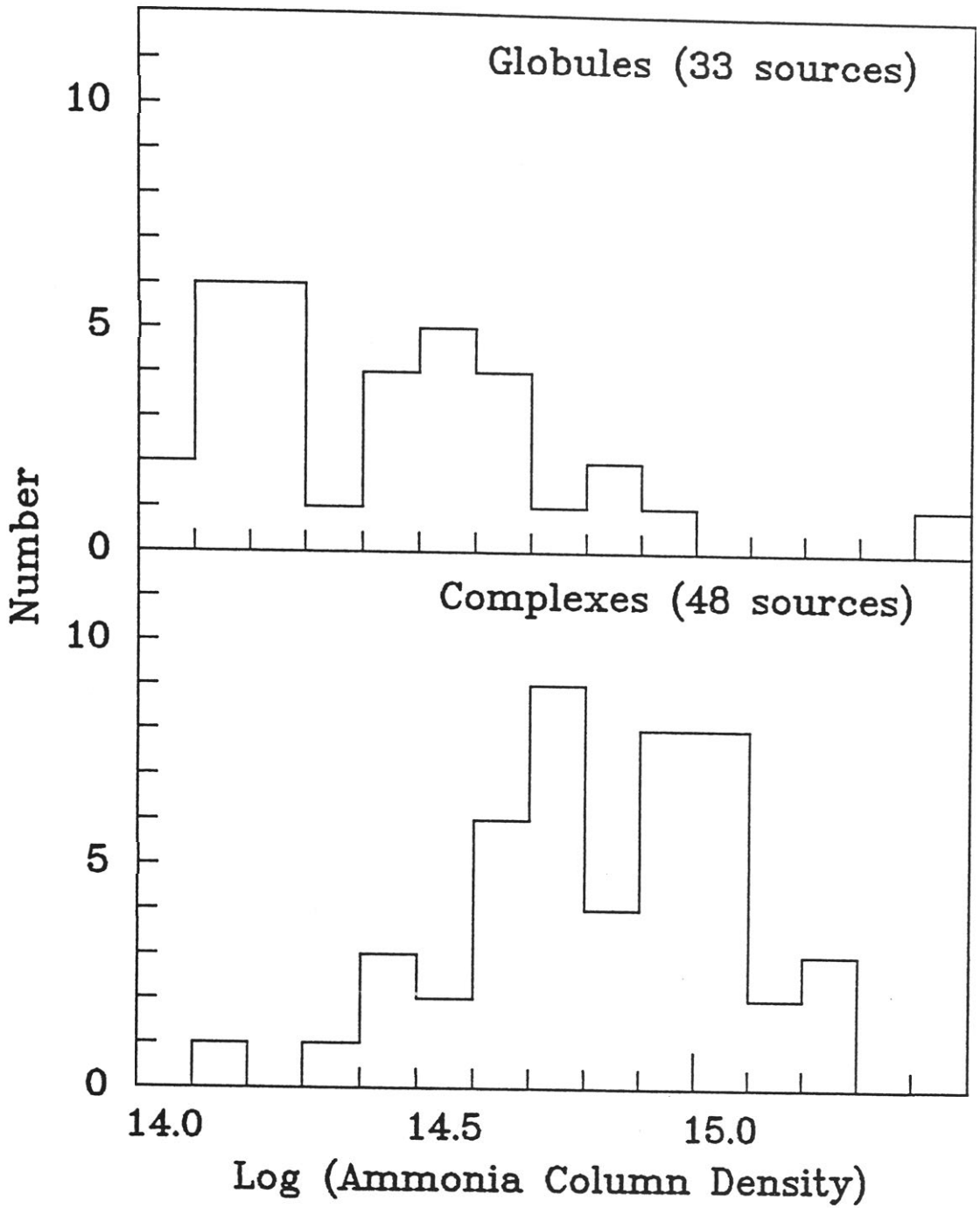


Figure 3.6: Histograms of the total ammonia column density for globules (top) and cores within complexes (bottom).

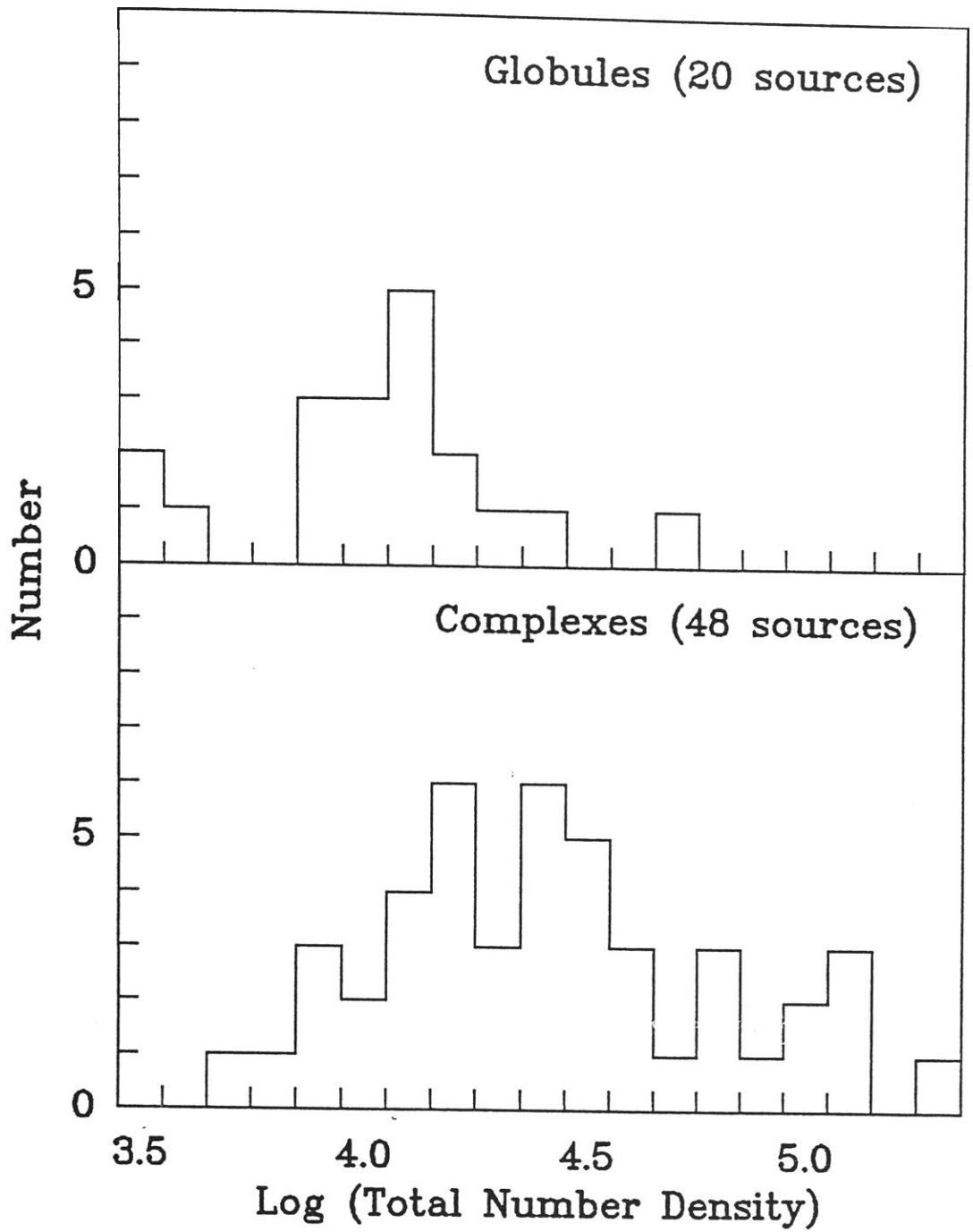


Figure 3.7: Histograms of the total number density for globules (top) and cores within complexes (bottom).

for small globules.

An attempt has been made to rule out distance effects in the above comparisons by removing the Taurus and Ophiuchus cores from the BM89 sample. However, the possibility that the effect of beam dilution is masking the true nature of the globules cannot be ruled out altogether, since BM89 showed that if they move their Taurus sources to a distance of 420 pc, then only 3 of that sample remain as strong detections. It is believed, however, that the difference observed between the globules and complexes may be real, and due primarily to the different environments in which they reside. What is clearly required are higher spatial resolution observations in order to prevent beam dilution being a major uncertainty.

For the beam averaged masses in this work we find a mean value of $M \sim 5 \pm 7 M_{\odot}$, with a median value in the range $2 - 3 M_{\odot}$ (see figure 3.8). BM89 find for their cores an average mass $\sim 50 \pm 140 M_{\odot}$, with a median value of $13 M_{\odot}$. However, they have used the core diameter as the radius in their mass calculations, so their mass estimates will be ~ 8 times greater for any one source. If they were to have used the core radius, they would have found an average core mass of $\sim 6 M_{\odot}$, with a median value of $\sim 2 M_{\odot}$. So we can see that the masses of the cores within globules and the cores within complexes are similar, despite the differences in their densities and opacities. Both samples consist of low mass cores.

3.5.2 Globule Sizes

It was suggested in section 3.5.1 that some globules may not have been detected in ammonia because of their size. If they are too small compared to the Parkes beam size at 23.7 GHz of $1.4'$, then they may have suffered from beam dilution.

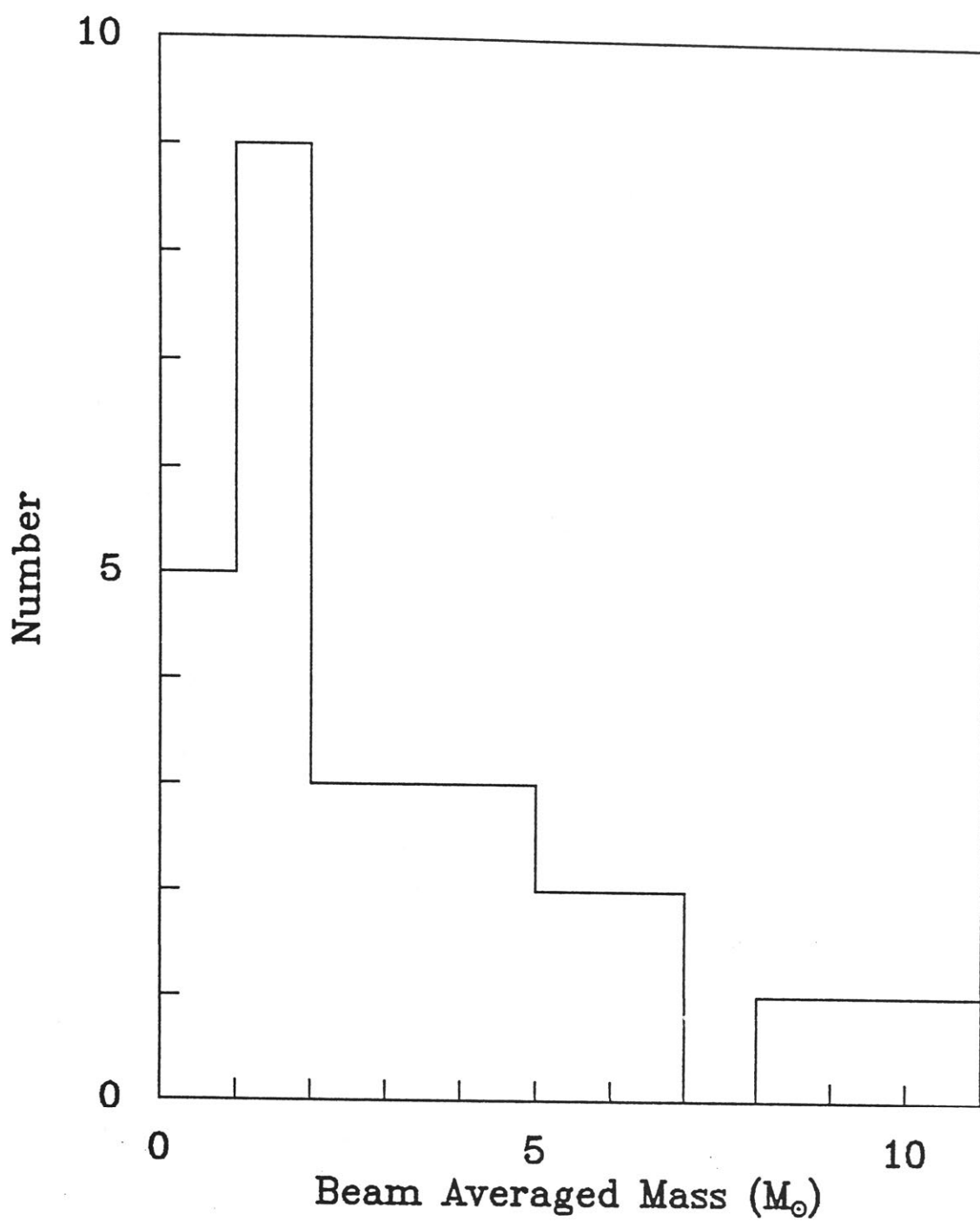


Figure 3.8: Histogram of the beam averaged masses of globules in this work. Excluded from this plot are 3 sources with masses greater than $10 M_{\odot}$.

If they are large we may not have observed the densest part of the globule. We will now look at the cloud sizes and the number of detections for each cloud size to see if there may be any evidence to support this conjecture. Table 3.4 shows the number of clouds detected in each size range. Column 1 lists the size ranges, column 2 the number of detections in each size range, column 3 the number of non-detections in each size range, and column 4 the number of detections as a percentage of the total number of clouds in each size range.

It can immediately be seen that the smaller globules ($< 2'$) are not readily detected (detection rate 36%). As suggested above, beam dilution is the likely reason, due to their apparent small size, for the small globules which do have dense cores. However, we also see a relatively low detection rate for the largest globules ($> 5'$) of 39%. Again, a likely reason has already been suggested. It is quite possible that with the large globules we have not observed the densest part of the globule, which is difficult to determine by eye when the globule expands more than a few arcminutes. In general only one position with each globule has been searched, so more positions within these globules should be searched for ammonia emission. It would, however, seem unlikely that many, if any, of the largest undetected globules will become strong ammonia detections, unless their core size is very small.

3.5.3 Cometary Globules

The Cometary Globules (CGs) associated with the Gum Nebula (Hawarden and Brand, 1976; Sandqvist, 1976; Reipurth, 1983; Zealey *et al.*, 1983) form an interesting subsample of the list of globules presented here. The favoured scenario for their formation has been discussed in Chapter 1 (Reipurth, 1983). They appear to have been subjected to a considerable external pressure in the

Table 3.4: The number of clouds in this survey detected in each size range is shown. The size is the geometric mean size as shown in table 2.1 of the previous chapter.

Size Range	Detections	Non-detections	% Detected
< 1'	1	2	33
1 - 2'	13	23	36
2 - 3'	31	25	55
3 - 4'	21	13	62
4 - 5'	9	8	53
> 5'	9	14	39

form of a wind or shock, which may have resulted in significant compression of their heads. Did they exist as cores within larger cloud complexes before they were disrupted, or were the cores formed by the passage of the wind or shock?

In this study there are 32 globules which have been identified as possibly associated with the Vela–Gum region (Reipurth, 1983; Zealey *et al.*, 1983) which we have observed for ammonia emission. We have also observed four of the Globular Dark Clouds (GDCs) identified by Reipurth (1983), these being GDC1 (=DC 267.4-7.5), GDC2 (DC 267.5-7.4), GDC4 (DC 267.2-7.2) and GDC5 (DC 267.7-7.4). Of this list of 36, 4 are found to be strong emitters of ammonia (11%) and 23 have detections greater than 3σ (64%). We thus find that as a group the CGs are detected more frequently than the other Bok globules in this study (75% compared with only 38% for the other globules). Such a high detection rate would suggest that the external forces which have been at work on the CGs have had a significant effect on their internal structure. Of the 9 CG with geometric head sizes $\leq 1'$, 7 were not detected in ammonia, while the two that were had the lowest antenna temperatures amongst the CGs. If beam dilution is the reason for their non-detections, then it may be that all the CGs in the Gum region contain dense cores. At an assumed distance of 400 pc the CGs with head sizes $\leq 1'$ have beam filling factors < 0.35 , so beam dilution is plausible.

What are the physical characteristics of the detected cometary globules? Four of the globules have been mapped in sufficient detail for their core sizes to be derived. For three of these the core size closely approximates the optical size of the globule head. Table 3.5 show the properties derived for the CGs based on the assumptions outlined below. Column 1 lists the CG name, according to Zealey *et al.* (1983) and Reipurth (1983), and column 2 the observed antenna temperature. Column 3 lists the optical head size in arcminutes, column 4 the beam filling factor, and column 5 the core diameter in parsecs, assuming a

common distance of 400 pc to the CGs. Column 6 lists the (1,1) column density, and column 7 the method used to derive the column density, where 1 indicates the model fit spectrum has been used, 0.5 indicates the integral over the satellite lines has been used, and 0 indicates that the integral has been performed over the main line group. Column 8 lists the total ammonia column density and column 9 the molecular hydrogen density. Column 10 indicates the approximate core mass, and column 11 the luminosity of any associated *IRAS* sources. The core size is assumed to equal the optical size of the CG head for the reason given above (except for GDC5, which we have mapped and has a core size less than the head size). This is most likely an overestimate in many cases, but it is the best approximation we can arrive at, and will not have a significant affect on our conclusions. For positions where it has not been possible to fit a model NH_3 spectra the cloud average for T_{ex} of 6 K has been assumed, again most likely an overestimate in many cases. An attempt has been made to determine the lower limit to the (1,1) column density using one of the methods outlined in the section on data analysis, either by fitting the ammonia hyperfine pattern to the observed spectra, or by integrating over the spectral lines and assuming optically thin conditions. For four of the CGs it has been possible to determine their kinetic temperatures. For two of the “true” CGs in the list (CG30 and CG31A), the values of $T_R \sim T_K$ is ~ 13 K, while for the other two (GDC1 and 5) the values of T_R are 16 K and 11 K respectively. Thus a value for the kinetic temperature of 13 K has been assumed for the cometary globules. The CGs appear slightly warmer than the average core as defined by the work of BM89 ($T_K \sim 10$ K), though the temperature of a larger number of CGs need to be determined to state this with certainty (Harju *et al.*, 1990, found $T_K = 15$ K for the core region of CG1, and studies of other CG-like globules also find higher than “average” temperatures, e.g. Cernicharo *et al.*, 1992). With these assumptions we are able to estimate the total column densities of NH_3 for the

detected CGs, and assuming a value for the ammonia abundance, their densities (lower limits).

It has been possible to estimate the ammonia abundance for 7 of the CGs, for which we find an average value of $4 \pm 3 \times 10^{-8}$. For the globule sample as a whole we find a median value of $\sim 3 \times 10^{-8}$, similar to that found by Harju *et al.* (1993). The abundance is thus assumed to be 3×10^{-8} in the calculations here. The masses may then be estimated by adopting a distance of 400 pc to the CGs. The luminosities of any associated *IRAS* sources may also be estimated. The flux quality of the *IRAS* associations has been ignored when selecting sources possibly associated with the CGs. Bhatt (1993) has shown that the *IRAS* sources found lying within the CG optical boundaries have a high probability of being true associations, by comparing the occurrence of *IRAS* sources lying toward the CGs with that of the surrounding sky.

The column densities for the CGs lie mainly in the range $8 \times 10^{13} \text{ cm}^{-2}$ to $3.2 \times 10^{14} \text{ cm}^{-2}$, with core densities in the range $n(H_2) \sim 2.5 \times 10^3 \text{ cm}^{-3}$ to $1 \times 10^4 \text{ cm}^{-3}$. The average value for the core mass is $\sim 3 M_\odot$, while the median value lies in the range $1 - 2 M_\odot$. Here half of the core geometric mean diameter (denoted d in table 3.5) has been used to calculate the mass. The assumptions we have made suggest that these values are probably lower limits in most cases. Therefore a “typical” CG in the Gum region has an ammonia column density $N(NH_3) \sim 3 \times 10^{14} \text{ cm}^{-2}$, density $\sim 10^4 \text{ cm}^{-3}$, and a core mass of $2 - 3 M_\odot$. For the associated *IRAS* sources, we find that the majority ($\sim 60\%$) have bolometric luminosities $L_{bol} \leq 3L_\odot$, with an average value of $\sim 5 L_\odot$ (with CG12 removed from the calculations).

The average properties of the CGs are thus very similar to those found in cores in dark cloud complexes (see e.g., BM89). BM89 show that if their Taurus cores were moved to a distance of 420 pc, then only 3 of their 13 strong detections

Table 3.5: Derived properties of Cometary Globules in the Vela/Gum Nebula Region.

Notes:

(a) Optical head size, except for GDC5 (see text).

(b) $m = 1.0$ $N(1, 1)$ determined from fit of model spectrum.

$m = 0.5$ if $N(1, 1)$ determined from integrating over the satellite lines.

$m = 0$ if $N(1, 1)$ determined from integrating over the main line group.

(c) Ammonia abundance of 3×10^{-8} assumed.

Name	T_a^* (K)	$a \times b^{(a)}$ (')	ϕ	d (pc)	$N(1,1)$ ($\times 10^{14} \text{ cm}^{-2}$)	$m^{(b)}$	$N(\text{NH}_3)$ ($\times 10^{14} \text{ cm}^{-2}$)	$n(\text{H}_2)^{(c)}$ ($\times 10^4 \text{ cm}^{-3}$)	M (M_\odot)	L_{bol} (L_\odot)
CG1	0.10	2' \times 2'	0.67	0.23	0.36	0.5	1.10	0.26	1.1	17.2
CG2	0.11	2' \times 2'	0.67	0.23	0.23	0	0.71	0.16	0.7	1.9
CG3	0.17	3' \times 1.5'	0.66	0.25	0.59	0.5	1.83	0.40	2.0	2.8
CG4	0.20	4' \times 1'	0.55	0.23	0.37	0	1.13	0.26	1.1	
CG5	0.09	1' \times 0.5'	0.20	0.08	0.52	0	1.59	1.05	0.2	1.3
CG6	0.19	3' \times 1'	0.53	0.20	0.48	0	1.49	0.40	1.1	
CG7	...	2' \times 1.5'	0.60	0.20						
CG11	...	2.5' \times 1.5'	0.64	0.23						
CG12	...	4' \times 3'	0.86	0.40	0.35	0	1.09	0.15	3.2	56.4
CG13	0.12	5' \times 3'	0.87	0.45	0.18	0	0.56	0.07	2.0	
CG14	0.11	3' \times 1'	0.53	0.20	0.26	0	0.82	0.22	0.6	1.9
CG15	0.19	3' \times 1'	0.53	0.20	0.36	0	1.13	0.30	0.8	1.1
CG16	0.21	2' \times 1'	0.48	0.16	1.04	1	3.21	1.05	1.6	
CG17	...	1' \times 1'	0.34	0.12						
CG18	...	0.5' \times 0.5'	0.11	0.06						
CG19	0.12	2' \times 1'	0.48	0.16	0.58	0.5	1.81	0.59	0.9	2.7
CG20	0.19	4' \times 1.5'	0.69	0.29	0.28	0	0.86	0.16	1.3	
CG21	...	7' \times 2'	0.80	0.44						
CG22	0.14	5' \times 3'	0.87	0.45	0.35	0.5	1.07	0.13	3.9	3.7
CG24	0.07	1' \times 1'	0.34	0.12	0.24	0	0.75	0.35	0.2	
CG26	0.23	2' \times 1'	0.48	0.16	0.68	0.5	2.09	0.68	1.0	0.9
CG27	0.22	2' \times 1'	0.48	0.16	0.50	0	1.56	0.51	0.8	1.1
CG28	...	1' \times 1'	0.34	0.12						1.3
CG29	...	1' \times 1'	0.34	0.12						
CG30	0.61	3' \times 2'	0.74	0.29	2.01	1	6.20	1.18	9.1	13.2
CG31A	0.35	4' \times 2'	0.77	0.33	0.72	0.5	2.22	0.36	4.3	
CG31B	0.19	2' \times 2'	0.67	0.23	0.34	0.5	1.04	0.24	1.0	
CG31C	0.24	3' \times 2'	0.74	0.29	0.54	0.5	1.68	0.32	2.4	
CG31D	...	1' \times 1'	0.34	0.12						
CG32	0.22	3' \times 1.5'	0.66	0.25	1.18	1	3.64	0.80	4.0	9.2
CG33	...	0.8' \times 0.6'	0.20	0.08						
CG34	0.24	3' \times 1'	0.53	0.20	0.94	1	2.9	0.78	2.1	
CG36	...	1' \times 1'	0.34	0.12						1.3
GDC1	0.39	4' \times 3'	0.86	0.40	0.97	1	2.99	0.40	8.7	17.6
GDC2	0.30	2' \times 2'	0.67	0.23	0.99	1	3.06	0.71	3.0	
GDC4	0.20	2' \times 2'	0.67	0.23	0.36	0.5	1.13	0.26	1.1	3.3
GDC5	0.75	2.5' \times 2.5'	0.76	0.29	1.85	1	5.71	1.06	8.7	4.4

remain strong, compared with 4 CGs at a similar distance. This supports the claim that the values derived here are lower limits, due in part to beam dilution. The large number of *IRAS* sources associated with the CGs suggests that star formation is enhanced compared with other Bok globules (Bhatt, 1993). This would argue against the idea that all isolated Bok globules have passed through a CG phase in their evolution, though certainly doesn't rule out the possibility that some of the CGs will eventually form isolated globules. The parameters derived here for the CGs indicate that only low mass star formation is occurring within the CGs. The efficiency of star formation would appear to be a few \times 10%, somewhat larger than that found in dark cloud complexes. All indications suggest that the event responsible for the formation of the CGs has a burst of triggered star formation within them.

3.5.4 *IRAS* sources in Globules and Complexes

The *IRAS* sources associated with the dark clouds in this work are shown in table 2.2 of the previous chapter. All *IRAS* sources which lie within the cloud boundaries are shown in this table regardless of the quality of their detections. It was stated in the previous chapter that if the *IRAS* flux sensitivity limits could be lowered from 3 Jy to 1 Jy then almost all globules would be detected at 100 μm , a result which was first shown by Clemens *et al.* (1991).

More stringent selection criteria will now be applied to the *IRAS* sources, in an attempt to identify true point sources associated with the globules. In order to compare the number of sources associated with globules with those found in the cores in complexes, the selection criteria of BM89 is used. To be included here the *IRAS* sources must have been detected in at least two of the four *IRAS* wavebands, with a greater flux density at the longer wavelength. A total of

Table 3.6: *IRAS* sources associated with small southern dark clouds satisfying the selection criteria of BM89. Distance estimates: (1) = Vela/Gum CG; (2) = proximity to Coalsack; (3) = Chamaeleon; others from reddening.

DC Name	<i>IRAS</i> Name	D (pc)	L_{IRAS} (L_{\odot})	ΔL (L_{\odot})	L_{bol} (L_{\odot})
255.3-14.4	07114-4352	400 ¹	1.1	0.8	1.9
256.2-14.1	07178-4429	400 ¹	14.3	2.9	17.2
262.5-13.4	07372-4945	400 ¹	1.1	0.8	1.9
260.7-12.4	07378-4745	400 ¹	1.7	1.1	2.8
257.2-10.3	07391-4342	400 ¹	0.9	0.4	1.3
253.3-1.6	08076-3556	400 ¹	9.1	4.1	13.2
252.5+0.1	08124-3422	400 ¹	5.7	3.5	9.2
267.4-7.5	08242-5050	400 ¹	12.6	5.0	17.6
267.2-7.2	08250-5030	400 ¹	1.9	1.5	3.3
267.7-7.4	08261-5100	400 ¹	3.5	0.9	4.4
253.6+2.9	08267-3336	400 ¹	2.5	1.2	3.7
259.9-0.0	08337-4028	500	278.8	168.7	447.5
259.9-0.0	08337-4024	500	6.1	4.7	10.8
256.9+2.6	08354-3926	400 ¹	0.9	0.5	1.3
275.9+1.9	09449-5052	300	2.0	1.1	3.1
289.3-2.8	10471-6206	250	1.6	1.2	2.9
297.7-2.8	11590-6452	150 ²	4.5	2.3	6.9
301.7-6.7	12345-6910	150 ²	0.5	0.2	0.7
302.1+7.4	12427-5508	300	0.9	0.6	1.5
303.8-14.2	13036-7644	150 ³	0.5	0.3	0.8
307.3+2.9	13224-5928	400	6.4	3.2	9.6
316.5+21.2	13547-3944	400 ¹	39.1	17.2	56.4
314.8-5.1	14451-6502	400	4.4	1.9	6.3
320.7-1.7	15148-5911	350	10.1	8.1	18.2
320.5-3.6	15215-6056	350	1.8	1.1	2.9
320.1-4.3	15223-6146	350	1.2	0.8	2.0
344.5+2.0	16510-4026	350	6.8	3.7	10.5
337.1-4.9	16554-5031	300	2.7	2.3	5.0
351.2+5.2	16590-3313	700	6.9	2.3	9.2
351.2+5.1	16594-3315	700	14.1	2.6	16.7
349.0+3.0	17011-3613	200	1.0	0.8	1.8
349.2+3.1A	17012-3603	200	1.0	0.7	1.7
354.2+3.2	17151-3202	200	1.8	0.9	2.8
353.3+2.4	17156-3312	200	2.6	1.5	4.2
354.1+2.9C	17157-3212	200	2.2	0.9	3.1
353.1+2.3	17159-3324	200	6.6	5.9	12.5
345.2-3.6	17172-4316	400	3.7	2.5	6.2
344.6-4.3	17181-4405	700	86.8	44.4	131.2
345.4-4.0	17193-4319	400	3.2	2.0	5.1
356.5-4.5	17518-3414	300	1.1	0.8	1.9

40 sources in 39 globules satisfy this criteria, while BM89 found 39 sources in 28 cores. The sources satisfying this criteria are shown in table 3.6. Column 1 lists the globule name, column 2 the *IRAS* name and column 3 the adopted distance. The distance estimates are derived from stellar reddening as described earlier, unless otherwise noted. Columns 4–6 list the derived luminosities. The bolometric luminosity, L_{bol} , may be estimated from $L_{bol} = L_{IRAS} + \Delta L$, where L_{IRAS} is obtained from (Parker, 1991):

$$L_{IRAS} = 4\pi D^2 \int_{12\mu m}^{100\mu m} S_\nu d\nu \quad (3.17)$$

$$\simeq 4.7 \times 10^{-6} D^2 \left(\frac{S_{12}}{0.79} + \frac{S_{25}}{2} + \frac{S_{60}}{3.9} + \frac{S_{100}}{9.9} \right) L_\odot$$

where D is the source distance in parsecs and S_ν is the flux at frequency ν . Since the flux is increasing with wavelength a significant fraction of the flux may be emitted at wavelengths longer than 100 μm . The bolometric correction to the luminosity for these wavelengths may be estimated from:

$$\Delta L = 5.33 \times 10^{-5} D^2 \left(\frac{S_{100}}{100} \right) \quad (3.18)$$

assuming that the maximum flux density over the entire spectrum occurs at 100 μm , and that the spectrum is a blackbody for wavelengths greater than 100 μm (Myers *et al.*, 1987). No correction has been made for the luminosity at wavelengths shorter than 12 μm . The mean bolometric luminosity of the sources in table 3.6 with $L_{bol} < 50 L_\odot$ (37 sources), is $6 \pm 5 L_\odot$, with a median value of 2–3 L_\odot . For the BM89 sample the mean *IRAS* luminosity, L_{IRAS} , is $\sim 2 \pm 3 L_\odot$, with a median in the range $L_{IRAS} = 0 - 1 L_\odot$. Both samples therefore consist primarily of low luminosity, low mass sources. Note that of the three sources we have excluded from our average, two are associated with bright reflection nebulosities (259.9–0.0 and 316.5+21.2), while the other (344.6–4.3) contains a near-infrared reflection nebulosity associated with the embedded source, as indicated by our near-infrared observations not reported in this thesis.

BM89 have included some sources which are obviously confused (e.g., the two sources in L1495N have identical flux densities in all 4 *IRAS* wavebands), so an attempt has been made to avoid this problem here. For this work we find that 6 of the 9 strong sources (67%) have an associated *IRAS* source, while BM89 found 27 sources in their 40 nearby ($D < 500$ pc) strong detections (68%), so the results are similar. Strong ammonia emission would seem to be a good indicator of low mass star formation, as suggested by BM89, regardless of the core type. For the moderate detections, only 21 of our 67 cores have an associated *IRAS* source (31%), while for the cores in complexes BM89 found 9 of 19 moderate detections have an *IRAS* source (47%). So for good ammonia detections ($> 3\sigma$) only 27 of 76 (36%) are associated with an *IRAS* point source, implying that for globules detection of ammonia is not necessarily a good indication of advanced low-mass star formation, while for cores in complexes the opposite conjecture appears valid, since 36 of 59 (61%) of nearby cores with good ammonia detections have an associated *IRAS* source. This result, combined with the findings of the previous section, indicates that while low-mass star formation is occurring in some globules (see e.g., Bourke *et al.*, 1993; Yun and Clemens, 1990) the efficiency of star formation appears lower than that for cores within larger dark cloud complexes.

3.6 Conclusions

The catalogue of small, isolated molecular clouds (globules) presented in chapter 2 has been surveyed with the Parkes radio telescope for emission in the (1,1) inversion transition of ammonia. Approximately half of the 169 clouds surveyed were detected, with only 5% of these detections being strong. This result indicates that approximately half of the globules have densities sufficient to suggest

that they may undergo contraction leading to star formation, or at least are gravitationally bound.

The properties of the cores found within the globules were compared with the cores found within the larger dark cloud complexes. It was found that the cores within globules are less opaque and less dense than those found within complexes. This is not surprising, since the cores within complexes are embedded in a larger diffuse region of matter while, by definition, the globules are not, and so are subjected to larger external pressures than the globules. The strength of the ammonia emission from the globules was on average less than that observed from the cores within complexes, with only 5% of the globules being strong detections, while $\sim 25\%$ of the cores within complexes are found to be strong. This may be a direct result of the globules being less opaque and less dense than the cores within complexes. The average values of the other properties of the cores within the globules, such as temperature, cores size, mass, and luminosity of associated *IRAS* sources, are similar to those of the cores within complexes.

Small globules ($< 2'$) were not as readily detected in ammonia emission as the larger globules, probably due to beam dilution, since the beam size used was $1.4'$. Clearly high resolution observations of these globules with a high density gas tracer are required. Large globules ($5' - 10'$) were also not readily detected. The reason for this is not clear, but may be due to the core being missed by the telescope beam, since in general only one position within each cloud was searched. These large globules should be searched in more detail for possible missed cores.

The Vela-Gum Nebula cometary globules, as a subsample of the globules surveyed, were detected in ammonia emission in a significantly higher percentage (75% compared to 38%) than the other globules surveyed, and appear to be more active sites of star formation. Their enhanced star formation would suggest that

while some CGs may evolve into isolated Bok globules, it would seem unlikely that all Bok globules have passed through a CG phase in their evolution. The properties of the CGs are similar to those of the cores within complexes, with densities $\sim 10^4 \text{ cm}^{-3}$, temperatures $\sim 15 \text{ K}$, masses $\sim 2\text{--}3 M_{\odot}$, and *IRAS* sources with luminosities a few $\times L_{\odot}$.

Subjecting our *IRAS* sources to the selection criteria of BM89, we find that a lower percentage of the cores in globules (as defined by the detection of ammonia) are associated with *IRAS* sources than are associated with the cores within complexes (36% compared to 61%). This may imply that the detection of ammonia toward a globule is not necessarily a good indication of a site of low mass star formation, unless the detection is strong. Combined with the results that cores in complexes are denser and more opaque, and that the CGs are more active sites of star formation, it becomes clear that the environment in which the core resides is playing a significant role in the general process of initiating star formation, and that the cores in complexes and CGs are strongly influenced by their environment.

Chapter 4

Ammonia Mapping and Dynamical Analysis

4.1 Introduction

In the previous chapter the results of the survey of the 169 small molecular clouds for ammonia emission were presented. In this chapter we present the results of the mapping observations of the strongest sources found in the survey, and that of the more northern globule B68. The results of the mapping are discussed and compared to previous observations of the globules where they exist.

The dynamical state of the mapped globules is investigated by comparing their derived mass with that required for equilibrium of an isothermal, self-gravitating sphere. The problems with comparisons of the derived masses and those of the idealized models are discussed briefly, and possible causes for the observed differences between theory and observation outlined.

A combined sample of 15 globules from this study and that of Benson and

Myers (1989; hereafter BM89) is examined to see whether the power-law correlations between Δv and R , and n and R found by previous investigators for clouds of a large range of sizes hold. The dynamical nature of the globules as a group are investigated in an attempt to identify the major factors influencing the physical state of the globules (i.e., magnetic fields, turbulence).

4.2 Observations and Data Reduction

The observations have been described in detail in the previous chapter, and so will not be repeated here. The contour maps have been produced with the in-house spectral line data reduction package (SPC) of the Australia Telescope National Facility (ATNF). The full width at half maximum (FWHM) of the gaussian beam of the Parkes telescope at 23.7 GHz is $1.4'$, and the spacing used between the observed positions was $1'$. The contouring package in SPC attempts to take into account the gaussian nature of the telescope beam when interpolating the data onto a grid for contouring, the grid spacing being defined by the user. As suggested in the SPC manual, the grid spacing used for the interpolation was $0.7'$, i.e., half of the FWHM beam size.

4.3 Results

4.3.1 Source Mapping

Ten sources have been mapped on a $1'$ grid in sufficient detail to enable the core sizes to be estimated. The core area is defined to be the area within the half power contour of the ammonia map (BM89; Menten *et al.*, 1984). In all

sources presented here the half power contour closely approximates an ellipse, and the major and minor axis of this contour have been estimated directly from the maps. Once the source size is known then the beam filling factor ϕ may be determined. The results of the mapping are presented in table 4.1 and the maps are presented in figure 4.2. In table 4.1, column 1 lists the cloud name. Columns 2 and 3 list the cloud's major and minor axes, where the cloud has been approximated by an ellipse, and the cloud size is the half power contour. The aspect ratio, i.e., major axis/minor axis, is listed in column 4, and the beam filling factor in column 5. Columns 6 and 7 indicate the cloud size in arcminutes and parsecs, and column 8 the adopted cloud distance. The value of d quoted in this table is the geometric mean half-power diameter of the map.

Included in the list of mapped sources is B68, which is not part of the survey because of its more northerly declination (-23°), but which has been observed in some detail during the observing sessions as part of another study. It is a fine example of an isolated Bok globule which does not appear to be undergoing star formation. It is reasonably well studied (Bok, 1977; Leung *et al.*, 1982; BM89) and importantly is the only quiescent source in the mapped list which has been studied in some detail in ammonia by other workers (Martin and Barrett, 1978; BM89).

It is apparent from even this small sample that cores in globules have a range of sizes, in this work ranging from 0.13 pc for B68 to 0.41 pc for DC 267.4-7.5. BM89 found a very tight range for their globule sizes about a value of 0.11 pc, with only one globule (B361) being larger at 0.32 pc, while the mean of the globules in this sample is 0.27 pc. However, these are the strongest sources in our list, and more of the weaker globules need to be mapped before we are able to draw meaningful conclusions about the 'typical' globule core size. However, combining our 10 mapped globules with the 6 mapped globules from BM89

Table 4.1: Mapping Analysis Results

Name	Major Axis (')	Minor Axis (')	Aspect Ratio	ϕ	d (')	d (pc)	Distance (pc)
253.1–1.7A	3.8	2.3	1.7	0.80	2.9	0.34	400 ¹
253.3–1.6	2.7	2.1	1.3	0.74	2.4	0.28	400 ¹
267.4–7.5	4.4	2.8	1.6	0.85	3.5	0.41	400 ¹
267.7–7.4	2.5	2.4	1.0	0.75	2.4	0.28	400 ¹
275.9+1.9	3.5	2.7	1.3	0.82	3.1	0.27	300 ²
295.0+3.4	3.6	2.4	1.5	0.81	2.9	0.30	350 ²
297.7–2.8	3.8	2.5	1.5	0.82	3.1	0.14	150 ³
327.2+1.8	2.7	2.0	1.3	0.73	2.3	0.17	250 ²
345.4–4.0	2.4	2.4	1.0	0.75	2.4	0.28	400 ²
B68	2.5	2.0	1.3	0.71	2.2	0.13	200 ⁴

Notes:

Distances:

- (1) Adopted distance to Vela–Gum CGs
- (2) From stellar reddening
- (3) Proximity to Coalsack ($D = 175$ pc; Rodgers, 1960)
- (4) Bok (1977).

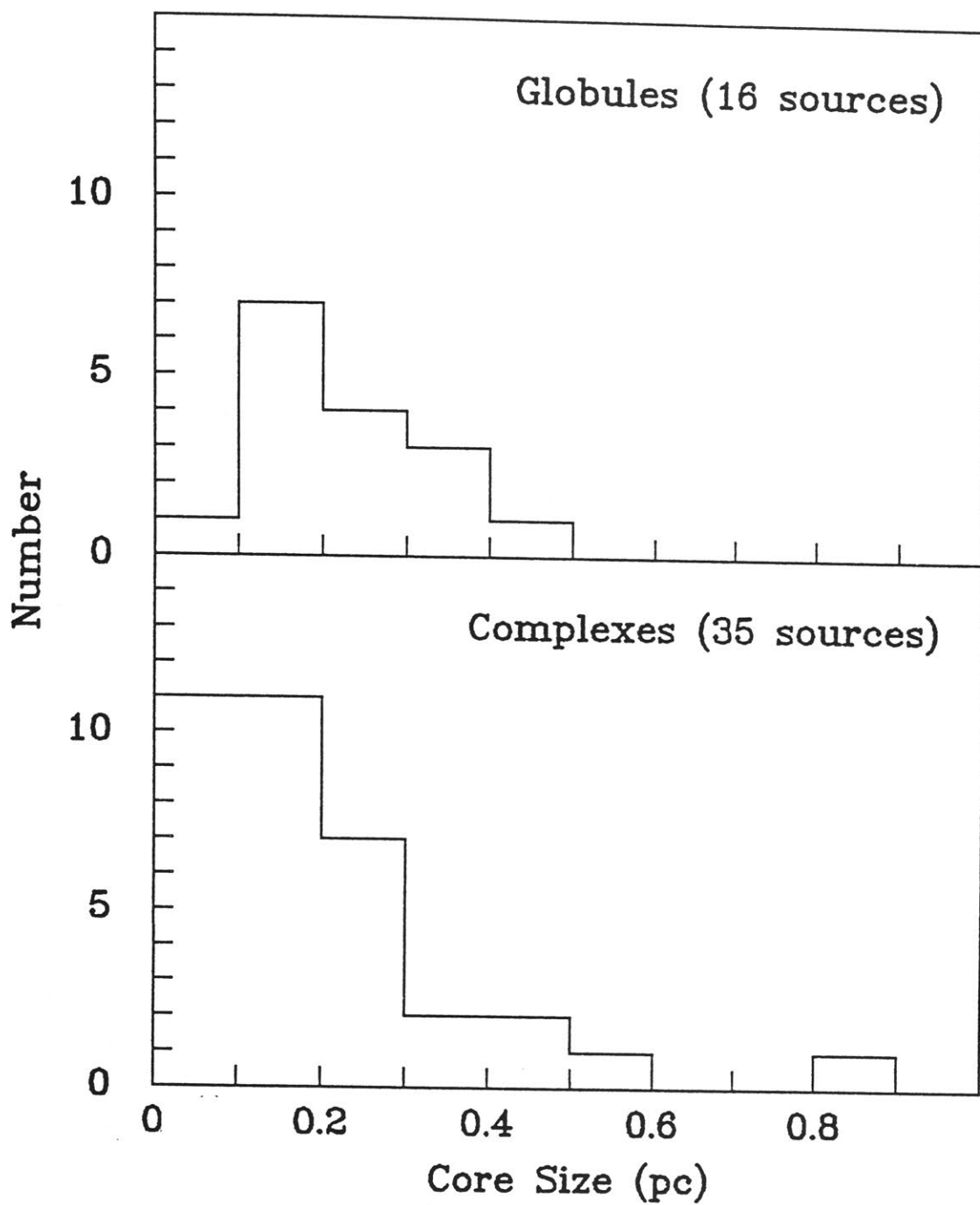


Figure 4.1: Histogram of the core sizes for isolated globules (top) and cores within complexes (bottom).

(L1512, L1544, L63, B335, B361 and L1262A), we find a mean globule core size of 0.21 ± 0.10 pc. For the mapped cores within complexes from BM89 (35 sources), we find a mean size of 0.20 ± 0.17 pc. So the average size of the two samples are similar, though the median size of the globules is slightly larger, as indicated by figure 4.1, which plots histograms of the cores sizes of the two samples.

The aspect ratios range from 1.0 to 1.6, with a mean value of 1.3 ± 0.2 , indicating that the cores are not round, but in general elongated. For the six mapped globules in the BM89 sample the mean is 1.6 ± 0.4 , with a combined mean of the two samples being 1.4 ± 0.3 . BM89 has suggested that this result implies that there are other significant forces present aside from random motions and self-gravity, such as magnetic fields and/or rotation, or that the cores are not in equilibrium. The filling factors range from 0.71 to 0.85 with a mean of about 0.75.

4.3.2 Mapped Sources

In this section the individual sources which have been mapped are discussed in light of the mapping results. Results of previous studies are presented and discussed, along with a description of the cloud characteristics as derived from our mapping analysis. Only a few of the clouds mapped have been observed previously, and very few in any detail. The masses quoted in this section have been calculated using half of the geometric mean half power NH_3 contour, i.e., $d/2$ in table 4.1.

DC 253.1–1.7A

Also known as CG31A, this cometary globule is located very close to the well studied CG30. It is a relatively unstudied globule, with few indications that star formation is currently taking place within any of the globules of the complex (Pettersson, 1987). Pettersson (1987) surveyed the CG31 complex for H_2CO absorption at 6 cm using a beam size of $4.4'$. He found the maximum absorption to occur at a position to the north-west of the optical centre of CG31A. This position is marked with an asterisk on the NH_3 contour map of CG31A.

Its proximity and similarity to CG30 makes it an ideal study companion, which may provide some insight into the differences between active and quiescent CGs. The contour map in figure 4.2(a) shows a departure from regularity which is more pronounced than in CG30. However, the core shape and size are similar to the optical appearance, with an optical head size of $\sim 4' \times 2'$, and a core size of $3.8' \times 2.3'$, which corresponds to 0.4×0.25 pc at a distance of 400 pc (the adopted distance to the Vela–Gum CGs). At the position of maximum intensity we find $T_g^* = 0.30$ K. However, the optical depth is very low and could not be determined accurately from the model best fit, which implied that $\tau_m < 0.2$. From the (2,2) line we derive a kinetic temperature of 14.4 K, similar to that found for CG30. Assuming optically thin conditions, we find the NH_3 column density to be $2.2 \times 10^{14} \text{ cm}^{-2}$, compared to $6.1 \times 10^{14} \text{ cm}^{-2}$ for CG30. The total number density of CG31A is $n \sim 1.2 \times 10^4 \text{ cm}^{-3}$ and the core mass is $13 M_\odot$. Although the two CGs have similar core sizes and temperatures, CG30 has a significantly larger optical depth and density, but a lower mass, and is known to be undergoing low mass star formation (see below).

DC 253.1-1.7A

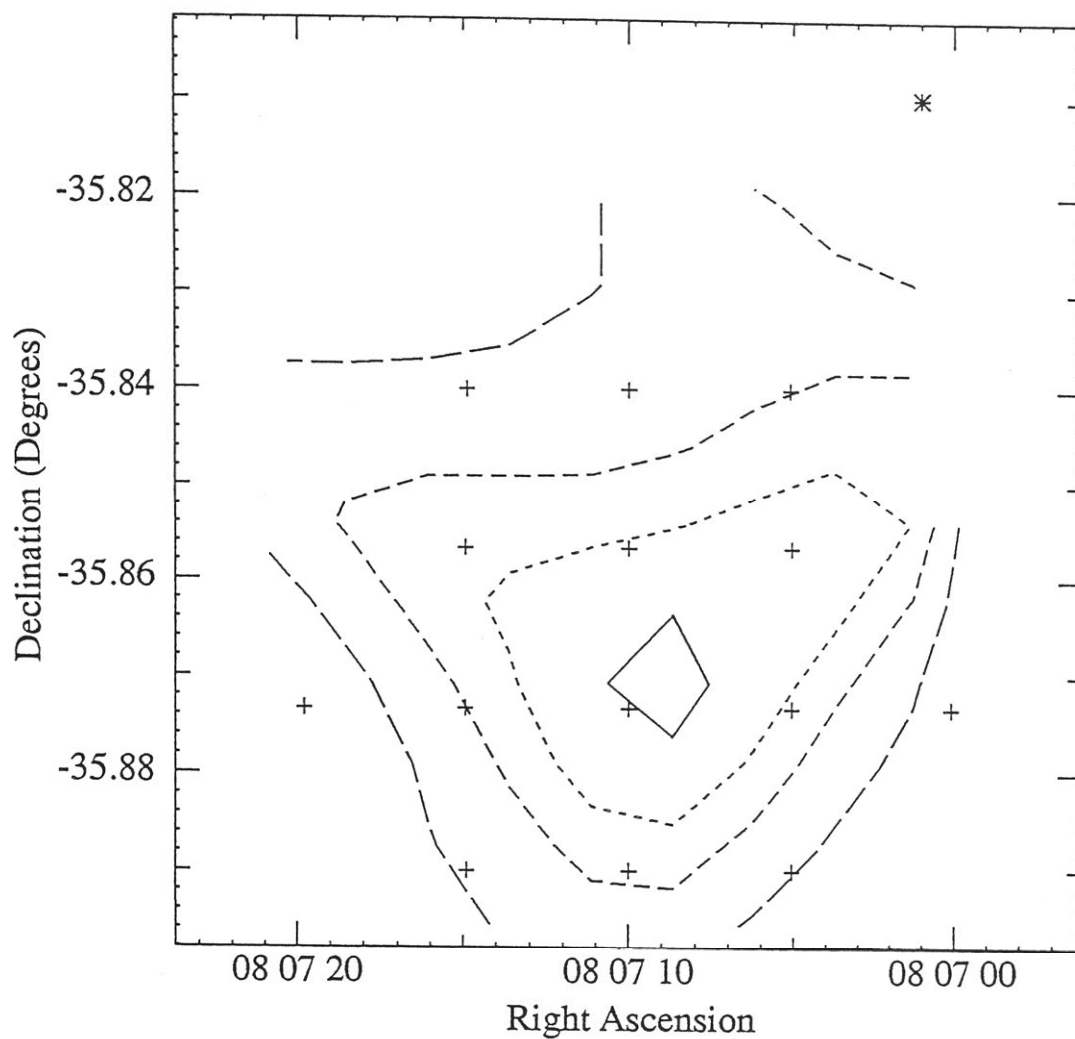


Figure 4.2: (a) Ammonia intensity contour map for DC 253.1-1.7A. The levels are 0.10, 0.15, 0.20 and 0.25 K. Crosses mark the observed positions. The asterisk marks the position of maximum H₂CO absorption seen by Petterson (1987).

DC 253.3-1.6

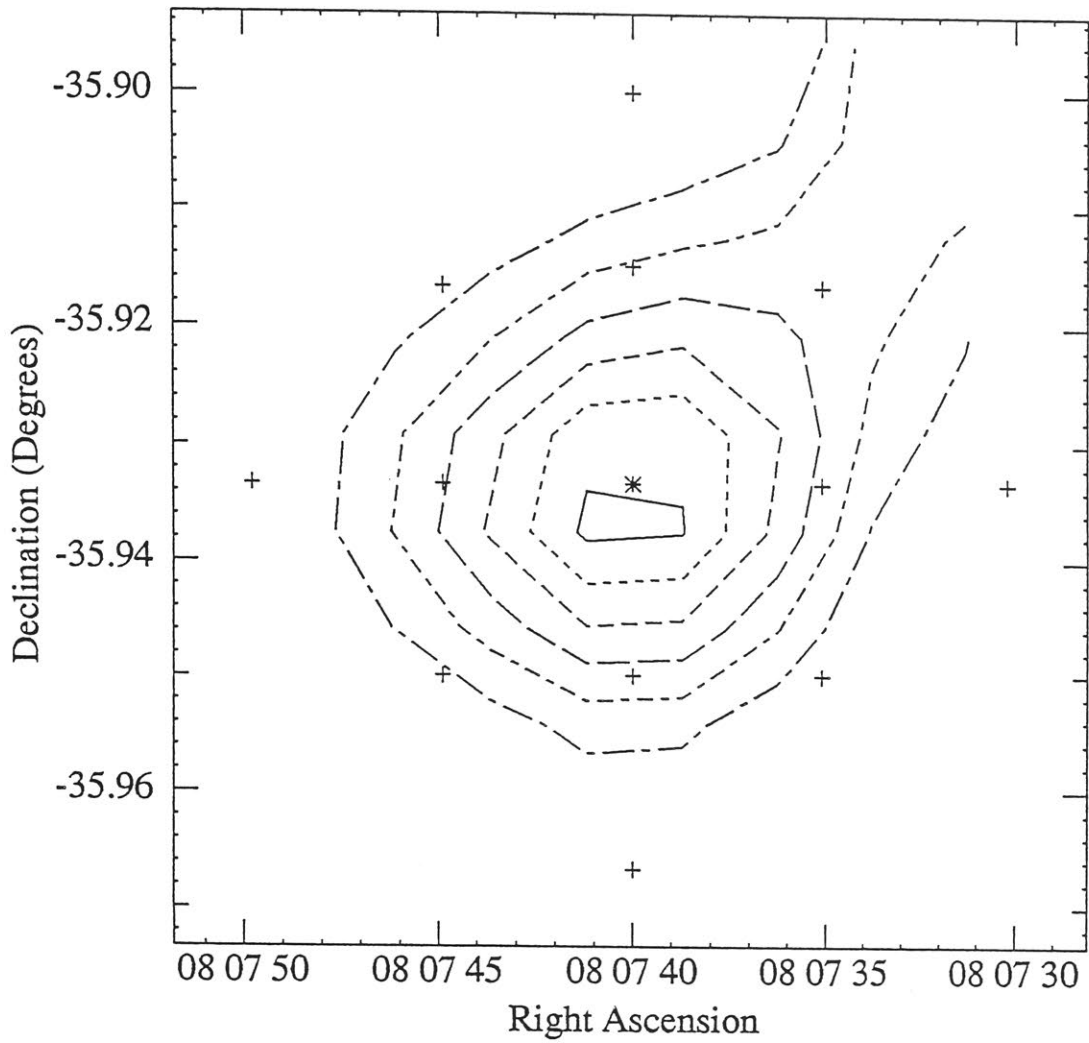


Figure 4.2: (b) Ammonia intensity contour map for DC 253.3–1.6. The levels are 0.15, 0.20, 0.25, 0.30, 0.35 and 0.40 K. The centre of the Vela–Gum Nebula is located to the south-east of the globule. The asterisk marks the position of the *IRAS* source (*IRAS* 08076–3556).

DC 267.4-7.5

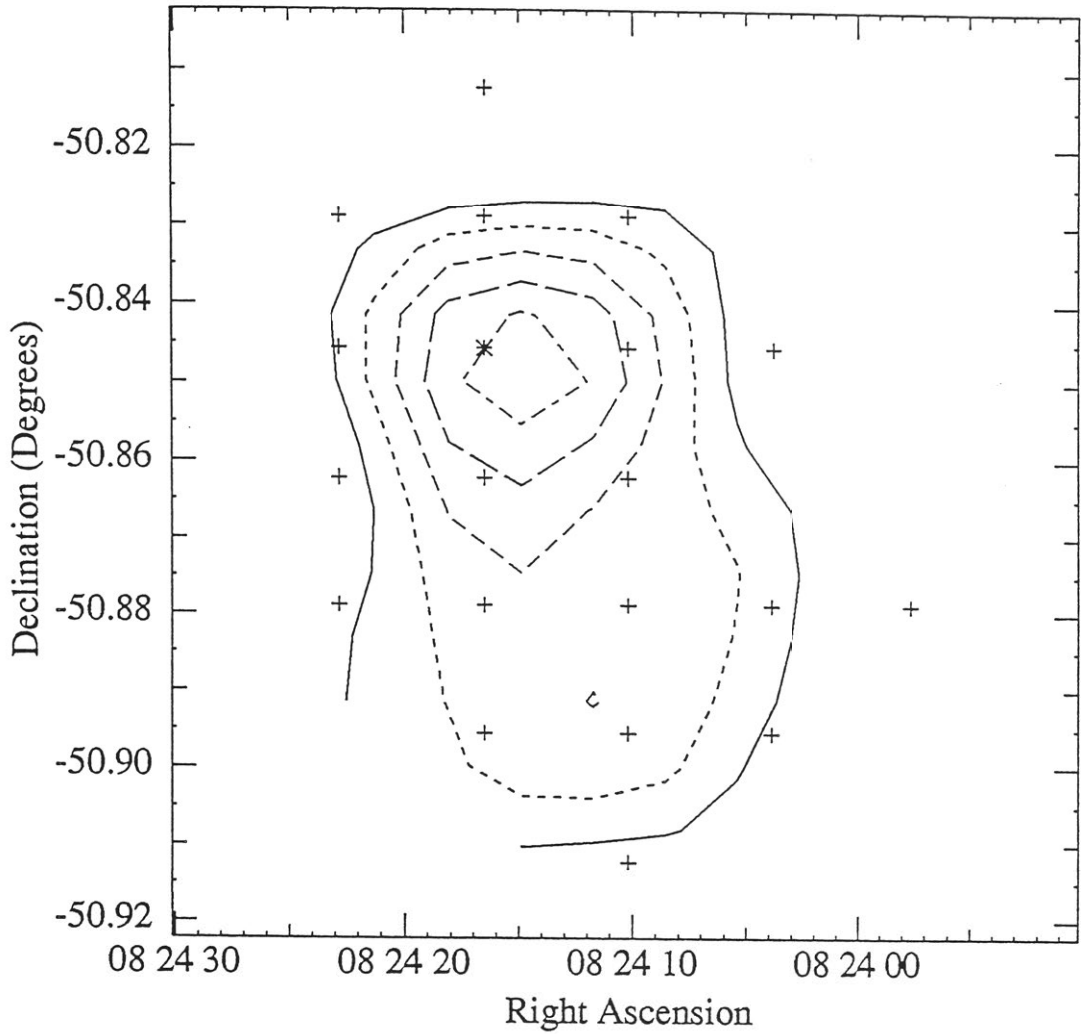


Figure 4.2: (c) Ammonia intensity contour map for DC 267.4-7.5. The levels are 0.15, 0.18, 0.21, 0.24, 0.27 K. The centre of the Vela-Gum Nebula is located to the north-west of the globule. The asterisk marks the position of the *IRAS* source (*IRAS* 08242-5050).

DC 267.7-7.4

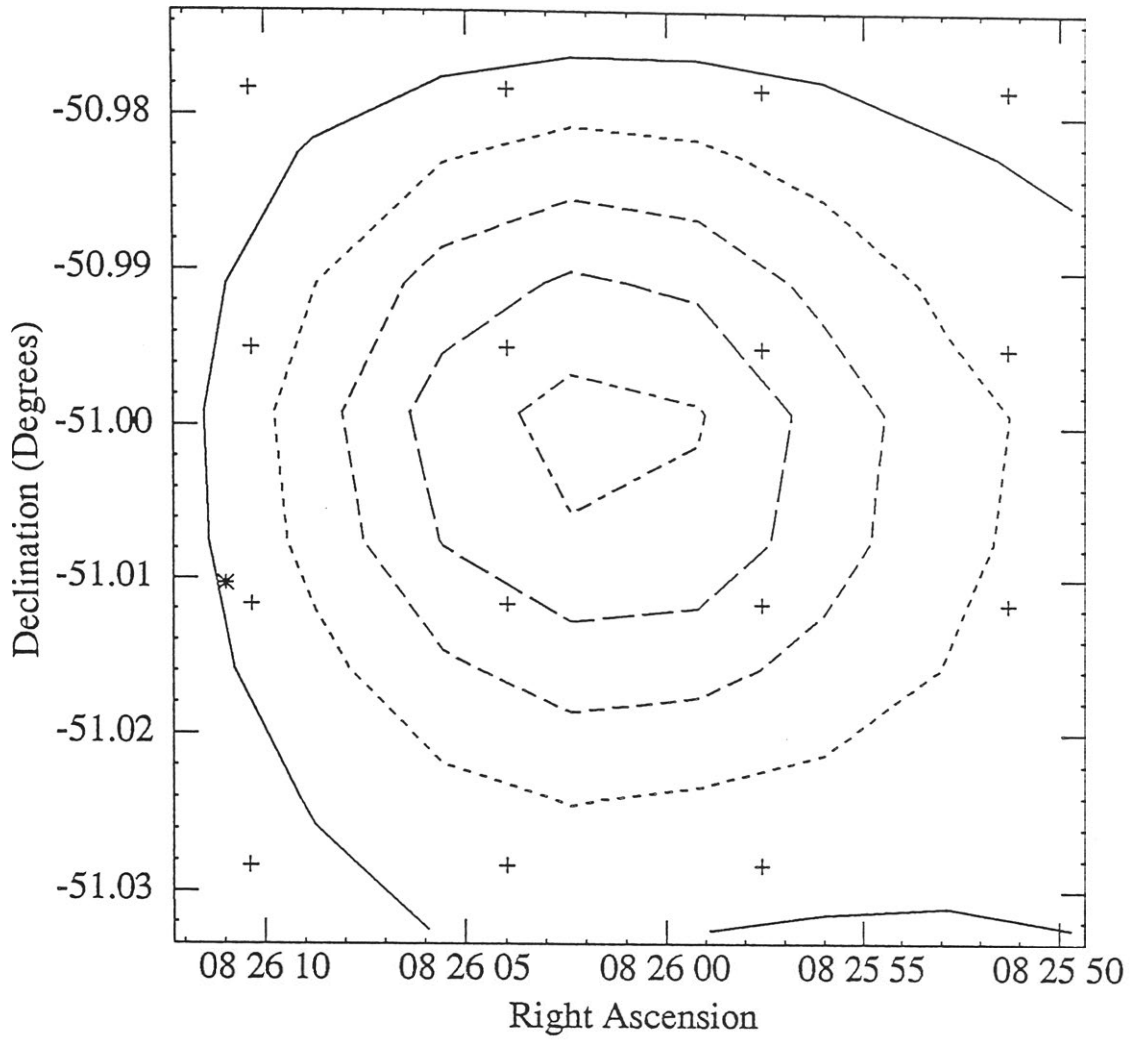


Figure 4.2: (d) Ammonia intensity contour map for DC 267.7-7.4. The levels are 0.15, 0.25, 0.35, 0.45 and 0.55 K. The asterisk marks the position of the *IRAS* source (*IRAS* 08261-5100).

DC 275.9+1.9

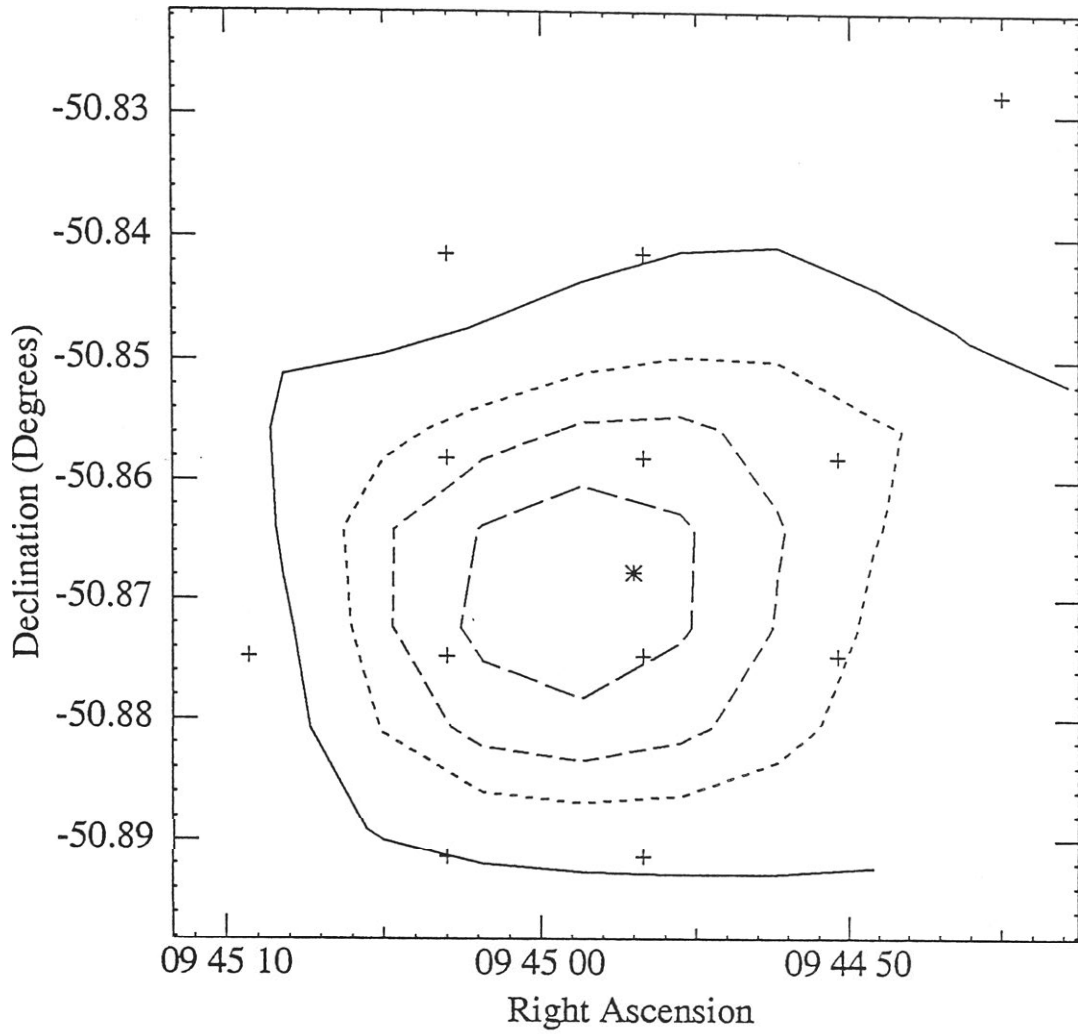


Figure 4.2: (e) Ammonia intensity contour map for DC 275.9+1.9. The levels are 0.15, 0.20, 0.25 and 0.30 K. The asterisk marks the position of the *IRAS* source (*IRAS* 09449-5052).

DC 295.0+3.4

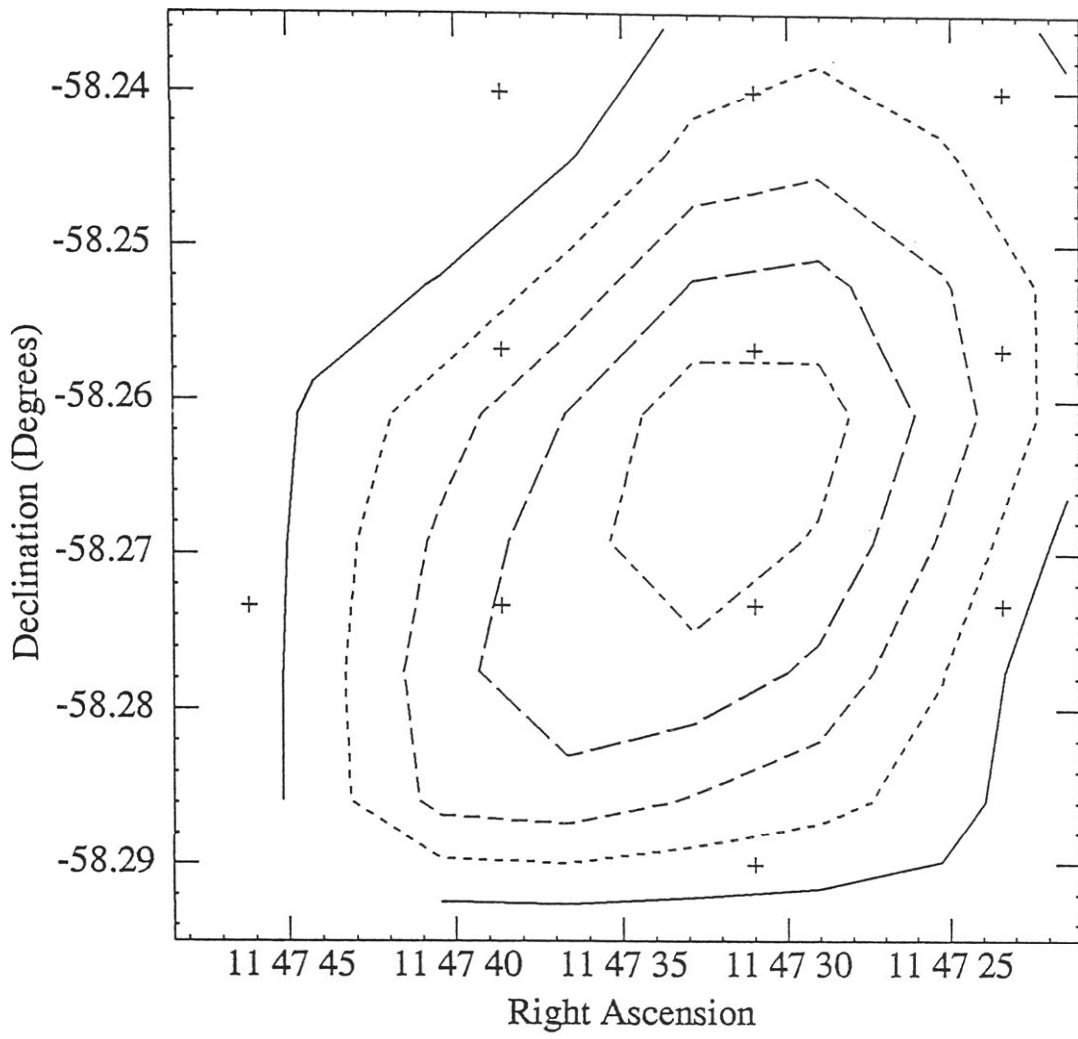


Figure 4.2: (f) Ammonia intensity contour map for DC 295.0+3.4. The levels are 0.15, 0.20, 0.25, 0.30 and 0.35 K.

DC 297.7-2.8

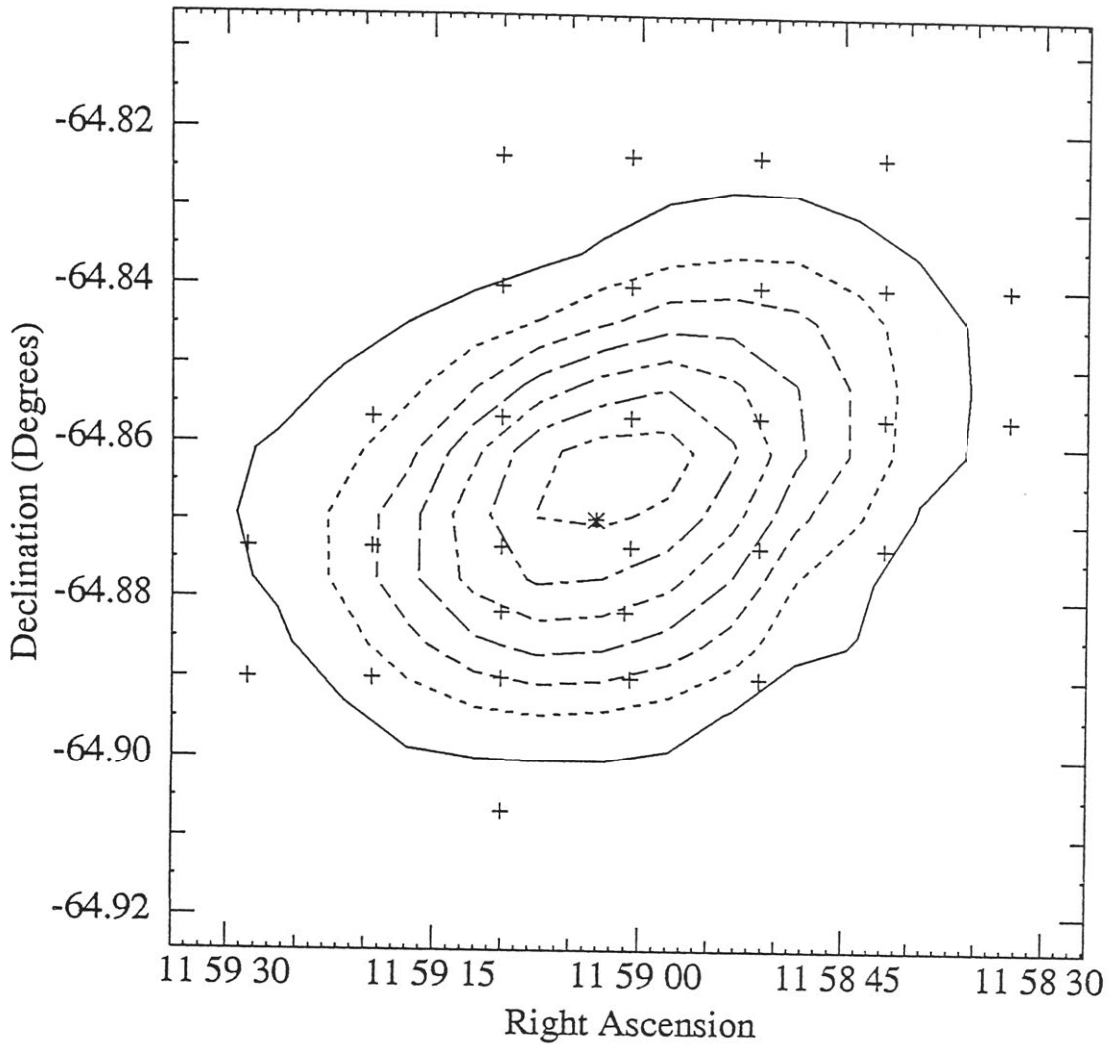


Figure 4.2: (g) Ammonia intensity contour map for DC 297.7-2.8. The levels are 0.2, 0.3, 0.4, 0.5, 0.6, 0.7 and 0.8 K. The asterisk marks the position of the *IRAS* source (*IRAS* 11590-6452).

DC 327.2+1.8

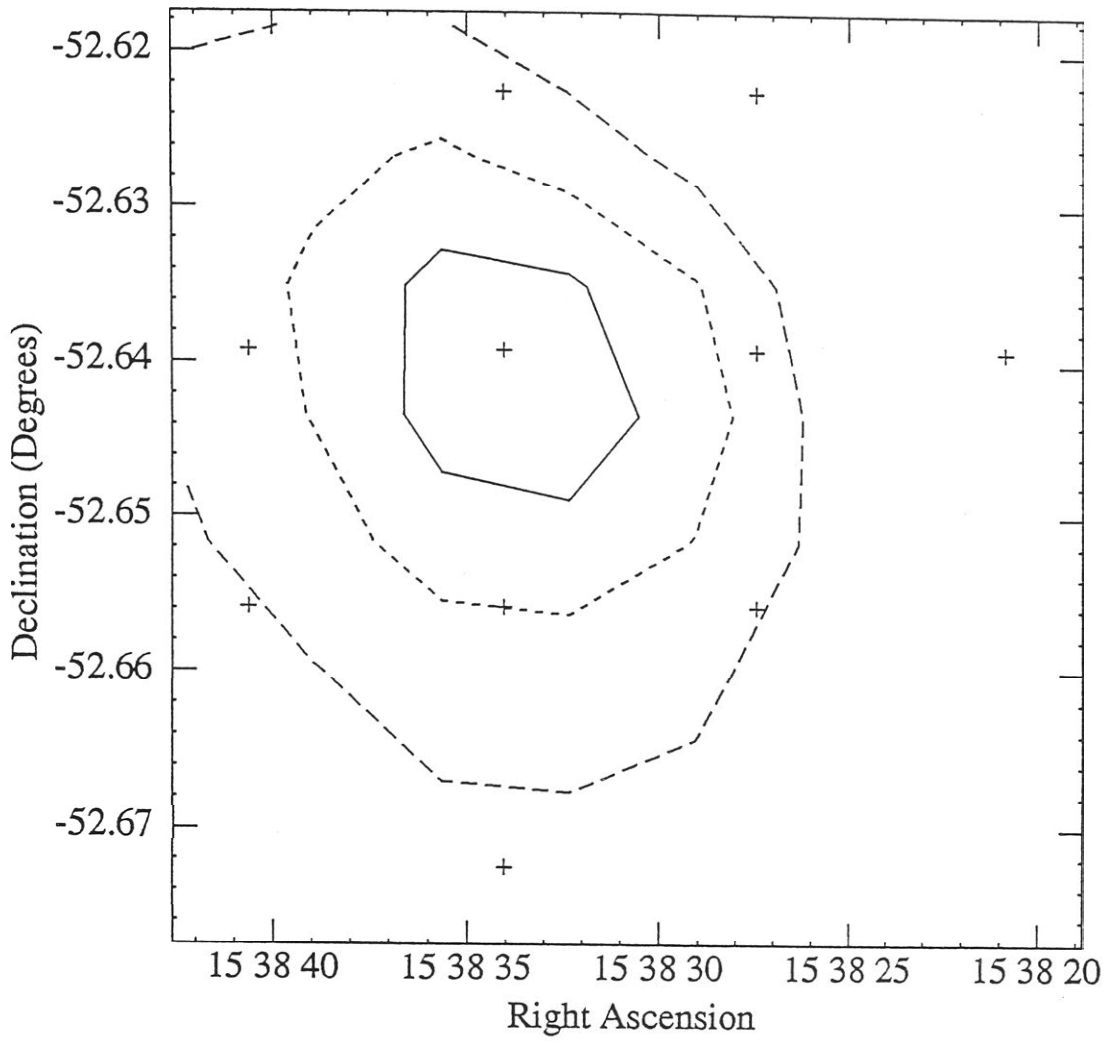


Figure 4.2: (h) Ammonia intensity contour map for DC 327.2+1.8. The levels are 0.14, 0.18 and 0.22 K.

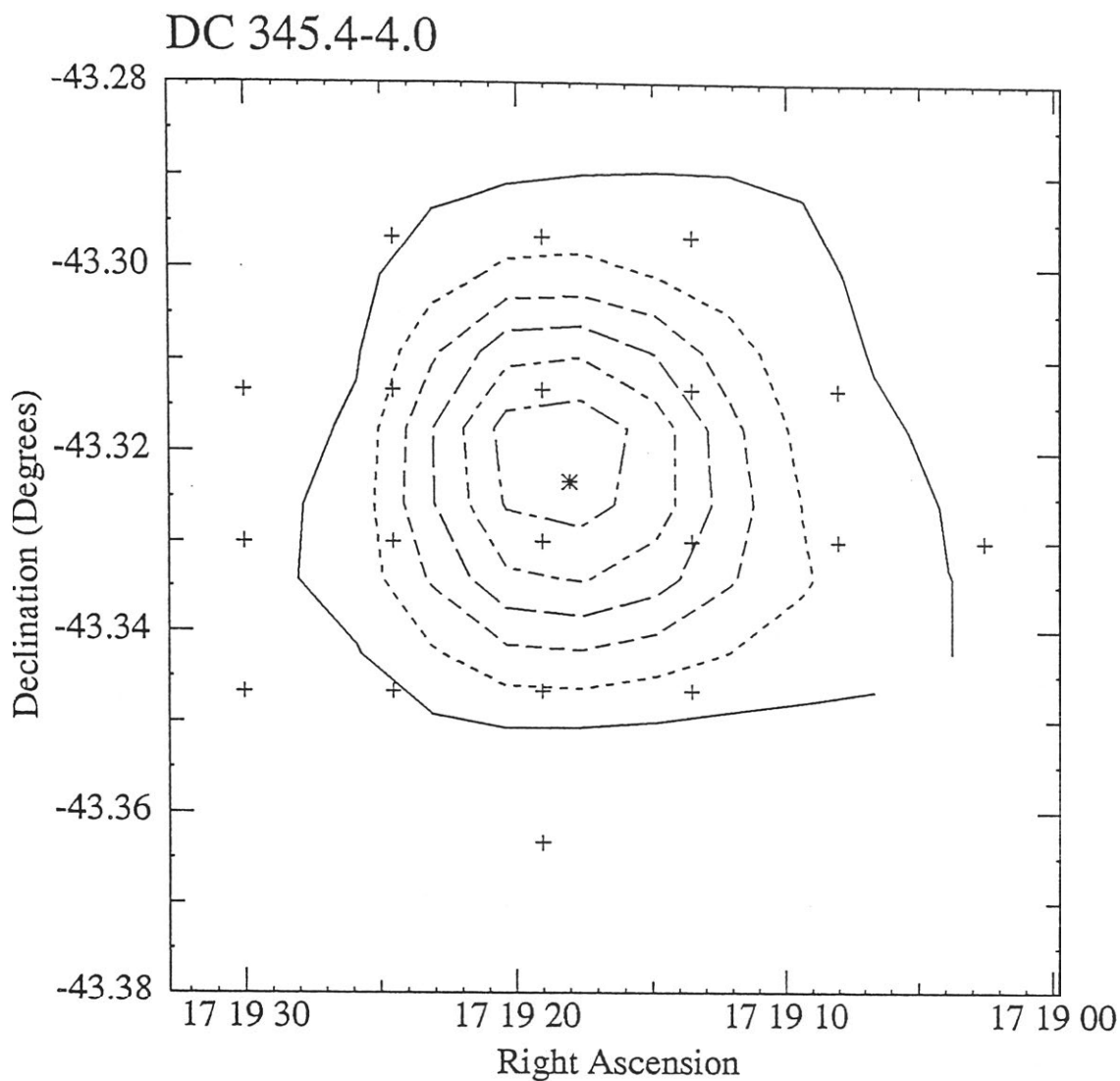


Figure 4.2: (i) Ammonia intensity contour map for DC 345.4-4.0. The levels are 0.15, 0.25, 0.35, 0.45, 0.55 and 0.65 K. The asterisk marks the position of the *IRAS* source (17193-4319).

B68

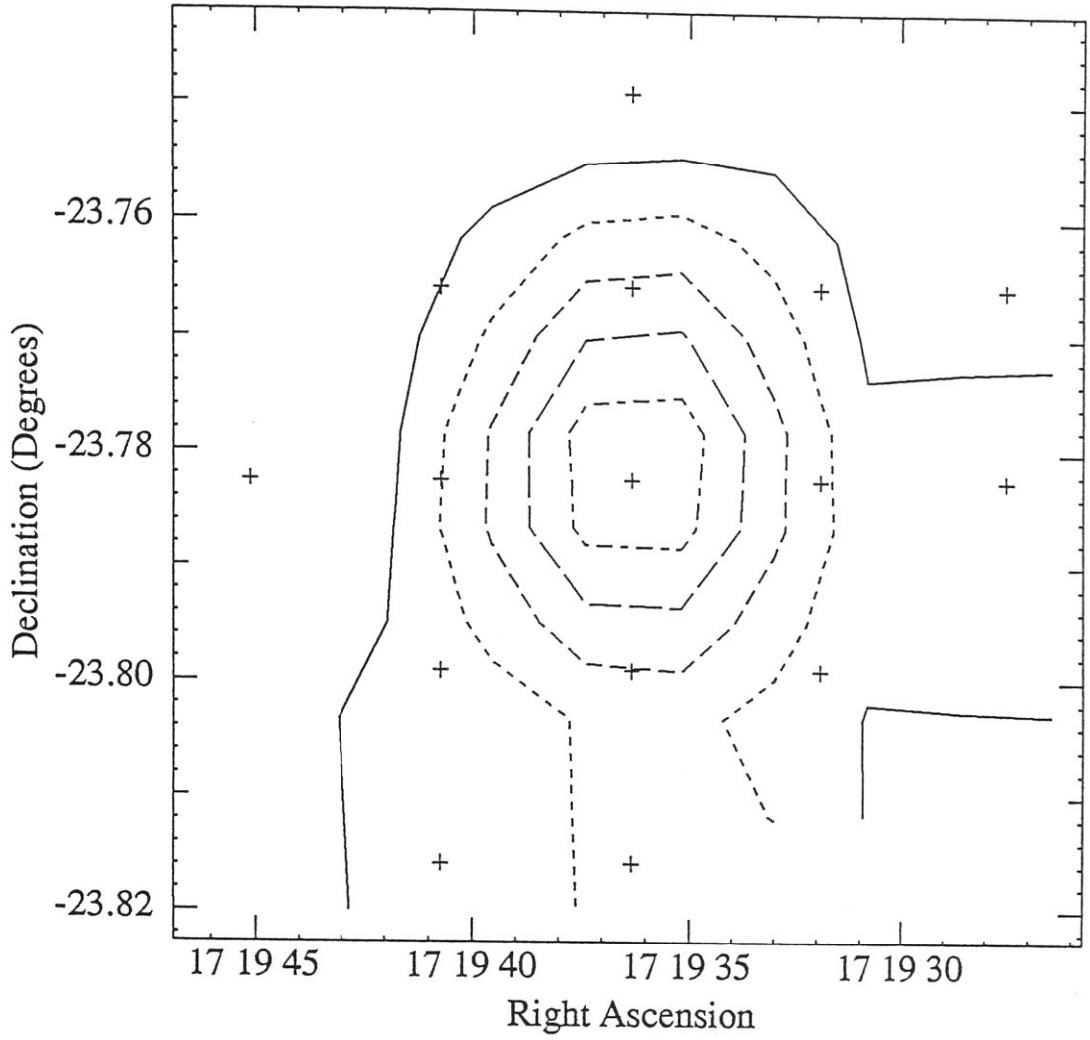


Figure 4.2: (j) Ammonia intensity contour map for B68. The levels are 0.12, 0.16, 0.20, 0.24 and 0.28 K.

DC 253.3–1.6

Better known as the cometary globule CG30, this is one of the most well studied isolated star forming globules in the sky. Optically we see a very opaque head of size $3' \times 2'$ with the Herbig-Haro object HH120 visible toward its centre (Reipurth, 1981; Pettersson, 1984). Near infrared studies reveal the presence of an embedded source located at the south eastern edge of HH120 (Pettersson, 1984; Graham and Heyer, 1989). This source has also been detected by *IRAS* (*IRAS* 08076–3556) which has allowed its bolometric luminosity to be estimated at $18 L_{\odot}$ (Cohen and Schwartz, 1987). Observations of CO suggest the possible presence of a mass outflow from the globule (de Vries *et al.*, 1984) and near infrared studies indicate the presence of shocked molecular hydrogen emission from HH120 (Schwartz *et al.*, 1987). Recently, Persi *et al.* (1993) have presented near infrared, millimetre continuum and NH_3 observations of CG30. They find a visual extinction, $A_V > 30$ magnitudes, and a 1–1300 μm luminosity of $19 L_{\odot}$, in agreement with earlier studies. They mapped the NH_3 emission from CG30 on a 5 point grid, but were unable to resolve the core, due to the low elevation of CG30 from their observation site (Haystack Observatory), resulting in low signal-to-noise data. The very steep SED of the embedded source indicates that it is a very young protostellar candidate.

The ammonia map presented in figure 4.2(b) shows that the core region of CG30 is regular in shape, but that the emission outside the core region is extended to the north west in a similar manner to its dust tail. The map is centered on the embedded source, and has a peak antenna temperature of 0.61 K, which corresponds to a beam brightness temperature, T_B , of 1.9 K, equal to that found by Persi *et al.* (1993), and an optical depth $\tau_m = 1.46$, again similar to that found by Persi *et al.*. The cloud velocity is $V_{l,sr} = 6.18 \text{ km s}^{-1}$ and the intrinsic line width at the centre is 0.80 km s^{-1} . The half power contour indicates

a core size of $2.7' \times 2.1'$, which at a distance of 400 pc (the adopted distance to the Vela–Gum CGs) corresponds to 0.32×0.25 pc. The core size is thus very similar to the optical size of the cloud head. The derived density of $n = 1.5 \times 10^4 \text{ cm}^{-3}$ corresponds to a core mass of $\sim 9 M_{\odot}$. From (2,2) observations we derived the kinetic temperature at the core centre to be 13.9 K, at which Persi *et al.* (1993) estimate a dust temperature of 20 K. Our observations indicate an ammonia abundance of 3.2×10^{-8} , which allows us to derive an H_2 column density of $2 \times 10^{22} \text{ cm}^{-2}$.

CG30 is a dense cometary globule undergoing active star formation. The similarities between CG30 and CG31A suggest that CG31A has all the properties required for a CG to undergo star formation, and may be at an earlier stage of the star formation process than CG30. Observations required here are high resolution CO observations of CG30 to examine the possible outflow, and high resolution continuum observations of CG31A in the millimetre waveband to examine whether it contains a very young cool, compact source, not detected by *IRAS*. Both globules require mapping in the near infrared to examine their dust density distributions.

DC 267.4–7.5

This globule, also known as ESO 210–6a, has been even more extensively studied than CG30. It was one of the first Bok globules to show evidence for low mass star formation in the form of two HH objects, HH46/47 (Schwartz, 1977), located either side of an embedded source which has been identified with *IRAS* 08242–5050, the luminosity of which has been estimated at $\sim 24 L_{\odot}$ (Cohen and Schwartz, 1987; Berilli *et al.*, 1989). Shocked H_2 emission has been observed from the HH objects (Elias, 1980; Wilking *et al.*, 1990), which is seen as an extensive bow shock in near infrared imaging (Zealey *et al.*, 1993; Eislöffel *et al.*,

1993). The embedded source exhibits a characteristic T Tauri spectra (Graham and Heyer, 1989). Previous ammonia studies (Kuiper *et al.*, 1987) have been interpreted as evidence for a circumstellar disk about the embedded source, with size ~ 7000 AU and mass $\sim 0.10 M_{\odot}$. Observations of CO show a bipolar molecular outflow aligned with the HH objects (Olberg *et al.*, 1992). The total mass of the globule has been estimated at between $10 M_{\odot}$ (Emerson *et al.*, 1984; Sahu *et al.*, 1989) and $25 M_{\odot}$ (Bok, 1978).

As can be seen in figure 4.2(c) the ammonia emission is extended to the south of the position of peak intensity and away from the bright rim facing the centre of the Gum Nebula. The optical size of the globule is $4' \times 3'$, and the core size as traced by the ammonia emission is $4.4' \times 2.8'$, which corresponds to 0.5×0.33 pc at 400 pc. The core and optical sizes are very nearly identical. At the position of peak intensity, which corresponds to the location of the embedded source, we find $T_a^* = 0.39$ K, $V_{lsr} = 5.28$ km s $^{-1}$, $\Delta v = 0.73$ km s $^{-1}$, and $\tau_m = 0.9$. From these observations we derive $n = 7.3 \times 10^3$ cm $^{-3}$, an ammonia abundance of 1.6×10^{-8} , and a column density of 1.5×10^{22} cm $^{-2}$. This implies the mass estimate of Kuiper *et al.* (1987) should be raised to $\sim 1 M_{\odot}$ for their disk, since they assumed an abundance of 10^{-7} . But Kuiper *et al.* based their interpretation of a disk structure on the fact that they did not observe strong ammonia emission from other positions within the cloud, which they claim indicates that the emission is not due to the globule. We can see clearly in the map that this is not the case, and that the ammonia emission is widespread throughout and clearly due to the globule, and so the disk interpretation does not seem valid. We find $T_K = 17.7$ K at the position of the *IRAS* source, in agreement with previous studies (Kuiper *et al.*, 1987; Olberg *et al.*, 1992). The core mass is estimated to be $13 M_{\odot}$, which is similar to some previous estimates of the total mass of the globule. The extended nature of the ammonia emission may result in the core mass being

overestimated. Higher angular resolution measurements of the core region in both the (1,1) and (2,2) lines are required to more accurately determine the gas density distribution.

DC 267.7–7.4

This dense globule is located in the same complex as DC 267.4–7.5, but appears shielded from the centre of the Gum Nebula, and so does not exhibit any bright rims. A nebula is visible on the north-eastern edge of the globule. Also on the eastern edge is located the *IRAS* source 08261–5100, which has an estimated luminosity at wavelengths longer than $12 \mu\text{m}$ of $4.4 L_{\odot}$. The *IRAS* colours are those of a T Tauri star, and a possible optical candidate appears on the Schmidt survey J print. However, it does not appear to coincide with the star embedded within the nebula, vbH16 (van der Bergh and Herbst, 1975). Herbst (1977) determines the distance to this star to be 400 pc, based on its reddening. Reipurth and Zinneker (1993) report that vbH16 is a spectroscopic T Tauri binary. They also identify the optical source we have suggested may coincide with the *IRAS* source with a pre-main-sequence binary, ESO H α 280.

The globule exhibits an extremely simple structure in ammonia emission. Its optical size is $5' \times 4'$, while its core size is $2.5' \times 2.4'$, corresponding to a linear size of 0.28 pc. It is thus not elongated, and its core size does not approximate its optical size, unlike the three globules directly facing the Gum Nebula described above. The position of peak intensity is located $1'N$ of the nominal cloud centre, and has $T_a^* = 0.75 \text{ K}$, $V_{lsr} = 5.43 \text{ km s}^{-1}$ and $\Delta v = 0.47 \text{ km s}^{-1}$, with an optical depth of $\tau_m = 2.42$. The kinetic temperature is found to be $\sim 11 \text{ K}$, and the total number density $n \sim 1.2 \times 10^4$. At the adopted distance of 400 pc the core mass is $\sim 7.5 M_{\odot}$, and the virial mass is $6.5 M_{\odot}$ (see next section). Of the mapped sources, this is the only one associated with an *IRAS* source where the source

lies outside the core. The ratio $\log(S_{60}/S_{25}) = 0.2$ is also the lowest of the *IRAS* sources associated with the mapped clouds, possibly indicating that it is the most well evolved of these *IRAS* sources. This globule certainly deserves much closer study, as it may have begun contracting, though no embedded source was detected by *IRAS*. It would appear that the star formation efficiency of this globule is relatively high, with two pre-main-sequences binaries located at its edge, and a dense core within. High resolution continuum observations of this globule in the millimetre waveband are required to search for the presence of any compact, young embedded sources.

DC 275.9+1.9

This globule appears embedded in a slightly larger region of obscuration. Its southern edge exhibits a rather sharp rim, while the visual opacity decreases gradually to the north and west. The ammonia map is slightly elongated in the E/W direction. Its optical size is estimated at $4' \times 3'$, though the extended obscuration covers a larger region, while the core size is $3.5' \times 2.7'$ (aspect ratio = 1.3), similar to its optical size. At the distance of 300 pc, estimated from stellar reddening, the core size is 0.3×0.24 pc. The position of peak intensity is at the core centre for which $T_a^* = 0.41$ K, $V_{lsr} = -5.41$ km s⁻¹, $\Delta v = 0.56$ km s⁻¹, and $\tau_m = 1.0$. However, the position of peak density is at (1'W, 1'N) for which $\tau_m = 2.4$. The associated *IRAS* source, *IRAS* 09449-5052, lies closest to the this position and has an estimated luminosity of $3 L_\odot$. Its colours are those of an embedded source, and there is no optically visible counterpart on the Schmidt plates. The kinetic temperature and density of the (0,0) position are 11 K and 1×10^4 cm⁻³ respectively. The estimated core mass is $5 M_\odot$. No other observations of this globule are known.

DC 295.0+3.4

A rather inconspicuous globule, despite its optical size of $6' \times 4'$. The ammonia core appears elongated along its NW/SE axis, which does not follow any particular orientation with respect to the optical appearance of the globule. The core has a projected size of $3.6' \times 2.4'$ which translates to a linear size of 0.37×0.25 pc at the adopted distance of 350 pc. At the position of peak intensity we find $T_a^* = 0.37$, $V_{lsr} = -7.55$ km s $^{-1}$, $\Delta v = 0.57$ km s $^{-1}$, and $\tau_m = 1.93$. For the kinetic temperature we find $T_K = 10.9$ K and a total number density of 8×10^3 cm $^{-3}$. The core mass is thus estimated to be $\sim 5 M_\odot$. No *IRAS* sources are found toward this globule. Goss *et al.* (1980) detected the globule in H $_2$ CO absorption and found $V_{lsr} = -7.7$ km s $^{-1}$, but they did not derive any globule properties from their observations. Apparently a quiescent globule with a dense core.

DC 327.2+1.8

Visually this cloud appears as two 'blobs', one to the north-west and the other to the south-east, connected by a narrow bridge of obscuration. The ammonia core is located within the north-east segment, though we have not examined the south-east segment in detail and so cannot rule out the possibility of it too containing a core. The core is elongated NE/SW, which puts it roughly perpendicular to the optical axis of the blob. The optical size of the north-east blob is $6' \times 4'$ while the core has a size $2.7' \times 2.0'$, which implies a linear size of 0.2×0.15 pc at the adopted distance of 250 pc. At the peak position we find $T_a^* = 0.49$ K, $V_{lsr} = 0.00$ km s $^{-1}$, $\Delta v = 0.41$ km s $^{-1}$, with $\tau_m = 1.3$. Derived properties are $T_K = 11.3$ K and $n = 1.3 \times 10^4$ cm $^{-3}$. The core mass is $2.1 M_\odot$. There are no *IRAS* sources located toward this globule. The visual appearance of the globule suggests it might be fragmenting into two. The lack

of correlation between the core axis and the globule axis may also imply that something interesting is happening to this globule, as for the other globules the two axes usually appear aligned. A determination of the magnetic field direction within this globule may be worthwhile.

B68

As indicated earlier, B68 is a relatively well studied isolated Bok globule, which has a possible association with the globular filament B72, also known as the snake. Bok (1977) studied it optically and estimated a distance of 200 pc based on star counts, and a visual extinction $A_V \geq 25$ magnitudes. Martin and Barrett (1978) observed B68 in NH_3 , and found a core size of $1.5'$ (0.09 pc) and mass $1.1 M_\odot$. They determined a core density of $8 \times 10^3 \text{ cm}^{-3}$ from their observed parameters, $T_a^* = 0.99 \text{ K}$, $\tau_m = 0.7$, and $T_{ex} = 6.7 \text{ K}$. Leung *et al.* (1982) observed the globule in both ^{13}CO and ^{12}CO . They defined the core as the area within the 0.1 K intensity contour and found a core size 0.19 pc, mass $5 M_\odot$, density $4 \times 10^3 \text{ cm}^{-3}$ and $T_K \sim 9 \text{ K}$. BM89 observed B68 in their survey for NH_3 cores, finding $T_a^* = 0.43 \text{ K}$, $V_{lsr} = 3.31 \text{ km s}^{-1}$, $\Delta v = 0.17 \text{ km s}^{-1}$, τ_o (total optical depth) = 3.5, and density $3 \times 10^4 \text{ cm}^{-3}$. Their observations also imply a kinetic temperature $T_K \sim 15 \text{ K}$.

Optically the globule appears kidney shaped (see chapter 1), though in ammonia it is clearly roundish but slightly elongated in the N/S direction. The core size is $2.5' \times 2.0'$, which at a distance of 200 pc corresponds to a linear size of $0.15 \times 0.12 \text{ pc}$. Our reddening plot indicates that 200–250 pc is the likely globule distance, in agreement with the estimate of Bok (1977). At the position of peak intensity we find $T_a^* = 0.51 \text{ K}$, $\Delta v = 0.28 \text{ km s}^{-1}$, $\tau_m = 1.98$ (which implies a total optical depth of ~ 4) and $T_{ex} = 5.4 \text{ K}$. Except for the excitation temperature these values are in good agreement with those of BM89. From these values and

observations of the (2,2) line we derive $T_K = 14.7$ K, $n = 8 \times 10^3$ cm⁻³ and mass $\sim 0.7 M_\odot$. Note that the density is significantly less than that found by BM89 due to the different values of T_{ex} , but that the kinetic temperatures are similar. Our values for the mass and density are similar to those found by Martin and Barrett (1978). The virial mass of the core is $\sim 1.2 M_\odot$. Leung *et al.* (1982) suggested that the cloud is in approximate virial equilibrium, a result which is supported by the above mass estimates. The ammonia abundance in B68 is found to be $\sim 4 \times 10^{-8}$. No *IRAS* point sources are found toward this globule, though Clemens *et al.* (1991) detected it in all 4 *IRAS* wavebands using coadded *IRAS* data, implying a 60/100 μ m dust temperature of ~ 26 K, while their CO results imply a kinetic temperature of 12.5 K. One of the unusual features of B68 is its narrow NH₃ line widths, much narrower than any of the other globules discussed here, and more in common with the line widths found in the Taurus region (BM89). It would appear the B68 is a very quiescent globule existing in a state of near virial equilibrium with no ongoing star formation.

DC 345.4–4.0

One of the largest globules in this work, with an optical size of $10' \times 6'$. The cloud lies in a rich part of the Milky Way, and a number of stars are seen projected against it. This may suggest that the globule is in fact relatively large and distant. The reddening curve, figure 3.4, indicates a possible distance of 400 pc for the cloud, though it may also be consistent with a distance of 700–800 pc, if it is believed to be distant. However, we have adopted a distance of 400 pc for this cloud, since the change in reddening is most pronounced at this distance. Only one previous observation of this cloud is known. Goss *et al.* (1980) observed the cloud in H₂CO absorption and found a brightness temperature of -0.22 K at a velocity $V_{lsr} = -8.2$ km s⁻¹.

In figure 4.2(i) we see that the core is quite round, with an elongation to the west in the envelope. The core has a size $2.4' \times 2.4'$ which implies a physical size of 0.28×0.28 pc. An *IRAS* source (*IRAS* 17193–4319) whose colours are those of an embedded source is located just north of the nominal cloud centre, and has an estimated luminosity of $5.1 L_{\odot}$. The position of the *IRAS* source coincides with the position of peak intensity, with $T_{\alpha}^* = 0.96$. However, the position of peak density appears to be the nominal cloud centre, for which $T_{\alpha}^* = 0.69$, $V_{lsr} = -8.33 \text{ km s}^{-1}$, $\Delta v = 0.99 \text{ km s}^{-1}$, and $\tau_m = 2.79$. At this position we find the kinetic temperature to be $T_K = 8.9 \text{ K}$, and the total density $n = 1.9 \times 10^4 \text{ cm}^{-3}$. These results imply a relatively large ammonia abundance of 9.4×10^{-8} , when compared with the other globules in this sample. The kinetic temperature at the position of the *IRAS* source is $T_K = 10.9 \text{ K}$, and at the 1'N position $T_K = 11.0 \text{ K}$, so that while the NH_3 column density is larger at both these positions than at (0,0), the derived total number density is slightly less, due to the greater kinetic temperature. The core mass is found to be $12 M_{\odot}$.

Figure 4.3 shows a contour plot of the observed velocity as a function of position for DC 345.4–4.0. We see that there is no appreciable velocity shift through the core region of the cloud, though in the envelope region we see the velocity drop at both the eastern and western edges. Benson (1983) has suggested that such a velocity profile could be a sign of core contraction, where the contraction on the edges is perpendicular to the line of sight, and the velocity of the front of the cloud is less because we see it moving away from us. However, the positions where we see the shift have low S/N ratios, and broad lines, so determining the line centre is sometimes difficult. Since the observed line shift is only 0.5 km s^{-1} , less than the intrinsic line width, the interpretation of contraction in this case should be treated with caution.

In figure 4.4 we see a contour plot of the NH_3 column density. The core

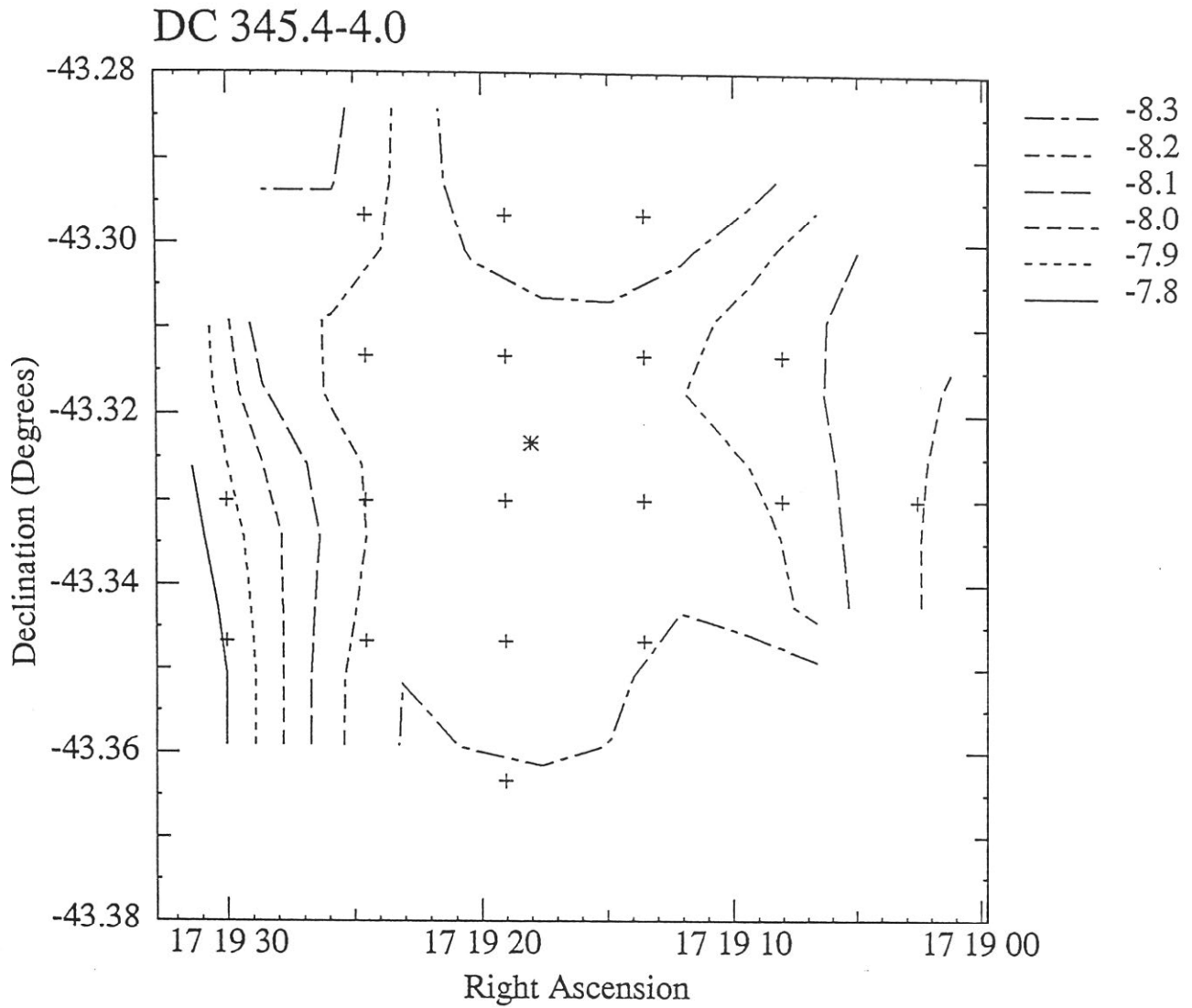


Figure 4.3: Map of ammonia velocity distribution in DC 345.4-4.0. The velocity levels are shown in the legend. It can be seen that there is very little velocity shift across the centre of the cloud.

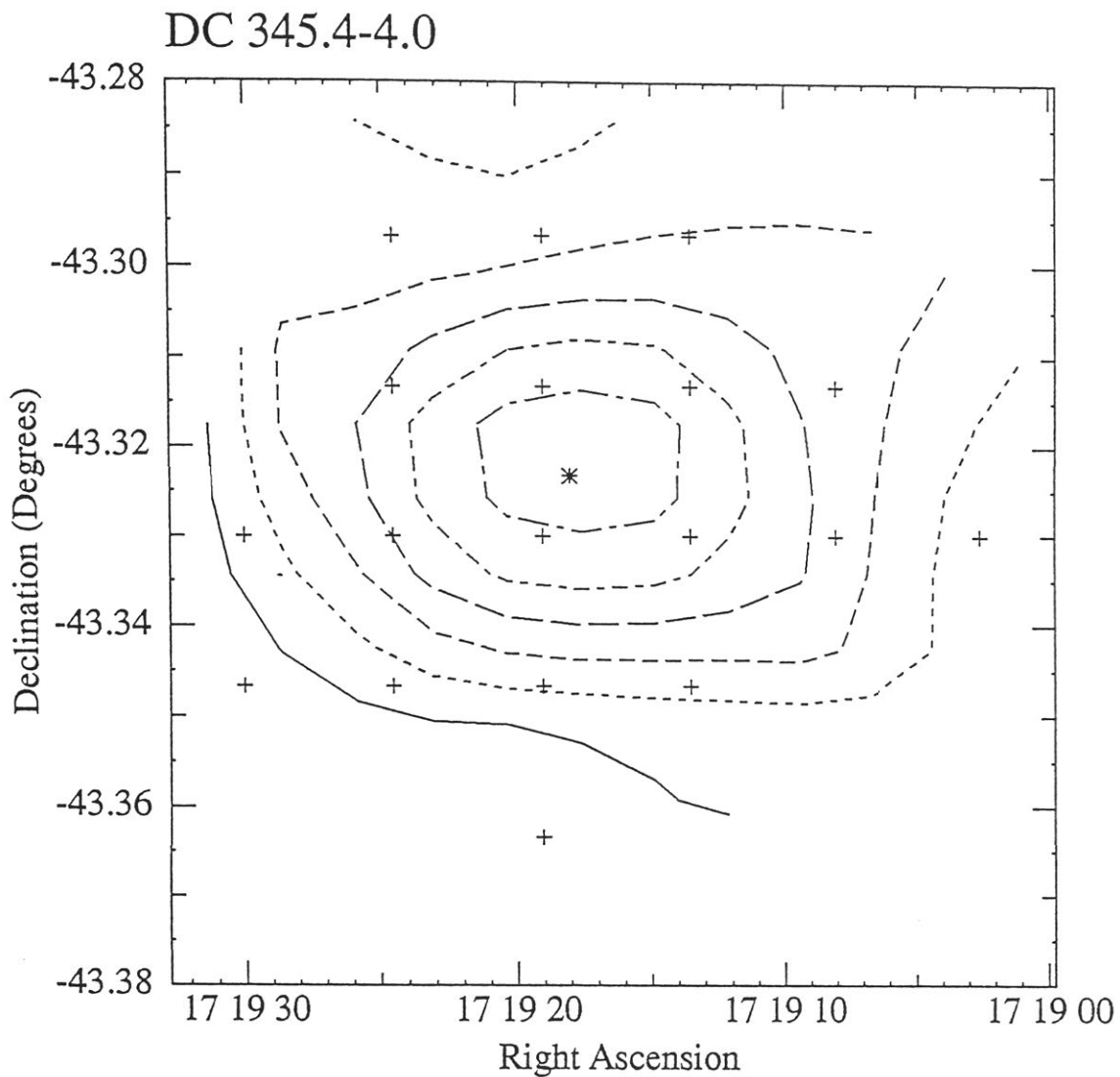


Figure 4.4: Contour map of ammonia column density for DC 345.4-4.0. The levels are $\log N(\text{NH}_3) = 14.0, 14.2, 14.4, 14.6, 14.8$ and 15.0 .

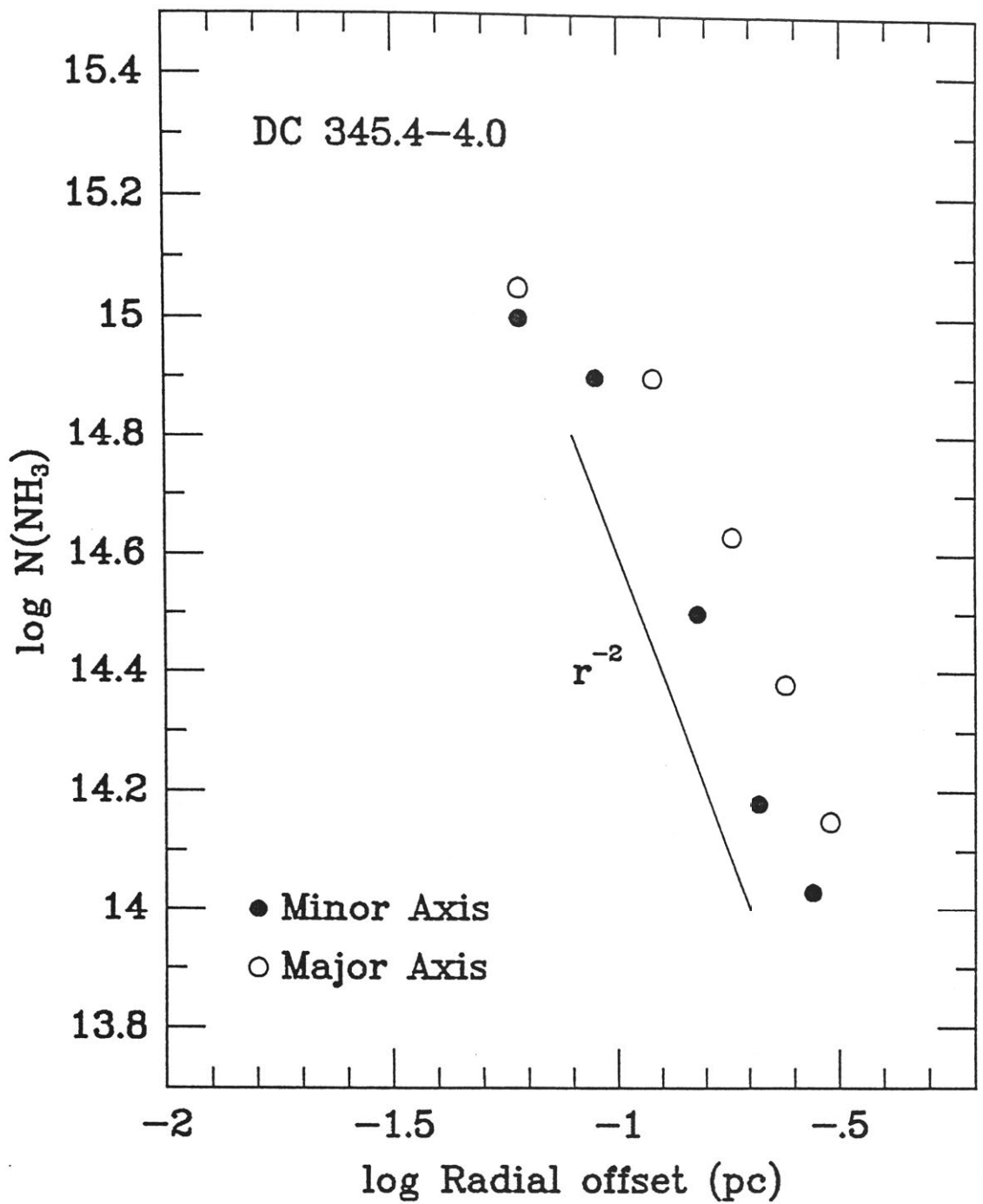


Figure 4.5: Sections through the N/S and E/W axes of the column density contour plot of DC 345.4-4.0. The density gradient along both axes follows an approximate inverse square law outside the core region.

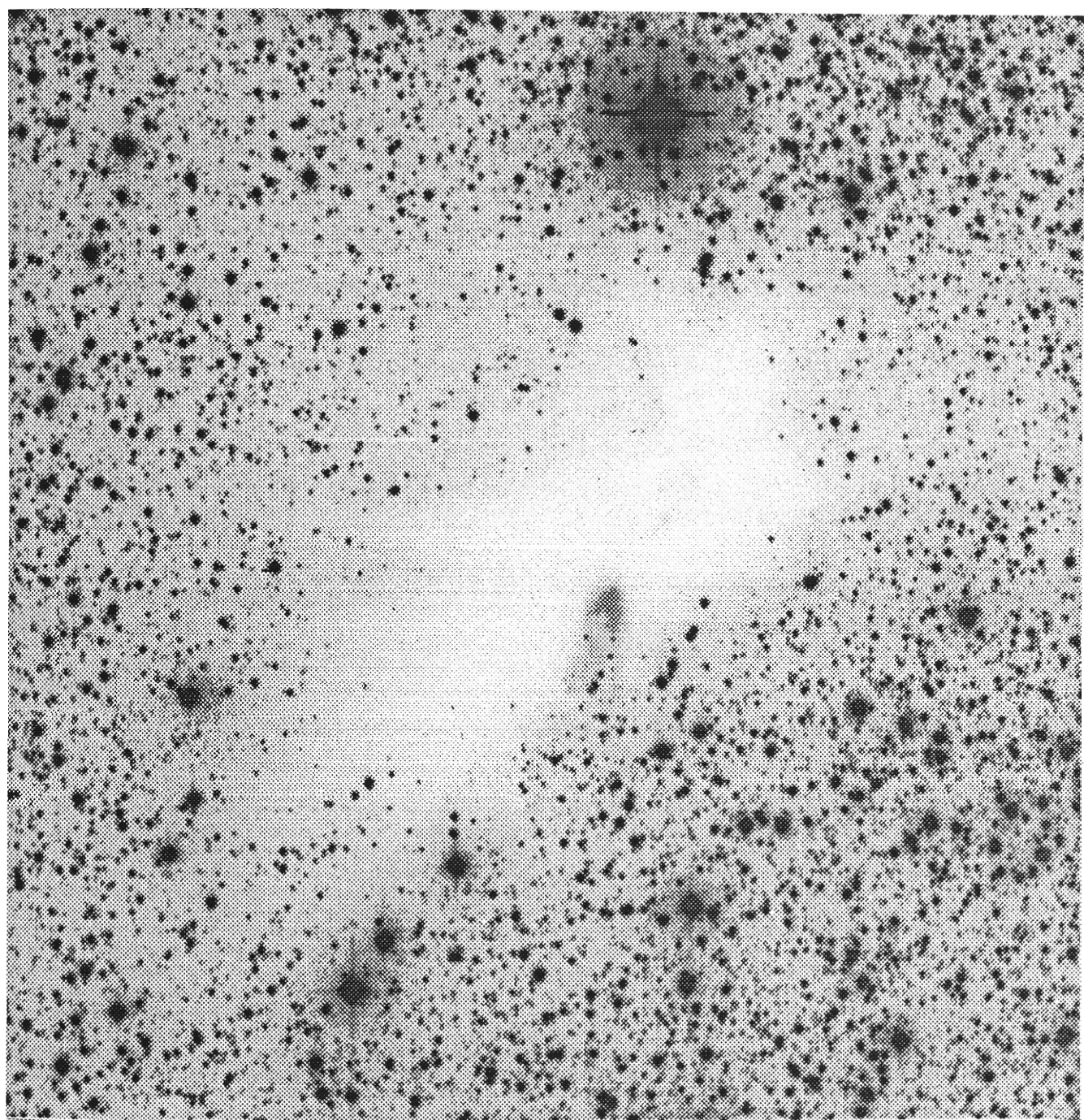
appears flatter in this map in the N/S direction than it does in the map of antenna temperature, and is more symmetric about its peak position along the N/S and E/W axes. Figure 4.5 shows $\log N(\text{NH}_3)$ vs $\log(\text{radial offset})$ plots through the N/S and E/W axes, where the values either side of the centre have been averaged in the plot. Also plotted are lines with slope -2 . Along both axes we see a drop in density which is very well approximated by an r^{-2} law in the envelope region. We also see that the core column density is very uniform with a much shallower gradient. These results are consistent with cloud collapse models (see e.g., Larson, 1969; Shu, 1977; Villere and Black, 1980) which predict that the density should fall off as r^{-2} outside the core, while the core exists at a nearly uniform density. However, it may be that we do not have sufficient resolution in our observations to detect a continual increase in the density as we get closer to the cloud centre.

DC 297.7–2.8

This is a beautiful example of an isolated globule with a very dense core, which is shown clearly in figure 4.6. Visible in this near-infrared ($0.8 \mu\text{m}$) image is a reflection nebula situated near the centre of the globule. The projected apex of this nebula coincides with the *IRAS* source, *IRAS* 11590–6452, whose colours are those of an embedded source. Goss *et al.* (1980) observed this globule in H_2CO absorption, finding a beam brightness temperature of -0.42 K. The globule also appears in the CO survey work of the Carina Arm by Grabelsky *et al.* (1987). In their figure 7 the globule appears clearly with a CO peak of ~ 10 K km s^{-1} . No other observations are known to us.

The map of antenna temperature observed towards the globule is shown in figure 4.2(g). The ammonia emission traces the optical extent of the globule very well. The globule is obviously non-circular, with a core size of $3.8' \times 2.5'$. The

Figure 4.6: *I* band image of DC 297.7–2.8 (wavelength $\sim 0.8 \mu\text{m}$). This image was taken with a Tektronix 1024×1024 CCD attached to the $40''$ reflector at Siding Spring Observatory. The field of view is $10.4' \times 10.4'$. Clearly visible is the elongated structure of the globule, and the nebula associated with the *IRAS* source. The image has north to the top and east to the left.



DC 297.7-2.8

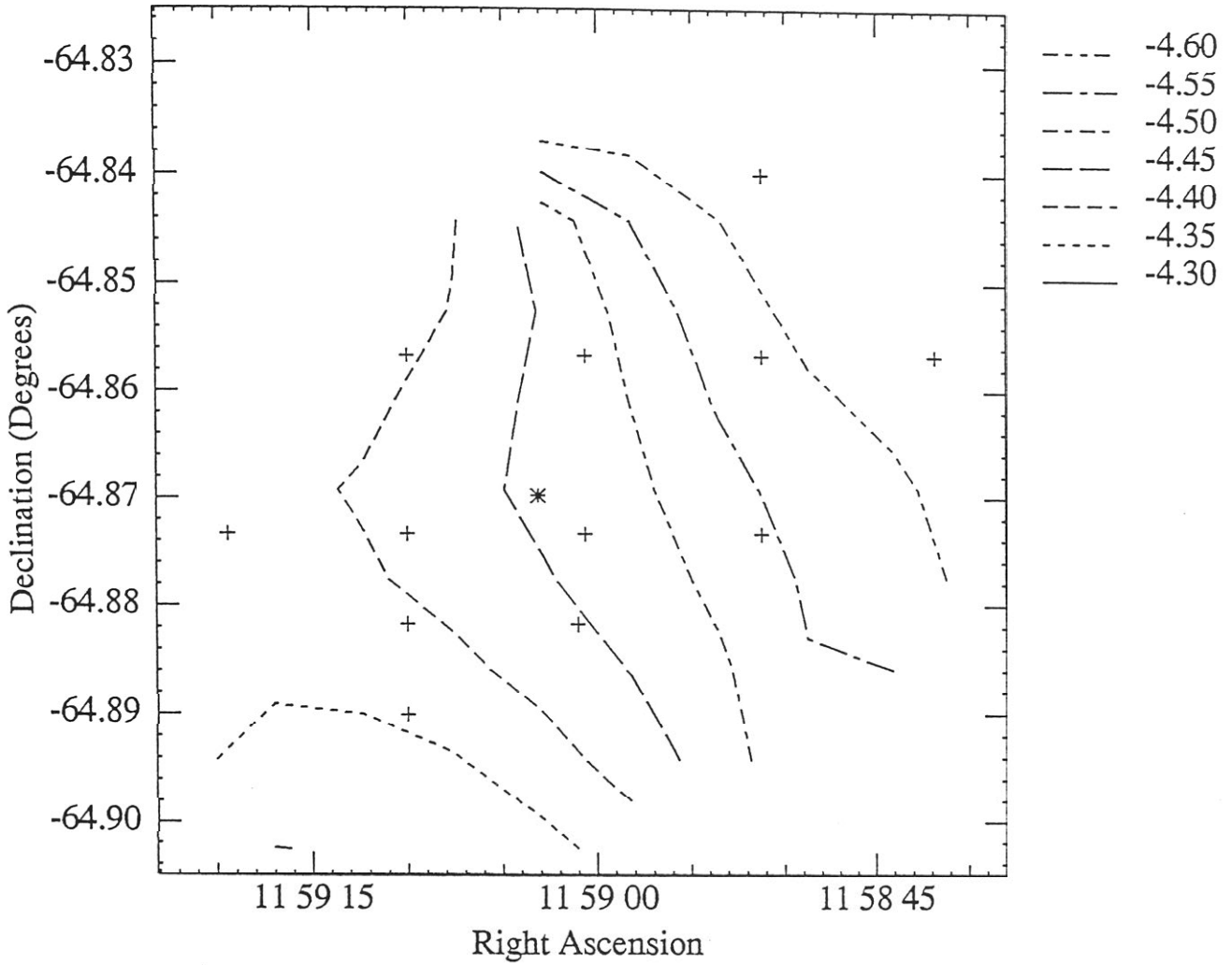


Figure 4.7: Contour plot of ammonia velocity distribution within the core region of DC 297.7–2.8. Only positions where $T_a^* > 0.2$ K are included. A clear velocity gradient is evident along the cloud major axis. The velocity levels are shown in the legend.

observed velocity, $V_{l,sr} = -4.4 \text{ km s}^{-1}$, and its proximity to the Southern Coalsack dark cloud complex implies the globule lies at a distance of about 150 pc, which in turn implies a true core size of $0.17 \times 0.11 \text{ pc}$. At the nominal cloud centre we find $T_a^* = 0.97 \text{ K}$, $\Delta v = 0.65 \text{ km s}^{-1}$ and $\tau_m = 1.83$. The values are very similar at the *IRAS* position, which lies just west of the centre, though not within the same telescope beam. For the central position we find a kinetic temperature $T_K = 11.9 \text{ K}$, and the total number density is $n = 2.44 \times 10^4 \text{ cm}^{-3}$. The ammonia abundance is thus implied to be 4.9×10^{-8} . At the *IRAS* position we find a slightly warmer kinetic temperature of $\sim 14 \text{ K}$. The core mass is estimated to be $1.9 M_\odot$. The luminosity of the *IRAS* source is found to be $6.9 L_\odot$ for wavelengths longer than $12 \mu\text{m}$.

Figure 4.7 shows a velocity contour plot for the central region of DC 297.7–2.8, where $T_a^* > 0.2 \text{ K}$. The line centre velocity becomes difficult to determine at levels lower than this, due to the non uniform line shapes combined with the lower signal-to-noise ratios, as indicated previously for DC 345.4–4.0. The figure shows a clear velocity gradient across the inner region of the globule. If we assume that this gradient is a result of the globule rotating about its minor axis, then we can calculate the rotational velocity, by assuming rigid body rotation without correcting for possible projection effects. With these assumptions we find a rotational velocity $\omega = 1.9 \text{ km s}^{-1} \text{ pc}^{-1}$ ($\equiv 6.1 \times 10^{-14} \text{ s}^{-1}$), which corresponds to an angular momentum of $J = 0.0066 M_\odot \text{ km s}^{-1} \text{ pc}$. For a uniformly rotating spherical cloud (Goldsmith and Arquilla, 1985) the required equilibrium angular momentum, ω_{eq} , is $\sim 0.037n^{0.5} \text{ km s}^{-1} \text{ pc}^{-1}$. Using the value of n given above, we find $\omega_{eq} \sim 6 \text{ km s}^{-1} \text{ pc}^{-1}$ for DC 297.7–2.8, which indicates that the rotation cannot support the globule in equilibrium, and so cannot be important in the globule dynamics. This view is supported by the value found for the ratio of potential to gravitational energy, $\beta = 3 \times 10^{-3} \omega^2/n$,

DC 297.7-2.8

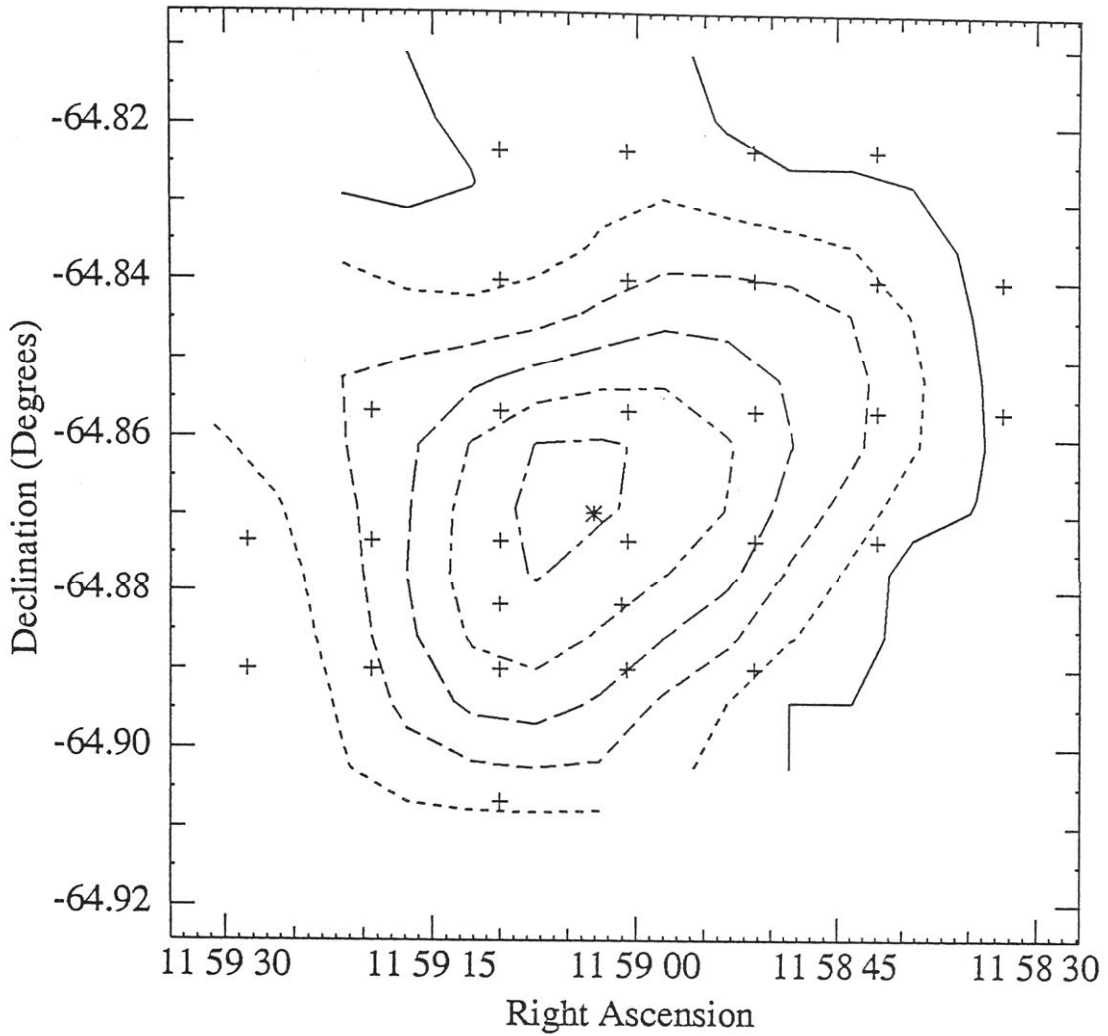


Figure 4.8: Contour plot of the ammonia column density distribution within DC 297.7-2.8. Comparison with the plot of antenna temperature shows that the major axis of the column density plot is slightly rotated with respect to the intensity map. Contour levels are $\log N(NH_3) = 13.7, 13.9, 14.1, 14.3, 14.5, 14.7$.

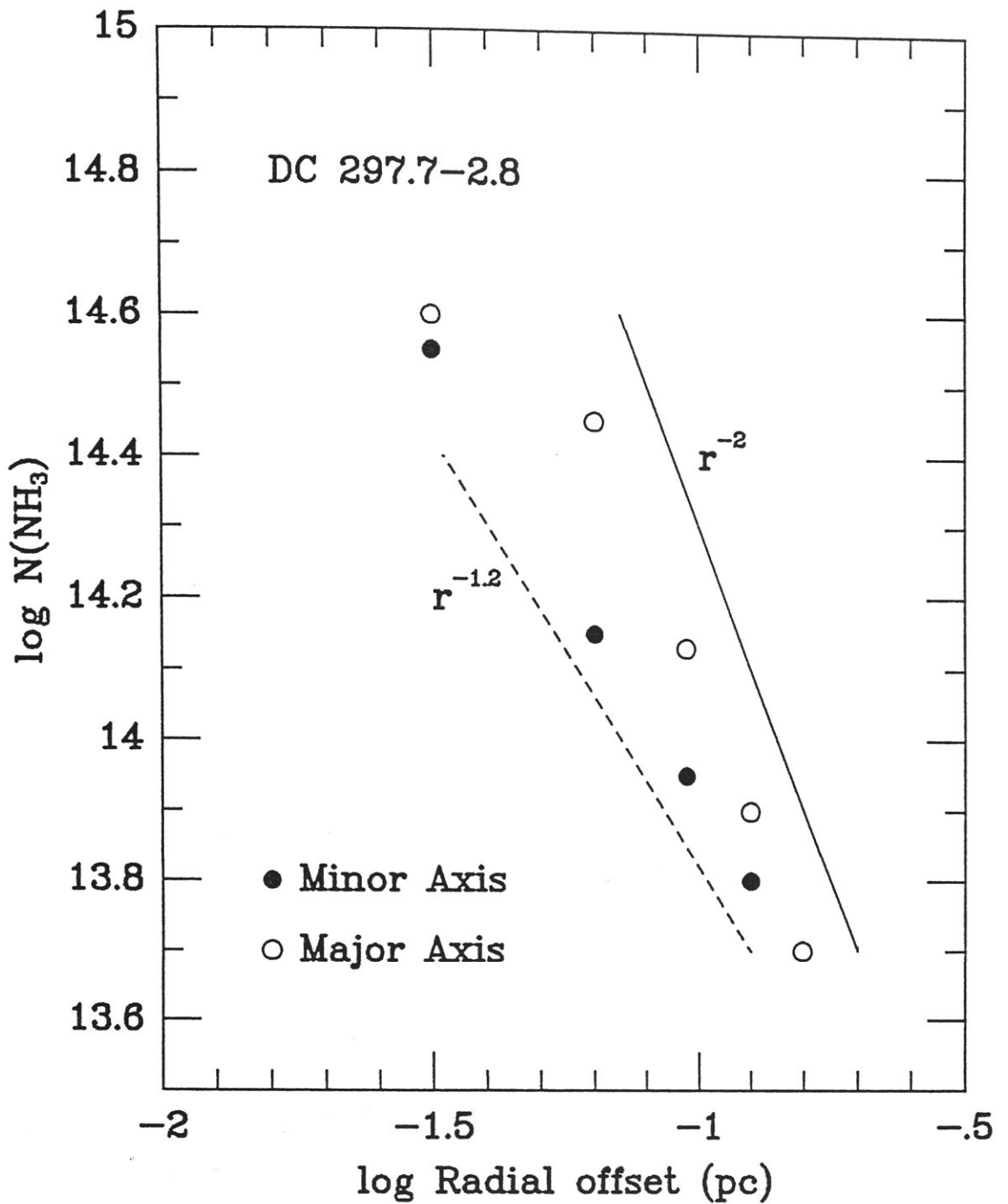


Figure 4.9: Plots of the density distribution along the major and minor axes of DC 297.7-2.8. The gradient along the major axis varies as r^{-2} and along the minor axis as $r^{-1.2}$.

Figure 4.10: Broadband image of DC 297.7–2.8 at K' ($2.11 \mu\text{m}$), taken with the infrared array camera IRIS (128×128) at the Anglo-Australian Telescope. The image is a 4×4 mosaic of 16 individual frames, and the field of view is $\sim 6.4' \times 6.4'$. A “bipolar” nebula is seen either side of the embedded source *IRAS* 11590–6452. The image has north to the top and east to the left.

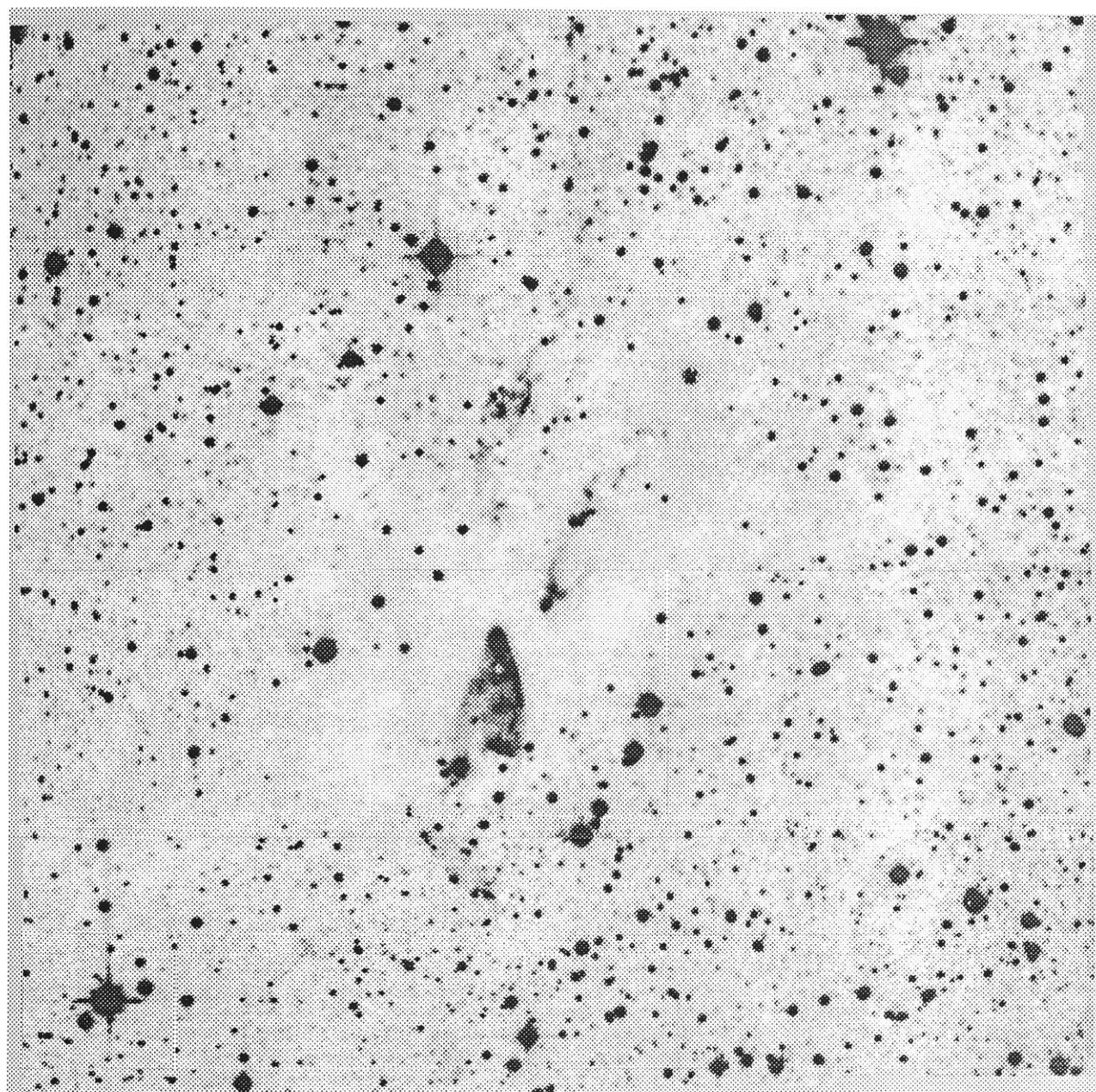
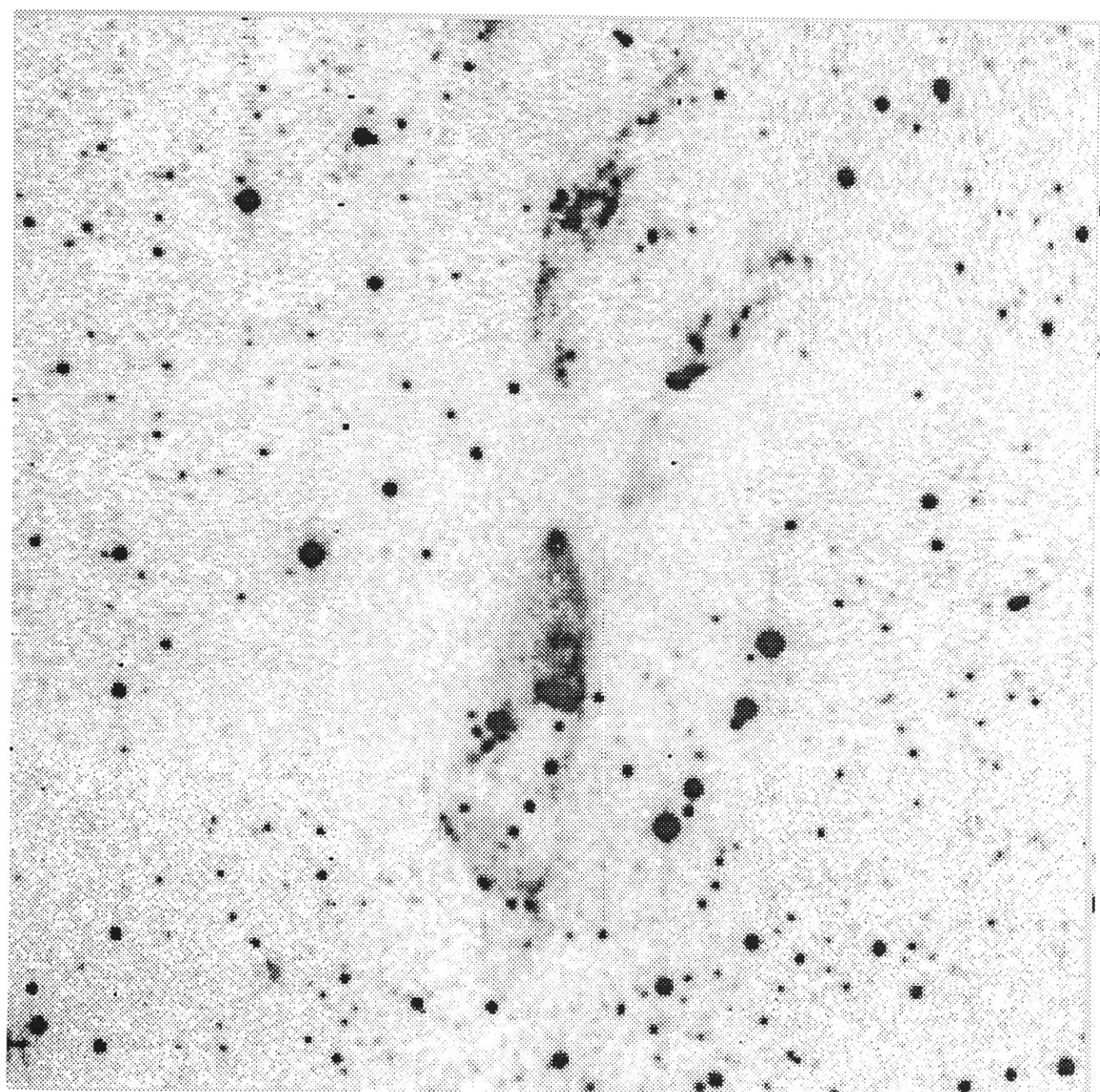


Figure 4.11: Narrow band image of DC 297.7–2.8 centered on the $2.12 \mu\text{m}$ $v = 1-0$ s(1) line of molecular hydrogen (1% bandpass). This image clearly indicates that the majority of the nebulosity seen at K' is due to molecular hydrogen emission, most likely caused by the impact of outflowing gas from the embedded source impacting on the surrounding ambient material, resulting in shocked emission. The image is a 3×3 mosaic taken with IRIS, and the field of view is $\sim 4.4' \times 4.4'$. North is to the top and east is to the left.



where ω is in units of 10^{-14} s^{-1} , and n is in 10^4 cm^{-3} (Menten *et al.*, 1984). We find that $\beta = 4 \times 10^{-2}$, clearly showing that if the observed velocity shift is due to core rotation, then this rotation is playing a negligible role in the core dynamics.

A contour plot of the derived NH_3 column densities is shown in figure 4.8. Though the structure is similar to that seen in the map of antenna temperature, the major axis of the density map appears slightly rotated in position angle compared to the intensity map. Figure 4.9 show the variation of ammonia column density with radial distance from the cloud centre along the major and minor axes. From the column density map we have take the *IRAS* position to be the cloud centre for these sections. What is clearly evident from the figure is the different density profiles along the two axes. Along the major axis the density varies as r^{-2} , which, as we have seen, is consistent with the profile expected in the envelope region of an isothermal self-gravitating sphere. We also see an indication that the density gradient drops toward the core centre, which would also be consistent with the self-gravitating sphere model. Higher resolution observations are needed in the core region to examine this possibility. However, along the minor axis the density drops as $r^{-1.2}$. Shu (1977) has shown that an isothermal self gravitating sphere will form a centrally condensed core with a spherical accretion flow following an $r^{-1.5}$ law around it (“inside-out collapse”), but DC 297.7–2.8 is clearly not spherical, and this does not explain the profile seen along the major axis. Cernicharo *et al.* (1985) used star counts to estimate the variation of density with radius for clouds in the Taurus and Perseus complexes. They found that the clouds follow an $r^{-1.3}$ profile. However, they were observing regions of moderate gas column densities, which is clearly not the case in DC 297.7–2.8. It may be that the mass is preferentially gathering along the cloud major axis (infall combined with rotation about the minor axis?), or that

the mass along the minor axis has somehow been depleted, perhaps due to a molecular outflow. The nebula visible in DC 297.7–2.8 is certainly suggestive of a cavity created by some mass outflow phenomena, where we see the nebula as light scattered from the cavity walls. The near-infrared broadband ($2.11 \mu\text{m}$) and narrowband ($\text{H}_2 v = 1 - 0 \text{ S}(1)$ transition at $2.12 \mu\text{m}$) images, figures 4.10 and 4.11, indicate that an extensive outflow is probably associated with *IRAS* 11590–6452, supporting the view that the mass along the minor axis may have been depleted by an outflow.

4.3.3 Dynamical Analysis

Cloud Masses and Equilibrium

To investigate whether a molecular cloud may or may not collapse, it is usual to compare the cloud's mass against some theoretically derived mass, based on other physical properties of the cloud, such as its size, density and temperature. In the most simplistic picture, one examines theoretically the properties of an isothermal self-gravitating sphere, where the only significant forces acting are those due to the cloud's self-gravity and internal pressure. Thus, forces such as rotation, turbulence and magnetic fields are often ignored, though they may be important.

In this section, three theoretical masses are examined and compared with the mass determined from the ammonia observations from the preceding section. These three masses, in theory, should be equivalent, but we shall see that they rarely agree numerically.

The virial mass provides an estimate of the mass at which the kinetic energy within the cloud stabilizes the cloud against gravitational collapse. Therefore,

clouds with masses larger than the virial mass should be unable to support themselves against gravitational collapse. The virial mass may be found from (Myers, 1987):

$$M_{vir} = \frac{5R}{8 \ln 2G} (\Delta v)^2$$

which simplifies to:

$$\frac{M_{vir}}{M_{\odot}} = 210 \frac{R}{\text{pc}} \left(\frac{\Delta v}{\text{km s}^{-1}} \right)^2 \quad (4.1)$$

This mass may also be expressed in terms of the cloud temperature and density, as outlined below.

Dyson and Williams (1980) show that the condition for collapse of an isolated self-gravitating sphere is that the free fall time for collapse must be less than the time taken for a sound wave to cross the cloud. In terms of the cloud mass, this may be expressed as:

$$M_{crit} \simeq \left(\frac{3\pi^5}{32} \right)^{1/2} a^3 G^{-3/2} \rho^{-1/2}$$

where M_{crit} is the critical mass, a the isothermal sound speed, and ρ the cloud density. This simplifies to:

$$\frac{M_{crit}}{M_{\odot}} = 1.4 \times 10^4 \left(\frac{T_K}{\text{K}} \right)^{3/2} \left(\frac{n}{\text{m}^{-3}} \right)^{-1/2} \quad (4.2)$$

where n is the total number density. Clouds with $M > M_{crit}$ should collapse, assuming there are no other means of internal support. However, for clouds with $M < M_{crit}$, both stable and unstable equilibria are possible, depending on the degree of central condensation (ratio of central to surface density). If the degree of central condensation is greater than about 14, then the equilibrium is unstable and a small perturbation is all that is required to cause the cloud to collapse (Spitzer, 1968; Shu, 1977). The critical mass is sometimes called the Jeans mass, M_J , and various expressions for it may be found in the literature. Lang (1974) derives the Jeans mass as:

$$M_J = \frac{\pi^{5/2}}{6} a^3 G^{-3/2} \rho^{-1/2}$$

which simplifies to:

$$\frac{M_J}{M_\odot} = 7.8 \times 10^3 \left(\frac{T_K}{K} \right)^{3/2} \left(\frac{n}{\text{m}^{-3}} \right)^{-1/2} \quad (4.3)$$

and so $M_{crit} \sim 2M_J$, even though they are derived from the same basic assumptions. We shall see that in some cases this difference is important.

Table 4.2 tabulates the values of the masses calculated with the above formulae, as well as the value determined from the ammonia observations (simply labelled M in this section). Column 1 lists the cloud name, and columns 2–5 the masses M , M_{vir} , M_{crit} and M_J respectively. Column 6 indicates whether there is an *IRAS* source lying within the cloud boundary. It can immediately be seen from table 4.2 that in all but one case the virial mass is greater than the cloud mass. While for clouds without *IRAS* sources, this may come as no surprise, since these clouds are showing no clear signs of star formation taking place, and may therefore be stable against collapse. For the clouds with *IRAS* sources, the situation is less clear. The virial equation uses the observed line width, and as has been observed by BM89, cores with stars (i.e., *IRAS* sources) have larger line widths than cores without stars. This is also observed in the globules studied here. It would seem apparent that the embedded sources are the cause of the enhanced line widths. These larger line widths, and their effect on the calculated virial mass, results in two possible interpretations of the result $M_{vir} > M$.

The first is that whatever process is resulting in the increased line widths (outflows, turbulence) is also providing support to the cloud against further collapse, at least until the current star formation process has quietened down. This support could be a result of the deposition of energy from the star or outflow into the gas within the core. It may also suggest that once single (or binary) star formation has begun, further star formation is unlikely. It is interesting to note that DC 267.7–7.4 has $M > M_{vir}$ but no *IRAS* source, suggesting it may be close to collapse, and that there are two T Tauri binaries at its periphery, which

Table 4.2: The cloud mass as determined from the ammonia observations, as well as the virial mass, critical mass and Jeans mass, for the mapped sources in this study.

Cloud	$M (M_{\odot})$	$M_{vir} (M_{\odot})$	$M_{crit} (M_{\odot})$	$M_J (M_{\odot})$	<i>IRAS</i>
253.1-1.7A	13	–	7	4	
253.3-1.6	9	19	6	3	Y
267.4-7.5	13	23	12	7	Y
267.7-7.4	8	7	5	3	
275.9+1.9	5	9	5	3	Y
295.0+3.4	6	10	6	3	
297.7-2.8	2	6	4	2	Y
327.7+1.8	2	3	4	2	
345.5-4.0	12	29	4	2	Y
B68	1	1	9	5	

may indicate that it was once a larger cloud which has undergone star formation in the past, and is ready to do so again, now that the stars have reached the (relatively) quiet T Tauri phase in their evolution. Parker (1989) has found that outflows from low mass YSOs are probably not the dominant mechanism of cloud support, but that they are capable of affecting the dynamics of the clouds.

The other possibility is that the large line widths are resulting in a false determination of the cloud's virial mass, i.e., it is being overestimated. It may be that the cloud is still contracting as a result of the star formation process, and that the process causing the enhanced line widths is not providing cloud support, but simply misleading us. Again this process could be something like turbulence or outflows, but not have the energy required for cloud support.

For the 5 clouds with *IRAS* sources, four have either $M \simeq M_{crit}$ or $M \simeq M_J$, while only one clearly has $M > M_{crit} > M_J$. If we believe these results, then they imply that some of these clouds seem to be in approximate critical equilibrium or are undergoing contraction, which is in contrast to that implied by the virial masses. It has been suggested by some authors (Larson, 1981; Leung *et al.*, 1982) that a cloud may be collapsing while appearing in approximate equilibrium.

For the 5 clouds without *IRAS* sources, 2 have $M > M_{crit} > M_J$ (CG31A, DC 267.7–7.4), and so may be collapsing or on the verge of collapse. They clearly require further study. Two have either $M \simeq M_{crit}$ or $M \simeq M_J$ and so may be unstable against collapse or in equilibrium, while B68 appears to have no chance of collapse in its current state.

The above analysis highlights the difficulties in using idealized models for studies of individual clouds (though for studying a number of clouds for an overall “feel” of their nature they may be useful, as shown in the next section). For example, both DC 267.4–7.5 and DC 297.7–2.8 have embedded near-infrared

Table 4.3: Ratio of core mass to virial mass for isolated globules from this work and from Benson and Myers (1989). Also indicated is whether there is an *IRAS* source lying within the core. A dividing line at $M/M_{vir} \sim 0.6$ appears to separate the cores with and without *IRAS* sources.

Cloud	$M (M_{\odot})$	$M_{vir} (M_{\odot})$	$\frac{M}{M_{vir}}$	<i>IRAS</i>
297.7–2.8	1.9	6.2	0.31	Y
B335	0.6	1.8	0.33	Y
L1544	0.3	0.9	0.33	N
345.4–4.0	11.8	28.8	0.41	Y
L1512	1.0	2.4	0.42	N
253.3–1.6	9.0	18.8	0.48	Y
L1262A	0.9	1.7	0.53	Y
275.9+1.9	4.9	8.8	0.56	Y
267.4–7.5	13.0	22.4	0.58	Y
295.0+3.4	6.1	10.4	0.59	N
B68	0.7	1.1	0.64	N
327.2+1.8	2.1	3.1	0.68	N
B361	13.7	16.5	0.83	Y
267.7–7.4	7.5	6.5	1.15	N
L63	2.2	0.78	2.8	N

sources and associated shocked molecular hydrogen outflows, but neither has $M > M_{vir}$ and DC 297.7–2.8 has $M_{crit} > M$, while it is obvious both clouds are undergoing star formation. These clouds add weight to the suggestion that an outflow is a possible mechanism for support of a cloud undergoing star formation. The isothermal self-gravitating sphere model ignores the effects of rotation, magnetic fields and turbulence, as well as adiabatic processes, all of which may be very important in cloud dynamics. In table 4.3 are listed the ratios of M to M_{vir} for the clouds in this work and the 6 globules from BM89, where the masses for the BM89 globules have been recalculated using half of the geometric mean core size as the radius. We can see in this table that the clouds with the smallest M/M_{vir} are the ones undergoing star formation, with the dividing line occurring around $M/M_{vir} \sim 0.6$. Once again we have support for the view that the onset of star formation in these isolated globules prevents further star formation in the immediate future. But we cannot say that these clouds will not collapse again once the most energetic phase of the star formation process have ended.

There are of course problems with the determination of cloud masses from the observations. For example, if the linear resolution of the observations is insufficient to resolve the central parts of the core, then we may be underestimating the core density and hence the core mass (when the mass calculations assume a uniform density, which in itself is unrealistic). This will not change the virial mass calculations, and will not affect the relationships between M , M_{crit} and M_J , but may bring M closer to M_{vir} . However, the lack of resolution may also result in the core size being overestimated, which would move M and M_{vir} further apart.

Another area of concern is the definition of the cloud size. As has been mentioned previously (chapter 3) some authors use the core “diameter” to define the cloud size, where the diameter is the geometric mean of the map half power

contour. This diameter is then used as the “radius” in further studies, such as mass calculations. Mass calculations, as indicated above, are usually based on the assumption of uniform densities, and the peak density is usually used in the mass calculations. It would seem that this would then result in a gross overestimate of the core mass, since we know the density may drop off dramatically toward the cloud edge. Using the “diameter” in the mass calculations here would result in $M \gg M_{crit}$ or M_J in almost all cases. One could then only conclude that all the cores will collapse, which would seem unlikely. In the next section, we shall see that when the core diameter as defined above is used in the mass calculations, then $M > M_{vir}$ in almost all cases, the complete opposite to what we have seen in this section (see figure 4.17). This inconsistency in definitions does not help in the investigation of the cloud’s dynamical state.

The choice of the density tracer is also important. Studies have shown that the use of CS emission as a high density tracer leads to derived core sizes greater than that traced by NH_3 by a factor of ~ 1.5 , and that the derived densities from CS observations are about a factor 10 greater than those derived from NH_3 (Zhou *et al.*, 1989). These two differences imply that the masses determined from CS observations will be much greater than from NH_3 observations, and so may result in completely different interpretations of the dynamical state of the clouds.

Power-Law Relationships

It has been found that over many decades in size, dark clouds exhibit well correlated power-law relationships between velocity dispersion and cloud size, and between mean density and cloud size, and that the law of virial equilibrium is satisfied (Larson, 1981; Myers, 1983). It has been suggested that these relationships can be understood if the observed non-thermal motions arise from magnetic

Table 4.4: Line widths, sizes, densities and temperatures for small Bok globules used in the analysis of the cloud dynamics. In this table R represents the geometric mean of the core half power diameter, and the mass is calculated using R as the cloud radius.

Cloud	R (pc)	T_K (K)	T_D (K)	Δv (km s ⁻¹)	Δv_{turb} (km s ⁻¹)	Δv_{tot} (km s ⁻¹)	n $\times 10^4$ cm ⁻³	M M_\odot
253.3–1.6	0.28	13.9	236.4	0.80	0.78	0.94	1.48	79
267.4–7.5	0.41	17.7	196.6	0.73	0.70	0.91	0.73	125
267.7–7.4	0.28	11.4	81.5	0.47	0.44	0.64	1.22	66
275.9+1.9	0.27	11.3	115.7	0.56	0.53	0.71	1.00	39
295.0+3.4	0.30	10.9	119.9	0.57	0.54	0.72	0.82	49
297.7–2.8	0.14	11.9	155.9	0.65	0.62	0.79	2.44	15
327.2+1.8	0.18	11.3	62.0	0.41	0.37	0.60	1.28	17
345.5–4.0	0.28	9.0	361.7	0.99	0.98	1.06	1.94	94
B68	0.14	15.8	28.9	0.28	0.19	0.59	0.86	5.6
L1512	0.05	10.0	16.3	0.21	0.13	0.46	25.12	7.6
L1544	0.10	9.8	33.2	0.30	0.25	0.51	1.00	2.4
L63	0.11	9.7	24.9	0.26	0.20	0.48	5.01	16
B335	0.11	9.9	59.0	0.40	0.37	0.57	1.26	4
B361	0.32	10.0	180.8	0.70	0.68	0.81	1.26	98
L1262A	0.12	10.3	50.5	0.37	0.33	0.56	1.58	6.6

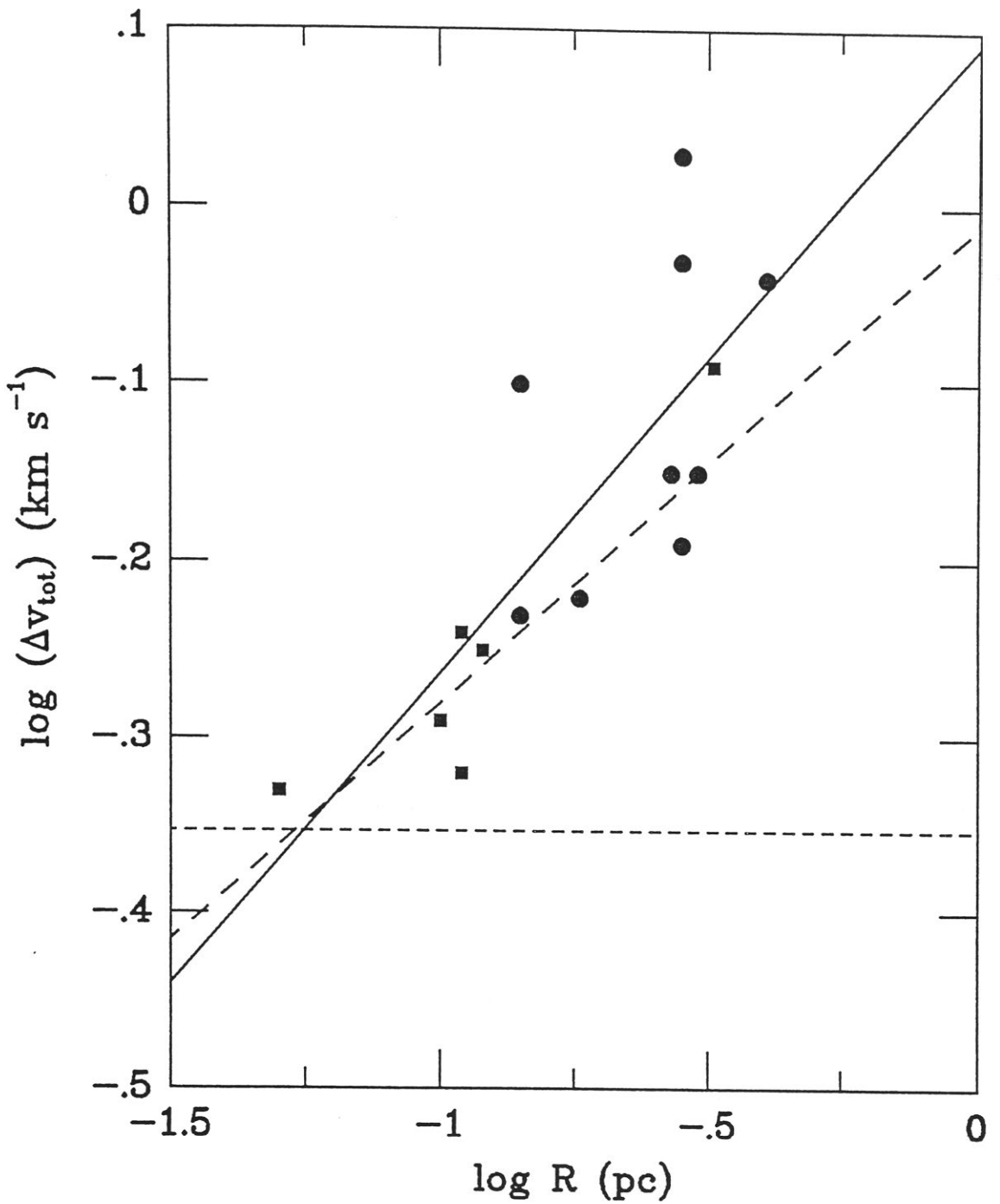


Figure 4.13: Log-log plot of total line width against cloud size for small Bok globules. The total line width is directly related to the overall velocity dispersion of the mean particle. Also shown is the line of best fit (solid line), with slope 0.36 and correlation coefficient 0.82. The short-dashed line represents the line width for pure thermal motions at 10 K, and the long-dashed line the best fit to Myers' data.

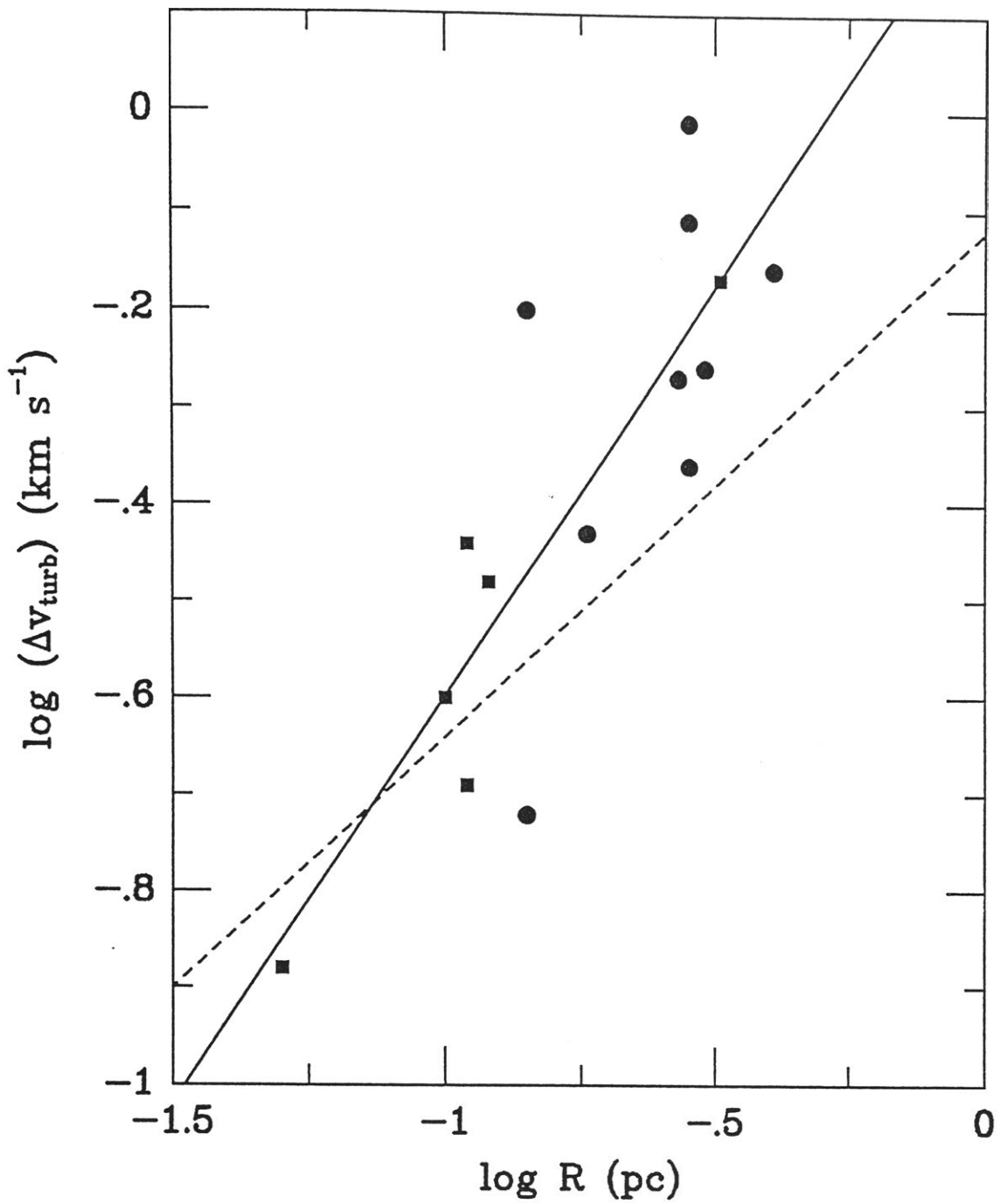


Figure 4.14: Log-log plot of the nonthermal, or turbulent line width against cloud size for small Bok globules. The best fit line is shown (solid line), with slope 0.84 and correlation coefficient 0.84, and the best fit to Myers' data (dashed line).

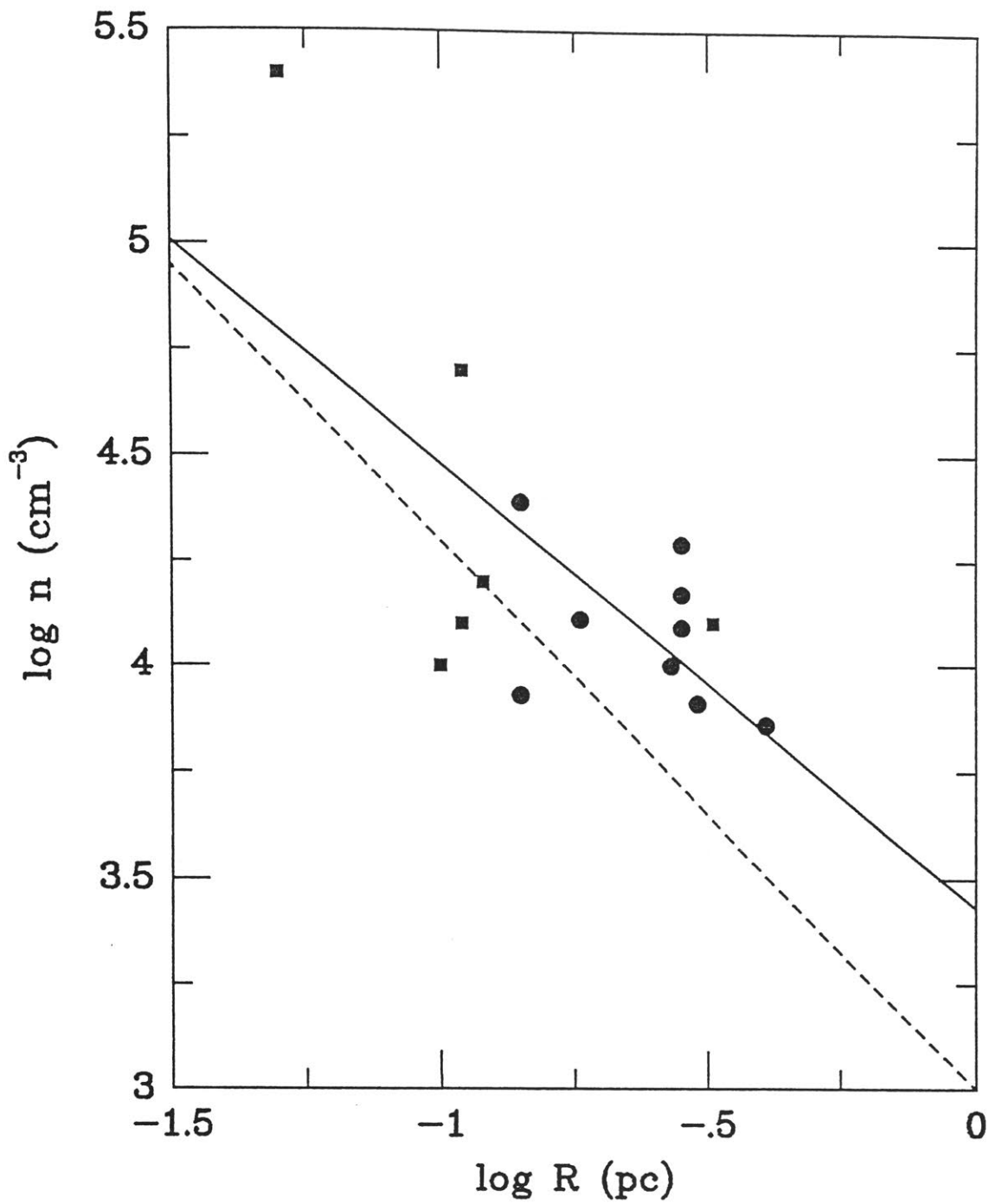


Figure 4.15: Log-log plot of total volume density against cloud size for small Bok globules. The best fit line is shown (solid line) with slope -1.1 and correlation coefficient 0.69 . Also shown is the best fit line to Myers (1983) data, with slope -1.3 (dashed line).

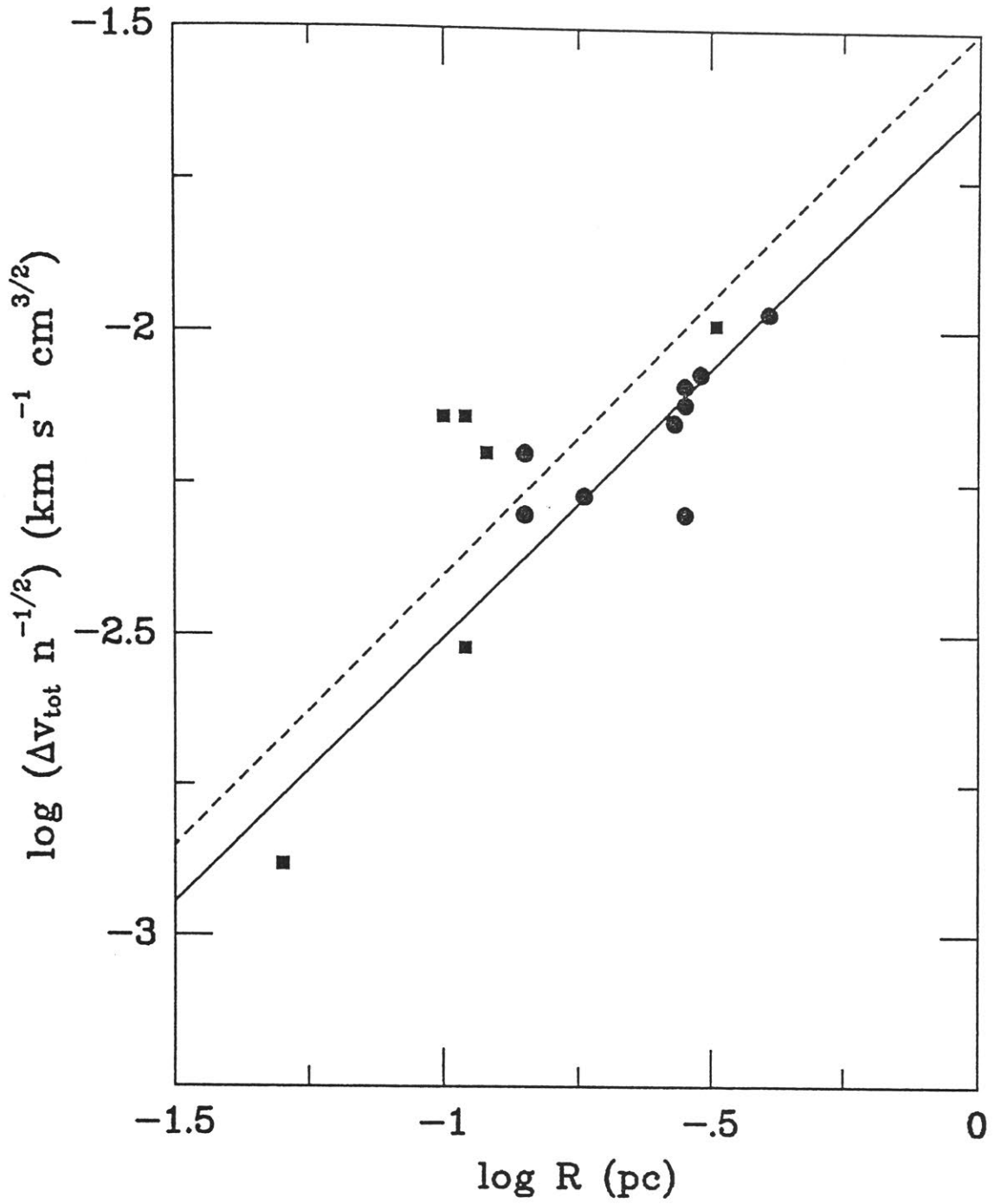


Figure 4.16: Log-log plot of $\Delta v_{\text{tot}} n^{-1/2}$ against cloud size for small Bok globules, for comparison with virial equilibrium. The line of best fit (solid line) has slope 0.88 and correlation coefficient 0.86. The best fit line to Myers' (1983) data is shown, which has slope 0.9 (dashed line).

fields with values typically 5–100 μG (Myers and Goodman, 1988; hereafter MG). We will examine in this section whether these power-law relationships hold for the small dense globules as a distinct sample. Myers (1983) found that the laws broke down when only considering the small dense cores detected in ammonia, but that a sample combining the dense cores with the large globules observed by Leung *et al.* (1982) showed the power-law relationships. These relationships have been observed by other investigators, e.g., Larson (1981), Sanders *et al.* (1985), and Dame *et al.* (1986), over a wide range of cloud types and sizes. Myers suggested that these trends thus only show themselves when a large range of cloud sizes are considered.

Here the results of this work, where size estimates and line widths have been determined for nine globules, have been combined with the results of six globules from BM89. The data used in the following analysis are presented in table 4.4. Column 1 lists the cloud name, and column 2 the cloud size (diameter of half power NH_3 contour). Column 3 lists the cloud kinetic temperature, and column 4 the “Doppler temperature”, $T_D = 369(\Delta v)^2$ (Myers and Benson, 1983). Columns 5–7 list the intrinsic ammonia line width, the turbulent line width, and the total line width, as defined below. Column 8 lists the total volume density and column 9 the cloud mass, where the core diameter, R , has been used to determine the mass, to be consistent with previous studies. The total volume density, n , has been recalculated for the BM89 sources using their values of T_{ex} and T_K to be consistent with the values determined in this work.

Three line widths are examined, Δv , the intrinsic NH_3 line width, Δv_{tot} , and Δv_{turb} . The width of the distribution of turbulent cloud motions, Δv_{turb} , is given by (Myers, 1983):

$$\Delta v_{turb} = \left[(\Delta v)^2 - \frac{8(\ln 2)kT_K}{m} \right]^{1/2} \quad (4.4)$$

where k is Boltzmann’s constant, and m is the molecular mass of the observed

tracer, which for NH_3 is 17 amu. A measure of the overall velocity dispersion of the mean cloud particle is (Myers, 1983):

$$\Delta v_{tot} = \left[(\Delta v_{turb})^2 + \frac{8(\ln 2)kT_K}{\mu} \right]^{1/2} \quad (4.5)$$

where μ is the mean mass per particle, which equals 2.33 amu assuming five hydrogen molecules to one helium atom. The cloud size is as previously defined, but in this section we use the geometric mean diameter to define the cloud radius, to be consistent with previous investigators.

Table 4.5 shows the derived relationships between the various parameters presented in table 4.4, together with the results found by Myers (1983). Columns 1 and 2 list the parameters plotted in figures 4.12 to 4.16. Column 3 indicates which sample is under consideration (see the legend in the table). Columns 4–6 lists the parameters of the line of best fit to the data indicated in columns 1–2, where m is the gradient, c the intercept on the vertical axis, and r is the linear correlation coefficient, i.e., the fit to the data is of the form $y = mx + c$.

In figure 4.12 we see the relationship between Δv and cloud size R in a log-log plot, with the line of best fit to the data indicated. Though the range of R is small, we see a well correlated fit ($r = 0.84$) with slope 0.66, in contrast to that found by Myers (slope 0.5). In figure 4.13 the relationship between the total velocity dispersion and size is shown. Since Δv_{tot} represents the motion of a particle of the mean mass rather than the line tracer, any correlation found here is likely to be more significant in terms of cloud dynamics (Myers, 1983). We again see a good correlation, this time with slope 0.36 and correlation factor of 0.82. This result is similar to that found by Myers (slope 0.27). Figure 4.14 shows the relationship between the turbulent, or “non-thermal” part of the velocity dispersion and size. A strong correlation is again present ($r = 0.84$) and the slope of the best fit line (0.84) is significantly steeper than that found by Myers (slope

Table 4.5: Power Law Correlations between line widths, density and cloud sizes for small Bok globules. Also shown are the laws found by Myers (1983) for clouds covering a larger range of sizes.

y	x	Sample ^(a)	m	c	$r^{(b)}$
$\log \Delta v$	$\log R$	This	0.66	0.16	0.84
		NH ₃	0.40	-0.13	0.40
		NH ₃ + CO	0.50	-0.03	0.92
$\log \Delta v_{tot}$	$\log R$	This	0.36	0.09	0.82
		NH ₃	0.15	-0.12	0.38
		NH ₃ + CO	0.27	-0.01	0.85
$\log \Delta v_{turb}$	$\log R$	This	0.84	0.24	0.84
		NH ₃	0.59	-0.05	0.58
		NH ₃ + CO	0.52	-0.12	0.90
$\log n$	$\log R$	This	-1.05	3.43	0.69
		NH ₃	-1.00	3.2	0.49
		NH ₃ + CO	-1.30	3.0	0.89
$\log[\Delta v_{tot} n^{-1/2}]$	$\log R$	This	0.88	-1.6	0.86
		NH ₃	0.66	-1.7	0.57
		NH ₃ + CO	0.90	-1.5	0.95

Notes:

(a) This \Rightarrow Globules shown in Table 4.4.

NH₃ \Rightarrow Myers (1983): 27 cores observed in ammonia.

NH₃ + CO \Rightarrow Myers (1983): 27 cores observed in ammonia + 16 globules observed in CO from Leung *et al.* (1982).

(b) Linear correlation coefficient.

$= 0.32$). Leung *et al.* (1982) have suggested that a strong correlation between Δv_{turb} and R indicates that the globules must be dominated by turbulence and not by gravitational collapse. They also suggest that if considerable dissipation of these turbulent motions occur (as indicated by the power law between Δv_{turb} and R having a coefficient greater than $1/3$, which is the law expected for a dissipationless turbulent cascade), and if the cloud is also gravitationally unstable, then the cloud may contract gravitationally while remaining in approximate virial equilibrium.

In figure 4.15 we see a plot of number density against cloud size. The correlation here (0.69) is not as good as those for the line widths and cloud size, and the slope of the line (-1.1) is different from that found for larger clouds (slope -1.3), but similar to that of virial equilibrium (-1). Thus this plot does not indicate any significant deviation from virial equilibrium, though a considerable scatter in the points about the best fit is evident, which may suggest the similarity of the best fit slope to that of virial equilibrium is a coincidence. Leung *et al.* (1982) suggested that the scatter of points for low n seen in their data may imply that these clouds may not be gravitationally bound. A similar scatter is seen here, but if the reason given by Leung *et al.* is true, then we might expect that the line of best fit in figure 4.16, which plots $\log(\Delta v_{tot} n^{-1/2})$ against $\log R$, would exhibit a slope steeper than the virial equilibrium line of 1. Instead we see the opposite is true, with the line of best fit having slope 0.88, which is not significantly different from the virial line, and correlation coefficient 0.86, implying the correlation is significant. This comparison may be more meaningful than that of M with M_{vir} in the previous section. The plot also shows the best fit to Myers' data, which has a slope of 0.9 and is also not significantly different from the virial line. Another argument for this finding is shown in figure 4.17, which shows a plot of Δv against $(M/R)^{1/2}$, and allows a more direct examination of

the dynamical state of the clouds. If a uniform cloud is in virial equilibrium, then (Myers, 1987):

$$\Delta v = \left(\frac{8 \ln 2GM}{5R} \right)^{1/2} \quad (4.6)$$

This relation is indicated by the solid line in the figure. Clouds lying on or near the line are believed to be in equilibrium, while clouds lying significantly below the virial line should be gravitationally bound, and may have undergone significant gravitational contraction. We see in this figure that all of clouds lie on or below the virial line, suggesting they are gravitationally bound, which argues against the interpretation that the scatter seen in the $\log n - \log R$ plot is due to the clouds being unbound. However, we have seen in the previous section that the choice of the cloud size has an effect on the interpretation of whether virial equilibrium is satisfied or not.

Figure 4.18 shows two variations of the plot of $\log n$ against $\log R$, which allows us to investigate possible equilibrium conditions within the globules, should they exist in equilibrium, by comparing the observed and derived parameters against those of an idealized pressure bounded isothermal sphere (Myers and Benson, 1983; hereafter MB). MB have shown that if equilibrium is present it will be stable if the internal density, n , satisfies:

$$n \leq n_{max} \equiv 8.44 \frac{T}{R^2} \quad (4.7)$$

for R in pc. They show, based on a number of simple arguments, that (a) equilibrium will be impossible if $n/n_{max} > 4.1$; (b) equilibrium may or may not be possible for clouds with $0.41 \leq n/n_{max} \leq 4.1$; and (c) equilibrium is possible for clouds with $n/n_{max} < 0.41$, and is stable if present. For case (b), where equilibrium may or may not be possible, the equilibrium will be (i) unstable if $1 < n/n_{max} < 4.1$; (ii) critical for $n/n_{max} = 1$; and (iii) stable for $0.41 \leq n/n_{max} < 1$. As indicated in the previous section, clouds in unstable equilibrium may

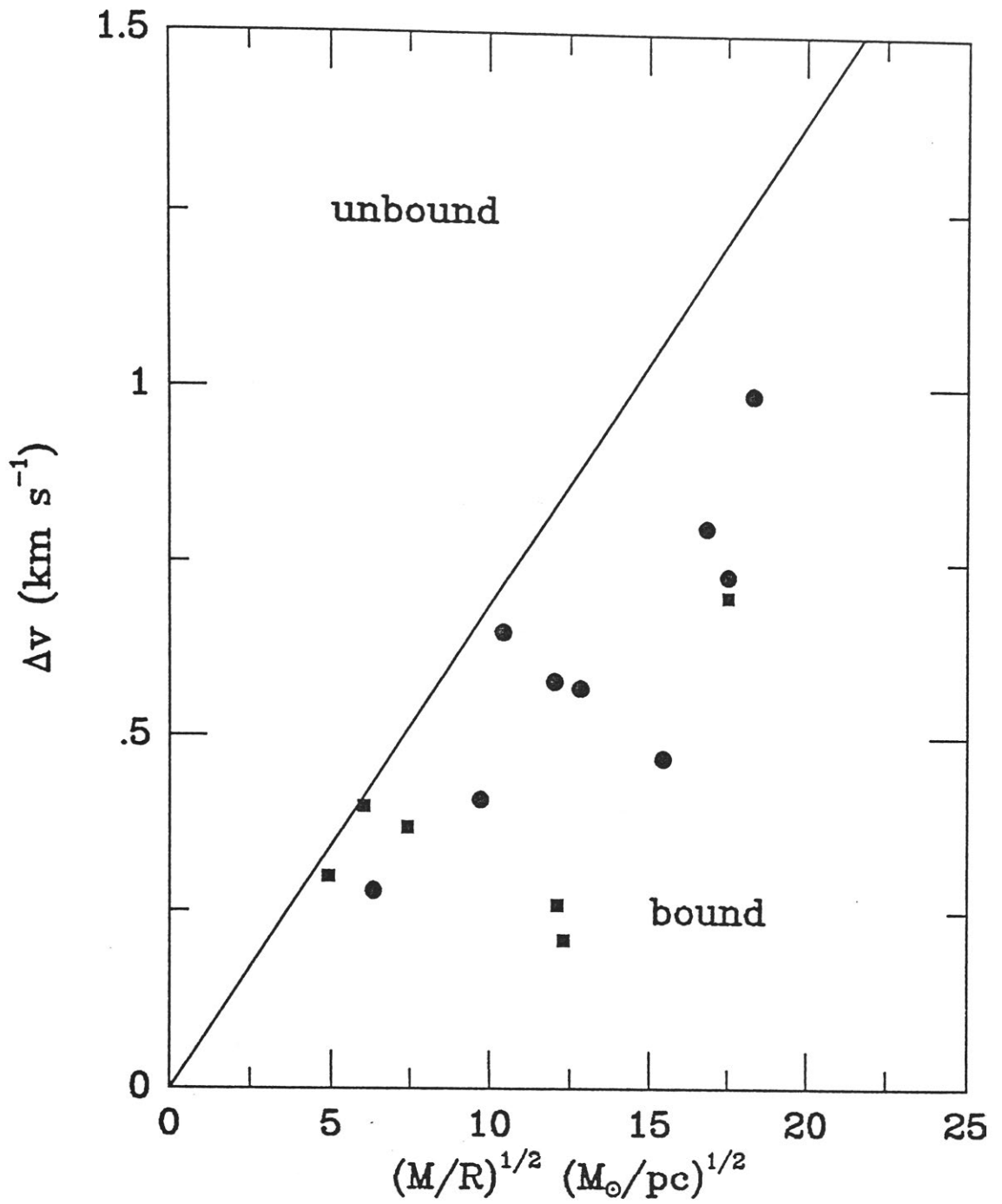


Figure 4.17: Plot of line width against $(M/R)^{1/2}$ for small Bok globules. The solid line indicates virial equilibrium. Clouds lying below this line should be gravitationally bound, while those above should be unbound.

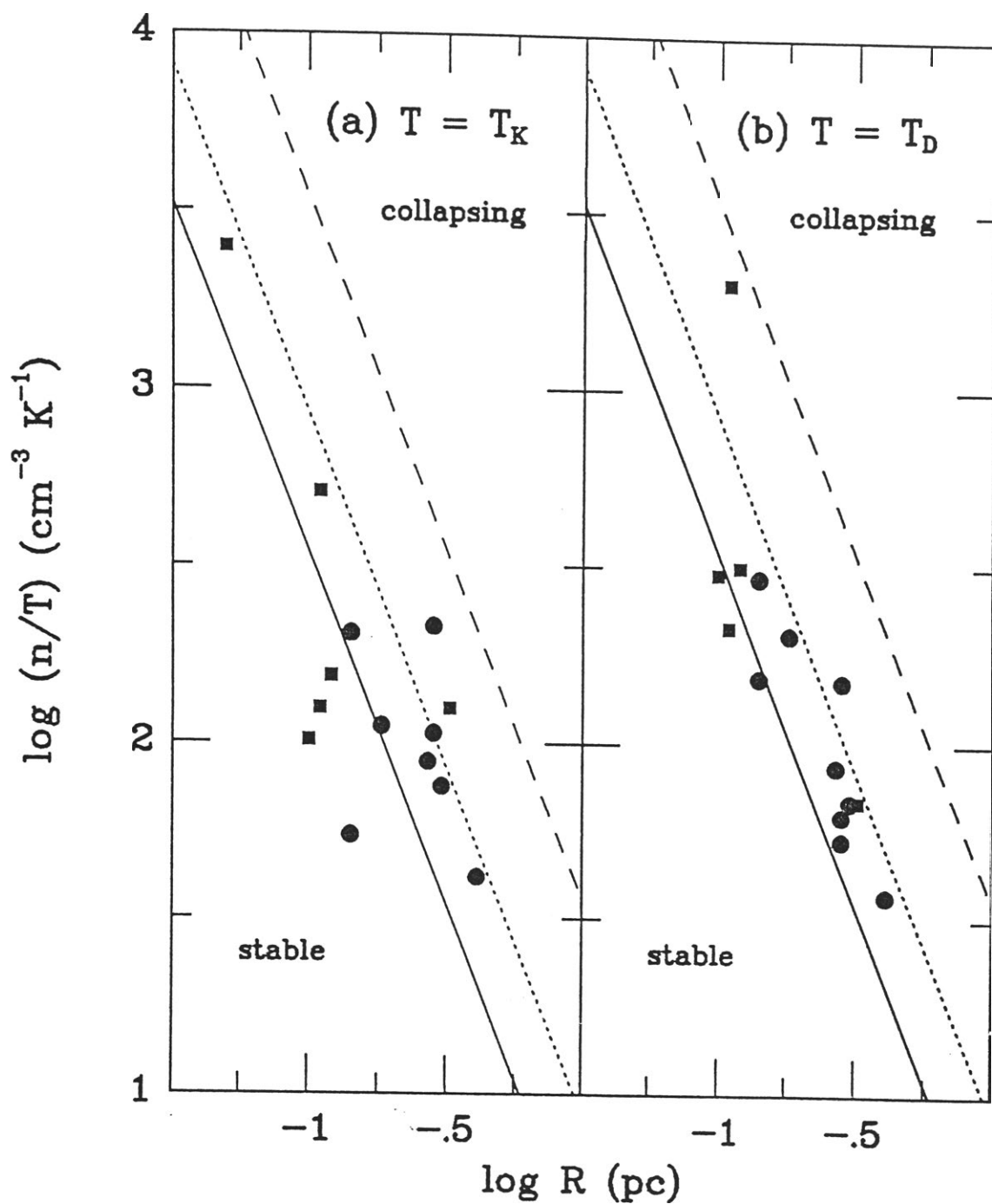


Figure 4.18: Plots showing an examination of possible equilibrium conditions for the Bok globules: (a) shows the possible cloud states assuming the cloud support motions are thermal, and (b) shows the possible cloud states assuming the clouds are supported by their Doppler motions.

collapse as the result of a small perturbation. In figure 4.18(a) we plot $\log(n/T_K)$ against $\log R$, where T_K is the cloud kinetic temperature. This plot allows us to investigate the possible cloud equilibrium states if the globules are supported only by thermal motions. Also shown in this plot are the lines representing $n/n_{max} = 4.1, 1$ and 0.41 . Points lying above the upper line represent clouds which may be collapsing. Points lying below the lower line will be stable if they are in equilibrium. Points lying between the upper and lower lines may or may not be in equilibrium, and this equilibrium may or may not be stable, as discussed in case (b) above. Figure 4.18(b) shows a similar plot, this time assuming the globules are supported by their internal turbulence, so that $T = 369(\Delta v)^2$ (MB).

Figures 4.18(a) and (b) suggest that the clouds in the sample exist in a state of near critical equilibrium, which is consistent with the results of figure 4.17. There is no support from figure 4.18 to suggest that any of the clouds are collapsing, which is more in line with the results of the previous section than with figure 4.17. However, Larson (1981) and Leung *et al.* (1982) have suggested that when turbulent gravitational collapse occurs, virial balance may still be closely satisfied, and so differentiating between contraction and equilibrium may be very difficult in practice. It would appear from the above analysis that the dense globules considered here are in a state of near equilibrium, with the possibility that some may be contracting. Clearly, differentiating between equilibrium and contraction needs to be done on a cloud by cloud basis, requiring high resolution observations over a wide range of wavelengths, to examine the smallest scale motions within the cloud. The comparison of the observed line profiles from a high density tracer on small linear scales (e.g., CS) may provide evidence for contraction by comparing the observed profile with theoretical studies (Zhou, 1992). Zhou (1992) has suggested that the best candidates for such a study are those clouds lying significantly above Myers' best fit line on the $\Delta v - R$ dia-

gram. Candidate clouds from table 4.4 would be DC 253.1–1.6, DC 267.4–7.5, DC 297.7–2.8, DC 345.4–4.0, B335 and B361.

Though we have shown here that power-law relations hold for the small globules, as found by previous studies for larger clouds, the power-law factors are different in some cases, as seen in table 4.4, particularly the $\Delta v - R$ relationships. Larson (1981) suggested that the $\Delta v - R$ law may terminate with objects so small their internal motions are no longer supersonic, with a corresponding minimum mass of $\sim 0.3 M_{\odot}$, and radius 0.04 pc. Myers (1983) found no evidence for such a cutoff in his data. The data in figure 4.13 suggests that for globules such a cutoff may exist, since the slope for globules is greater than that for all clouds, and greater still than the cores in complexes (which Myers suggested, based on his data, show an asymptotic approach to some limiting value of Δv , but not of R). We also find only one of the globules has a radius lower than ~ 0.1 pc. The intersection of the best fit line with the thermal line suggests the lower limit may be $R \sim 0.06$ pc, with a corresponding mass of $\sim 0.4 M_{\odot}$, assuming the power law found here between n and R is valid. These values are similar to those found by Larson (1981). The possibility that a lower limit in R exists may become clearer when we have mapped our weaker sources (where the core size may be smaller), though we may not be able to accurately determine line widths due to noise problems. What is required are observations at higher angular resolutions to study the smallest globules, as suggested by Myers (1983). This is also important to rule out selection effects, which may have resulted in the exclusion of the globules with the smallest sizes in our study from the above analysis. It has been noted by some authors (e.g., Zhou *et al.*, 1989) that the $\Delta v - R$ relationship may break down somewhere between 0.1 and 1 pc, which is supported somewhat by the data presented here. This may indicate some important process is occurring at these small scales to cause this breakdown, the

most likely being star formation (Zhou *et al.*, 1989).

Myers (1983) suggested that if the correlation between Δv and R is significantly better than the correlation between n and R , then it may be a more fundamental relationship, and may imply that virial equilibrium rather than a turbulent energy cascade is the dominant process underlying the observed relationships, since the $n - R$ relationship would then follow from the $\Delta v - R$ law and the tendency of the clouds towards virial equilibrium. Indeed, we find here that the $\Delta v - R$ relationship has a higher correlation than the $n - R$ relationship, and so this may be so. This adds support to the earlier findings which suggested that the globules are in a state of near equilibrium. However, the strong correlation between Δv_{turb} and R supports the turbulent cascade picture, and so clearly no definite conclusions can be drawn from these comparisons.

If the turbulent support picture is the correct one then we expect to see a power law relation between Δv_{turb} and R , but no prediction about a possible relation between Δv_{tot} and R can be made (Myers, 1983). The converse is true if the clouds are in virial equilibrium. For the correlations seen in the data presented here neither scenario can be rejected based on the above arguments, since both Δv_{turb} and Δv_{tot} have strong power-law relationships with R .

However, a simple explanation to the power-law relations has been given by Myers (1987) and MG, who show that if virial cores are magnetically supported by fields with strengths, $B \sim 5\text{--}100 \mu G$ then the power-law relations follow naturally. MG assume that for a uniform, isothermal, self-gravitating sphere supported by both thermal and nonthermal motions, the nonthermal kinetic energy is approximately equal to the magnetic energy density. They show in plots of turbulent velocity dispersion ($= \Delta v / \sqrt{8 \ln 2}$) against R and n against R that the clouds are well bound by curves for virial models with fields 5–100 μG . Plotting the 9 globules of this work directly onto these two plots shows

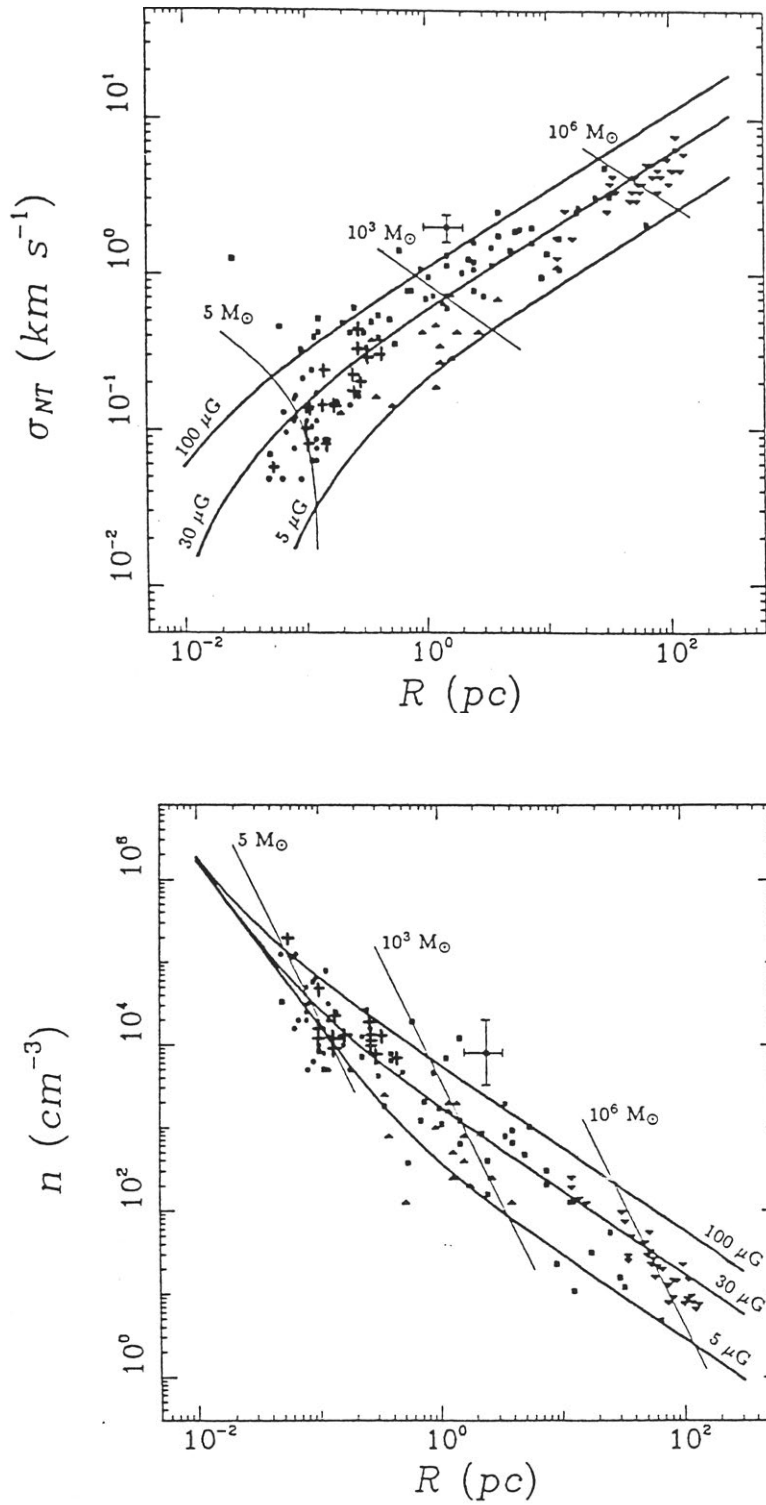


Figure 4.19: Plots of velocity dispersion against cloud size, and density against cloud size (from Myers and Goodman, 1988, figures 1 and 2). The crosses indicate the globules from this section, showing that they are well bound by the virial equilibrium models with magnetic fields in the range 5–100 μG .

they too are well bounded by the theoretical curves of MG, with a scatter about the line $B = 30 \mu G$ (see figure 4.19). That the globules may exist in a state of equilibrium supported by magnetic fields of the order of $30 \mu G$ is certainly a possible explanation of their dynamical state, based on the data presented here, but does not rule out the possibility of turbulence contributing significantly to their support, nor the possibility that some clouds are collapsing or are unstable against collapse.

Clearly, what is needed are direct measurements of strengths of the magnetic fields within the globules, should they exist. The determination of magnetic field strengths towards dark clouds has proved very difficult (Heiles, 1987), though it is sometimes possible through the observation of Zeeman splitting of the OH line at 18 cm (Heiles, 1987). At the least upper limits to the field strengths are required. Perhaps the first step is to determine whether appreciable magnetic fields exist in the globules, through the use of near-infrared studies of the polarization of starlight from stars lying behind the globules (Jones *et al.*, 1984; Klebe and Jones, 1990).

4.4 Conclusions

From the ammonia mapping, we have seen that the sizes of cores within globules are similar to the cores within complexes. The maps also show that the globules are in general not spherical, but elongated (average aspect ratio 1.4), indicating that forces other than random motions and self-gravity are important in the cloud dynamics, such as magnetic fields and turbulence. An examination of the density distribution of two star forming globules shows that they have radial distribution consistent with collapse models for isothermal self-gravitating spheres. However, the non-spherical nature of the globules indicates that non-spherical

modelling may be needed to fully examine their evolution. One globule shows evidence for rotation (DC 297.7–2.8), but the resulting angular momentum is insufficient to support the globule in equilibrium, and cannot be important in the globule dynamics. This is consistent with previous results for both active and quiescent globules.

The discussion of the results for the individual sources points to a number of future observations which should be undertaken to completely characterise these globules. These include: (a) higher angular resolution molecular line measurements, to investigate the gas density structure in the inner region of the core, (b) near infrared observations of stars lying behind the globules in order to determine their dust density distributions, (c) millimetre and far-infrared high resolution continuum observations to search for cool, compact sources which may have been missed by *IRAS*, and to investigate further the known far-infrared sources found by *IRAS*, and (d) CO observations to search for possible outflows.

The dynamical analysis indicates that the cause of the large line widths observed towards cores with *IRAS* sources needs to be investigated. Are they due to mass outflows, or turbulence, or magnetic fields combined with ambipolar diffusion, and is the underlying mechanism able to provide support to the clouds, as suggested by the observations?

It has been shown that the power law relationships which exist between Δv and R , and n and R for clouds covering a much larger range of sizes also exist for the globules as a distinct sample. However, the relationship between Δv and R has a significantly larger exponent than found previously, suggesting that some important process is acting at the smallest scales, resulting in an observed Δv which is larger than predicted by the power law relationships for clouds of a larger range of sizes. As discussed above, this may be a direct result of the star formation process, with the influence of such processes as stellar mass outflows

becoming important in cloud dynamics at the smallest scales. Globules in this work with known near-infrared embedded sources (CG30, DC 267.4–7.5 and DC 297.7–2.8) lie significantly above the best fit line for the larger clouds, as shown by figure 4.12, supporting this view. There is some evidence in the $\Delta v - R$ relationship that Δv may terminate at some small R (when the internal motions are no longer supersonic), and so indicates the possibility that there may exist a minimum protostellar mass of $\sim 0.4 M_{\odot}$. Unlike the dense cores in complexes studied by Myers (1983) in ammonia, the power law relationships for globules have a high correlation. This may be due to the globule sample being more rigorously defined than the cores in complexes sample, which combines data from different dark cloud complexes.

Comparisons between observation and theory suggests that the globules appear to be in a state of near critical equilibrium, probably supported by magnetic fields and turbulence, with the possibility that some may be contracting (as indicated by the presence of embedded sources) while appearing to remain in equilibrium. Determination of the magnetic field direction and strength for these globules is important to enable the magnetic support scenario to be confirmed or rejected. Comparisons of the line profiles of a high density tracer at small linear scales (e.g., CS) with those predicted by theory for contracting clouds should be undertaken for a number of globules to search for signs of infall.

Chapter 5

Conclusions and Future Work

5.1 Results of this Thesis

The main results of the work of each part of this investigation are presented in the conclusions section of each chapter, and so will not be repeated here verbatim. Instead they will be discussed in the context of the unanswered questions and aims of the thesis presented in chapter 1, and suggestions for future work will be discussed. A number of these questions have been answered directly by this investigation, and insights and directions for future research have been gained for most of them.

Star Formation and the Environment

A significant result of this study is that the CGs are a more active group of star forming globules than the other more isolated globules detected in ammonia (see section 3.5.3). This argues against the idea that all isolated globules pass through a CG phase. It would also seem unlikely that the isolated globules

could have originated solely from dense cores within complexes, if any do so at all, since the cores within globules appear to be significantly less active sites of star formation than those within complexes (section 3.5.4). The globules appear to be a truly separate group from the cores within complexes, as outlined below. However, it is possible that the CGs eventually evolve into star forming isolated globules, since their morphology suggests that they may be in a transient phase between being a core within a complex which is being disrupted by the effects of some energetic event, such as high mass star formation, and an isolated globule. The fact that the few globules within filaments surveyed here do not appear to be active star forming sites may suggest that the filaments could be an origin for a number of the isolated globules. The possible connection between B68 and the filament B72 was noted in chapter 1.

We have seen that approximately half of the globules have densities sufficient to suggest that they may undergo star formation (as evidenced by the detection of ammonia emission; table 3.3), a similar number to the dense cores surveyed by Benson and Myers (1989). A sufficient number of globules in this study have been resolved to enable dilution effects as the cause for the non-detection of ammonia to be ruled out. However, we have identified a number of important differences between the globules and the cores within complexes. The globules are less opaque and less dense, and are less efficient sites of star formation, than the cores within complexes (section 3.5.1). These results provide strong evidence that the environment in which the core resides has a large influence on its evolution, and leads to the inference that the outside influences are a dominant cause for the initiation of the star formation process. Spontaneous contraction in some cases cannot be ruled out, but the virial mass paradox outlined later may indicate the necessity of external influences triggering the collapse. Indeed, the fact that CGs have been subjected to outside influences not experienced by

most isolated globules and are more active sites of star formation supports this view.

Density Distribution in Star Forming Globules

In this investigation the gas density distributions of only two globules (DC 345.4–4.0 and DC 297.7–2.8) have been studied in any detail, and both are star forming globules. Both show density profiles between $r^{-1.2}$ and r^{-2} , where r is the radial distance from the cloud centre (see figures 4.5 and 4.9, and pages 165 and 177). These profiles are similar to that expected from the collapse of an isothermal self-gravitating sphere. Both globules appear to have density gradients which are shallower in the central core regions than in the cloud envelope regions, again consistent with most cloud collapse models. However, more of the globules in our list need to be examined at higher spatial resolution than has been possible here, in particular the quiescent globules where star formation does not appear to be taking place, to see whether any important differences can be identified. We have seen that most of the globules studied here are not spherical, and so higher resolution studies may require that a different approach to theoretical modelling be taken if the observations are to be realistically interpreted.

Rotation

Only one of the ten mapped globules shows any signs of a significant systematic velocity shift across it (DC 297.7–2.8; page 172). Interpreting this shift as evidence for globule rotation, we have seen that this rotation is not generating sufficient angular momentum to support the globule in equilibrium. In fact the ratio of potential to gravitational energy shows that the rotation is playing a negligible role in the core dynamics of the globule. This is in agreement with

earlier studies of small dark clouds, Bok globules and dense cores (Goldsmith and Arquilla, 1985; Fuller and Myers, 1987), where it has been found that rotation cannot be important in the cloud energetics, and is always less important than turbulence. It would seem from the lack of rotation in all the globules investigated in this study (and previous studies) that cloud rotation is unimportant in the formation of low mass stars.

Globule Dynamics

The question of whether globules are or are not in virial equilibrium is a difficult one to answer, as many investigators have found. A comparison of the core masses with the virial masses derived from the velocity dispersion measurements suggests that hardly any of the globules studied here are in virial equilibrium or gravitationally bound (table 4.2). But we know that some globules are forming stars, if only by the mere presence of *IRAS* and near-infrared sources embedded within them, so collapse has occurred at some point in the history of a few globules. The virial masses suggest that there is either not enough mass present for the globules to contract (for the globules without embedded sources), or that there is more than sufficient support for the globules (for the star forming globules) against further contraction. For the star forming globules it may be the star formation process itself which provides the support against further contraction, through a mechanism such as increased turbulence or molecular outflows. It could be that the velocity dispersions are indicating that the globules themselves are beginning to disperse. On the other hand, studies of the critical/J Jeans masses, and plots of density against cloud size, suggest that the globules may be in a state of critical equilibrium, with the possibility that some are undergoing contraction (which we know must be true) or may do so in the future. This paradoxical situation needs to be addressed. In particular, the most

detailed modelling studies need to be compared more directly with the observations, which has not been the case to date. The idea that cores may be collapsing while appearing to be in approximate equilibrium needs to be examined in more detail.

5.2 Future Work

Observationally a number of further studies should be undertaken on the globules. A subsample of the globules studied here should be selected for further detailed study. This group should contain globules both with and without indications of star formation, and with and without dense ammonia cores. The most useful information will come from millimetre and near infrared studies. A number of observations which should be undertaken are outlined below:

- a) The subsample should be studied at high angular resolution in ^{12}CO to search for signs of mass outflows, and to determine the temperature at a number of different locations within the globules, which may be difficult with ammonia because of the low intensities observed and low angular resolutions available at present.
- b) High resolution observations of CO isotopes, in particular C^{18}O , are required to examine in detail the gas density structure of the globules. Beamwidths used in millimetre studies are typically less than $1'$ and much less than the size of the ammonia beam width used here, and so the millimetre observations are able to provide higher resolution observations. C^{18}O is usually optically thin in dark clouds, and is able to probe high density gas, and so is an ideal diagnostic to follow-up the ammonia work.

- c) To search for possible signs of infall, high resolution observations of the high density gas tracer CS should be undertaken, in particular the isotope $C^{34}S$, and compared with theoretical studies such as those performed by Zhou (1992).
- d) Submillimetre continuum observations should be undertaken to examine the dust emission from the globules and/or from any embedded compact, cool sources within the globules. The earliest stages of cloud collapse and star formation may be investigated in this way.
- e) A number of studies are possible in the near-infrared. Determination of the near-infrared reddening of background field stars enables the dust density distribution within the core region to be investigated, and the small size of the globules in this study enables this type of investigation to be undertaken in a reasonable time with current near-infrared array cameras. At the same time embedded sources may be identified by their near-infrared colours, and combined with *IRAS* data (should it exist), their evolutionary state may be investigated. We have near-infrared observations of a subsample of 25 globules from this work, both with and without signs of star formation, which will be used for these purposes in the near future.
- f) In the near-infrared polarization studies of background stars would enable the magnetic field direction within the globule to be determined. Importantly, such studies would determine whether a magnetic field of any possible significance exists within the globules.
- g) Magnetic field strengths need to be measured. However, determination of magnetic field strengths towards globules may prove very difficult as indicated by earlier studies. In particular, the small size of the globules makes the use of OH Zeeman splitting at 18 cm difficult, since beam sizes

may be larger than the globules themselves.

- h) Finally, the database of measurements of the densities, sizes, and line widths for the smallest globules needs to be expanded to hopefully strengthen the relationships we have found for these globules, and thus provide important information on the dynamics of these smallest star forming clouds for their detailed theoretical modelling.

It is clear from this study, and previous investigations of small molecular clouds and Bok globules, that future observations and analyses of these isolated clouds offers the greatest promise for identifying and understanding the important factors in the formation of low mass stars.

References

- Adams, F.C. and Shu, F.H., 1986, *Astrophys. J.*, **308**, 836.
- Adams, F.C., Lada, C.J., and Shu, F.H., 1987, *Astrophys. J.*, **321**, 788.
- Bachiller, R., Guilloteau, S., Kahane, C., 1987, *Astron. Astrophys.*, **173**, 324.
- Barnard, E.E., 1919, *Astrophys. J.*, **49**, 1.
- , 1927, *A Photographic Atlas of Selected Regions of the Milky Way*,
ed. E.B. Frost and M.R. Calvert (Washington: Carnegie Institute).
- Beichman, C.A., Jennings, R.E., Emerson, J.P., Baud, B., Harris, S., Rowan-
Robinson, M., Aumann, H.H., Gautier, T.N., Gillett, F.C., Habing, H.J.,
Marsden, P.L., Neugebauer, G., and Young, E., 1984, *Astrophys. J. (Let-
ters)*, **278**, L45.
- Beichman, C.A., Myers, P.C., Emerson, J.P., Harris, S., Mathieu, R., Benson,
P.J., and Jennings, R.E., 1986, *Astrophys. J.*, **307**, 337 (BM86).
- Benson, P.J., 1983, *Microwave Observations of Dense Cores in Local Interstel-
lar Clouds*, PhD Thesis, Massachusetts Institute of Technology.
- Benson, P.J., Myers, P.C., and Wright, E.L., 1984, *Astrophys. J. (Letters)*,
279, L27.

- Benson, P.J. and Myers, P.C., 1989, *Astrophys. J. Suppl. Ser.*, **71**, 89 (BM89).
- van den Bergh, S. and Herbst, W., 1975, *Astron. J.*, **80**, 208.
- Bernes, C., 1977, *Astron. Astrophys. Suppl. Ser.*, **29**, 65.
- Berrilli, F., Ceccarelli, C., Liseau, R., Lorenzetti, D., Saraceno, P., and Spinoglio, L., 1989, *Mon. Not. R. Astr. Soc.*, **237**, 1.
- Bertout, C., 1989, *Ann. Rev. Astron. Astrophys.*, **27**, 357.
- Bevington, P.R., 1969, *Data Reduction and Error Analysis for the Physical Sciences* (New York: McGraw-Hill).
- Bhatt, H.C., 1993, *Mon. Not. R. Astr. Soc.*, **262**, 812.
- Blitz, L., 1991, in *The Physics of Star Formation and Early Stellar Evolution*, ed. C.J. Lada and N.D. Kylafis (Dordrecht: Kluwer), p. 3.
- Blitz, L. and Shu, F.H., 1980, *Astrophys. J.*, **238**, 148.
- Blitz, L., Magnani, L. and Mundy, L., 1984, *Astrophys. J. (Letters)*, **260**, L9.
- Bok, B.J., 1955, *Astron. J.*, **60**, 146.
- , 1977, *Publ. Astron. Soc. Pac.*, **89**, 597.
- , 1978, *Publ. Astron. Soc. Pac.*, **90**, 489.
- Bok, B.J. and Reilly, E.F., 1947, *Astrophys. J.*, **105**, 255.
- Bok, B.J. and Cordwell, C.S., 1971, *A Study of Dark Nebulae* (Tuscon: Uni. of Arizona).
- Bok, B.J., Cordwell, C.S., and Cromwell, R.H., 1971, in *Dark Nebulae, Globules, and Protostars*, ed. B.T. Lynds (Tuscon: Uni. of Arizona), p. 33.

- Bok, B.J. and McCarthy, C.C., 1974, *Astron. J.*, **79**, 42.
- Bok, B.J., Sim, M.E., and Hawarden, T.G., 1977, *Nature*, **266**, 145.
- Bonsack, W.K. and Greenstein, J.L., 1960, *Astrophys. J.*, **131**, 83.
- Bourke, T.L., Hyland, A.R., Robinson, G., and James, S.D., 1993, *Proc. Astron. Soc. Aust.*, **10**, 236.
- Bowers, R.L. and Deeming, T., 1984, *Astrophysics II: Interstellar Matter and Galaxies* (Boston: Jones and Bartlett).
- Cernicharo, J., Bachiller, R., and Duvert, G., 1985, *Astron. Astrophys.*, **149**, 273.
- Cernicharo, J., Bachiller, R., Duvert, G., González-Alfonso, E., and Gómez-González, J., 1992, *Astron. Astrophys.*, **261**, 589.
- Cheung, A.C., Rank, D.M., Townes, C.H., Thornton, D.D., and Welch, W.J., 1968, *Phys. Rev. Lett.*, **21**, 1701.
- Churchwell, E., 1991, in *The Physics of Star Formation and Early Stellar Evolution*, ed. C.J. Lada and N.D. Kylafis (Dordrecht: Kluwer), p. 221.
- Clavel, J., Viala, Y.P., and Bel, N., 1978, *Astron. Astrophys.*, **65**, 435.
- Clemens, D.P. and Barvainis, R., 1988, *Astrophys. J. Suppl. Ser.*, **68**, 257 (CB).
- Clemens, D.P., Yun, J.L., and Heyer, M.H., 1991, *Astrophys. J. Suppl. Ser.*, **75**, 877.
- Clube, S.V.M., 1967, *Mon. Not. R. Astr. Soc.*, **137**, 189.
- Cohen, M. and Kuhi, L.V., 1979, *Astrophys. J. Suppl. Ser.*, **41**, 743.

- Cohen, M., Harvey, P.M., Schwartz, R.D., and Wilking, B.A., 1984, *Astrophys. J.*, **278**, 671.
- Cohen, M. and Schwartz, R.D., 1987, *Astrophys. J.*, **316**, 311.
- Comerón, F., Torra, J., and Gómez, A.E., 1992, *Astr. Space Sci.*, **187**, 187.
- Dame, T., Elmegreen, B.G., Cohen, R.S., and Thaddeus, P., 1986, *Astrophys. J.*, **305**, 892.
- Danby, G., Flower, D.R., Valiron, P., Schilke, P., and Walmsley, C.M., 1988, *Mon. Not. R. Astr. Soc.*, **235**, 229.
- De Luca, M., Blanco, A., and Orofino, V., 1993, *Mon. Not. R. Astr. Soc.*, **262**, 805.
- Dickman, R.L., 1975, *Astrophys. J.*, **202**, 50.
- , 1978, *Astrophys. J.*, **37**, 407.
- Dickman, R.L. and Clemens, D.P., 1983, *Astrophys. J.*, **271**, 143.
- Dieter, N.H., 1973, *Astrophys. J.*, **183**, 449.
- Dyson, J.E. and Williams, D.A., 1980, *The Physics of the Interstellar Medium* (New York: Wiley).
- Eislöffel, J., Davis, C.J., Ray, T.P., and Mundt, R., 1993, *Astrophys. J. (Letters)*, in press.
- Elias, J.H., 1980, *Astrophys. J.*, **241**, 728.
- Emerson, J.P., Harris, S., Jennings, R.E., Beichman, C.A., Baud, B., Beintema, D.A., Marsden, P.L., and Wesselius, P.R., 1984, *Astrophys. J. (Letters)*, **278**, L49.

- Emerson, J.P., 1987, in IAU Symposium 115, *Star Forming Regions*, ed. M. Peimbert and J. Jugaku (Dordrecht: Reidel), p. 19.
- Evans, N.J. II, 1978, in *Protostars and Planets*, ed. T. Gehrels (Tucson: Uni. of Arizona), p. 153.
- , 1981, in IAU Symposium 96, *Infrared Astronomy*, ed. C.G. Wynn-Williams and D.P. Cruikshank (Dordrecht: Reidel), p. 107.
- Federman, S.R. and Willson, R.F., 1982, *Astrophys. J.*, **260**, 124.
- Feitzinger, J.V. and Stüwe, J.A., 1984, *Astron. Astrophys. Suppl. Ser.*, **58**, 365.
- FitzGerald, M.P., Stephens, T.C., and Witt, A.N., 1976, *Astrophys. J.*, **208**, 709.
- Frerking, M.A., Langer, W.D., and Wilson, R.D., 1982, *Astrophys. J.*, **262**, 590.
- Fulkerson, S.A. and Clarke, F.O., 1984, *Astrophys. J.*, **287**, 723.
- Fuller, G.A. and Myers, P.C., 1987, in *Physical Processes in Interstellar Clouds*, ed. G.E. Morfill and M. Scholer (Dordrecht: Reidel), p. 137.
- Genzel, R., 1991, in *The Galactic Interstellar Medium*, ed. D. Pfenniger and P. Bartholdi (Berlin: Springer-Verlag), p. 275.
- Goldsmith, P.F., 1987, in *Interstellar Processes*, ed. D.J. Hollenbach and H.A. Thronson Jr. (Dordrecht: Reidel), p. 51.
- Goldsmith, P.F. and Langer, W.D., 1978, *Astrophys. J.*, **222**, 881.
- Goldsmith, P.F., Snell, R.L., Hemeon-Heyer, M., and Langer, W.D., 1984, *Astrophys. J.*, **286**, 599.

- Goldsmith, P.F. and Arquilla, R., 1985, in *Protostars and Planets II*, ed. D.C. Black and M.S. Matthews (Tuscon: Uni. of Arizona), p. 137.
- Goss, W.M., Manchester, R.N., Brooks, J.W., Sinclair, M.W., Manefield, G.A., and Danzinger, I.J., 1980, *Mon. Not. R. Astr. Soc.*, **191**, 533.
- Grabelsky, D.A., Cohen, R.S., Bronfman, L., and Thaddeus, P., 1987, *Astrophys. J.*, **315**, 122.
- Graham, J.A. and Heyer, M.H., 1989, *Publ. Astron. Soc. Pac.*, **101**, 573.
- Harju, J., Sahu, M., Henkel, C., Wilson, T.L., Sahu, K.C., and Pottasch, S.R., 1990, *Astron. Astrophys.*, **233**, 197.
- Harju, J., Walmsley, C.M., and Wouterloot, J.G.A., 1993, *Astron. Astrophys. Suppl. Ser.*, **98**, 351.
- Hartley, M., Manchester, R.N., Smith, R.M., Tritton, S.B., and Goss, W.M., 1986, *Astron. Astrophys. Suppl. Ser.*, **63**, 27.
- Hawarden, T.G. and Brand, P.W.J.L., 1976, *Mon. Not. R. Astr. Soc.*, **175**, 19p.
- Hayashi, C., 1966, *Ann. Rev. Astron. Astrophys.*, **4**, 171.
- Hayashi, C., Hoshi, R., and Sugimoto, D., 1962, *Prog. Theor. Phys. Suppl.*, **22**, 1.
- Heiles, C., 1968, *Astrophys. J.*, **151**, 919.
- Heiles, C., 1987, in *Interstellar Processes*, ed. D.J. Hollenbach and H.A. Thronson Jnr. (Dordrecht: Reidel), p. 171.
- Henkel, C., 1989, *ESO Messenger*, **57**, 8.

- Herbig, G.H., 1957, *Astrophys. J.*, **125**, 612.
- , 1962, *Adv. Astron. and Astrophys.*, **1**, 47.
- , 1974, *Publ. Astron. Soc. Pac.*, **86**, 604.
- , 1977, *Astrophys. J.*, **214**, 747.
- Herbst, W., 1977, *Publ. Astron. Soc. Pac.*, **89**, 795.
- Ho, P.T.P., Martin, R.N., and Barrett, A.H., 1978, *Astrophys. J. (Letters)*, **221**, L117.
- Ho, P.T.P. and Townes, C.H., 1983, *Ann. Rev. Astron. Astrophys.*, **21**, 239.
- Hyland, A.R., 1981, in IAU Symposium 96, *Infrared Astronomy*, ed. C.G. Wynn-Williams and D.P. Cruikshank (Dordrecht: Reidel), p. 125.
- Hyland, A.R., Bourke, T.L., and Robinson, G., 1993, in ASP Conference Series Vol. 43, *Sky Surveys: Protostars to Protogalaxies*, ed. B.T. Soifer (San Francisco: ASP), p. 49.
- Jones, T.J., Hyland, A.R., Robinson, G., Smith, R.G., and Thomas, J., 1980, *Astrophys. J.*, **242**, 132.
- Jones, T.J., Hyland, A.R., and Bailey, J., 1984, *Astrophys. J.*, **282**, 675.
- de Jong, T., Dalgarno, A., and Boland, W., 1980, *Astron. Astrophys.*, **91**, 68.
- Joy, A.H., 1945, *Astrophys. J.*, **102**, 168.
- , 1949, *Astrophys. J.*, **110**, 424.
- Kazes, I. and Crovisier, J., 1981, *Astron. Astrophys.*, **101**, 401.
- Keene, J., Harper, D.A., Hildebrand, R.H., and Whitcomb, S.E., 1980, *Astrophys. J. (Letters)*, **240**, L43.

- Keene, J., 1981, *Astrophys. J.*, **245**, 115.
- Keene, J., Davidson, J.A., Harper, D.A., Hildebrand, R.H., Jaffe, D.T., Loewenstein, R.F., Low, F.J., and Pernic, R., 1983, *Astrophys. J. (Letters)*, **274**, L43.
- Klebe, D. and Jones, T.J., 1990, *Astron. J.*, **99**, 638.
- Krautter, J., 1991, in ESO Scientific Report 11 *Low Mass Star Formation in Southern Molecular Clouds*, ed. B. Reipurth (München: ESO), p. 127.
- Krügel, E., Stenholm, L.G., Steppe, H., and Sherwood, W.A., 1983, *Astron. Astrophys.*, **127**, 195.
- Kuhi, L.V., 1964, *Astron. Astrophys. Suppl. Ser.*, **15**, 47.
- Kuiper, T.B.H., Peters, W.L. III, Forster, J.R., Gardner, F.F., and Whiteoak, J.B., 1987, *Publ. Astron. Soc. Pac.*, **99**, 107.
- Kylafis, N.D., 1991, in *The Physics of Star Formation and Early Stellar Evolution*, ed. C.J. Lada and N.D. Kylafis (Dordrecht: Reidel), p. 269.
- Lada, C.J., 1987, in IAU Symposium 115, *Star Forming Regions*, ed. M. Peimbert and J. Jugaku (Dordrecht: Reidel), p. 1.
- , 1991, in *The Physics of Star Formation and Early Stellar Evolution*, ed. C.J. Lada and N.D. Kylafis (Dordrecht: Reidel), p. 329.
- Lang, K.R., 1974, *Astrophysical Formulae* (Berlin: Springer-Verlag).
- Larson, R.B., 1969, *Mon. Not. R. Astr. Soc.*, **145**, 271.
- , 1981, *Mon. Not. R. Astr. Soc.*, **194**, 809.
- Lee, M.A. and Rogers, C., 1987, *Astrophys. J.*, **317**, 197.

- Leung, C.M., 1975, *Astrophys. J.*, **199**, 340.
- , 1978, *Astrophys. J.*, **225**, 427.
- , 1985, in *Protostars and Planets II*, ed. D.C. Black and M.S. Matthews (Tuscon: Uni. of Arizona), p. 104.
- Leung, C.M., Kutner, M.L., and Mead, K.N., 1982, *Astrophys. J.*, **262**, 583.
- Leung, C.M., O'Brien, E.V., and Dublisch, R., 1989, *Astrophys. J.*, **337**, 293.
- Lynden-Bell, D. and Pringle, J.E., 1974, *Mon. Not. R. Astr. Soc.*, **168**, 603.
- Lynds, B.T., 1962, *Astrophys. J. Suppl. Ser.*, **7**, 1.
- , 1968, in *Nebulae and Interstellar Matter*, ed. B.M. Middlehurst and L.H. Aller (Chicago: Uni. of Chicago), p. 119.
- Magnum, J.G. and Wootten, A., 1993, *Astrophys. J. Suppl. Ser.*, in press.
- Martin, R.N. and Barrett, A.H., 1978, *Astrophys. J. Suppl. Ser.*, **36**, 1.
- McGregor, P.J., 1992, *Aust. J. Phys.*, **45**, 411.
- Mendoza, V.E., 1966, *Astrophys. J.*, **143**, 1010.
- , 1968, *Astrophys. J.*, **151**, 977.
- Menten, K.M., Walmsley, C.M., Krügel, E., and Ungerechts, H., 1984, *Astron. Astrophys.*, **137**, 108.
- Mezger, P.G. and Smith, L.F., 1977, in IAU Symposium 75, *Star Formation*, ed. T. de Jong and A. Maeder (Dodrecht: Reidel), p. 133.
- Milman, A.S., 1977, *Astrophys. J.*, **211**, 128.

- Morris-Kennedy, P., 1983, *MK Classification Extension* (Canberra: Mt Stromlo Obs.), also in The Astronomical Data Centre CD-ROM Selected Astronomical Catalogs, Vol. 1, 1989.
- Mouschovias, T. Ch., 1991, *Astrophys. J.*, **373**, 169.
- Myers, P.C., 1983, *Astrophys. J.*, **270**, 105.
- , 1985, in IAU Symposium 115, *Star Forming Regions*, ed. M. Peimbert and J. Jugaku (Dordrecht: Reidel), p. 33.
- , 1987, in *Interstellar Processes*, ed. D.J. Hollenbach and H.A. Thronson Jnr. (Dordrecht: Reidel), p. 71.
- Myers, P.C., Ho, P.T.P., Schneps, M.H., Chin, G., Pankonia, V., and Winfoerg, A., 1978, *Astrophys. J.*, **220**, 864.
- Myers, P.C., Linke, R.A., and Benson, P.J., 1983, *Astrophys. J.*, **264**, 517.
- Myers, P.C. and Benson, P.J., 1983, *Astrophys. J.*, **266**, 309 (MB).
- Myers, P.C., Fuller, G.A., Matthieu, R.D., Beichman, C.A., Benson, P.J., Schild, R.E., and Emerson, J.P., 1987, *Astrophys. J.*, **319**, 340.
- Myers, P.C. and Goodman, A.A., 1988, *Astrophys. J.*, **329**, 392 (MG).
- Nyman, L.-Å, Bronfman, L., and Thaddeus, P., 1989, *Astron. Astrophys.*, **216**, 185.
- Ogura, K. and Hasegarva, T., 1983, *Publ. Astron. Soc. Japan*, **35**, 299.
- Olberg, M., Reipurth, B., and Booth, R.S., 1992, *Astron. Astrophys.*, **259**, 252.
- Palmer, P., Zuckerman, B., Buhl, D., and Snyder, L.E., 1969, *Astrophys. J. (Letters)*, **156**, L147.

- Parker, N.D., 1989, *Studies of Star Formation in Dark Molecular Clouds*, PhD Thesis, University of Cambridge.
- Pauls, T.A., Wilson, T.L., Bieging, J.H., and Martin, R.N., 1983, *Astron. Astrophys.*, **124**, 23.
- Penzias, A.A., Solomon, P.M., Jefferts, K.B., and Wilson, R.W., 1972, *Astrophys. J. (Letters)*, **174**, L43.
- Persi, P., Ferrari-Tomolo, M., Busso, M., Origlia, L., Robberto, M., Scaltriti, F., and Silvestro, G., 1990, *Astron. J.*, **99**, 303.
- Persi, P., Ferrari-Toniolo, M., Marenzi, A.R., Anglada, G., Chini, R., Krugel, E., and Sepulveda, I., 1993, *Astron. Astrophys.*, in press.
- Pettersson, B., 1984, *Astron. Astrophys.*, **139**, 135.
- Pettersson, B., 1987, *Astron. Astrophys.*, **171**, 101.
- , 1991, in ESO Scientific Report 11 *Low Mass Star Formation in Southern Molecular Clouds*, ed. B. Reipurth (München: ESO), p. 69.
- Phillips, T.G. and Huggins, P.J., 1981, *Astrophys. J.*, **251**, 533.
- Reipurth, B., 1983, *Astron. Astrophys.*, **117**, 183.
- Reipurth, B., Heathcote, S., and Vrba, F., 1992, *Astron. Astrophys.*, **256**, 225.
- Reipurth, B. and Zinnecker, H., 1993, *Astron. Astrophys.*, in press.
- Rickard, L.J., Palmer, P, Buhl, D, and Zuckerman, B., 1977, *Astrophys. J.*, **213**, 654.
- Rodgers, A.W., 1960, *Mon. Not. R. Astr. Soc.*, **120**, 163.
- Rohlfs, K., 1986, *Tools of Radio Astronomy* (Berlin: Springer-Verlag).

- Rucinski, S.M., 1985, *Astron. J.*, **90**, 2321.
- Rydbeck, O.E.H., Sume, A., Hjalmarson, Å, Elldér, J., Rönnäng, B.O., and Kollberg, E., 1977, *Astrophys. J. (Letters)*, **215**, L35.
- Rydgren, A.E., Strom, S.E., and Strom, K.M., 1976, *Astrophys. J. Suppl. Ser.*, **30**, 307.
- Sahu, M., Sahu, K.C., and Pottasch, S.R., 1989, *Astron. Astrophys.*, **218**, 221.
- Sanders, D.B., Scoville, N.Z., and Solomon, P.M., 1985, *Astrophys. J.*, **289**, 373.
- Sandford, M.T. II, Whitaker, R.W., and Klein, R.I., 1982, *Astrophys. J.*, **260**, 183.
- , 1984, *Astrophys. J.*, **282**, 178.
- Sandqvist, Aa., 1977, *Astron. Astrophys.*, **57**, 467.
- Sandqvist, Aa. and Lindroos, K.P., 1976, *Astron. Astrophys.*, **53**, 179.
- Schmidt, E.G., 1975, *Mon. Not. R. Astr. Soc.*, **172**, 401.
- Schneider, S. and Elmegreen, B.G., 1979, *Astrophys. J. Suppl. Ser.*, **41**, 87.
- Schwartz, R.D., 1977, *Astrophys. J. (Letters)*, **212**, L25.
- , 1991, in ESO Scientific Report 11 *Low Mass Star Formation in Southern Molecular Clouds*, ed. B. Reipurth (München: ESO), p. 93.
- Schwartz, R.D., Cohen, M., and Williams, P.M., 1987, *Astrophys. J.*, **322**, 403.
- Scoville, N.Z. and Sanders, D.B., 1987, in *Interstellar Processes*, ed. D.J. Hollenbach and H.A. Thronson Jnr. (Dordrecht: Reidel), p. 21.

- Shu, F.H., 1977, *Astrophys. J.*, **214**, 488.
- Shu, F.H., Adams, F.C, and Lizano, S., 1987, *Ann. Rev. Astron. Astrophys.*, **25**, 23.
- Snell, R.L., 1981, *Astrophys. J. Suppl. Ser.*, **45**, 121.
- Snell, R.L., Langer, W.D., and Frerking, M.A., 1982, *Astrophys. J.*, **255**, 149.
- Solomon, P.M., Sanders, D.B., and Rivolo, A., 1985, *Astrophys. J. (Letters)*, **292**, L19.
- Spencer, R.G. and Leung, C.M., 1978, *Astrophys. J.*, **222**, 140.
- Spitzer, L., 1968, in *Nebulae and Interstellar Matter*, ed. B.M. Middlehurst and L.H. Aller (Chicago: Uni. of Chicago), p. 1.
- Stutzki, J., Jackson, J.M., Olberg, M., Barrett, A.H., and Winnewisser, G., 1984, *Astron. Astrophys.*, **139**, 258.
- Stutzki, J. and Winnewisser, G., 1985a, *Astron. Astrophys.*, **144**, 13.
- , 1985b, *Astron. Astrophys.*, **148**, 254.
- Sugitani, K., Fukui, Y., and Ogura, K., 1991, *Astrophys. J. Suppl. Ser.*, **77**, 59.
- Tapia, S., 1973, in IAU Symposium 52, *Interstellar Dust and Related Topics*, ed. J.M. Greenberg and H.C. van de Hulst (Dordrecht: Reidel), p. 43.
- Tarafdar, S.P., Prasad, S.S., Huntress, W.T. Jnr., Villere, K.R., and Black, D.C., 1985, *Astrophys. J.*, **289**, 220.
- Thorne, A.P., 1988, *Spectrophysics* (London: Chapman and Hall).
- Tomita, Y., Saito, T, and Ohtani, H., 1979, *Publ. Astron. Soc. Japan*, **31**, 407.

- Turner, B.E., 1978, in IAU Symposium 84, *The Large-Scale Characteristics of the Galaxy*, ed. W.B. Burton, (Dordrecht: Reidel), p. 257.
- , 1988, in *Galactic and Extragalactic Radio Astronomy*, ed. G.L. Verschur and K.I. Kellermann (New York: Springer-Verlag), p. 154.
- Ungerechts, H., Walmsley, C.M., and Winnewisser, G., 1980, *Astron. Astrophys.*, **88**, 259.
- , 1982, *Astron. Astrophys.*, **111**, 339.
- , 1986, *Astron. Astrophys.*, **157**, 207.
- Villere, K.R. and Black, D.C., 1980, *Astrophys. J.*, **236**, 192.
- de Vries, C.P., Brand, J., Israel, F.P., de Graauw, Th., Wouterloot, J.G.A., van de Stadt, H., and Habing, H.J., 1984, *Astron. Astrophys. Suppl. Ser.*, **56**, 333.
- Walker, M.F., 1972, *Astrophys. J.*, **175**, 89.
- Walmsley, C.M. and Ungerechts, H., 1983, *Astron. Astrophys.*, **122**, 164.
- Walter, F.M., 1987, *Publ. Astron. Soc. Pac.*, **99**, 31.
- Westin, T.N.G., 1985, *Astron. Astrophys. Suppl. Ser.*, **60**, 99.
- Whitter, D.C.B., 1992, *Dust in the Galactic Environment* (London: Institute of Physics).
- Wilking, B.A., 1991, in ESO Scientific Report 11 *Low Mass Star Formation in Southern Molecular Clouds*, ed. B. Reipurth (München: ESO), p. 159.
- Wilking, B.A., Schwartz, R.D., Mundy, L.D., and Schultz, A.S.B., 1990, *Astron. J.*, **99**, 344.

- Wilson, R.W., Jefferts, K.B., and Penzias, A.A., 1970, *Astrophys. J. (Letters)*, **161**, L43.
- Winnewisser, G., Churchwell, E., and Walmsley, C.M., 1979, in *Modern Aspects of Microwave Spectroscopy*, ed. G.W. Chantry (London: Academic), p. 313.
- Yun, J.L., 1992, *Star Formation in Small Molecular Clouds - A Characterization of Young Stellar Objects in Bok Globules: Infrared Imaging, Spectral Energy Distributions, and Molecular Outflows*, PhD Thesis, Boston University.
- Yun, J.L. and Clemens, D.P., 1990, *Astrophys. J. (Letters)*, **367**, L73.
- , 1992, *Astrophys. J. (Letters)*, **385**, L21.
- Zealey, W.J., Ninkov, Z., Rice, E., Hartley, M., and Tritton, S.B., 1983, *Astrophys. Lett.*, **23**, 119.
- Zealey, W.J., Suters, M.G., and Randall, P.R., 1993, *Proc. Astron. Soc. Aust.*, **10**, 203.
- Zhou, S., Wu, Y., Evans, N.J. II, Fuller, G.A., and Myers, P.C., 1989, *Astrophys. J.*, **346**, 168.
- Zhou, S., 1992, *Astrophys. J.*, **394**, 204.

Appendix A

Molecular Excitation and Radiative Transfer

The main references used in these appendices are Winnewisser *et al.* (1979), Ho and Townes (1983), Benson (1983), Stutzki and Winnewisser (1985b), Ungereschts *et al.* (1986), Rohlfs (1986), Thorne (1988), Turner (1988), and Genzel (1991).

A.1 Molecular Excitation

Molecules may change their state by spontaneous emission of a photon, by stimulated emission, or by collisions. Consider a two level system. The probability that a spontaneous transition will occur from the upper (u) to the lower (l) level is given by the Einstein A coefficient:

$$A_{ul} = \frac{64\pi\mu_{ul}^2\nu_{ul}^3}{3hc^3} \quad (\text{A.1})$$

where μ_{ul} is the transition moment matrix element. The probability that a stimulated transition will occur from the upper to the lower level is by given the product of the Einstein coefficient for stimulated emission, B_{ul} :

$$B_{ul} = \frac{c^3}{8\pi h\nu_{ul}^3} A_{ul} \quad (\text{A.2})$$

and the specific energy density of the surrounding radiation, $U(T_r)$:

$$U(T_r) = \frac{8\pi h\nu^3}{c^3} \frac{1}{\exp(h\nu/kT_r) - 1} \quad (\text{A.3})$$

where T_r is the temperature of the surrounding radiation at the frequency ν_{ul} , thus:

$$B_{ul}U(T_r) = A_{ul}F(T_r) \quad (\text{A.4})$$

where:

$$F(T) = \frac{1}{\exp(h\nu/kT) - 1} \quad (\text{A.5})$$

as defined in Chapter 3. The probability that absorption will occur between the two levels is related to the probability of emission by the ratio of statistical weights of the states, or the degeneracy of the states:

$$B_{lu} = \frac{g_u}{g_l} B_{ul} \quad (\text{A.6})$$

where g_i is the statistical weight of the state i .

Collisional transitions between the upper and lower states are described by the collision rates, C_{ul} and C_{lu} . The collision rate from the upper to the lower lever is given by:

$$C_{ul} = C_{u \rightarrow l} = n\gamma_{ul} = n \langle \sigma_{ul}v \rangle \quad (\text{A.7})$$

where σ_{ul} is the cross section for the collision $u \rightarrow l$ at the velocity v , n is the volume density, and γ_{ul} is the overall collisional rate coefficient for $u \rightarrow l$. The equation of detailed balance then gives the rate coefficient in the opposite direction:

$$C_{lu} = C_{ul} \frac{g_u}{g_l} \exp\left(-\frac{h\nu}{kT_k}\right) \quad (\text{A.8})$$

and the excitation temperature for the transition $T_{ex} = T_{ul}$ is defined by:

$$\frac{n_u}{n_l} = \frac{g_u}{g_l} \exp\left(-\frac{h\nu}{kT_{ex}}\right) \quad (\text{A.9})$$

The excitation temperature is therefore an equivalent Planck temperature that describes the population of the states u and l through a Boltzmann population.

At equilibrium the number of molecules leaving a given level per second is equal to the number of molecules entering that level. For the two level system this may be expressed as:

$$n_u(A_{ul} + B_{ul} + nC_{ul}) = n_l\left(\frac{g_u}{g_l}B_{ul} + n\frac{g_u}{g_l}C_{ul}\exp\left(-\frac{h\nu}{kT_k}\right)\right) \quad (\text{A.10})$$

where n is the total number density of the collision partner(s). Combining the above equation with the equation of detailed balance allows the volume density of the collision partner to be calculated. In molecular clouds the collision partner is almost always molecular hydrogen, hence:

$$n(H_2) = \frac{A_{ul} F(T_{ex}) - F(T_{bg})}{C_{ul} F(T_k) - F(T_{ex})} [1 + F(T_k)] \quad (\text{A.11})$$

A.2 Radiative Transfer

The intensity of line radiation we observe from a molecular cloud depends on the radiative transportation properties of the cloud. The change in line intensity as radiation of frequency ν passes through a cloud of thickness dz may be expressed as:

$$\frac{dI_\nu}{dz} = \epsilon_\nu - \kappa_\nu I_\nu \quad (\text{A.12})$$

where ϵ_ν is the emission coefficient and κ_ν the absorption coefficient. The absorption along the line of sight is known as the optical depth, τ_ν :

$$\tau_\nu = -\int_0^z \kappa_\nu dz \quad (\text{A.13})$$

The source function, S_ν , is defined as the ratio of the emission coefficient to the absorption coefficient:

$$S_\nu = \frac{\epsilon_\nu}{\kappa_\nu} = \frac{2h\nu^3}{c^2} \left[\frac{n_l g_u}{n_u g_l} - 1 \right]^{-1} = \frac{2h\nu^3}{c^2} F(T_{ex}) \quad (\text{A.14})$$

Integrating along the line of sight then gives the expression for the observed line intensity:

$$I_\nu = I_{bg} \exp(-\tau_\nu) + S_\nu(1 - \exp(-\tau_\nu)) \quad (\text{A.15})$$

where I_{bg} is the background intensity.

When the observed emission is due purely to line emission, the intensity observed at the telescope is the line intensity in excess of the background continuum:

$$\Delta I = I_\nu - I_B = (S_\nu(T_{ex}) - I_{bg})(1 - \exp(-\tau)) \quad (\text{A.16})$$

The conversion of intensity into units of temperature is given by

$$T \equiv \frac{c^2}{2k\nu^2} I \equiv \frac{h\nu}{k} F(T)$$

and so the intensity observed at the telescope may then be expressed as the brightness temperature, T_B :

$$T_B = [F(T_{ex}) - F(T_{bg})](1 - \exp(-\tau)) \quad (\text{A.17})$$

where T_{bg} is the continuum background temperature = 2.7 K. Astronomical sources rarely fill the telescope beam in radio astronomy, so in practice T_B cannot be derived directly without a knowledge of the source size. If the telescope beam is approximated by an gaussian of FWHM θ_b , and the line source by a gaussian of FWHM $\theta_x \times \theta_y$, then the beam filling factor may be determined:

$$\phi = \left\{ \left[1 + \left(\frac{\theta_b}{\theta_x} \right)^2 \right] \left[1 + \left(\frac{\theta_b}{\theta_y} \right)^2 \right] \right\}^{-1/2} \quad (\text{A.18})$$

Taking the telescope beam efficiency, η , into account, the relation between the observed antenna temperature, T_a^* , and the brightness temperature, T_B , is:

$$T_a^* = \phi\eta T_B \quad (\text{A.19})$$

where T_a^* is the observed antenna temperature corrected for the variation of gain with elevation and atmospheric attenuation.

The absorption coefficient may be written as:

$$\kappa_\nu = \frac{h\nu l_u}{4\pi} n_{ul} B_{ul} \left(1 - \frac{n_l g_u}{n_u g_l} \right) \varphi_\nu \quad (\text{A.20})$$

where φ_ν is the line shape function, which gives the probability per frequency interval that a photon is emitted at frequency ν ($\int \varphi_\nu d\nu = 1$). The column density in the upper state N_u ($= \int_0^z n_u dz$) is then found from:

$$N_u = \frac{8\pi\nu^2}{\varphi_\nu A_{ul} c^2} \tau_\nu \left(\frac{n_l g_u}{n_u g_l} - 1 \right)^{-1} \quad (\text{A.21})$$

The line shape function is related to the line width $\Delta\nu$ via

$$\varphi = \frac{c}{\nu 1.064 \Delta\nu}$$

for a gaussian line, and so with the equation of detailed balance, the column density can be written as:

$$N_u = \frac{8\pi\nu^3 1.064}{A_{ul} c^3} F(T_{ex}) \Delta\nu \tau \quad (\text{A.22})$$

In the optically thin limit, $\tau \ll 1$, we have:

$$\begin{aligned} \tau \Delta\nu &\simeq \int \tau_\nu d\nu \\ &\simeq \frac{1}{\phi [F(T_{ex}) - F(T_{bg})]} \int T_B(\nu) d\nu \\ &= \frac{\nu}{\phi c} \frac{1}{F(T_{ex}) - F(T_{bg})} \int T_B(\nu) d\nu \end{aligned} \quad (\text{A.23})$$

and so in the optically thin limit the column density may be found from:

$$N_u = \frac{8\pi\nu^4 1.064}{\phi A_{ul} c^4} \frac{1}{1 - \frac{F(T_{bg})}{F(T_{ex})}} \int T_B(\nu) d\nu \quad (\text{A.24})$$

The total column density for the transition, assuming a Boltzmann distribution, is then:

$$N(\nu) = N_u + N_l = N_u \left(1 + \frac{g_l}{g_u} e^{h\nu/kT_{ex}} \right) \quad (\text{A.25})$$

and the total column density for the molecule is:

$$N_{tot} = \sum_i N(\nu_i) \quad (\text{A.26})$$

Appendix B

The Ammonia Molecule

B.1 Physics of the Ammonia Molecule

Ammonia (NH_3) is a symmetric top with inversion. The rotational state of the molecule may be expressed in terms of two quantum numbers, the total angular momentum, J , and its projection onto the axis connecting the nitrogen atom to the plane of the hydrogen atoms, K ($K \leq J$). The symmetry of the molecule means that radiative transitions are only allowed between J states in a given K ladder, i.e., the selection rules are $\Delta J = \pm 1, \Delta K = 0$. States with $J = K$ are metastable with respect to radiative transitions.

Two distinct species of NH_3 exist, due to the different possible orientations of the hydrogen spins. When all the spins are parallel the species is known as ortho- NH_3 , which have $K = 3n$, where n is an integer, while para- NH_3 ($K \neq 3n$) does not have the hydrogen spins aligned. Transitions between ortho- and para- NH_3 are forbidden.

Each rotational (J, K) state may exist in one of two further states, depending

on whether the nuclear wavefunction is symmetric or antisymmetric with respect to the plane of the hydrogen atoms. Classically this vibrational inversion occurs when the nitrogen atom “tunnels” through the potential barrier set up by the plane of the hydrogen atoms. This barrier is small enough so that this tunnelling occurs often, resulting in many transitions around $\lambda = 1.2$ cm. These inversion doublets are further split by hyperfine interactions, mainly from interactions between the nitrogen atom and the electric field of the electrons, and coupling of the nitrogen spin with J , and H–H and H–N spin–spin interactions. For the (1,1) transition, 18 hyperfine components result from these interactions, which allows the optical depth of the transition to be obtained directly. Figure B.1 shows the energy levels of the NH_3 molecule and figure B.2 shows the hyperfine transitions of the (1,1) level with their relative intensities and frequency offsets.

B.2 Ammonia as a Diagnostic Probe

Since transitions between the various metastable levels ($J = K$) are induced mainly by collisions, observations of the various inversion transitions should allow the kinetic temperature of the molecular cloud to be directly determined. Column densities are also directly obtainable from the inversion transitions due to the observation of the hyperfine structure. Due to the relative closeness of the inversion transitions in frequency, the relative calibration errors should be small.

The most easily observed NH_3 transitions in typical molecular clouds ($T = 10\text{--}100$ K) are the (1,1) and (2,2) inversion transitions at 23.694495 and 23.722633 GHz respectively. The Boltzmann equation gives the rotational tem-

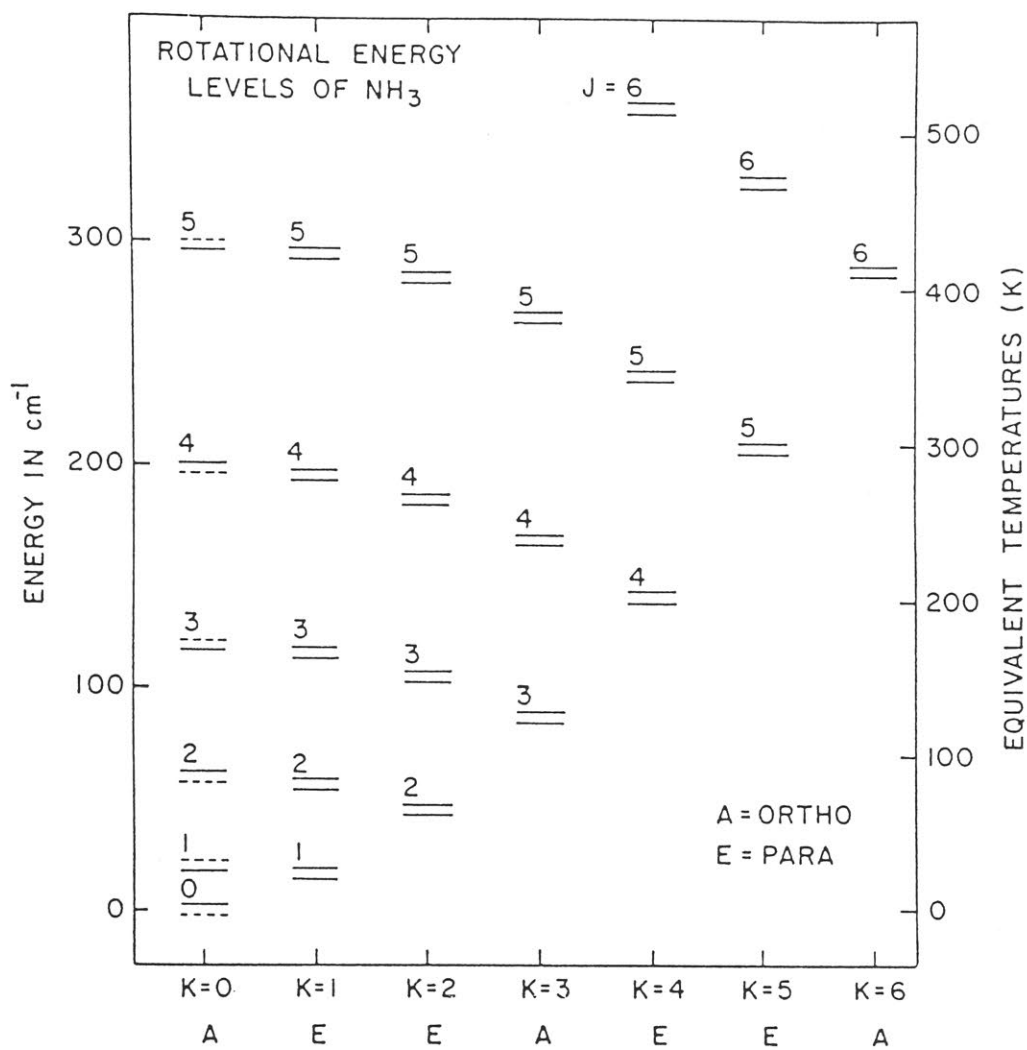
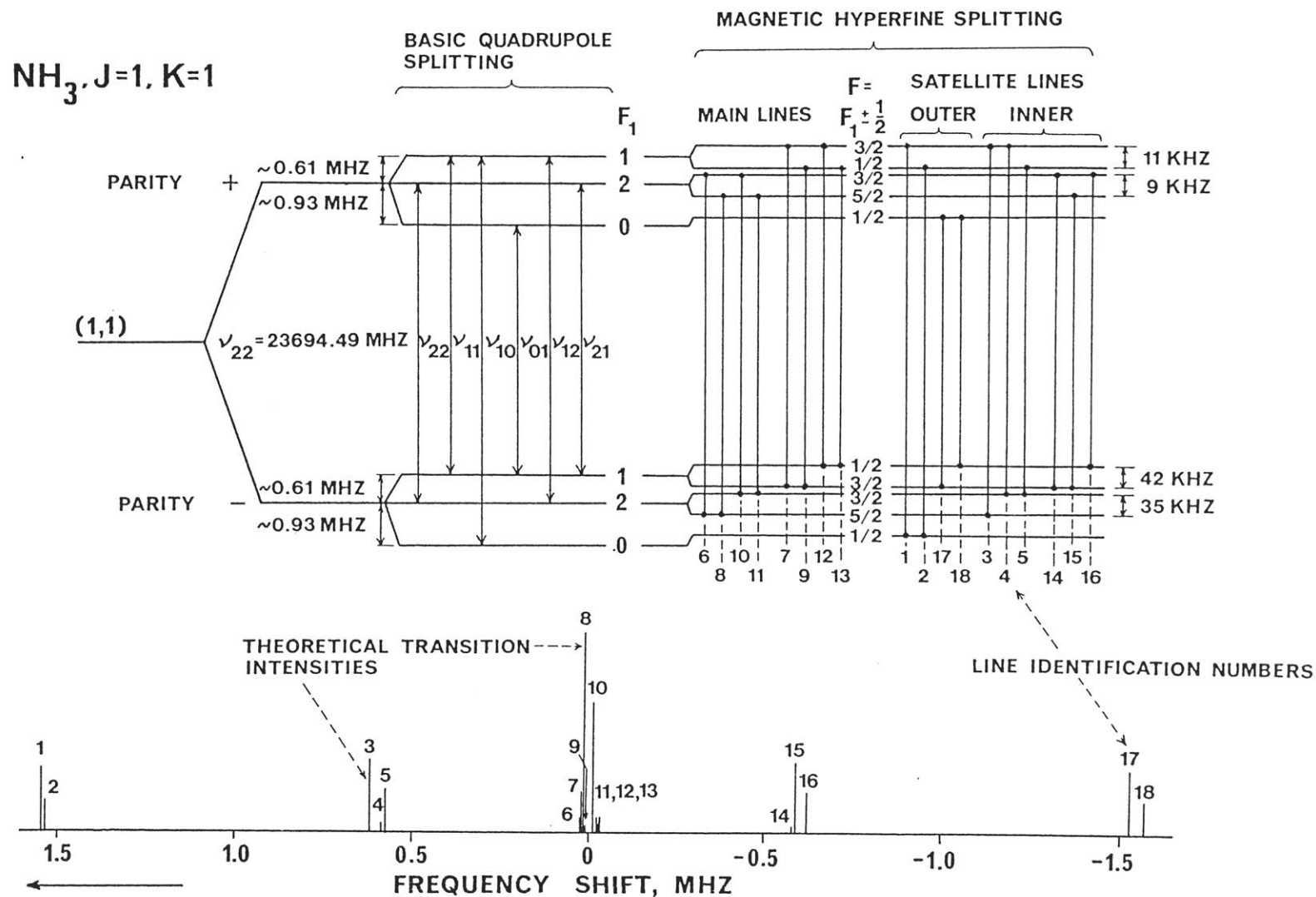


Figure B.1: The energy level diagram of the rotation-inversion states of ammonia (taken from Ho and Townes, 1983, figure 1).

Figure B.2: Hyperfine splitting, allowed transitions and relative intensities of the (1,1) hyperfine transitions (from Rydbeck *et al.*, 1977, figure 1).



perature, T_{12} , between the two states:

$$\frac{N_{22}}{N_{11}} = \frac{g_{22}}{g_{11}} \exp\left(-\frac{\Delta E_{12}}{kT_{12}}\right) \quad (\text{B.1})$$

where N is the column density, g the statistical weight, and ΔE_{12} is the energy difference between the two levels ($= 41.5$ K). Since the hyperfine components of the (2,2) are not always visible in molecular clouds due to their relatively low intensity, the column density of the (2,2) state may not always be well determined. In this case the relative intensities of the observed brightness temperatures may be used to determine T_{12} , since they are proportional to the optical depths and hence to the column densities. The rotational temperature may then be found from:

$$T_{12} = \frac{\frac{\Delta E_{12}}{k}}{\ln \left[-\frac{g_{11}}{g_{22}} \frac{A_{11}}{A_{22}} \left(\frac{\nu_{22}}{\nu_{11}}\right)^3 \frac{1}{s_{22}\tau_{11}} \ln \left(1 - \frac{T_B^{22}}{T_B^{11}} (1 - \exp(-s_{11}\tau_{11})) \right) \right]} \quad (\text{B.2})$$

where A is the Einstein coefficient for spontaneous transitions, ν the frequency of the inversion transition, and s_{JK} is the relative intensity of the main line group with respect to the main line group of the (1,1) transition.

For the temperatures considered here, only the (1,1) and (2,2) metastable transitions need be considered to have significant populations. The rate equation for exchange of population between the $K = 1$ and $K = 2$ ladders is then:

$$n_{22}(C_{22 \rightarrow 11} + C_{22 \rightarrow 21}) = n_{11}C_{11 \rightarrow 22} \quad (\text{B.3})$$

where $C_{JK \rightarrow J'K'}$ represents the rate of collisional transfer of population between the (J,K) and $(J'K')$ levels. The values for C where molecular hydrogen is the collision partner may be found in Danby *et al.* (1988).

Applying the equation of detailed balance, and assuming $T_{ex}(1,1) = T_{ex}(2,2)$, then gives the expression relating T_{12} and T_K :

$$T_{12} = \frac{T_k}{1 + \frac{kT_k}{\Delta E_{12}} \ln \left(1 + \frac{C_{22 \rightarrow 21}}{C_{22 \rightarrow 11}} \right)} \quad (\text{B.4})$$

A knowledge of the kinetic temperature then allows the volume density to be calculated, as shown in Appendix A.

thesis 1994 Bourke
Studies of star formation in s
mall molecular clouds and B...
Bourke, Tyler Leonard
BARCODE 301255 BRN 259914
ADFA Library 08 DEC 1994